AN INTEGRATED GEOLOGICAL, GEOCHEMICAL AND PETROGENETIC STUDY OF A PART OF THE ARCHEAN LARDER LAKE GROUP AT THE ADAMS MINE, NORTHEASTERN ONTARIO

AN INTEGRATED GEOLOGICAL, GEOCHEMICAL AND PETROGENETIC STUDY OF A PART OF THE ARCHEAN LARDER LAKE GROUP AT THE ADAMS MINE, NORTHEASTERN ONTARIO

By

GORDON D. McROBERTS, B.Sc.

A Thesis
Submitted to the School of Graduate Studies
in Partial Fulfilment of the Requirements
for the Degree
Master of Science

McMaster University
April, 1986

MASTER OF SCIENCE (1986) McMASTER UNIVERSITY
Geology Hamilton, Ontario

TITLE: An Integrated Geological, Geochemical and Petrogenetic Study of a Part of the Archean Larder Lake Group at the Adams Mine, Northeastern Ontario

AUTHOR: Gordon David McRoberts, B.Sc. (McMaster)

SUPERVISOR: Dr. James H. Crocket

NUMBER OF PAGES: xxviii, 386

Abstract

. The thesis map area is located in northeastern Ontario in and west of the Adams Mine site. The Adams Mine produces iron ore and is situated 15 km southeast of the town of Kirkland Lake. Kirkland Lake is the largest population centre in the Kirkland Lake-Larder Lake gold camp. The Adams Mine lies south of this camp.

The thesis map area is underlain by volcanics (most of which are komatiitic), clastic, chemical and pelitic sediments and various intrusives (peridotite sills, layered peridotite-gabbro and gabbro sills, discordant gabbro bodies, alkali-rich dykes and diabase dykes. The syenitic Lebel Stock forms the northern boundary of the map area.

The map area lies entirely within the Larder Lake Group which forms the lower part of the second major volcanic cycle (cycke II) in the Archean aged Abitibi greenstone belt. The Kinojevis and Blake River Groups overlie the Larder Lake Group north of Kirkland Lake and are also part of cycle II. The Skead Group constitutes the upper most part of cycle I. The top of this group marks the southern boundary of the map area.

The fold axis of the Lebel Syncline passes through the northern half of the map area. This fold is isoclinal

and has no plunge. The fold axis and the stratigraphy are broadly conformable to the shape of the Lebel Stock. Tight folds with north-south trending axial surface traces and a drag fold occur on the south limb of the Lebel Syncline.

The Lebel Syncline and these second-order folds are believed to pre-date intrusion of the Lebel Stock. The stock may have modified the trend of the Lebel Syncline fold axis so that it and the strata parallel the stock's shape.

Five faults with unknown but apparently little displacement were recognized. Faulting is not prominent in the map area.

The northern half of the map area has been metamorphosed to the hornblende hornfels facies. This occurred during contact metamorphism following intrusion of the Lebel Stock. Greenschist facies mineralogy is present in the southern half of the map area and developed during an earlier regional metamorphic event.

There are eight volcanic sequences on the south limb of the Lebel Syncline. Seven of these are komatiitic. There are three komatiitic sequences on the north limb. Komatiitic sequences are characterized by volcanic flows which show decreases in MgO contents stratigraphically upwards. Komatiites occur at the base of each sequence and are overlain by one or more of high MgO komatiitic basalt, high MgO komatiitic andesite, low MgO komatiitic basalt,

low MgO komatiitic andesite, low Al_2O_3 komatiitic dacite, high Al_2O_3 komatiitic basalt, andesite and dacite and high Fe_2O_3, Al_2O_3 komatiitic basalt.

Most low MgO komatiitic basalts and andesites on the south limb of the Lebel Syncline have anomously high Cr (>1000 ppm) and Ni (>200 ppm) contents when compared to similar lithologies in other Archean terranes. The high Cr abundances are linked to high chromite contents.

Sequences with Cr and Ni-rich volcanics do not contain high Al_2O_3 komatiitic volcanics; the latter have low Cr (approximately 400 ppm) and Ni (approximately 80 ppm) contents. High Fe_2O_3, Al_2O_3 komatiitic basalt occurs in sequences with high Al_2O_3 komatiitic basalts. High Al_2O_3 and high Fe_2O_3, Al_2O_3 komatiitic basalts are not found in other Archean terranes. Cr and Ni-rich komatiitic volcanics are found in Destor Township in Quebec (within the Abitibi greenstone belt). They are not otherwise found.

Sequence 1 basalts are regarded as tholeiitic or calc-alkalic. There are no ultramafic or high MgO flows in this sequence and lithological variation with stratigraphic height is not observed.

The high Cr and Ni contents in the komatiitic basalts and andesites are explained by rapid cooling in a magma chamber. This process stops or reduces olivine and chromite crystallization in the magma as it reaches a MgO content of 12 % to 15 %. The residual magma is thus

enriched in Cr and Ni. The production of high Al_2O_3 komatiitic volcanics can also be explained by rapid cooling in a magma chamber. This process lowers the temperature of plagioclase crystallization resulting in Al_2O_3 enrichment in the magma.

Many of the sedimentary rocks in the map area are deposits from submarine debris flows and turbidity currents. The flow mechanism is not known for massive sandstones. The presence of conglomerates (debris flow deposits) suggests a proximal depositional environment, using a submarine fan model. The source area is comprised of sedimentary, volcanic and plutonic lithologies.

Peridotite sills are believed to syn-volcanic with komatiitic volcanism. Peridotite-gabbro and gabbro sills are likely syn-volcanic with tholeiitic volcanism now preserved in the Kinojevis Group north of Kirkland Lake. The discordant gabbro intrusions are believed to be syn-volcanic with calc-alkalic volcanism now preserved in the Blake River Group north of Kirkland Lake. Lateral equivalents to both groups may have once overlain the Larder Lake Group but have since been eroded. This is consistent with the fact that higher metamorphic grades prevail south of the Larder Lake Break.

The sills and discordant gabbros were emplaced prior to regional metamorphism. The Lebel Stock, syenite, biotite lamphrophyre, feldspar porphyry and diabase dykes

were emplaced following deformation and greenschist metamorphism. The alkali-rich intrusions are likely contemporaneous with Archean trachytic volcanism now preserved in the Timiskaming Group.

ACKNOWLEDGEMENTS

The writer wishes to thank Dr. James H. Crocket for suggesting the topic and for his supervision throughout the project. The writer also expresses gratitude to Mr. Andy Fyon, Dr. B. Burley, Dr. P.M. Clifford, Dr. R.H. McNutt and Mr. Keith Oliver for numerous valuable discussions and to Albert Chong, Mark Hughes and Brent McInnes for their invaluable field assistance.

Thanks is also extended to Mr. J. Whorwood who helped produce and prepare photographs, Mr. L. Zwicker who prepared thin sections for petrographic analyses, Mr. O Mudrock who gave instructions in pressed and powder pellet preparation and in the use of the x-ray fluorescence spectrometer and to Mrs. L. Fyon who typed the manuscript and who helped organize the tables.

Financial support was provided through a grant to Drs. J.H. Crocket, R.H. McNutt, H.P. Schwarcz and the late Dr. C.E. Rees from the Geoscience Research Grants Program.

Table of Contents

Table of Contents (continued)

List of Figures

List of Plates

List of Tables

List of Maps (in the back pocket)

Chapter 1

Introduction

1-1 Purpose and Scope of this Study

In Archean greenstone terranes, economic concentrations of gold occasionally occur in Algoma type banded iron formations (B.I.F.) a volumetrically minor lithology. Examples in Canadian greenstone belts are indicated in figure 1-1. There is some controversy as to the origin of this precious metal in relation to the genesis of B.I.F..

Two types of genetic relationships have been suggested. Fyon et al. (1983) suggest that the subeconomic gold-bearing Carshaw and Malga iron formations in northeastern Ontario (figure 1-1) were chemogenic sinks for gold when oxides were replaced by sulphides. On the other hand, Page (1983) suggests that sulphide facies B.I.F. at the Lupin Mine in the North West Territories concentrated gold during sedimentation. Exhalative volcanism was thought to enrich the depositional environment in metals.

Crocket (1981) proposed that geological, isotopic and geochemical study of B.I.F. and their enclosing strata, might determine whether precious and base metal enrichment in B.I.F. was syndepositional and whether this metal enrichment and the B.I.F. were genetically related to

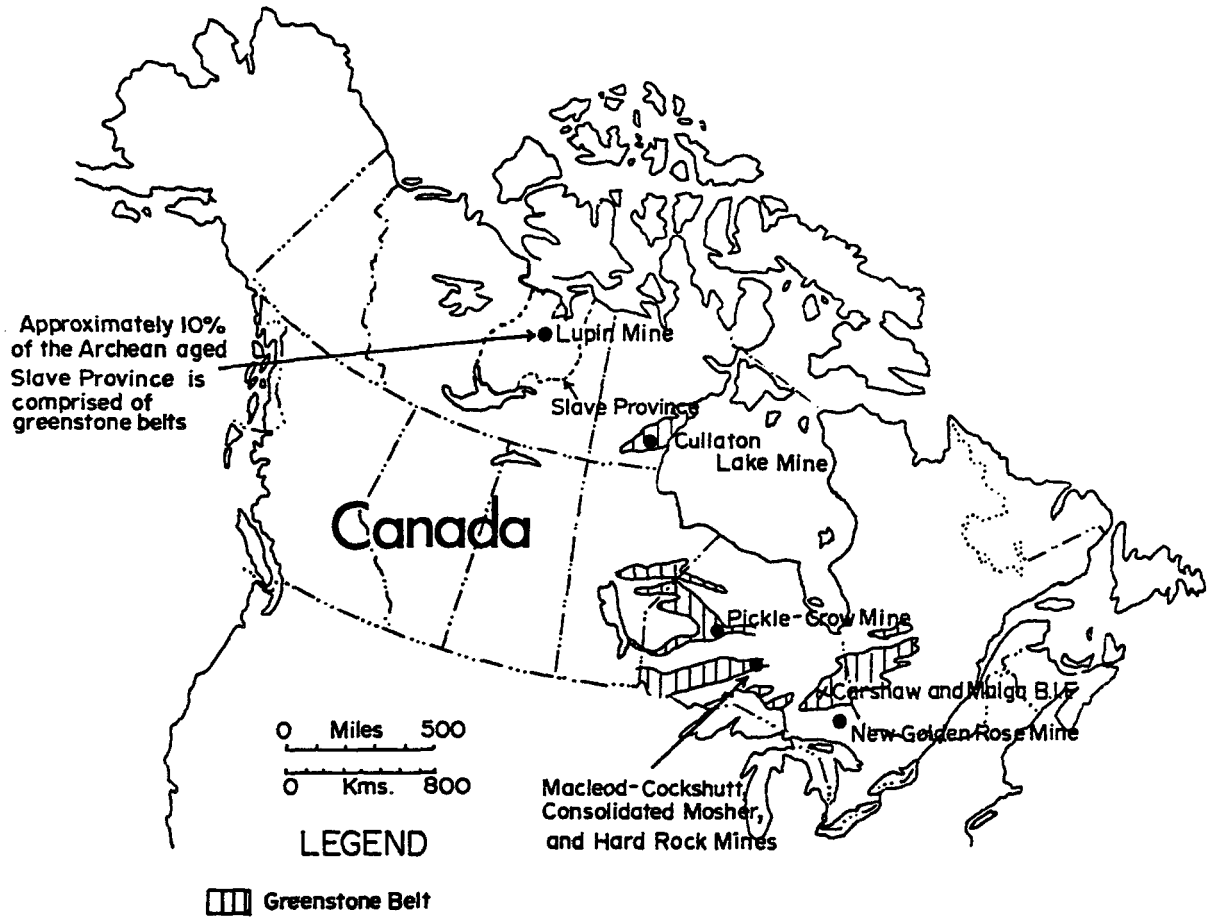

FIGURE 1-1 Location of Canadian gold producers that are hosted by B.I.F. (Also shown is the location of the Carshaw and Malga iron formations).

volcanism.

Two areas with B.I.F. were selected for study which provided good contrast in terms of host rock lithologies, metamorphic grade and proximity to a major mining camp. One is the Adams Mine area located 15 km south of the Kirkland Lake-Larder Lake gold camp, and the other is the Sherman Mine near Temagami (figure 1-2) where no major gold or base metal deposits are known.

Mapping of B.I.F. complimented by study of lithologies laterally equivalent to the B.I.F. units was initiated to establish the stratigraphic relationships of B.I.F. to sedimentary and volcanic rocks on a regional basis. At the Adams Mine site, the lithologies, stratigraphy and structure of the economic B.I.F. units and their lateral equivalents to the west were poorly defined. As such, correlations between the thick economic B.I.F. and their western lateral equivalents, also poorly defined, were uncertain. This thesis was initiated to produce a geological map which would establish these correlations and which could be combined with geological maps produced by contemporaneous field mapping east of the western end of the Adams Mine site in order to characterize the volcano-sedimentary setting associated with the iron formations. The map is accompanied by an integrated geological, geochemical, petrographic and petrogenetic study of the area mapped.

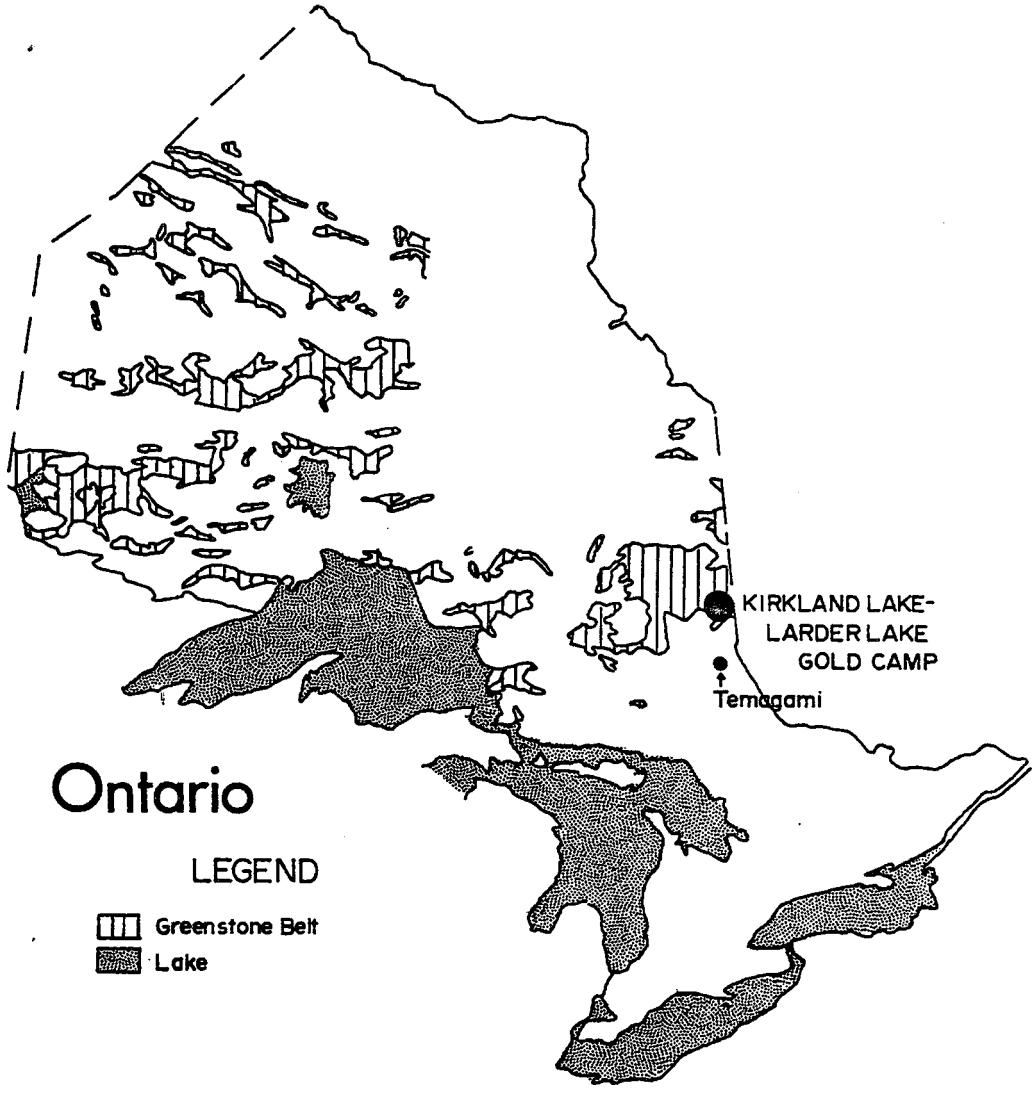

FIGURE 1-2 Location of the Kirkland Lake-Larder Lake gold camp and the town of Temagami.

1-2 Location and Characteristics of the Thesis Map Area

The Boston Iron Range trends in an east-west arc across the northern part of Boston Township (figure 1-3). The Adams Mine lies in the thicker part of the range in northeastern Boston Township, 12 km southeast of the town of Kirkland Lake and 15 km southwest of the town of Larder Lake. Kirkland Lake hosts two current gold producers, the Macassa and the Lake Shore Mines and six past gold producers. Fifteen past producing gold mines are located between Kirkland Lake and Larder Lake and immediately northeast of Larder Lake and southwest of Kirkland Lake (figure 1-3). The Kerr Addison Mine located east of Larder Lake is a current gold producer. The Adams Mine produces iron ore and is not a part of the Kirkland Lake-Larder Lake gold camp.

Figure 1-4 shows the boundaries of the thesis map area with respect to the iron range, the mine site, the mine's open pits and two areas mapped by Norbert Blum, (Ph.D. thesis, 1986) a member of the B.I.F. study group. The map area covers approximately 9 km^2 and is centered immediately west of the west end of the Adams Mine site. This coverage encompassed the stratigraphy which encloses the economic iron formations in the western part of the mine site and their westward extensions. The map area lies adjacent to NB-1 and NB-2 map areas shown in figure 1-4. NB-1 was mapped by Norbert Blum in October of 1982 prior to

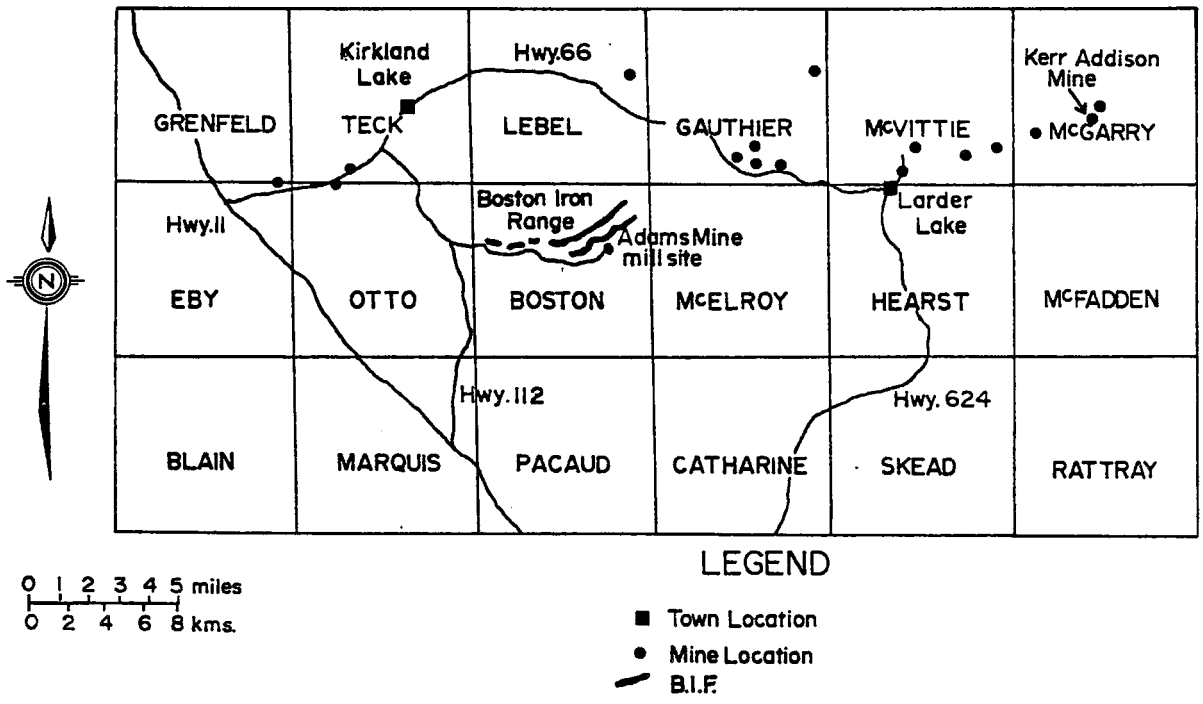

FIGURE 1-3 Location of Kirkland Lake and the past and present producing gold mines which make up the Kirkland Lake-Larder Lake gold camp. Also shown is the location of the Boston Iron Range and the Adams Mine mill site. The location of the gold mines is from Thompson (1948).

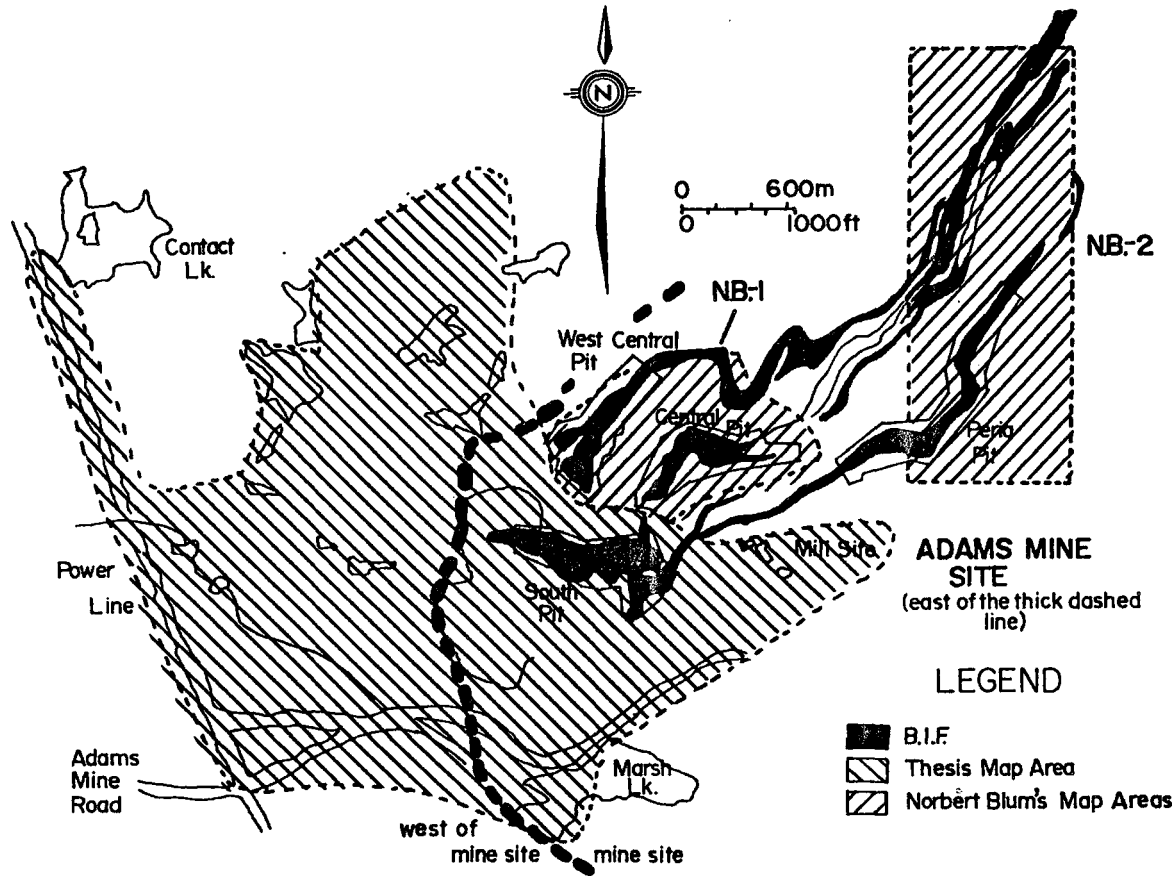

FIGURE 1-4: Location of the thesis map area and map areas NB-1 and NB-2. The terms NB-1 and NB-2 have been adopted by and for this study only.

the initiation of this thesis work. NB-2 was mapped by Norbert Blum in May and August of 1983. Together NB-1 , NB-2 and this thesis map area cover a strike length of approximately 6 km which represents a significant portion of the Boston Iron Range.

1-3 Field Methods

The thesis map area west of the mine site is largely bush-covered (plate 1-1). Here, outcrops were located on a grid of lines spaced roughly 75 to 100 meters apart and flagged at 25 meter intervals. The lines were tied into the Adams Mine road or the east-west trending power line in the south, both of which are shown in O.M.N.R. aerial photos 78-1-40-114, 115. Figure 1-5 is a photocopy of these aerial photos while figure 1-6 highlights the names of lakes and identifies such features as the Adams Mine road. In the northern and central parts of the thesis map area, lines were tied into several small lakes. The names of these lakes, Beaver, Dry, Spider, North, Finger and Fault are not recognized geographical names but have been created for the purposes of this thesis. The Dane-Larder road east of the northwest trending power line and north of the east-west trending power line is distinctly seen on the aerial photos but, unfortunately, has been partly flooded since the aerial photo was taken and as such was of limited use for aerial photo location of outcrops.

PLATE 1-1 View looking west over the thesis map area from the dump near the west end of the South Pit. The birch trees are 100 meters away.

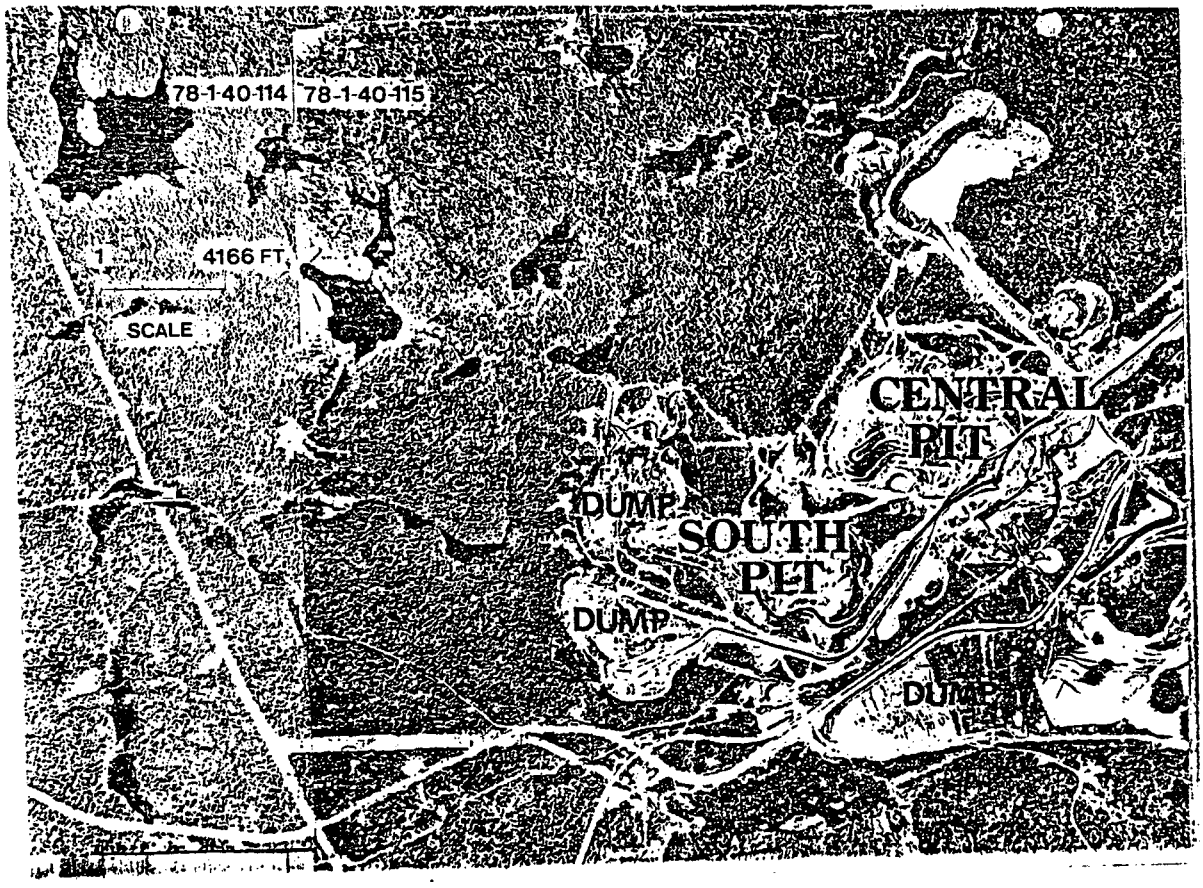

FIGURE 1-5: A photocopy of Ontario Ministry of Natural Resources aerial photos 78-1-40-114 and 78-1-40115. The former makes up the left 1/5 of the photocopy. The aerial photos are at a scale of 1 inch to 50,000 feet.

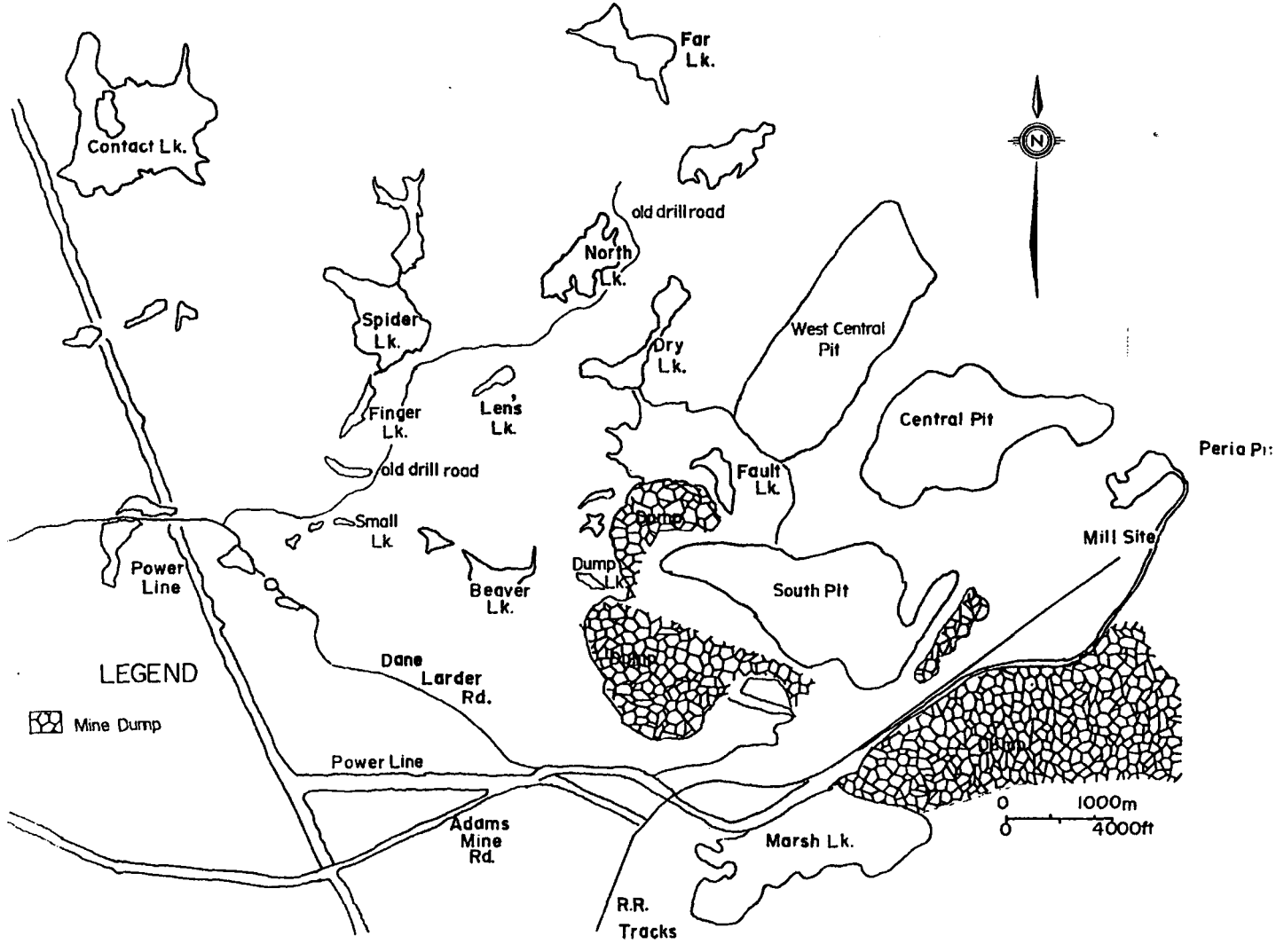

FIGURE 1-6: Outline of the lakes, roads, power lines, open pits and dump sites in the map area.

The lines used for mapping are shown in figure 1-7. Approximately one-third of these lines were reflagged from pre-existing lines. To install lines immediately west of the South Pit and south of Beaver Lake, the sundial was used to accommodate directional uncertainty caused by magnetic disturbances from B.I.F. lenses. A drill road shown in figure 1-6 provided good access to the north central part of the thesis map area from the intersection of the Dane-Larder road and the northwest trending power line.

The mine site was largely free of bush (plate 1-2) and outcrop locations could be plotted directly on the aerial photos. The mapping was carried out at a scale of 1" to 400' over a total period of nine weeks, divided into four periods, late May 1983, late August 1983, late May 1984 and late September 1984.

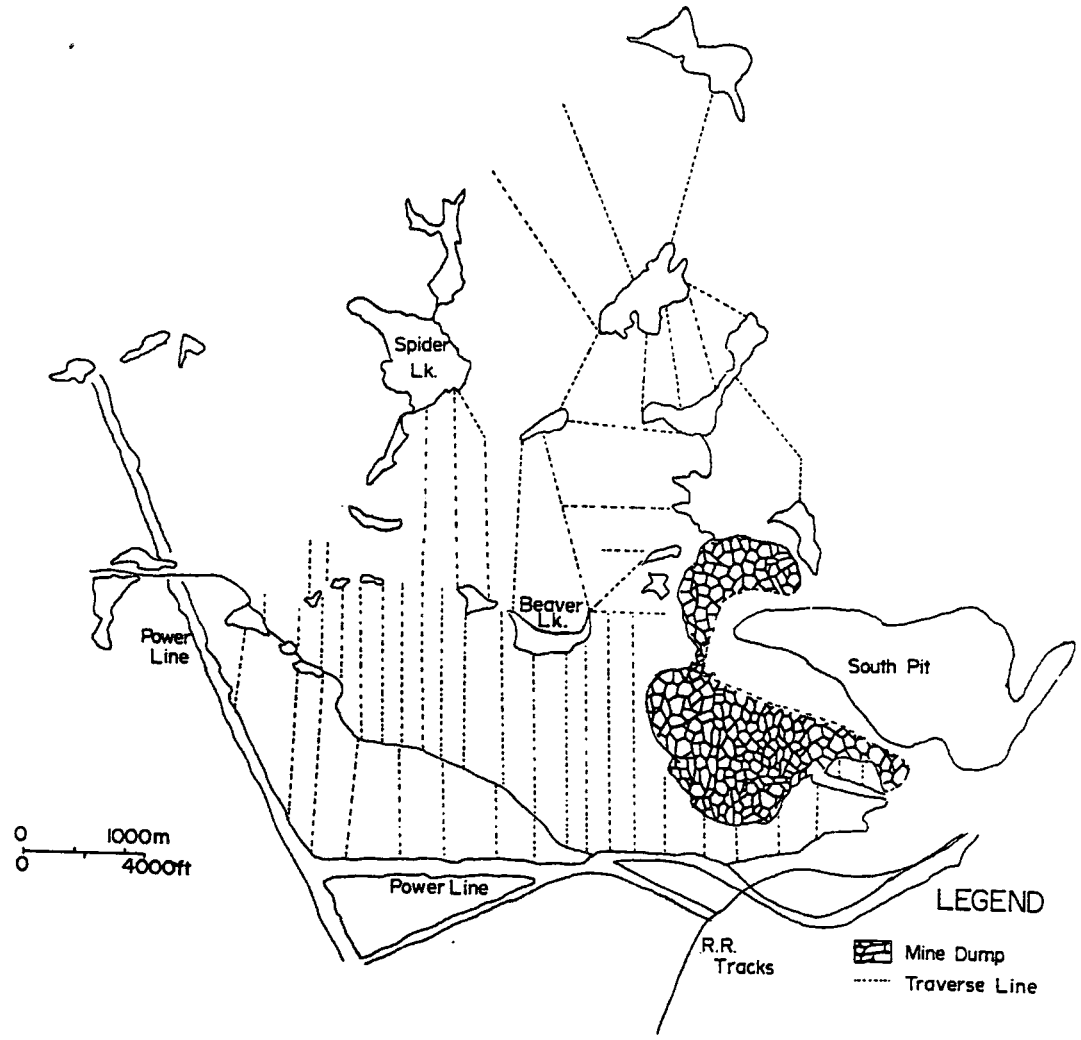

FIGURE 1-7 Outline of traverse lines used for mapping purposes.

PLATE 1-2 View looking east from the west end of the South Pit. The Adams Mine mill site is visible in the distance.

Chapter 2

General Geology of the Abitibi Greenstone Belt and of the Kirkland Lake Area and Previous Work in the Thesis Map Area

2-1 The Abitibi Greenstone Belt: General Geology

The Boston Iron Range and the enclosing lithologies are part of the Archean age Abitibi greenstone belt. Figure 2-1 shows a general outline of this belt which stretches across northeastern Ontario and into north central Quebec. The belt covers an area of approximately 650 km^2 and is bounded to the east and south by the Grenville Province and by Proterozoic cover, to the north by the Quetico Belt and to the west by the Kapuskasing gneiss belt.

The Abitibi Belt stratigraphic sequence consists of two volcanic cycles, each grading upwards from komatiitic and tholeiitic basalt sequences to a highly differentiated basalt to rhyolite sequence of tholeiitic to calc-alkalic character at the top (Dimroth, 1982). Figure 2-2 shows that rocks of cycle I are exposed only in the core of the Lake Abitibi Anticline and at the Round Lake Dome.

Large tonalite-trondjhemite and granodiorite plutons underlie more than 40% of the northern portion of the belt and less than 20% of the southern part (Dimroth, 1982). Submarine, largely turbiditic sediments are intercalated with volcanic rocks near the base of cycle II, south of the

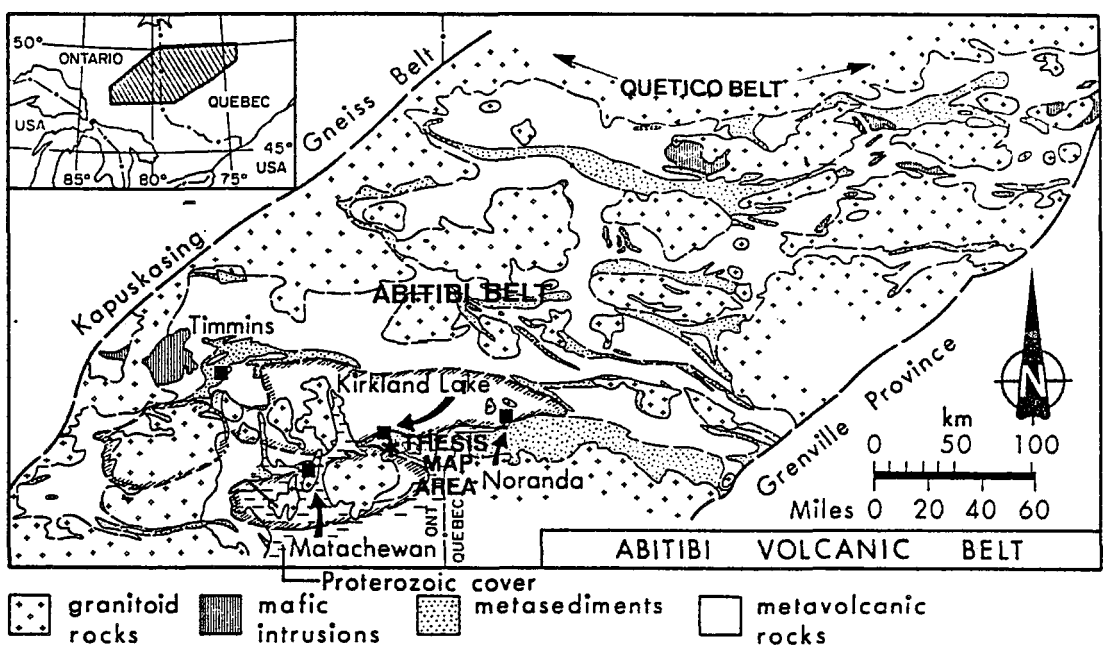

FIGURE 2-1 General outline of the Abitibi greenstone belt from Goodwin (1982).

Legend

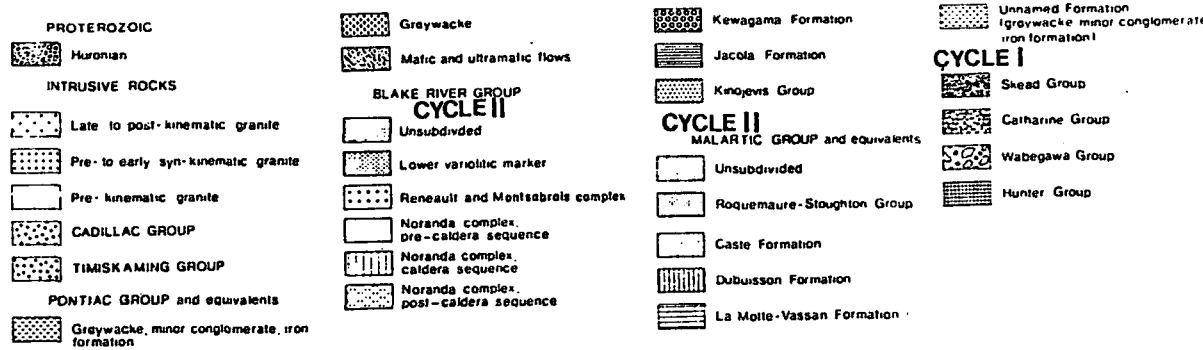

FIGURE 2-2: Stratigraphic and generalized structural map of the Abitibi Belt in the Kirkland Lake, Rouyn-Noranda areas from Dimroth (1983a). Major fold structures: LLA = Lake Abitibi Anticline; LMA = La Motte Anticline; RLD = Round Lake Dome; BRS = Blake River Synclinorium. The two major fault structures indicated are the Duparquet-Destor Break (D.D.B.) and the Cadillac Break (C.B.). The latter is referred to as the Larder Lake Break where it occurs in Ontario by Jensen (1983) and others. The name Larder Lake Break will be used in this study.

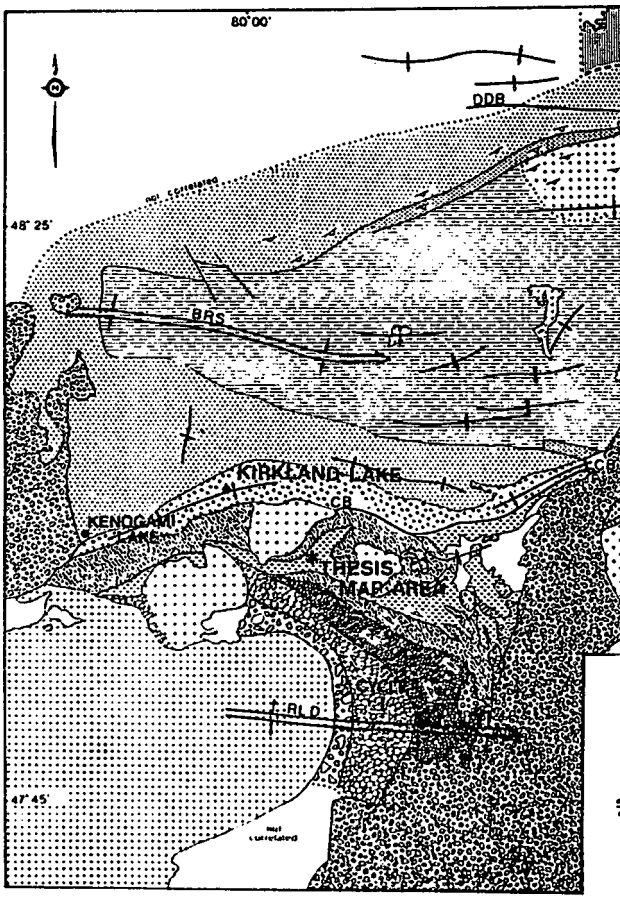
80°00'
DDB
48° 25'
BRS
KIRKLAND LAKE
CB
KENOGAMI LAKE
THESIS MAP AREA
CYCLE
RLD
47° 45'

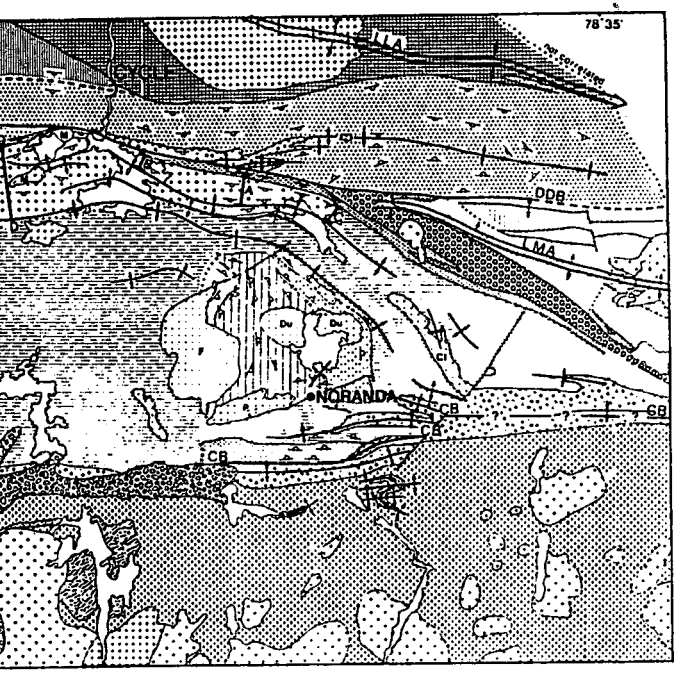

SYMBOLS

- Stratigraphic contact
- Stratigraphic top
- Unconformity
- Anticline
- Syncline
- break DDB Duparquet Destor
  CB Cadillac-Larder Lake
- Major fault
- Section line

- F Flavrian granite
- M Montsabrais granite
- Du Dufault granite
- Cl Clericy granite
- P Powell granite

0 5 15
kilometres

Larder Lake Break and north of the Duparquet-Destor Break near Timmins.

The Abitibi Belt is characterized by a pattern of generally east-trending isoclinal folds with subvertical axial planes (Dimroth, 1983a). Figure 2-2 outlines the major fold axes in the belt. First order folds (the Round Lake Dome, Lake Abitibi Anticline and Blake River Syncline) are defined as those with a half-wavelength of about 30 km while second order folds (not named in figure 2-2) have a half-wavelength of 1 to 10 km and are set on the limbs of the first order folds. The folds have steep plunges, exceeding 60 degrees, making folds laterally discontinuous (Dimroth, 1983a).

2-2 Kirkland Lake Area: General Geology

The thesis map area lies between the axes of the Blake River Synclinorium and the Round Lake Dome shown in figure 2-2 and south of the Larder Lake Break. The Break is an east-trending structural discontinuity (Watson and Kerrich, 1983) which extends from south of Kenogami Lake to east of Kirkland Lake and into the Noranda area in Quebec. Figure 2-3 shows the generalized stratigraphy between the two major axes in the Kirkland Lake area. Figure 2-4 outlines the groups listed and the major lithologies within each group. Jensen (1977, 1978a,b,c, 1979, 1980, 1983) has made use of the Jensen Cation Plot shown in figure 2-5 to

Figure 2-3

Geological map of the Kirkland Lake Area showing the distribution of volcanic groups.

LEGEND

Proterozoic	12	Cobalt Group
Archean	11	Granodiorite, monzonite, quartz -monzonite, syenite
	10	Massive to gneissic quartz diorite, tonalite trondhjemite.
Upper Supergroup (Cycle II)	9	9a Timiskaming Group
	8	8a,8b Blake River Group
	7	7a,7b Kinojevis Group
	6	6a Larder Lake Group
		6b Stoughton Roquemaure Group
		6c Lower Fm., Tisdale Group
	5	5c Porcupine Group
Lower Supergroup (Cycle I)	4	4a Skead Group
		4b Hunter Mine Group
	3	3a Catherine Group
	2	2a Wabewawa Group
	1	1a Pacaud Tuffs

The terms Upper Supergroup and Lower Supergroup are from Jensen (1980). The terms cycle I and cycle II are Dimroth's (1982). The legend and map are from Jensen (1980). In this study the terms cycle I and cycle II are used.

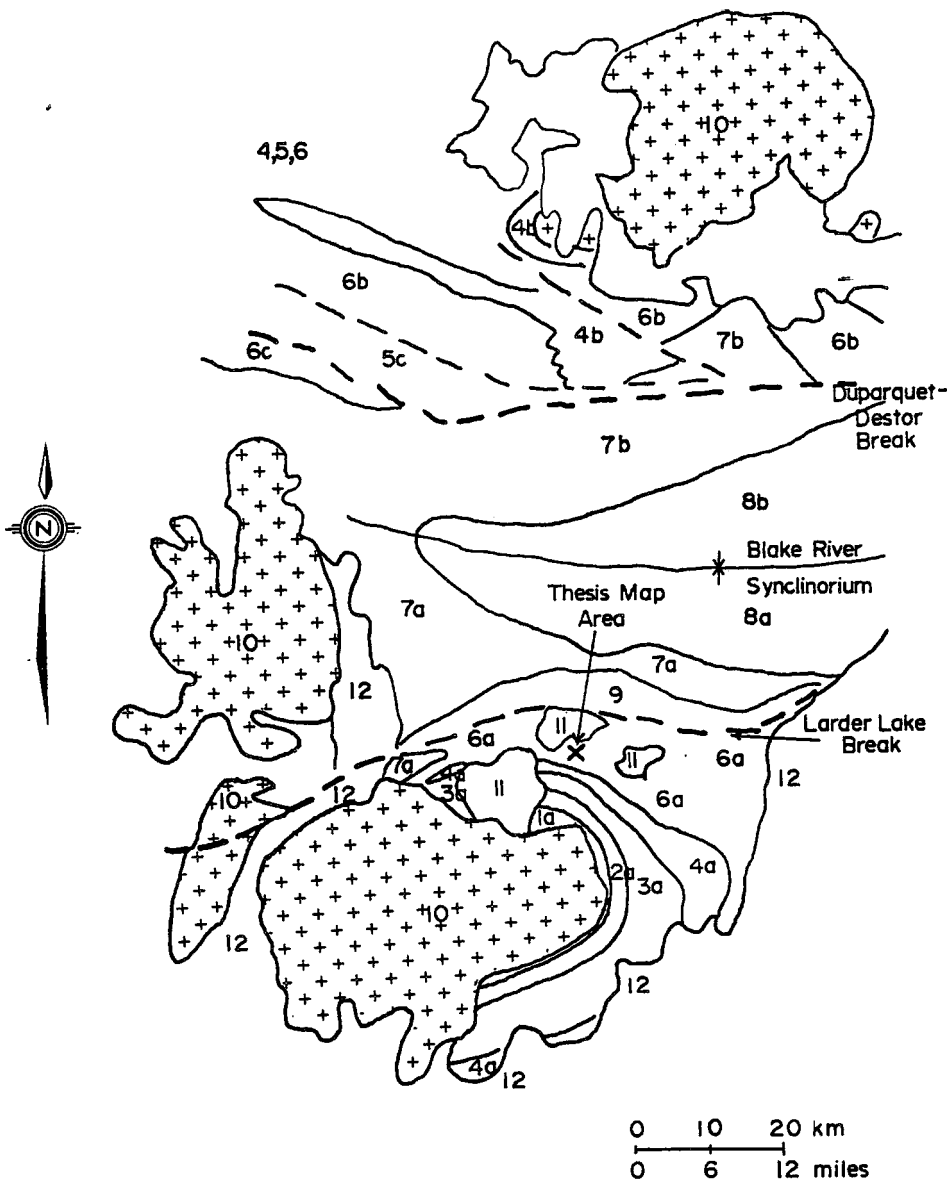
4,5,6
10
4b
6b
6b
4b
7b
6b
6c
5c
Duparquet-
Destor
Break
7b
8b
Blake River
Synclinorium
Thesis Map
Area
8a
7a
7a
9
12
11
6a
Larder Lake
Break
6a
12
7a
4a
3a
11
6a
10
12
1a
2a
3a
4a
10
12
12
4a
12
N
0 10 20 km
0 6 12 miles

STRATIGRAPHIC SUCCESSION OF THE KIRKLAND LAKE AREA.

SOUTH LIMB OF SYNCLINORIUM

Upper Supergroup

Timiskaming Group
- Volcanic rocks: Mafic, intermediate, felsic trachyte, and K-rich dacite and rhyolite flows and tuffs.
- Sedimentary rocks: Fluvial conglomerate, sandstone, and argillite.
- Intrusions: Stocks and dikes of syenodiorite, syenite, quartz monzonite, and lamprophyre.

Blake River Group
- Volcanic rocks: Calc-alkalic basalt, andesite dacite and rhyolite flows and tuffs.
- Sedimentary rocks: Volcaniclastic slump deposits.
- Intrusion: Stocks and dikes of gabbro, quartz gabbro, hornblende gabbro, diorite, quartz diorite, and subvolcanic rhyolite domes.

Kinojevis Group
- Volcanic rocks: Mg-rich and Fe-rich tholeiitic basalts, and tholeiitic andesite, dacite and rhyolite flows and tuffs.
- Sedimentary rocks: Thin interflow argillite and chert.
- Intrusions: Sills of Mg-rich and Fe-rich gabbro.

Larder Lake Group
- Volcanic rocks: Flows of peridotitic and basaltic komatiite, and Mg-rich tholeiitic basalt, and minor Fe-rich tholeiitic basalt, and minor Fe-rich tholeiitic basalts and interflow rhyolite tuff- breccias.
- Sedimentary rocks: Turbiditic conglomerate, greywacke and argillite, and iron formation chert, limestone, and dolostone.
- Intrusions: Sills and stocks of peridotite, pyroxenite, and gabbro.

Lower Supergroup

(Unnamed Unit)
- (Conglomerate with trachyte and syenodiorite pebbles).

Skead Group
- Volcanic rocks: Mainly calc-alkalic rhyolite tuff-breccia with some calc-alkalic basalt, andesite and dacite flows and tuff- breccias.
- Sedimentary rocks: Chert and cherty argillite.
- Intrusions: Stocks of feldspar porphyry and quartz diorite.

Catherine Group
- Volcanic rocks: Mg-rich and Fe-rich tholeiitic basalts.
- Sedimentary rocks: Interflow chert.
- Intrusions: (None mapped)

Wabewawa Group
- Volcanic rocks: Peridotitic and basaltic komatiite, Mg-rich tholeiite basalt and minor Fe-rich tholeiitic basalt, and a few interflow rhyolite tuffs.
- Sedimentary rocks: (None mapped)
- Intrusions: Layer sills (possibly flows) of dunite, pyroxenite, and gabbro.

Pacaud Tuffs (Ridler 1970)
- Volcanic rocks: Calc-alkalic andesite, dacite, and rhyolite tuffs.
- Sedimentary rocks: Chert, argillite, iron formation.
- Intrusions: Trondhjemite of Round Lake Batholith.

FIGURE 2-4 Generalized stratigraphy of the Abitibi Belt in northeastern Ontario from Jensen (1980).

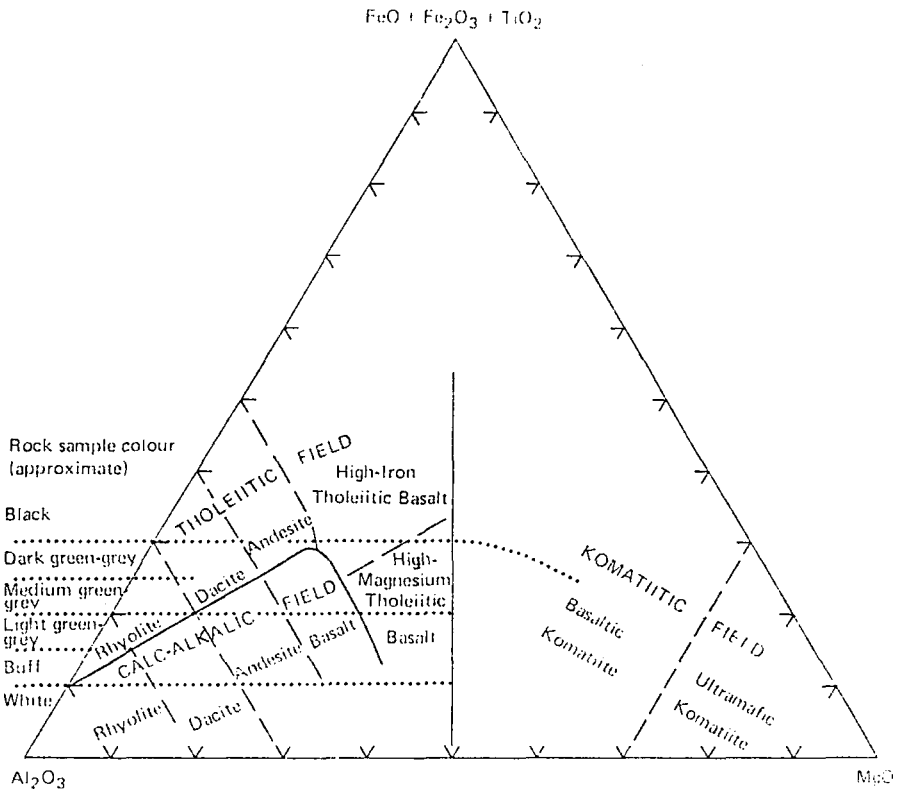

FIGURE 2-5: Jensen Cation Plot involving the cation percentages of Al_2O_3, FeO + Fe_2O_3 + TiO_2 and MgO from Jensen (1976a). Cation percentages refer to mole percent oxide where the oxide formula is based on units containing one cation (ie. the actual molecular formula used for alumina is $AlO_{1.5}$).

classify the volcanic rocks in the Kirkland Lake area.

The Wabewawa, Catherine and Skead Groups constitute a part of Dimroth's (1982) cycle I volcanics while the Larder Lake, Kinojevis and Blake River Groups constitute cycle II volcanics. The thesis area lies within the Larder Lake Group. Jensen (1979) indicates that the Pacaud Tuffs, which underlie the Wabewawa Group and border the Round Lake Batholith, may be the top of a volcanic cycle older than that of which the Wabewawa Group is a part.

The strike of cycle I volcanics and the disconformable contact (Jensen, 1979) between the Skead and Larder Lake Groups generally follows the outline of the Round Lake Batholith (figure 2-3) and dips at subvertical angles. Tops face away from the batholith, which is of quartz diorite to granodiorite composition and is massive in texture, except for a strongly sheared margin.

The Larder Lake Group which was more complexly folded than the cycle I volcanics to the south, extends from Larder Lake near the Quebec border westward for 30 km, to Eby Township (figure 2-6). South and southeast of Larder Lake, this group occupies 5 km of section. In this interval, Thompson (1941, 1947) and Abraham (1950) mapped numerous anticlinal and synclinal folds having variable trends and with limited apparent lateral extent. The distribution of volcanic rock types here is largely unknown, therefore the stratigraphy and structure is still poorly defined. The

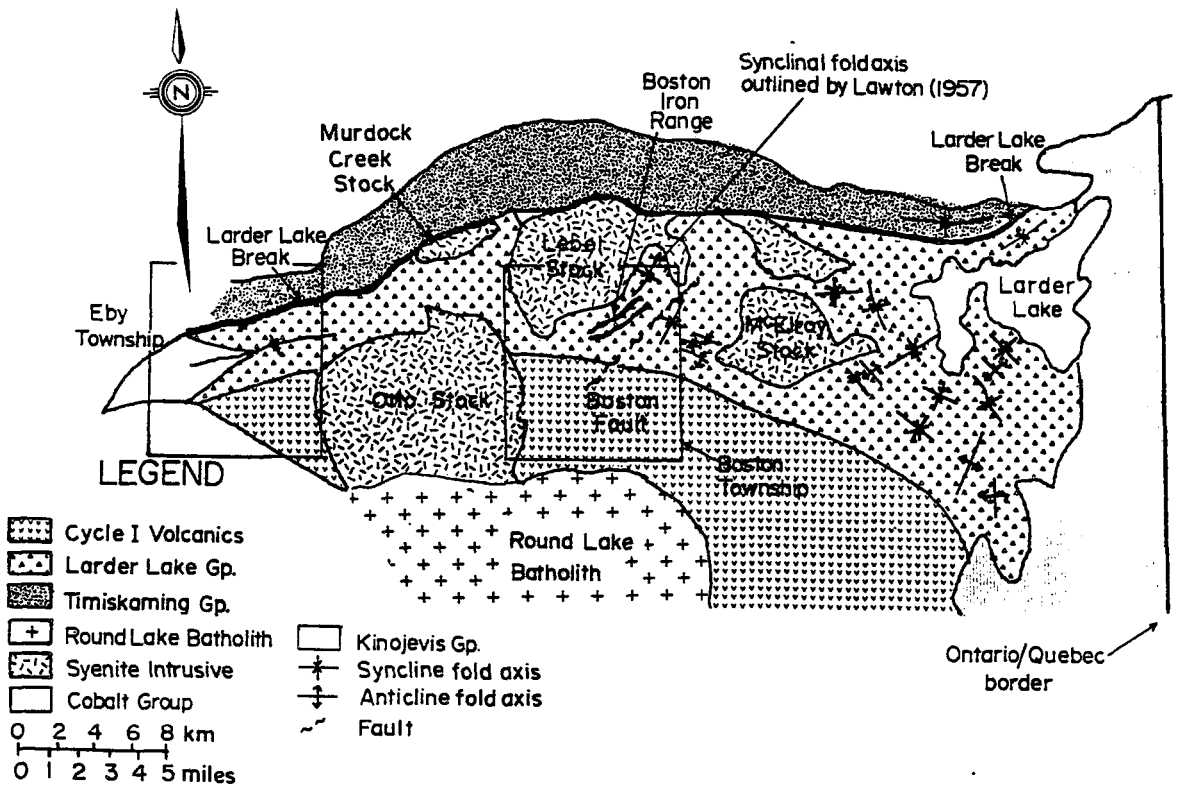

FIGURE 2-6: Geological map of the Kirkland Lake-Larder Lake area after Jensen (1979). Folds in the Larder Lake Group are from Thompson (1941, 1947), Abraham (1950) and Lawton (1957).

Larder Lake Group thins westward. In Eby Township, 2 km of the Larder Lake Group is exposed in an east-west trending syncline and is conformably overlain by the Kinojevis Group (Jensen, 1983).

The thesis area lies within the Larder Lake Group and is bounded to the south by the Skead Group of cycle I and the north by the Lebel Stock. This stock is one of five large, syenitic bodies which are intrusive into the Larder Lake Group. The others, as seen in figure 2-6 are the Otto, Murdock Creek and McElroy Stocks and an unnamed stock 5 km east of the Lebel Stock.

The Boston Iron Range forms an arc which generally conforms to the southeastern and southern boundary of the Lebel Stock. In northeast Boston Township, Lawton (1957) determined that one of the B.I.F. units was caught in a synclinal fold with a northeast-trending fold axis and a steep southwest plunge. This fold, outlined in figure 2-6, had not been traced to the southwest and west prior to initiation of this thesis.

The northeast striking Boston Fault as delineated by Lawton (1957) is situated between the Lebel and McElroy Stocks in figure 2-6 and along the southeastern edge of the thesis map area. East of this fault, a band of clastic sediments with a thickness of 2 km has a northwest strike. West of the fault, B.I.F. at the Peria Pit and volcanics above and below the B.I.F. strike southwest. The existence

of the Boston Fault is refuted in section 3-9.

The clastic sediments east of the Boston Fault as shown in figure 2-7 comprise 40% of the Larder Lake Group and are referred to as the McElroy Formation by Hyde (1978). Hyde determined that this formation consists of three end members:

(1) graded, thin to very thick bedded, fine to coarse grained sandstones interbedded with argillite; the sandstones are interpreted as turbidites.

(2) granule-pebble conglomerate with graded bedding deposited from gravel laden turbidity currents.

(3) ungraded, pebble-cobble conglomerates which are interpreted as debris flows. Clasts consist of quartz, feldspar, mafic and felsic volcanic fragments and chert fragments.

The Proterozoic Cobalt Group forms a 12 km wide cover along the Ontario-Quebec border separating the Larder Lake Group from the Bellecombe gneiss belt (figure 2-7). The Cobalt Group unconformably overlies both the Larder Lake Group and the Bellecombe gneiss belt. The Bellecombe gneiss belt is comprised of greater than 99% quartzites and argillites. Pebble conglomerate and iron formation are local intercalations. The quartzites are regarded as turbidites and consist of greater than 90% quartz with minor amounts of albite, biotite and rare zircon and chromite (Lajoie and Ludden, 1984). Rock fragments of chert and

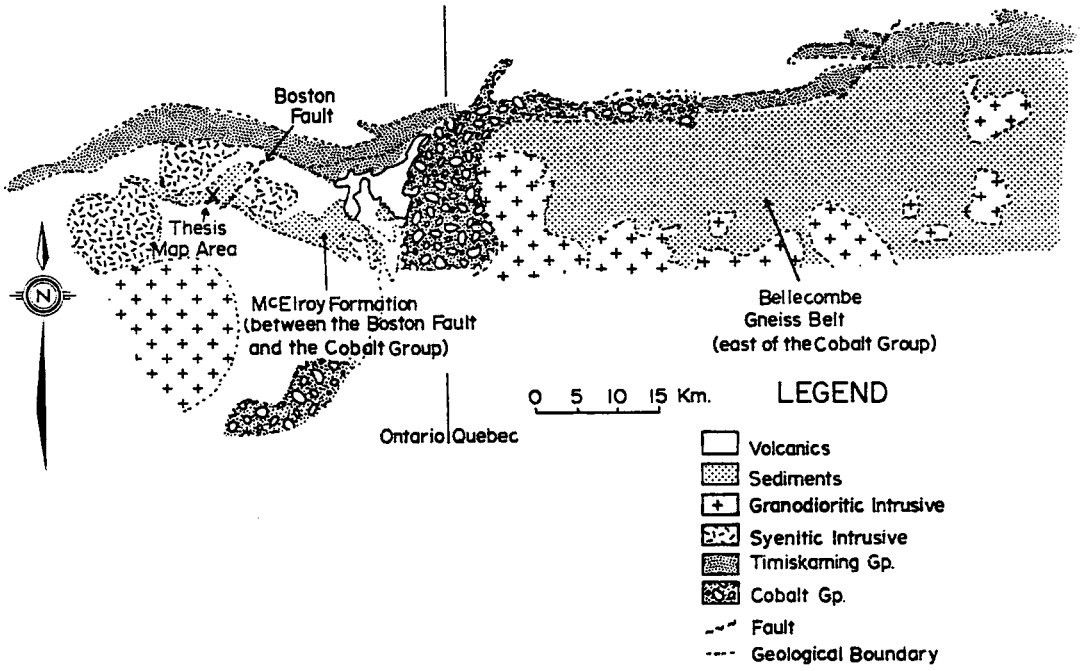

FIGURE 2-7: Geological map emphasizing the location of the McElroy Formation and the Bellecombe gneiss belt.

quartzite are rare. Komatiitic and basaltic volcanics underlie the sediments.

The Bellecombe gneiss belt and Larder Lake Group are regarded here as lateral equivalents and join beneath the Proterozoic sediments at the Quebec-Ontario border. There is no evidence of a major north-south fault north of the Larder Lake Break where the Cobalt Group cover is absent. Dimroth's (1982) contention that the komatiites in the Bellecombe gneiss belt are correlatable in Ontario to those of the Larder Lake Group is consistent with the above interpretation.

The Timiskaming Group which forms an east trending belt 0.5 to 5 km in width north of the thesis map area (figure 2-6) is comprised of fluvial sediments and alkalic volcanics. The Timiskaming unconformably overlies the Kinojevis Group to the north and is in fault contact with the Larder Lake Group to the south (Jensen, 1979). The Timiskaming has vertical dips and southern facings and is part of the north limb of a syncline (Hewitt, 1963). Both limbs of this syncline are exposed north of Larder Lake (figure 2-6). The Larder Lake Break is at or close to the south edge of the Timiskaming Group (figure 2-6).

Nunes and Jensen (1980) have dated the Hunter Mine Group near the top of cycle I at 2,710±2 Ma and the Blake River Group near the top of cycle II at 2,703±2 Ma by the U-Pb method on zircons. The Timiskaming Group, which

truncates folded strata of the second cycle, is clearly the youngest group. There are no precise age determinations on zircons from igneous rocks of this group. However, Matachewan diabase dyke swarms cut all Archean igneous rocks in the Kirkland Lake area (Jensen, 1983) and have Rb-Sr whole-rock isochron ages of 2,690±9.3 Ma (Gates and Hurley, 1973) which places a lower limit on the age of the Timiskaming Group.

2-3 Thesis Map Area: Previous Work

In 1951, Dominion Gulf Company optioned a number of claims which covered much of the Boston Iron Range in Boston Township. The company subsequently carried out a detailed geological mapping programme over the claims at a scale of 1"-200'.

H.D. McLeod of Dominion Gulf produced a map which covers the central and eastern portions of the thesis map area. Figure 2-8 shows his work. It is seen that McLeod (1952) outlined the general configuration of the iron formations and quartzites and noted the presence of drag folding and large peridotite-gabbro intrusives. McLeod (1952) classified the volcanics as either 1) massive andesite, 2) mafic agglomerate/fragmental or 3) tuffs and attempted to trace out individual volcanic lithologies. Parks (1952) produced a map of the west-central part of the thesis map area which is also shown in figure 2-8. However,

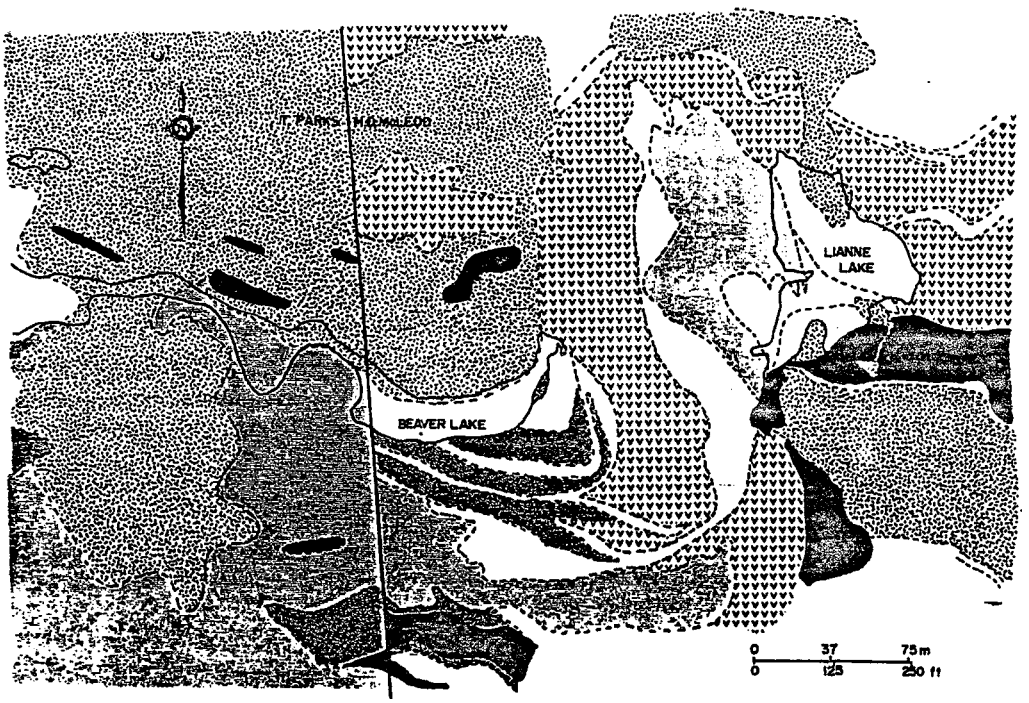

FIGURE 2-8: A compilation of McLeod's (1952) and Park's (1952) work. A line marks the boundary between Park's geology in the west and McLeod's in the east. Lianne Lake is now covered by the dump at the western end of the South Pit. Beaver Lake is observable in the central portion of this figure. The geological patterns were added by the author of this thesis.

LEGEND

- Peridotite
- Gabbro
- B.I.F.
- Quartzite
- Andesite
- Agglomerate
- Tuff
- ---- Geological Boundary (approx.)

his map is more generalized than that of McLeod's and the stratigraphy and structure are largely undefined.

Boston Township was mapped at a scale of 1" to 1000' by Lawton (1957). Shown in figure 2-9 is that part of Lawton's map which covers the thesis map area. Basic to intermediate volcanics are subdivided on the basis of grain size and/or distinctive field structures. There is no stratigraphic distribution to the various subdivisions. Felsic tuffaceous rocks are widespread and are commonly associated with sediments. Geochemical analyses were not used by Lawton (1957), McLeod (1952) or Parks (1952) to aid in rock classification.

Lateral correlation between small iron formation lenses and chert west of the mine site to the thicker iron formation horizons on the mine site is limited. This is best seen in a larger scale map of the area taken from Dubuc (1966a) and based on Lawton (1957)(figure 2-10).

Jensen (1978a) mapped a small area of the Larder Lake Group stratigraphy immediately north and south of the Peria Pit at the Adams Mine site in map area NB-2. Jensen determined that the Peria Pit was underlain by massive and pillowed magnesium-rich tholeiitic basalt and pyritic tuff and overlain by cherty quartzite andy ultramafic komatiite. Jensen (1978a) used the Jensen Cation Plot to classify the volcanic rocks.

LEGEND

CENOZOIC

RECENT AND PLEISTOCENE*

Clay, sand, gravel, and boulders.

GREAT UNCONFORMITY

PRECAMBRIAN

KEWEENAWAN OR MATACHEWAN

12 — *Diabase (12).*

INTRUSIVE CONTACT

ALGOMAN

9 — *Basic syenite (9); syenite and porphyritic syenite (9a); syenite porphyry (9b); quartz porphyry (9c); granite (dikes and small stocks) (9d); lamprophyre (9f); diorite and metadiorite (9g); quartz-feldspar porphyry (9p); felsite (9r).*

Batholithic granite (Round Lake batholith) (9s).

HAILEYBURIAN (?)

7 — *Diorite (7a); gabbro (7b); hornblendite (7c); serpentinite (7d); diorite porphyry (7e).*

INTRUSIVE CONTACT

TIMISKAMING

6 — *Fine-grained sedimentary rocks: greywacke (6a); arkose (6b); quartzite (6c); slate (6d).*

5 — *Conglomerate (5a); conglomerate with some interbedded arkose, slate, and greywacke (5b).*

GREAT UNCONFORMITY

POST-KEEWATIN (?)

4 — *Diorite and metadiorite (4a).*

INTRUSIVE CONTACT

KEEWATIN**

3 — *Basic and intermediate volcanics: greenstone (3); brecciated and carbonate-veined greenstone (3a); andesite, basalt, and pillow lava (3b); dioritic, diabasic, and gabbroic lava (3c)***; amphibolite (3d); sheared basic lava (3l); fragmental lava (3q); basic lava containing horizons of tuff (3h); injection gneisses, and metamorphosed basic lavas and tuff adjacent to the Lebel and Otto syenite stocks (3k); variolitic lava (3v).*

2 — *Intermediate and acid volcanics: fragmental volcanics, generally porphyritic (2); porphyritic andesite, dacite, and rhyolite, containing horizons of acid and cherty tuff (2a); dacite (2b); andesite, occasionally fragmental (2c).*

1f — *Iron formation (1f).*

1 — *Acid volcanics, tuff, quartzite, etc.: rhyolite (1a); acid tuff and cherty tuff (1b); agglomerate, conglomerate (1c); tuffs and sediments interbedded with volcanic rocks (1d); tuff and iron formation (1e); tuff, tuffaceous sediments, and their altered equivalents (1g); cherty quartzite (1k).*

FIGURE 2-9: Geology of north central Boston Township as mapped by Lawton (1957). On this page is the legend, on the opposite page is the map. Lawton (1957) mapped at a scale of 1 inch to 1000 feet. The names of lakes etc. in bold letters have been added by this writer. The scale is shown in the upper left corner.

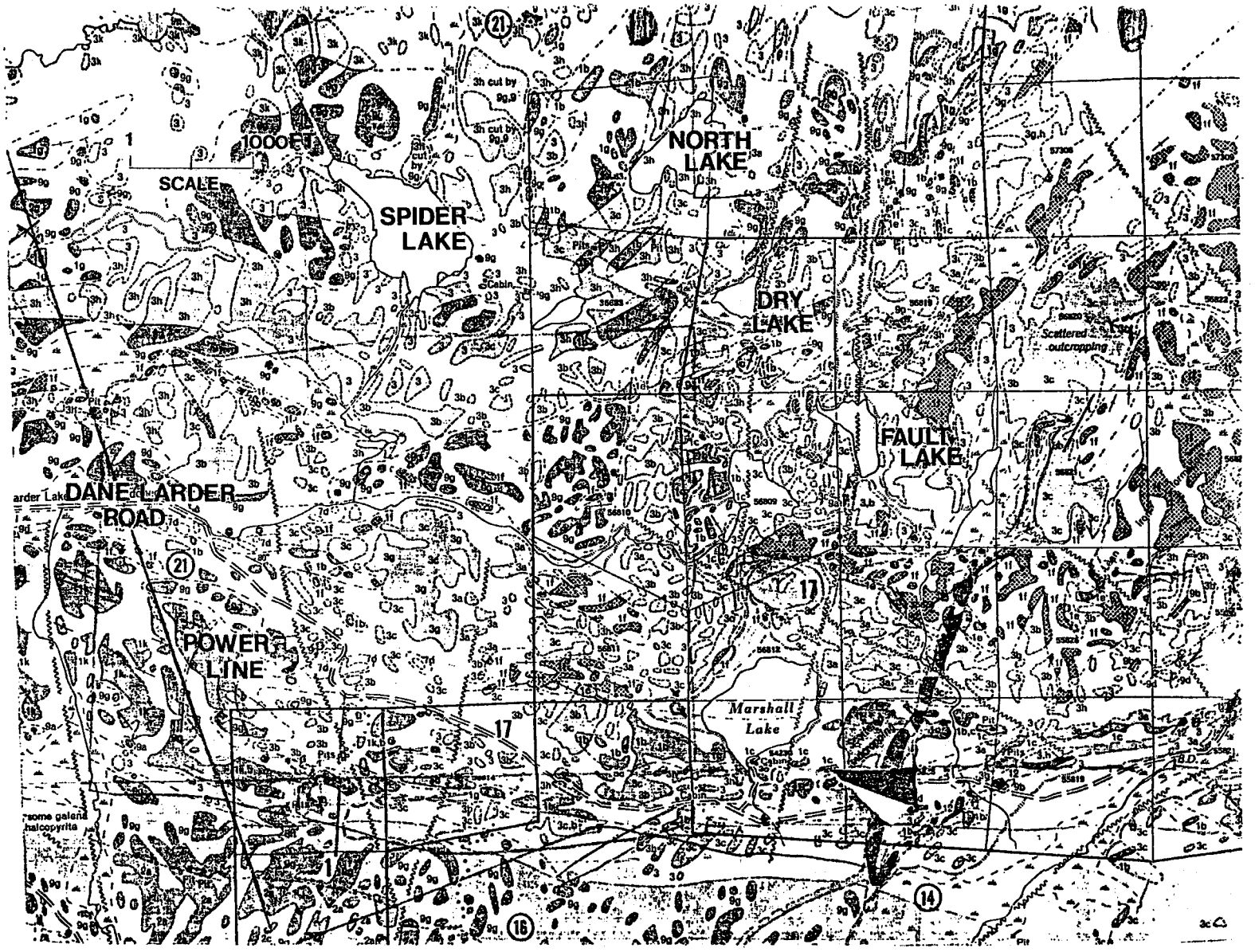
1000FT
SCALE
SPIDER LAKE
NORTH LAKE
DRY LAKE
Scattered outcropping
FAULT LAKE
DANE-ARDER ROAD
POWER LINE
Marshall Lake
some galena chalcopyrite

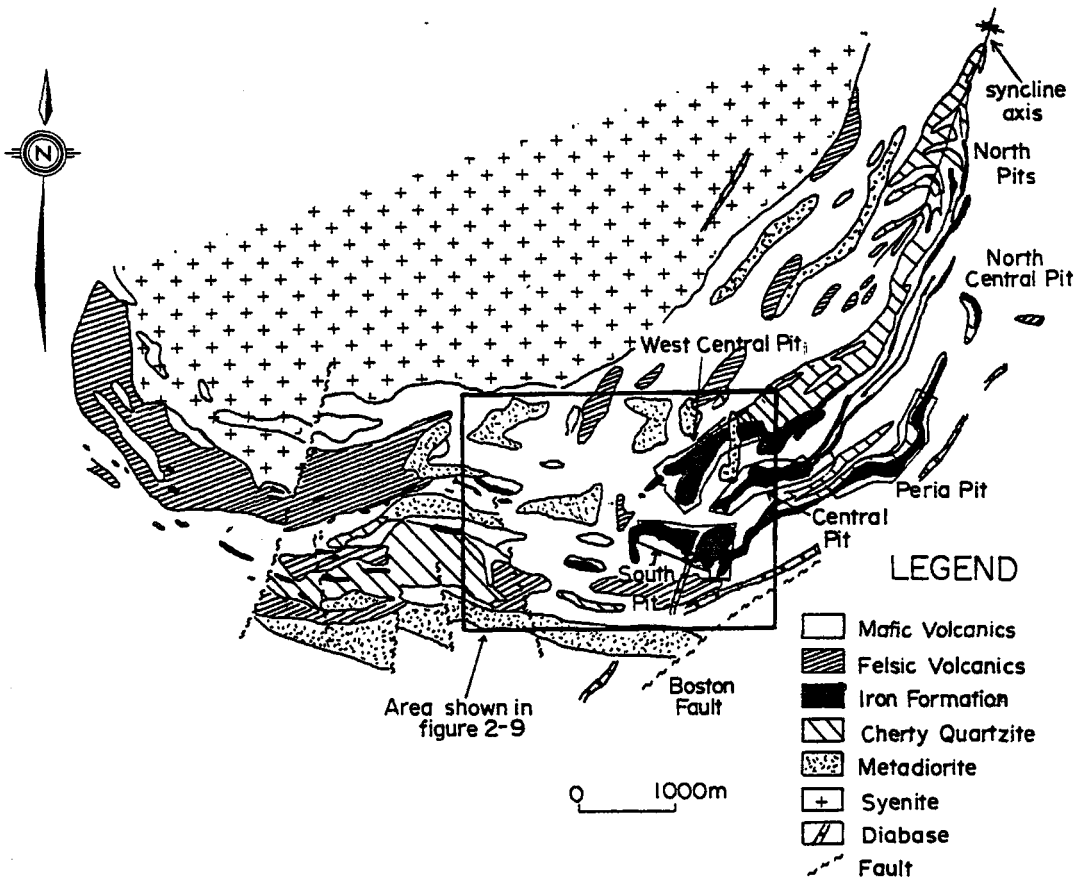

Figure 2-10: Geology of the Adams Mine area from Dubuc (1966). Dubuc was a mine geologist at the time of publication of this map and to the author's knowledge, his mapping was confined to the ore bodies. His simplified version of the northern Boston Township geology is derived from Lawton (1957). The solid outline is the area covered in figure 2-9.

Chapter 3

Geology of the Thesis Map Area

3-1 General Geology: Thesis Map Area

The volcanics are mainly komatiitic. Together with intercalated clastic, chemical and pelitic sediments, they have been intruded by several peridotitic, layered peridotite-gabbro and gabbroic sills, discordant gabbroic plugs, mafic dykes and alkali-rich dykes (maps 2,3,4,5,6). This package has been preserved on both limbs of a syncline, here named the Lebel Syncline. The fold axis of this syncline passes through the northern part of the thesis map area and is the same synclinal structure noted to the northeast by Lawton (1957). The syncline is isoclinal, in that all bedding on both limbs is of vertical or near vertical dip. The fold axis is refolded into an S-shaped drag fold at the western end of the mine site. There is no recognizable plunge to the fold axis of the Lebel Syncline in the map area. The southern part of the area has been metamorphosed to the greenschist facies. Hornblende hornfels facies mineralogy is present in the northern part.

As noted previously, but emphasized here again, the southern boundary of the thesis map area is marked by the Skead Group of cycle I. The northern boundary is the Lebel Stock. Before giving a more detailed description of the map

area, it is necessary to discuss the rock classification scheme used herein which is different from that used for much of the Kirkland Lake area by Jensen (1977, 1978a,b,c, 1979, 1980, 1983).

3-2 Volcanic Rock Classification: Komatiites and Komatiitic

As most of the volcanic rocks in the map area are considered to be komatiitic, it is important to define the term komatiite and what constitutes komatiitic. Arndt and Nisbet (1982) define a komatiite as an ultramafic volcanic rock with greater than 18 % MgO. It is characterized by textures and structures indicative of an extrusive origin and mineralogical and chemical features pointing to an ultramafic composition. The diagnostic textural, compositional and mineralogical features of a komatiite are summarized in table 3-1 which is taken from Arndt and Nisbet (1982). Nisbet et al. (1982) point out that komatiites satisfy criteria such as high MgO and low incompatible element contents, which indicate high percentage melting of mantle material.

Arndt and Nisbet (1982) refer to mafic volcanic rocks which are part of a komatiitic series as komatiitic basalts. The characteristic features of these basalts as outlined by Arndt and Nisbet (1982) are shown in table 3-2. Arndt and Nisbet (1982) regard highly magnesian pigeonite and unusually sodic plagioclase as possibly diagnostic.

Table 3-1

Diagnostic features of a komatiite from Arndt and Nisbet (1982)

Features indicating volcanic origin	Chilled flow tops, polyhedral jointing, well-developed spinifex texture, pillows, fragmental structures (tuffs and breccias). Rapid-cooling textures, abundant glass.
Features indicating ultramafic composition	A predominance of olivine and pyroxene in a once-glassy groundmass, MgO>18% (anhydrous basis). This value corresponds roughly to 20-35% modal olivine, 15-30% normative olivine, and 65-70% normative mafic minerals.

Table 3-2: Characteristic features of komatiitic basalts as indicated by Arndt and Nisbet (1982).

Geological	Spatial associations with komatiite; ideally within volcanic sequences within which the lava compositions change progressively from ultramafic to mafic.
Petrographic	Most characteristic are spinifex textures: the olivine type in lavas with MgO between 18 and 9%. Olivine porphyritic textures do occur, but in certain cases a linkage between lavas with this texture and komatiite is difficult to verify. Basalts with MgO<10% have few diagnostic features.
	Highly magnesian pigeonite (Arndt & Fleet 1979) and unusually sodic plagioclase (Binns et al., 1982) are possibly diagnostic.
Chemical	High Mg, Ni, Cr; low alkalies, TiO_2, Fe:Mg; high SiO_2 at given MgO; $CaO:Al_2O_3$>0.8-1.0. All of these features are characteristic but not necessarily diagnostic.

Arndt and Nisbet (1982) note that in the ideal geological setting, komatiitic basalts occur in volcanic sequences within which the flow composition changes progressively from ultramafic to mafic. In this study, komatiitic basalts are those which overlie komatiites in a group of flows (a volcanic sequence) which shows a progressive decrease in MgO stratigraphically upwards.

Spinifex texture and polygonal jointing, characteristic of a komatiite are found in the map area basalts which are classified as komatiitic by the above criteria. Moreover, these basalts have major and trace element compositions consistent with derivation from a parent ultramafic liquid. However, spinifex texture alone is not diagnostic of komatiitic affinity. Rapidly grown crystals with acicular habit are known from non-komatiitic rocks.

The high grade of metamorphism in the map area has destroyed primary pyroxenes and plagioclase. Thus it is not possible to determine whether highly magnesian pigeonite or unusually sodic plagioclase previously existed in any rocks.

The rock classification scheme to be used in this thesis is shown in table 3-3. The division between komatiite and komatiitic basalt is consistent with Arndt and Nisbet (1982).

Komatiitic basalts are further subdivided into high MgO and low MgO komatiitic basalts at MgO = 12 %. The range

Table 3-3 Volcanic rock classification scheme

Komatiite	MgO > 18%
High MgO Komatiitic Basalt	MgO > 12% MgO ≤ 18%
Low MgO Komatiitic Basalt	MgO 4-12% SiO_2 < 54% Al_2O_3 < 16%
High MgO Komatiitic Andesite	MgO > 12% SiO_2 54-62% Al_2O_3 < 16%
Low MgO Komatiitic Andesite	MgO 4-12% SiO_2 54-62% Al_2O_3 < 16%
Low Al_2O_3 Komatiitic Dacite	MgO 4-12 % SiO_2 62-67% Al_2O_3 < 16%
High Al_2O_3 Komatiitic Basalt	MgO 1-12% SiO_2 < 54% Al_2O_3 ≥ 16%
High Al_2O_3 Komatiitic Andesite	MgO 1-12% SiO_2 54-62% Al_2O_3 ≥ 16%
High Al_2O_3 Komatiitic Dacite	SiO_2 62-67% Al_2O_3 ≥ 16%
High Fe_2O_3, Al_2O_3 Komatiitic Basalt	Fe_2O_3 18-20% Al_2O_3 ≥ 16%

N.B. 1) Major element abundances are from data which has been normalized to 100% on a volatile-free basis. 2) Rocks classified as low MgO komatiitic basalt, for example, must satisfy the chemical requirements outlined above, and also must occur within a sequence which grades from komatiite stratigraphically upwards into less MgO-rich compositions. Tholeiitic basalts have chemical compositions similar to low MgO komatiitic basalts but are not linked to komatiites by field associations as komatiitic basalts are.

in MgO for these komatiitic basalts in the map area is 6.5 % to 17.24 % and 12 % falls roughly in the middle. However, this is coincidental. This division is made to be compatible with the field observation that komatiitic basalts with greater than 12 % MgO generally show more easily recognizable polygonal jointing than do those below 12 %. Moreover, the two can generally be distinguished in hand specimen. As such, high and low MgO komatiitic basalts could easily be mapped separately in the field.

Volcanics with $SiO_2 \geq 54$ %, and which are associated with the komatiites in sequences which change stratigraphically upward from ultramafic to mafic: intermediate, are referred to as low or high MgO komatiitic andesites (table 3-3). The andesite/basalt division is taken at 54 % SiO_2 following the terminology used by Gelinas et al. (1977)(table 3-4). These andesites resemble the low MgO komatiitic basalts in major element composition and locally show textures and structures characteristic of komatiites, namely spinifex texture and polygonal jointing respectively.

The term komatiitic andesite has been used previously by Cameron and Nisbet (1982). However for this thesis, this term was not taken from them. This writer was unaware of their usage of it when the term was first applied to some of the map area komatiitic volcanics. Cameron and Nisbet (1982) use the term briefly. They discuss the

Table 3-4

Terminology used to subdivide basalts, andesites and dacites as a function of SiO_2 abundances (volatile free) after Gelinas et al. (1977).

basalt	<54% SiO_2	(volatile free)
andesite	54-62% SiO_2	(volatile free)
dacite	62-67% SiO_2	(volatile free)

problems of CaO:Al_2O_3 ratios as a means of labelling a particular volcanic rock as a komatiitic basalt or andesite. The term andesite is referred to only once.

High Al_2O_3, komatiitic basalts, andesites and dacites are those with $Al_2O_3 \geq 16$ % and which are linked spatially to komatiites in a manner similar to that of low MgO komatiitic andesites and basalts. The value of 16 % Al_2O_3 or greater carries some universal weight as far as a boundary to define the designation high Al_2O_3. Irvine and Baragar (1971) refer to high-Al volcanics as those with $Al_2O_3 > 16$ % in noting that Cenozoic calc-alkalic basalts and andesites are generally high-Al volcanics whereas tholeiites have low Al_2O_3 abundances between 12 and 16 %. Naldrett and Smith (1981) note that basalts which are commonly referred to as Al-rich in Archean terranes are those with Al_2O_3 contents in the range 15 to 22 %. Associated andesites have 16 to 20 % Al_2O_3. Kuno (1960) refers to high-Al basalts as aphyric basalts with Al_2O_3 higher than 17 % and rarely as low as 16 %. Clearly the value of 16 % Al_2O_3 used for thesis area rocks is compatible with previous literature usage.

The adjective low MgO is not required (high Al_2O_3, low MgO komatiitic basalt) because MgO abundance in basalts with high Al_2O_3 abundances is less than 12 %.

High Fe_2O_3, Al_2O_3 komatiitic basalts are those with $Al_2O_3 \geq 16\%$ (to be consistent with the above) and Fe_2O_3

between 18-20%.

Low Al_2O_3 komatiitic dacites are those volcanics with SiO_2 (62-67%) Al_2O_3<16% and which are spatially linked to the komatiites in the manner similar to that of the low MgO komatiitic andesites. The prefix low MgO is not required for these dacites because MgO abundances do not exceed 12 %.

3-3 Komatiitic versus Non-Komatiitic: Use of the Jensen Cation Plot

The Jensen Cation Plot used extensively by Jensen in the Kirkland Lake area is not sufficient to distinguish komatiitic volcanics from tholeiitic or calc-alkalic volcanics. This plot relies on major element composition while ignoring geological relationships which are important in recognizing komatiitic volcanics.

Samples regarded as komatiitic for geological reasons are plotted on the Jensen Cation Plot in figure 3-1. It is seen that M-47, a low MgO komatiitic basalt, plots as a magnesium-rich tholeiitic basalt. M-302, a high Al_2O_3 komatiitic basalt plots as a calc-alkalic basalt. Low MgO komatiitic andesites plot in both the magnesium-rich tholeiitic basalt field (M-3) and the calc-alkalic field (M-126, M-395). The other representative komatiitic volcanic samples (M-353, M-260, M-197) with less than 10 to 11% MgO plot in the tholeiitic or calc-alkalic fields. Those with greater than 10 to 11% MgO plot as komatiites (M-436, M-522,

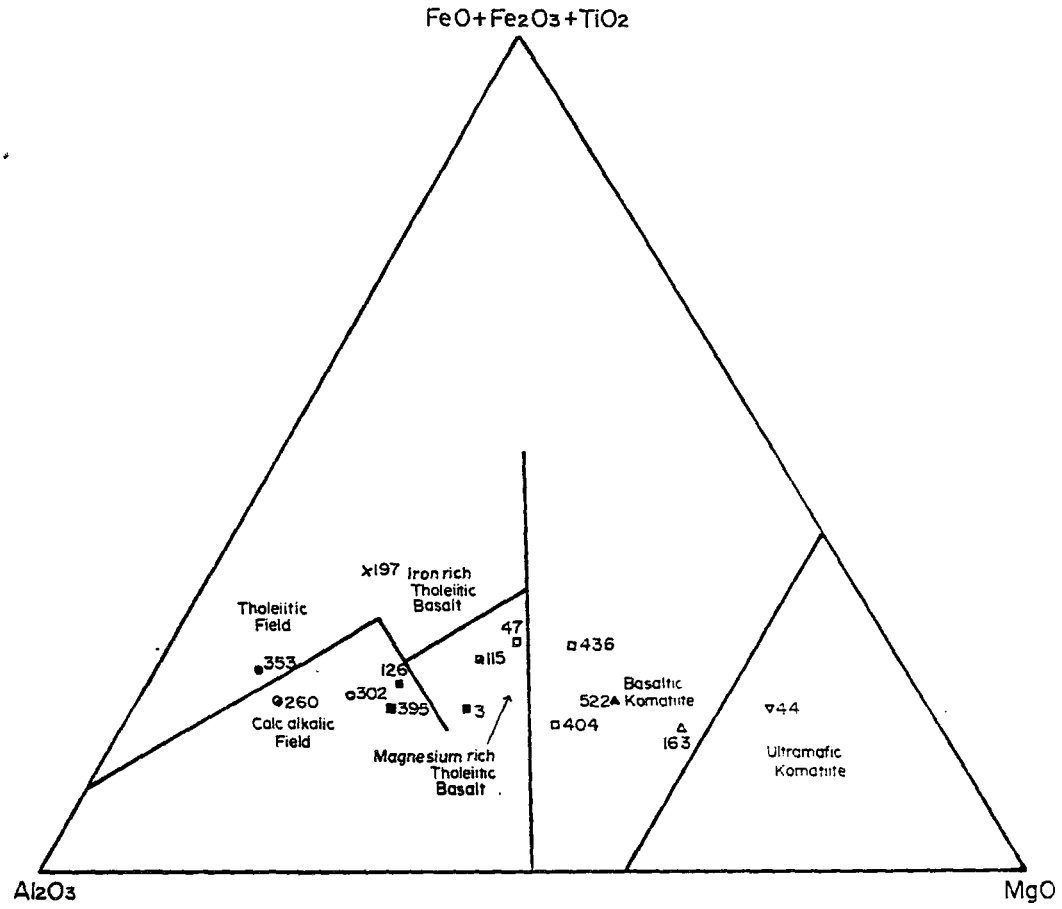

FIGURE 3-1: Representative komatiite and komatiitic volcanics plotted on the Jensen Cation Plot.

- ▽ Komatiite
- ▲ High MgO Komatiitic Basalt
- ▲ High MgO Komatiitic Andesite
- □ Low MgO Komatiitic Basalt
- ■ Low MgO Komatiitic Andesite
- ◪ Low Al_2O_3 Komatiitic Dacite
- o High Al_2O_3 Komatiitic Basalt
- ● High Al_2O_3 Komatiitic Andesite
- ◍ High Al_2O_3 Komatiitic Dacite
- × High Fe_2O_3, Al_2O_3 Komatiitic Basalt

M-404, M-163, M-44).

Tholeiitic and calc-alkalic volcanics should be regarded as genetically different from the komatiitic volcanics in that the former two were not derived by fractional crystallization from an ultramafic liquid. As such, one should not, for instance, classify a komatiitic basalt as a tholeiitic basalt if geological field relations suggest otherwise.

3-4 Komatiitic versus Non-Komatiitic: The Value of TiO_2 Contents

Nesbitt et al. (1979) make an interesting point in suggesting that the principal difference between komatiites and tholeiites is in the degree of melting and that diagrams to discriminate between komatiitic and tholeiitic basalts must be based on parameters that can be interpreted in terms of such genetic processes.

TiO_2 abundances are an important parameter in this light. TiO_2 is an incompatible element and preferentially enters the liquid during partial melting of the mantle. Clearly, with higher degrees of melting, TiO_2 abundances in the liquid decrease as the element is diluted by addition of other more refractory TiO_2-poor phases. A primitive high MgO (ultramafic) liquid would have low TiO_2 abundances. Low MgO komatiitic basalts derived from this liquid by fractional crystallization of olivines and pyroxenes will have higher TiO_2 abundances than the liquid due to loss of

non-Ti bearing phases. These basalts, however, may have lower TiO_2 abundances than basalts with similar major element compositions but parented by a mafic liquid which was derived through lower degrees of partial melting of the mantle. In this light, TiO_2 contents are one of the more diagnostic major elements in recognizing rocks of komatiitic kindred.

This is consistent with the literature which shows that basalts regarded as komatiitic have TiO_2 values in the order of 0.5 to 0.8 %. Basalts regarded as tholeiitic (from Archean terranes, younger mid-ocean ridges and island arc terranes) usually have greater TiO_2 abundances. This generalization also applies to komatiitic basalts versus calc-alkalic basalts.

Clearly, the best way to recognize a non-komatiitic basalt (tholeiitic or calc-alkalic) with major element chemistry and petrography similar to a komatiitic basalt, is to focus on field relationships, textures and discrimination diagrams such as SiO_2 vs TiO_2 and MgO vs TiO_2.

As discussed in section 3-2, field relationships are of ultimate importance in recognizing a komatiitic volcanic. Textures and composition may compliment field relationships but alone, are not diagnostic.

TiO_2 contents will be useful in chapter 8 when deciding whether the layered peridotite-gabbro and gabbroic intrusions noted in section 3-1 are of komatiitic or non-

komatiitic affinity.

3-5 Tholeiitic versus Calc-alkalic

Basaltic volcanic rocks which are not regarded as komatiitic can be referred to as tholeiitic or as calc-alkalic. Calc-alkalic rocks (aphyric and porphyritic) have higher Al_2O_3 contents and lower FeO/MgO ratios than the tholeiites with similar silica contents (Wilkinson, 1968).

Tholeiitic rocks often define a trend of increasing total iron enrichment on the Jensen Cation Plot and the A.F.M. plot shown in figures 3-2 and 3-3, respectively. Calc-alkalic rocks on the other hand may define a trend of increasing total alkalies on the A.F.M. plot. Irvine and Baragar (1971) point out that most high Al_2O_3 samples (Al_2O_3 > 16%) plot on the calc-alkalic field on the A.F.M. plot. On the Jensen Cation Plot, volcanics in the Blake River Group with greater than 15% Al_2O_3 and less than 10% Fe_2O_3 plot in the calc-alkalic field while volcanics with 13 to 16% Al_2O_3 and 9.75 to 18.08 % Fe_2O_3 plot in the tholeiitic field (Jensen, 1978b).

For this work, the Jensen Cation Plot will be used to designate a non-komatiitic volcanic as either tholeiitic or calc-alkalic. Irvine and Baragar's plot is not used because: (1) it uses $Na_2O + K_2O$ abundances which, as shown later in section 4-10 commonly do not reflect primary igneous composition. (2) Jensen (1976a) points out that the

FIGURE 3-2: The Jensen Cation Plot from Jensen (1976a). The Skaergaard trend represents a tholeiitic trend.

FIGURE 3-3: The A.F.M. diagram. The boundary between the tholeiitic and calc-alkalic fields is after Irvine and Baragar (1971). The typical calc-alkalic trend (stippled area) and the Skaergaard differentiation trend (dashed line) are from Best (1982). The Skaergaard trend represents a tholeiitic trend.

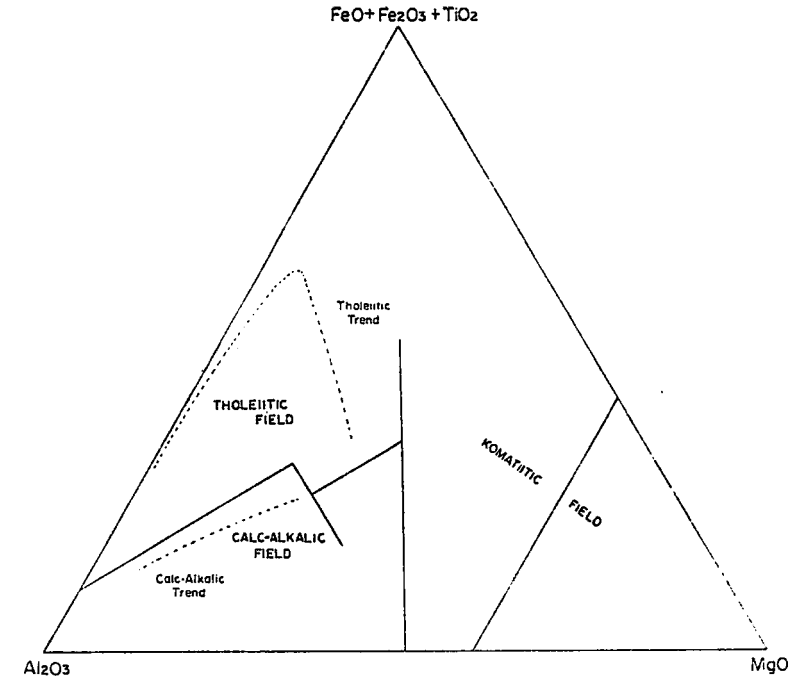
FeO+Fe2O3+TiO2
Tholeiitic Trend
THOLEIITIC FIELD
KOMATIITIC FIELD
CALC-ALKALIC FIELD
Calc-Alkalic Trend
Al2O3
MgO

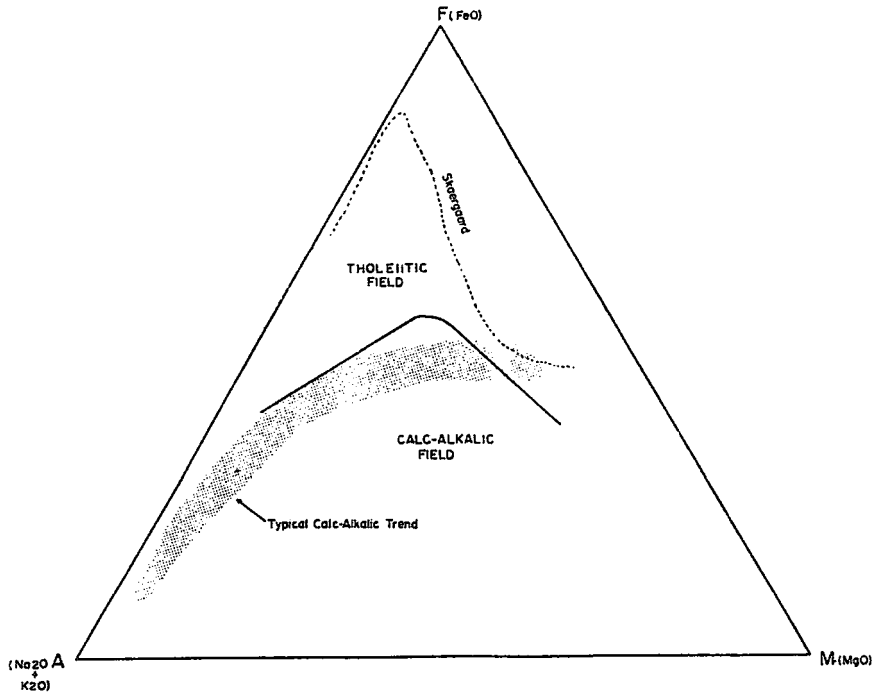
F(FeO)
Skaergaard
THOLEIITIC FIELD
CALC-ALKALIC FIELD
Typical Calc-Alkalic Trend
(Na2O + K2O)
A
M(MgO)

curved line dividing the calc-alkalic and tholeiitic fields on the Jensen Cation Plot corresponds closely to those employed on the A.F.M. plot and the Al_2O_3 versus normative plagioclase composition diagram proposed by Irvine and Baragar (1971). Since the division between the two fields on the Jensen Cation Plot is consistent with that on the A.F.M. plot such that samples will generally plot in the same field on both plots, the use of both is not necessary.

The use of the Jensen Cation Plot to classify non-komatiitic volcanic rocks makes the application of the terms tholeiitic and calc-alkalic consistent with previous usage in the literature.

3-6 Intrusive Rock Classification

Intrusive rocks are classified according to one of four criteria

1. igneous mineralogy
2. metamorphic mineralogy
3. major element chemistry
4. distinctive textures

The I.U.G.S. system shown in figure 3-4 is applicable to unmetamorphosed igneous rocks. Names derived from this are syenite and gabbro-diabase. The type of feldspar was determined petrographically. Abundance of minerals was estimated visually.

Metamorphosed ultramafic intrusive rocks with

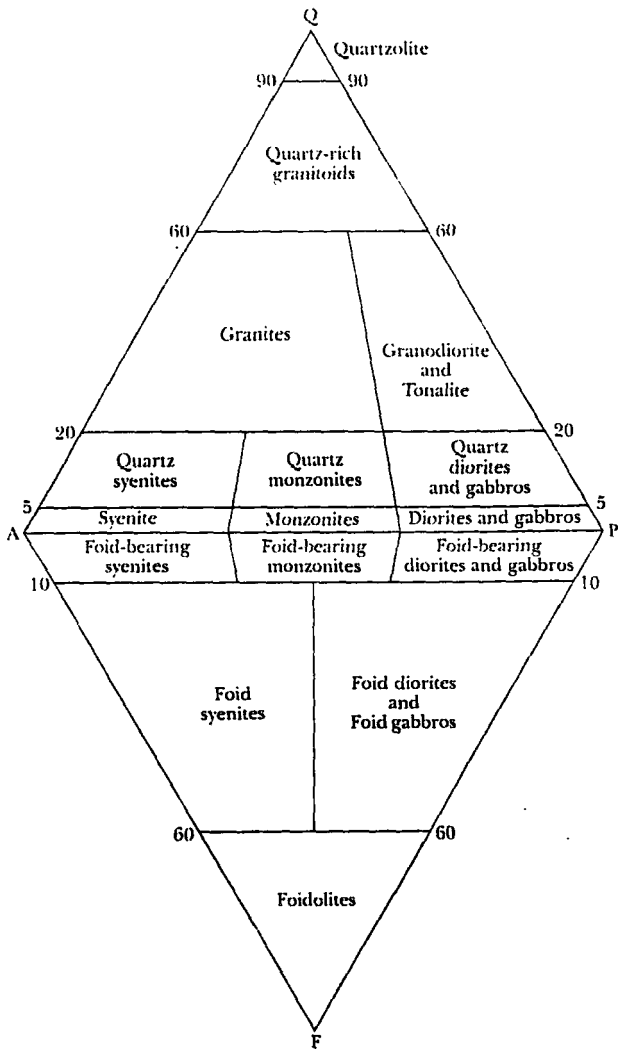

FIGURE 3-4: General classification and nomenclature of plutonic rocks according to the International Union of Geological Sciences (I.U.G.S.). (Streckeisen, 1975)

antigorite and minor amounts of Mg-rich chlorite and tremolite are referred to as peridotite. Antigorite and chlorite are considered to have formed from olivine while tremolite is a metamorphosed product of pyroxene. Pyroxenitic rocks are those composed largely of actinolite-tremolite (after pyroxene) with minor antigorite and feldspar. This classification is consistent with those shown in figures 3-5a and b. The terms hornblende pyroxenite or olivine pyroxenite were not used because the term pyroxenite was a convenient and general field term.

Metamorphosed medium to coarse grained mafic rocks are referred to as gabbro. These rocks are composed of clinozoisite, albite and equal amounts of amphibole. They commonly contain less than 54 % SiO_2. The primary igneous mineralogy is believed to have been plagioclase and pyroxene/hornblende. The term gabbro is consistent with Gelinas et al. (1977) who designate basalts as SiO_2<54 %

Unmetamorphosed intrusive dykes were classified in the field according to distinctive textures and the field classification terminology is used in this text. Names such as biotite lamprophyre and feldspar porphyry are examples.

Syenite, biotite lamprophyre and feldspar porphyry dykes are also collectively referred to as alkali-rich dykes. High potassium and/or sodium abundances are known to be a characteristic of these dykes (Jensen, 1978b; Ridler, 1970).

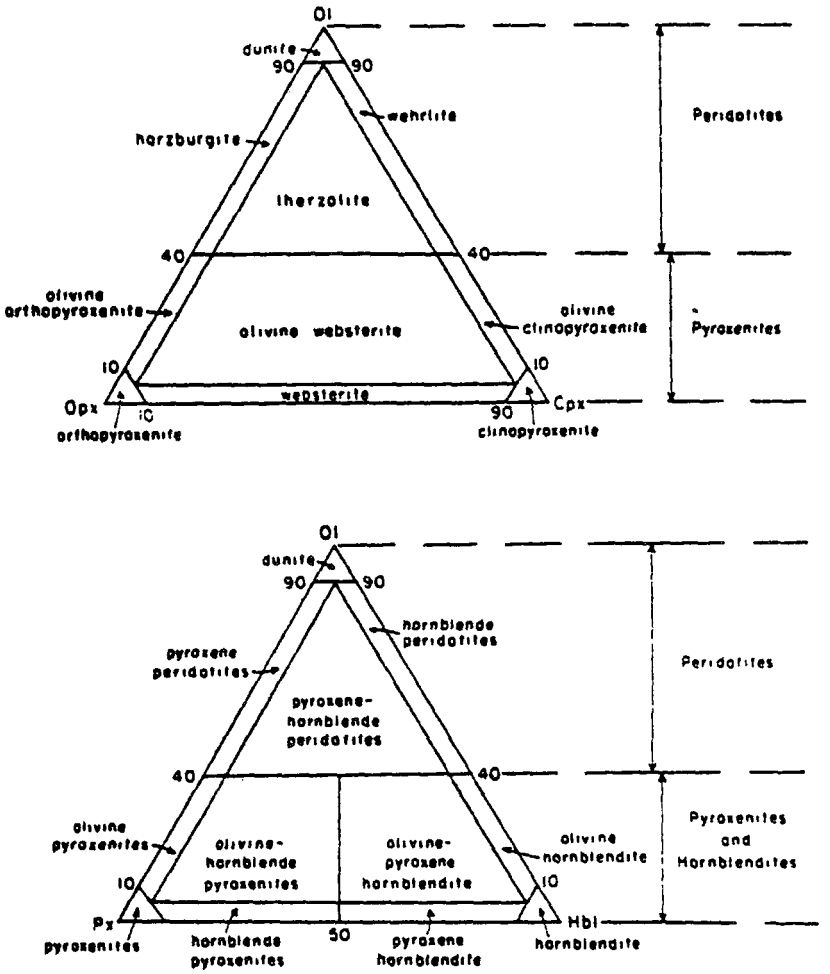

FIGURE 3-5a) Classification and nomenclature of ultramafic rocks composed of olivine, orthopyroxene and clinopyroxene according to the I.U.G.S.. (Streckeisen, 1975).

b) Classification and nomenclature of ultramafic rocks that contain hornblende, according to the I.U.G.S.. (Streckeisen, 1975).

3-7 Geology on the South Limb of the Lebel Syncline

The south limb hosts the three economic B.I.F.. In the mine site, these units and chert are the dominant sedimentary rock types. Less voluminous bands of clastic sediments are observed at the western end of the mine site below the South Pit, southeast of the Central Pit and between the Central and West Central Pits (map 6). West of the mine site, a total of ten separate units, commonly mixed clastic, chemical and pelitic sediments are observed, three of which correlate with the three economic B.I.F. (map 6). B.I.F. is a minor lithology west of the mine site.

The abundance of volcanic rocks varies laterally across the area mapped on the south limb (maps 3, 4). South of Beaver Lake and west of the mine site, eight volcanic sequences (groups of flows) are recognized whereas at the northwest trending power line in the west, only three are observed. In the mine site, four or possibly five sequences are observed. In map areas NB-1 and NB-2, volcanic rocks comprise 70 to 80 % of the stratigraphy.

The strata are tightly folded about north-south axial surfaces near the western end of the mine site where thinly bedded B.I.F. is abundant. The traces of these axial surfaces are marked with a 'B' in figure 3-6. B.I.F. to the northeast of these traces and the mill in map area NB-2 (map 6) does not seem to be as tightly folded, judging from their outline as mapped by Lawton (1957). The strata and the fold

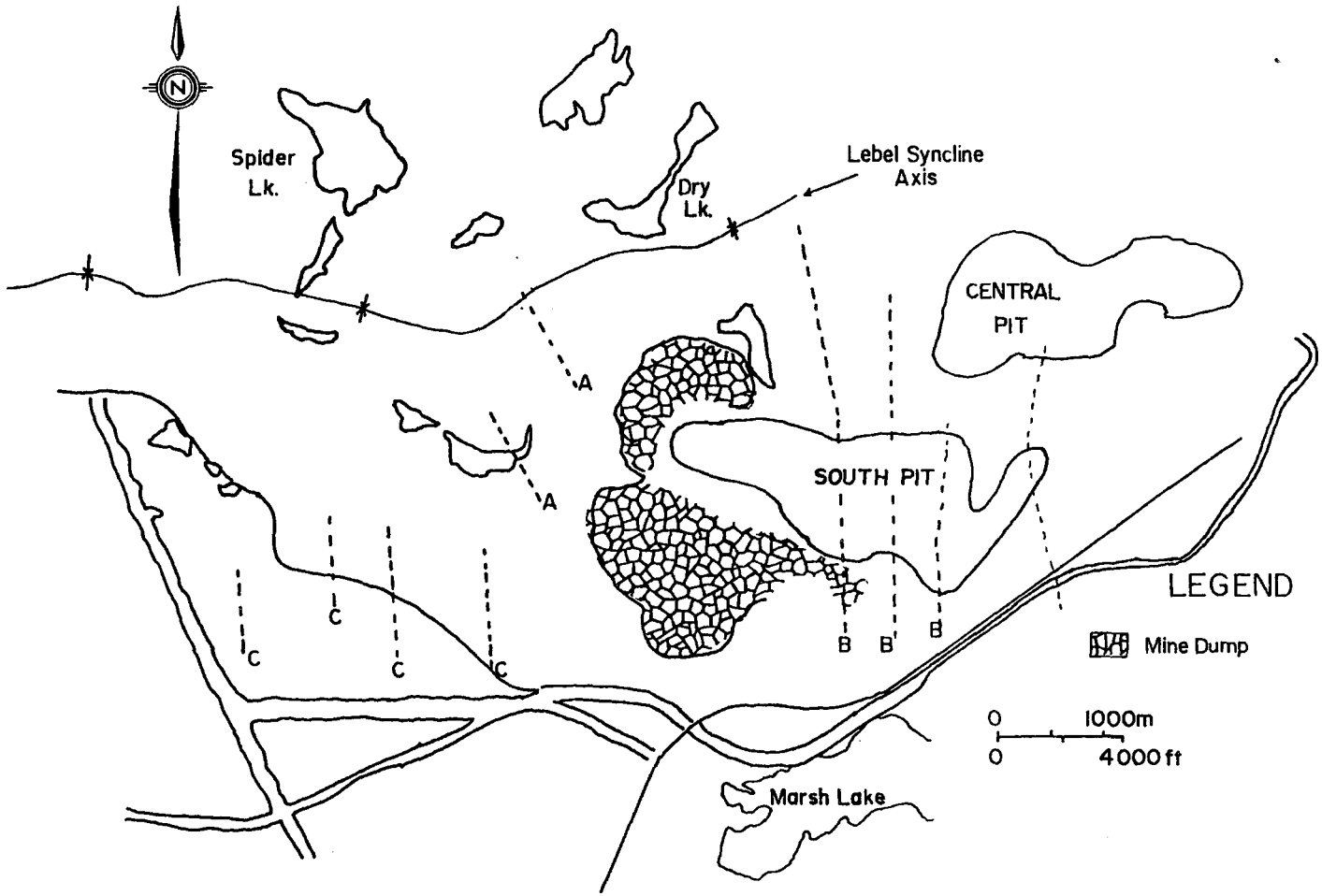

FIGURE 3-6: Traces of the fold axial surfaces on the south limb of the Lebel Syncline. The traces of axial surfaces at A mark the S-shaped drag fold. Axial surfaces traces at B mark very tight folds in the South Pit. Axial surfaces at C are defined by mild undulations in the stratigraphy.

axis of the Lebel Syncline are caught up in an S-shaped drag fold along the western mine site boundary as noted previously in section 3-1. This fold is indicated in figure 3-6 by the axial surface traces at 'A'. The Larder Lake/Skead Group contact may be caught up in this same fold. Lawton (1957) mapped an unusually wide sequence of the Skead Group 450 meters southwest of Marsh Lake and south of the observed drag fold in the map area and attributes this thickening to the presence of a large drag fold there. West of the mine site, warping of the strata is more open than observed at the western end of the mine site. Traces of the axial surface at 'C' in figure 3-6 are more widely spaced than those which cross the South Pit.

Distribution of the units is not thought to be controlled significantly by faulting. Some faulting does occur, for example, south of the Dane-Larder road causing an apparently minor but unknown displacement of the units. However, to emphasize the lack of significant strata offset due to faulting, one should look at the outline of the three major B.I.F. units derived from mapping prior to open pit mining (Lawton, 1957; map 6). No evidence of major displacement attributable to faulting can be found. Moreover, the easily mapped contact between the Skead and Larder Lake Groups does not show fault related displacement.

Figure 3-7 outlines the distribution of the eight volcanic sequences on the south limb of the Lebel Syncline

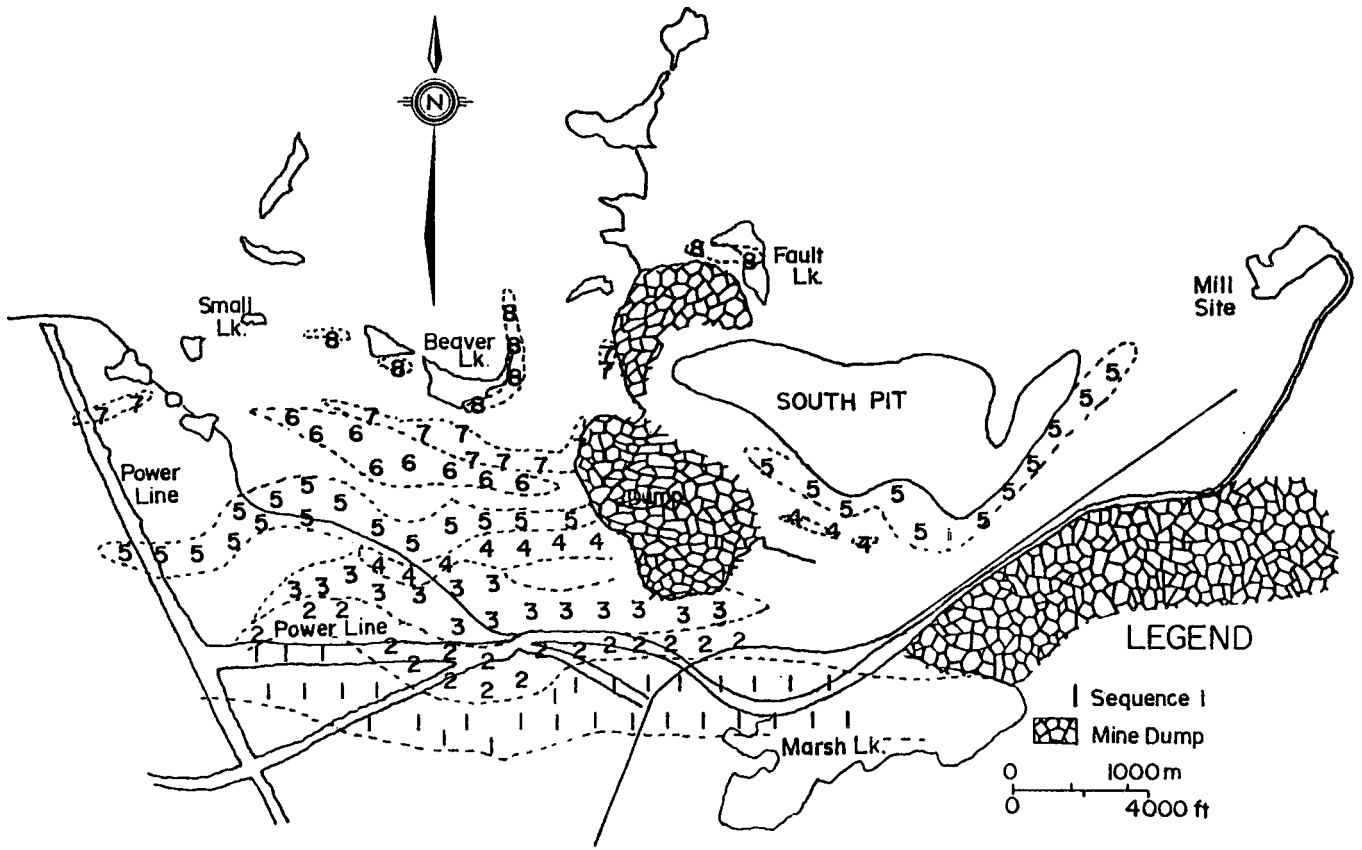

FIGURE 3-7: General outline of the eight volcanic sequences on the south limb of the Lebel Syncline.

while maps 2,3 and 4 outline the distribution of the volcanic lithologies. Seven of the eight volcanic sequences recognized are komatiitic.

A komatiitic sequence is composed of an indeterminate number of flows which are grouped together in the field through recognition of two common features:

1) the presence of komatiite flows at the base,
2) the presence of flows less magnesian than komatiites at the top. These uppermost flows are recognized by the fact that they are overlain by komatiites except in sequence 8, which is overlain by B.I.F. and sills.

Komatiitic volcanic sequences in the thesis map area show a lithological variation stratigraphically upwards which reflects decreasing magnesian contents in the flows. These variations are outlined in section 3-8. These sequences have variable degrees of lateral continuity and are commonly bounded by sediments.

Sequence 1 which forms the base of the Larder Lake Group is tholeiitic to calc-alkalic. This group of flows does not show a lithological variation with stratigraphic height. Sequence 1 basalts are easily recognized as sequence 1 flows in the field. Their appearance in hand specimen and at the outcrop contrasts with that of most of the overlying komatiitic basalts. This is discussed further in chapter 4. Sequence 1 does not have ultramafic or high

MgO flows.

Two units of clastic sediments are intercalated with sequence 1 (map 3). Chert and clastic sediments overlie it. Sedimentary rocks underlie and overlie komatiitic sequences but generally are absent within them.

The stratigraphically lowermost B.I.F. unit west of the mine site is correlatable with the South Pit B.I.F. and overlies four of the komatiitic sequences and the tholeiitic-calc-alkalic sequence.

Sequence 5 which directly underlies this B.I.F. is traced from the northwest trending power line to the mill site, a distance of 3 km (figure 3-7). This is the most extensively exposed volcanic sequence in the map area. Sequence 4 is outlined from the Dane-Larder road to south of the South Pit. Sequences 1,2, and 3 are observed mainly west of the mine site. They could not be traced far into the mine site due to poor exposure and a tailings pond which lies east and northeast of Marsh Lake. Sediments locally separate sequences 2 from 3 and 3 from 4.

West of the mine site, the sixth volcanic sequence overlies the stratigraphically lowest B.I.F.. The seventh and eighth sequences are best observed south and east of Beaver Lake. The sixth and eighth sequences can be traced west to south of Small Lake, while the seventh sequence is recognizable to the northwest trending power line (figure 3-7).

The eighth volcanic sequence south of Beaver Lake is overlain by a gabbroic sill. This sill is one of four sills which overlie the stratigraphically highest volcanic sequences west of the mine site on the south limb. On map 5 various phases of the sills (peridotitic, pyroxenitic, gabbroic and microgabbroic) are shown as they were mapped in the field. The stratigraphic order for these sills is also indicated on map 5. Two of the four sills show easily recognized lithological variation with stratigraphic height. South of Finger Lake, only the stratigraphically lowermost sill shows all four phases. North of Beaver Lake where three sills are exposed, peridotite is not observed and pyroxenite only locally. South of Dry Lake and immediately west of the drainage ditch, two gabbroic sills are observed. East of the drainage ditch, one is observed. Further to the east, between the Central and West Central Pits, concordant intrusive rocks of this character are not observed.

The outcrops of B.I.F. found immediately below and between the sills west of the mine site (figure 3-8) likely constituted one sedimentary unit prior to sill emplacement. This unit has been split by the concordant intrusives. These outcrops mark the stratigraphically highest sedimentary unit on the south limb of the Lebel Syncline. The outline of high magnetic intensities (figure 3-8) south of Dry Lake shows that these isolated B.I.F. outcrops are part of a horizon which includes B.I.F. in the West Central

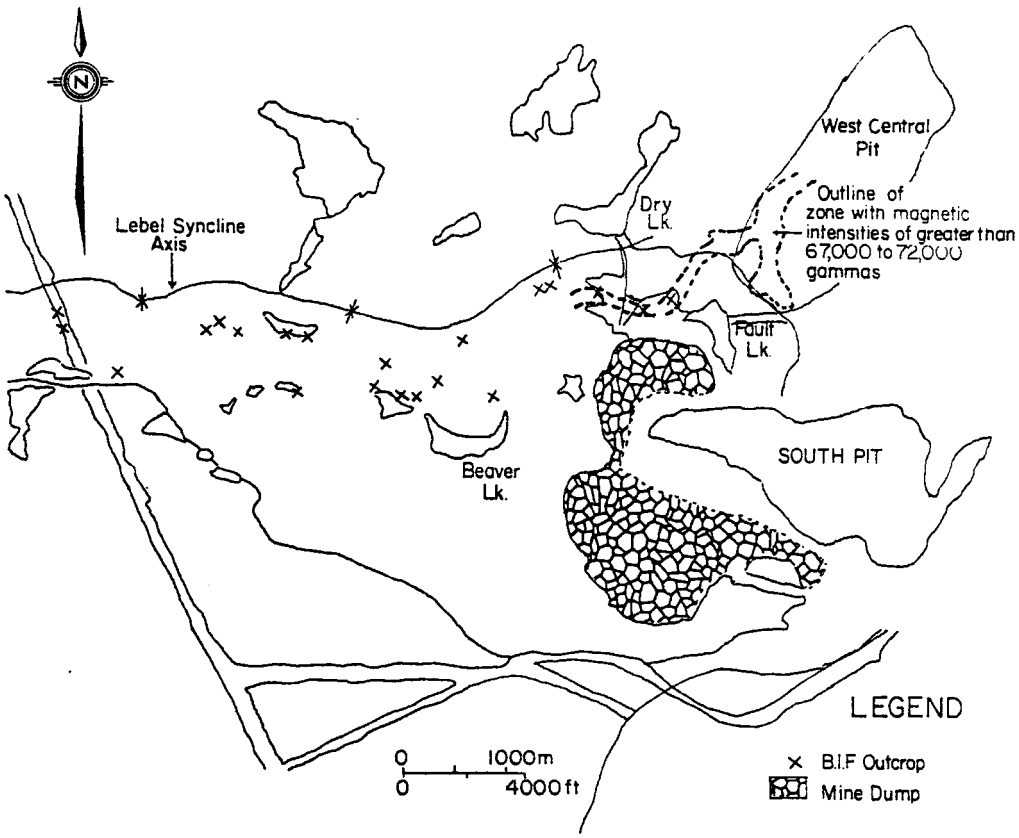

FIGURE 3-8: Location of B.I.F. outcrops which immediately underlie or occur between peridotite-gabbro and gabbro sills. The outline of high magnetic intensities south and southeast of Dry Lake is from Ratcliffe (1951).

Pit. B.I.F. in this pit is part of the stratigraphically highest major B.I.F. horizon in the mine site.

The B.I.F. and overlying chert in the area between Fault and Dry Lakes are not folded into tight folds as is found in the South Pit to the south. However, B.I.F. east of Fault Lake at the western end of the West Central Pit locally appears to be tightly folded as judged by its shape (figure 3-9). The trace of one fold axial surface is shown in figure 3-9.

A komatiite/gabbro/B.I.F. sequence is traceable, in parts and intermittently, from Beaver Lake north-south and then east-west to south of Dry Lake (figure 3-9). It best outlines the S-shaped drag fold noted previously in this section and in section 3-1.

The eighth volcanic sequence is observed on both sides of Fault Lake. On the east side of the lake, banded mafic tuff and chert underlie komatiites of this sequence. The chert thus occupies the same stratigraphic interval as 1) north-striking chert, carbonaceous chert and conglomerate found immediately west of the dump site and to the northeast of Dump Lake, and 2) the sediments between the seventh and eighth sequence southeast of Beaver Lake (figure 3-10). These sediments are considered to occupy the same stratigraphic horizons as the B.I.F. at the Central Pit. There are no outcrops of sedimentary rocks between Fault Lake and the Central Pit.

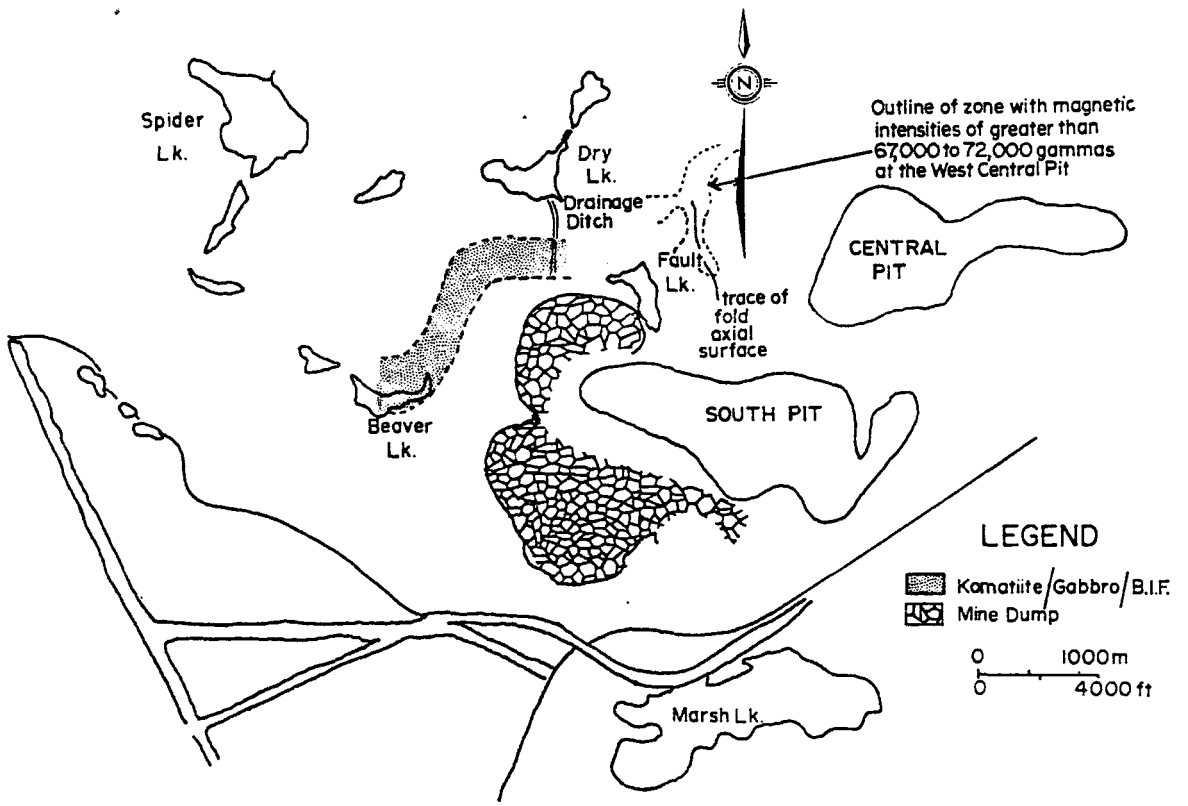

FIGURE 3-9: Trace of komatiite/gabbro/B.I.F. sequence through an S-shaped drag fold west of the mine site and the trace of fold axial surface at the West Central Pit.

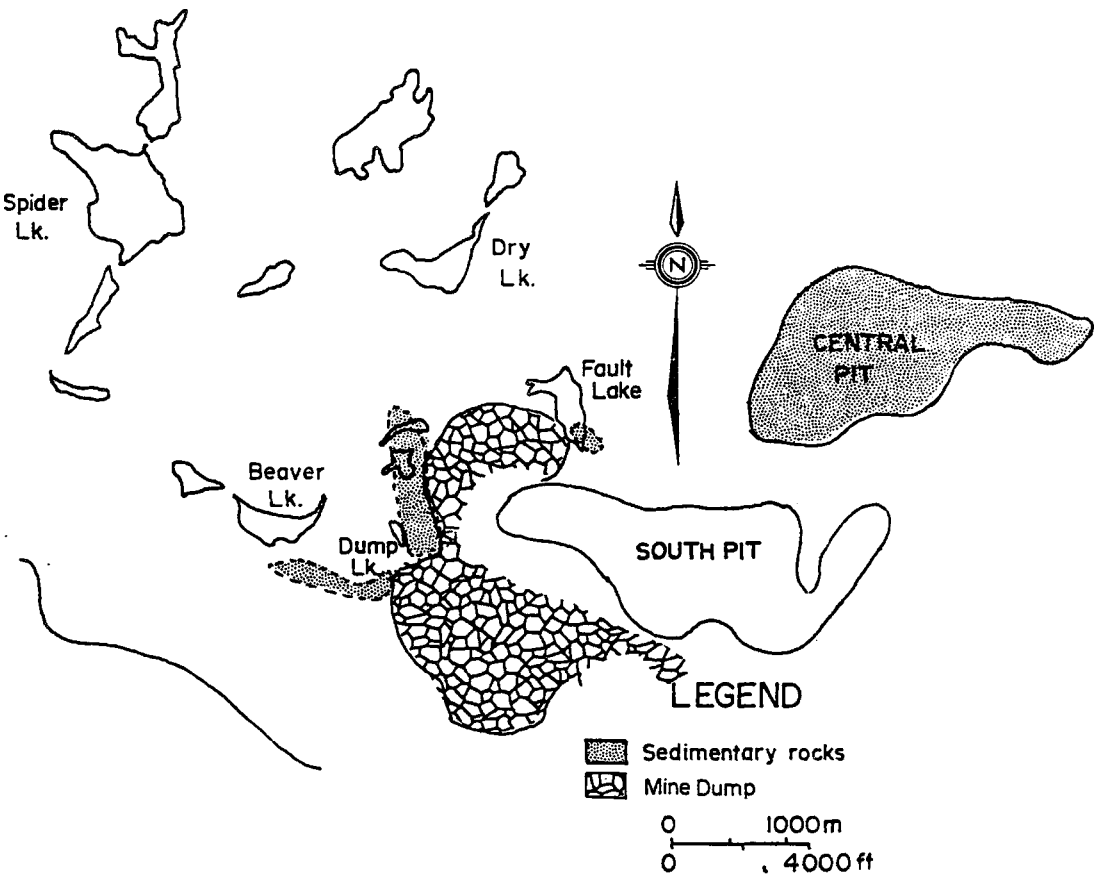

FIGURE 3-10: The dotted areas represent areas of outcrop of sedimentary rocks which are considered to represent the same stratigraphic unit.

Two large discordant gabbroic intrusions are found on the south limb of the Lebel Syncline (map 5). The eastern body referred to as the South Pit Gabbro is most voluminous immediately below the west end of the South Pit where it occupies a roughly circular area approximately 200 meters in diameter. Outcrops of the same gabbro are found north and south of this locality in sequences 8 and 1 respectively, (map 5) and may represent the same magma solidified in a conduit system.

The western discordant intrusion consists of two discordant, medium-grained gabbroic bodies which are 100 meters apart and occupy an area between the northwest trending power line and the Dane-Larder road on the west side of the map area (map 5). The northern body is rectangular in shape extending east-west for 240 meters and north-south for 120 meters. The circular southern body is 90 meters in diameter. In hand specimen, the two bodies appear similar and resemble the South Pit Gabbro. It is possible the two closely spaced bodies are joined and represent one intrusion as exposure between the two is very poor. These two bodies are referred to collectively as the Power Line Gabbro.

3-8 Characterization of Komatiitic Volcanic Sequences

As noted previously, the south limb of the Lebel Syncline hosts eight volcanic sequences, seven of which are

komatiitic. They are outlined in figure 3-7.

The complete upward stratigraphic progression in the seven komatiitic sequences from MgO rich flows to flows with lower abundances in MgO (komatiite to a low MgO komatiitic basalt for example) is not observable everywhere in the map area. This may be due to poor exposure. The most complete sections are noted below.

Sequence 2: The lithological order for this sequence as shown in figure 3-11 is well recognized immediately south of the intersection between the east-west trending power line and the Adams Mine road. Two samples were analyzed by X.R.F. from this locality (figure 3-12). Their MgO abundances are shown in table 3-5. MgO abundances for two analyzed samples located on the east-west trending power line are also given in table 3-5.

Sequence 3: The progression from high MgO komatiitic basalt to low MgO andesite and low Al_2O_3 dacite shown in figure 3-11 is observed north of the east-west trending power line and Adams Mine road intersection. Three samples (figure 3-12)(table 3-5) were analyzed from this locality. In figure 3-11, the base of sequence 3 is shown to be a komatiite which pinches out to the east. M-138 shown in figure 3-12 is considered as the basal komatiite to this sequence.

Sequence 4: Low MgO komatiitic basalt and andesite overlie high MgO komatiitic basalt at M-127 (figure 3-12) northeast of the Dane-Larder road. Komatiite at M-141 overlies

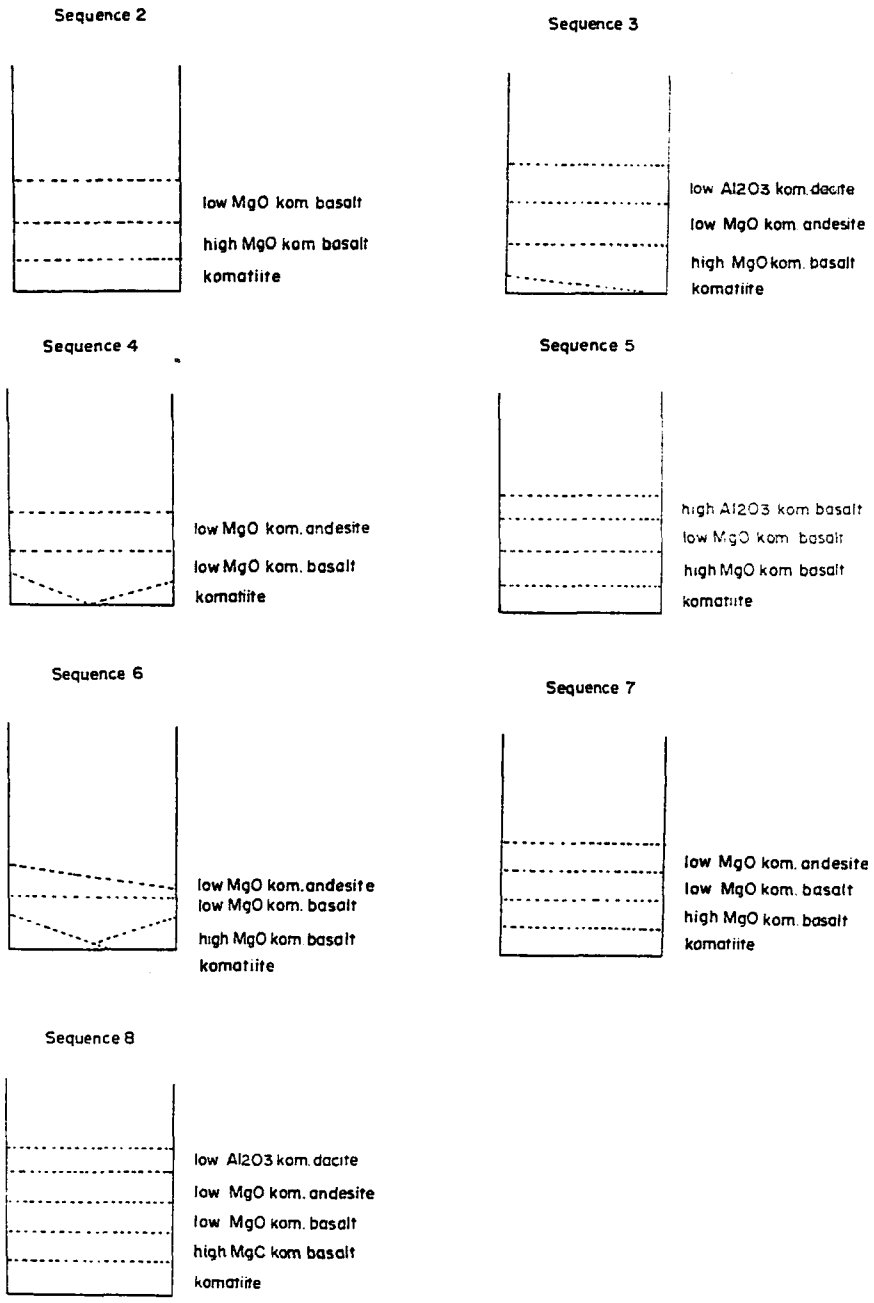

FIGURE 3-11: Generalized stratigraphy for each komatiitic volcanic sequence on the south limb of the Lebel Syncline. The diagrams are not intended to indicate thickness. Thickness of individual lithologies (a group of komatiitic flows for example) is difficult to determine owing to incomplete exposure.

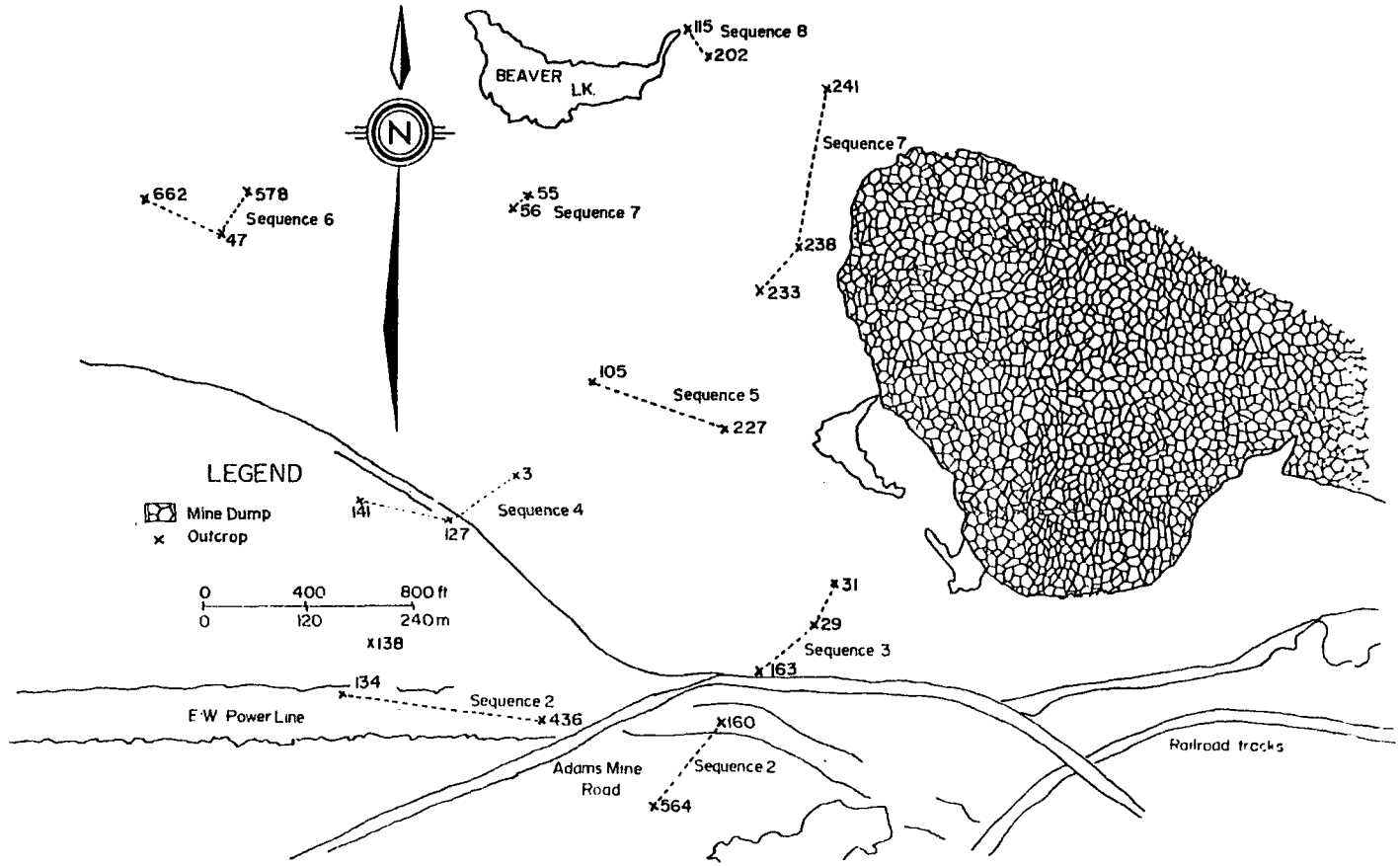

FIGURE 3-12: Location of closely spaced samples analyzed by X.R.F. which aid in characterizing the komatiitic volcanic sequences.

Table 3-5

Wt.% MgO for samples from closely spaced outcrops. Their locations are shown in figure 3-14

Sample Number	MgO%
Sequence 2	
M-564	21.68
M-160	11.04
M-134	12.59
M-436	11.81
Sequence 3	
M-163	16.57
M-29	12.11
M-31	4.96
Sequence 4	
M-141	26.80
M-127	12.29
M-3	6.74
Sequence 5	
M-227	23.74
M-105	3.28
Sequence 6	
M-47	8.69
M-578	6.00
Sequence 7	
M-233	20.63
M-238	13.30
M-241	6.56
M-56	23.15
M-57	15.05
Sequence 8	
M-202	19.60
M-115	7.72

sediments and is interpreted as the base of sequence 4 there. Three samples M-141, M-127 and M-3 were analyzed from this locality (table 3-5).

Sequence 5: The order shown in figure 3-11 is observed immediately south of the South Pit on the mine site. Sampled high Al_2O_3 basalt (M-105) overlies sampled komatiite (M-227) (figure 3-12) immediately west of the dump.

Sequence 6: M-662 (figure 3-12) is interpreted as the basal komatiite to this sequence. M-662 is overlain by low MgO basalts and andesites. M-47, a basalt underlies M-578, an andesite in figure 3-12. These two rocks are difficult to distinguish from each other in the field.

Sequence 7: Lithological variation with stratigraphic height (figure 3-11) is observable between the dump site and Beaver Lake. Shown in figure 3-12 are the locations of five analyzed samples from two localities which define the MgO variation (table 3-5) with stratigraphic height.

Sequence 8: Lithological variation with stratigraphic height (figure 3-11) is best recognized immediately east of Beaver Lake. M-202 and M-115 (figure 3-12 and table 3-5) are analyzed samples from this locality.

3-9 Correlation and Comparison of Volcanic Lithologies in Map Areas NB-1 and NB-2 with those in the Thesis Map Area

Blum's (1986) two map areas, designated as NB-1 and NB-2 in this study are shown in figure 3-13. Blum recognized three volcanic groups in NB-2 between the McElroy

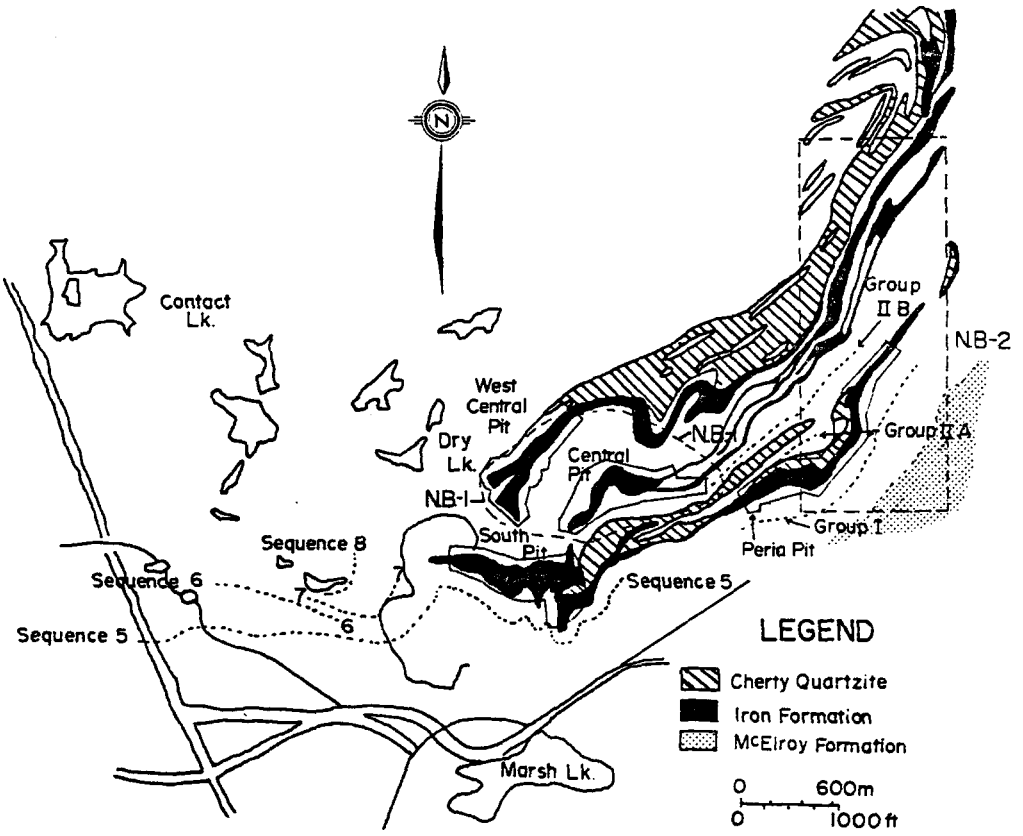

FIGURE 3-13: Geological map tracing out three volcanic sequences (5,6, and 7) in the map area and their lateral equivalents north and south of the Peria Pit. Also shown is the trace of sequence 8. The dashed line is drawn approximately through the middle of each sequence and group.

Formation and B.I.F. northeast of the Central Pit. These are referred to as groups I, IIA and IIB by Blum (1986). Their traces are shown in figure 3-13.

Group I which lies stratigraphically between the McElroy Formation and B.I.F. in the Peria Pit (figure 3-13) is best correlated with sequence 5 in the thesis map area. Both underlie the same B.I.F. unit. Sequence 4 cannot be correlated to the east. Group I contains komatiite, high and low MgO komatiitic basalt and high Al_2O_3 komatiitic basalt in the stratigraphic order observed in the map area. Low MgO komatiitic andesite is not found in either Group I or sequence 5.

Sequences 6 and 7 west of the mine site lie between sedimentary rocks regarded as laterally equivalent to B.I.F. in the Peria and Central Pits. In NB-2 map area, groups IIA and IIB occupy this stratigraphic interval. The suggested correlàtion is group IIA with sequence 6 and group IIB with sequence 7.

In NB-2, Group IIA is composed of komatiite flows which occupy the same stratigraphic level as high Al_2O_3 komatiitic basalts which lie immediately north of the South Pit in the thesis map area. West of the mine site, minor amounts of komatiite and abundant low MgO komatiitic basalts and andesites make up sequence 6. There is apparently variability in volcanic lithology type across the two map areas.

Sequence 7 (figure 3-14) is composed of komatiite, high and low MgO komatiitic basalts and low MgO komatiitic andesites. Group IIB in NB-2 contains high Al_2O_3 komatiitic basalts in addition to komatiites and high and low MgO komatiitic basalts. In the thesis map area, high Al_2O_3 komatiitic volcanics are not found in sequences which contain low MgO komatiitic andesites. The correlation between sequence 7 and Group IIB is thus unusual.

3-10 Correlation of the McElroy Formation with the Sedimentary Unit Overlying Sequence 3

The sedimentary unit shown in figure 3-15 which immediately underlies the fourth and fifth volcanic sequences is believed to be on the same stratigraphic level as the McElroy Formation. This is based on two observations: 1) the pebble and cobble conglomerate in this unit outcropping southwest of the mill (figure 3-15) are similar in composition and character to those in the McElroy Formation 600 meters to the east. 2) The similarity in stratigraphy below both the Peria and South Pits. Stratigraphic sections are shown in figure 3-16 for comparison.

It is not believed that a fault (the Boston Fault specifically) exists south and southeast of the Peria Pit as indicated by Lawton (1957). Three observations support this. At B in figure 3-16, the dioritic intrusive (9g) and gabbroic flow (3c) mark the Boston Fault (Lawton, 1957)

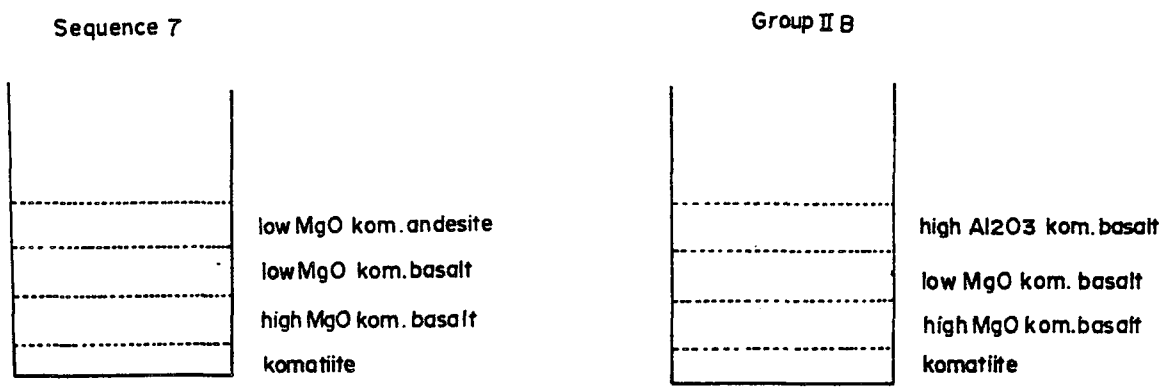

FIGURE 3-14: Generalized stratigraphy for sequence 7 and Group IIB. The sections are not intended to indicate thickness.

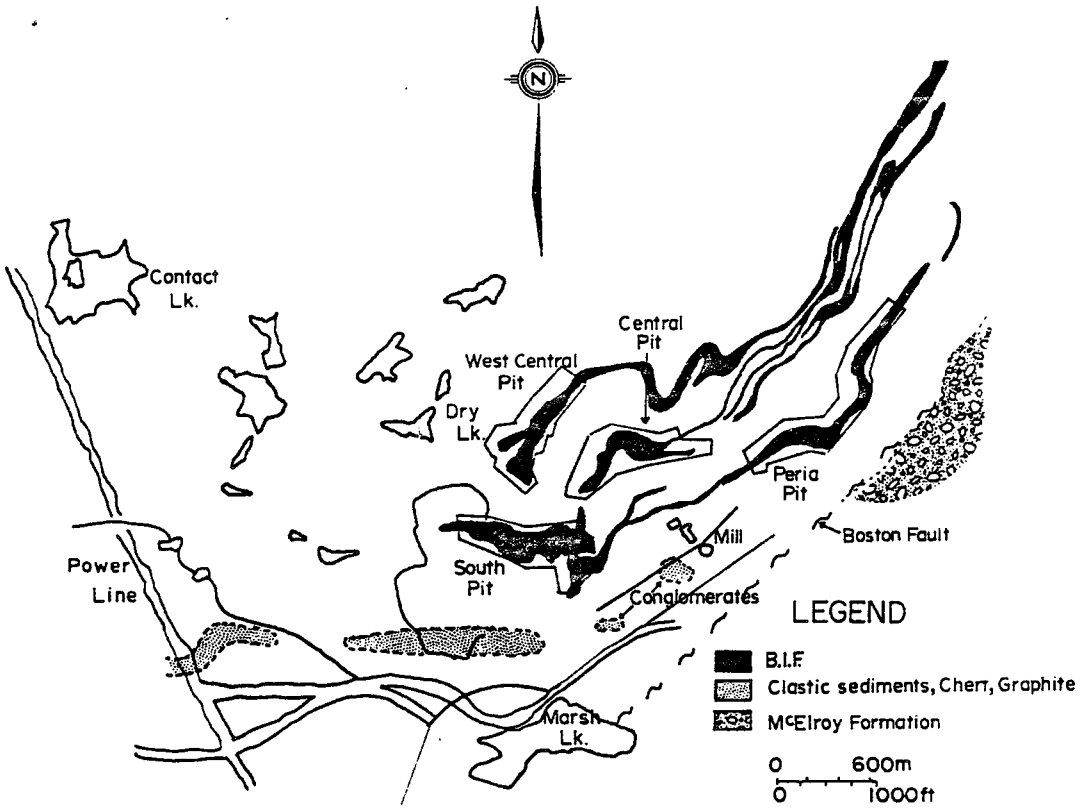

FIGURE 3-15: Outline of sediments which are considered to be a westward extension of the McElroy Formation.

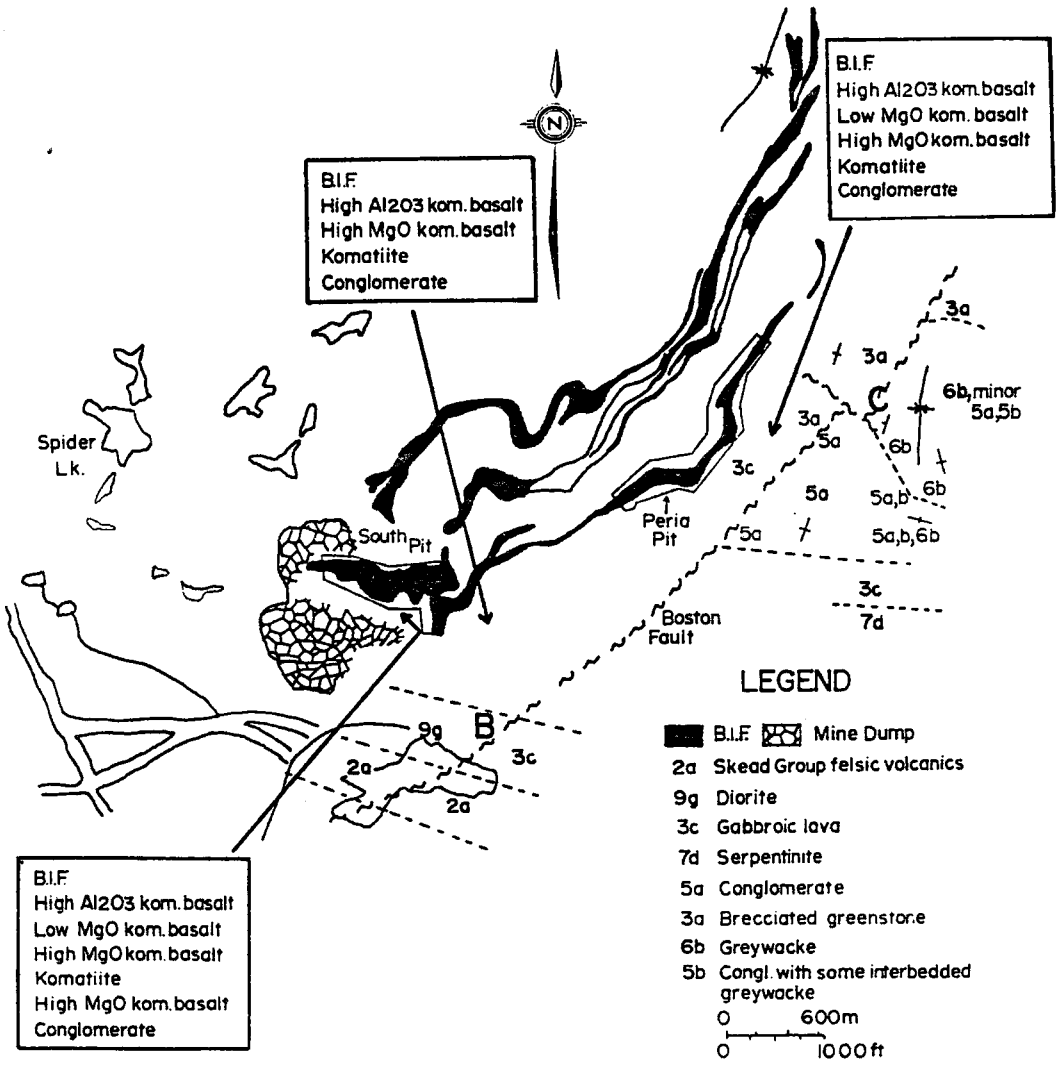

FIGURE 3-16: Geological map emphasizing: (1) the lithological contacts in the vicinity of the Boston Fault as mapped by Lawton (1957). The letters B and C highlight points made in the text. (2) Stratigraphic sections below the South and Peria Pits.

south of the South Pit. These are however the same lithology, sequence 1. Also at B, the felsic volcanic (2a)/9g-3c contact is not offset by the Boston Fault as one might expect. At C, the strike of greywacke (6b) on the east side of the Boston Fault parallels that of the volcanics and B.I.F. on the west side. There is not a structural discordance here to support the presence of a fault.

The contact delineated by Lawton (1957) between conglomerate dominated sediments (5a, 5a-b)(5a-b, 6b) and greywacke dominated sediments (6b) strikes northwest near and at the Boston Fault into southwest trending volcanics and B.I.F. This apparent discordance in the stratigraphy is likely the reason why Lawton delineated the Boston Fault. However (5a, 5a-b) and (5a, 5b, 6b) sediments may be on the same stratigraphic level as (6b) sediments to the north. This is possible if a sharp facies change exists.

Lawton (1957) indicates that there is approximately 1200 meters of stratigraphy between conglomerates (5a) and felsic volcanics (2a) east of this Boston Fault. This section likely represents the eastward extension of one or more of sequences 1, 2 and 3 between the McElroy Formation and the Skead Group. These sequences are intercalated with sediments and a peridotite sill.

3-11 Geology of the North Limb of the Lebel Syncline

On the northern limb, six bands consisting of clastic and chemical sediments, three volcanic sequences and a minimum of five intrusive sills are recognized (map 3). B.I.F. is observed only near the Lebel Syncline axis southwest of Dry Lake. On map 3 the strata are shown as gently warping. However, strongly deformed pillows at Spider Lake indicate that folding may be more complex than implied by the map.

The Lebel Syncline axis is shown in map 3 as folded by the S-shaped drag fold. This second-order fold does not appear to influence the strike of the stratigraphy on the north limb as it does on the south limb. The north limb stratigraphy is not folded into the S-shape as is the south limb stratigraphy.

Komatiites are observed at three stratigraphic levels on the north limb (map 2). North of North Lake, komatiites are overlain by high and low MgO komatiitic basalts. High Al_2O_3 komatiitic basalts outcrop along strike to the southwest of the komatiites. Komatiites south of North Lake are overlain by high and low MgO komatiitic basalt and by low MgO komatiitic andesite. Low MgO komatiitic andesite outcrops along strike to the west of the komatiites. Basalts and andesites along the north side of North Lake and at Dry Lake are considered to be komatiitic. These flows resemble komatiitic flows seen in other parts of

the map area in outcrop, in hand specimen and geochemically.

The gabbroic phase is prevalent in the intrusive sills in the western part of the north limb. In the eastern part, the gabbro phase predominates but the peridotite and pyroxenite phases occur. These sills are in general more abundant in the eastern part of the north limb mapped (map 6). West of Len's Lake for instance, four sills are observed. East of Len's Lake, six are observed. Thinner, peridotitic sills are relatively abundant between Dry Lake and North Lake and north of North Lake.

The massive, medium grained Contact Gabbro borders the Lebel Stock at all locations mapped and appears to be thickest along the northwest trending power line (maps 3,5). Here, north of Spider Lake and at Far Lake, this gabbro is characterized by abundant xenoliths, most of which are mafic volcanics. Iron formation xenoliths are also abundant south of Far Lake. This gabbro appears to be discordant to strata north of Spider Lake as judged by its outline. Gabbro/host rock contacts were not observed except for dykes of gabbro cutting host rocks.

3-12 Evidence for the Lebel Syncline

The Lebel Syncline shown in map 2 is clearly the major structural feature in the map area. Having described the geology in terms of the north and south limbs, evidence for a synclinal structure will be documented.

Northeast of the area mapped, the synclinal axis can be projected from west of the North Pits southwestward parallel to the B.I.F. units so that it passes between Dry and Fault Lakes (figure 3-17). The few strike measurements and the outline of sedimentary units mapped by Lawton (1957) in this interval are on the north limb of the fold and are parallel to the strike of the main B.I.F. horizons. This indicates that there is not a significant plunge to the fold axis, and thus that it does not for example trend into the Lebel Stock.

In the Dry and Fault Lakes area, there is evidence for the synclinal axis and it's approximate location.

1) The similarity in appearance in the field of high MgO komatiitic basalts at Dry Lake (north limb) and at Fault Lake (south limb, eighth sequence) is remarkable. Both have a very dark green surface which is seen elsewhere only in the third sequence on the south limb. The high MgO komatiitic basalts at Dry and Fault Lakes may thus be folded equivalents.
2) North of the West Central Pit clearing, pyroxenite outcrops (M-715) lie 10 meters north of gabbro outcrops (M-714). This suggests tops are to the south if the outcrops represent one layered intrusion. However, exposure is discontinuous, and this is not certain.
3) A drainage ditch located in figure 3-17 is cut perpendicular to the strike of the units south of Dry

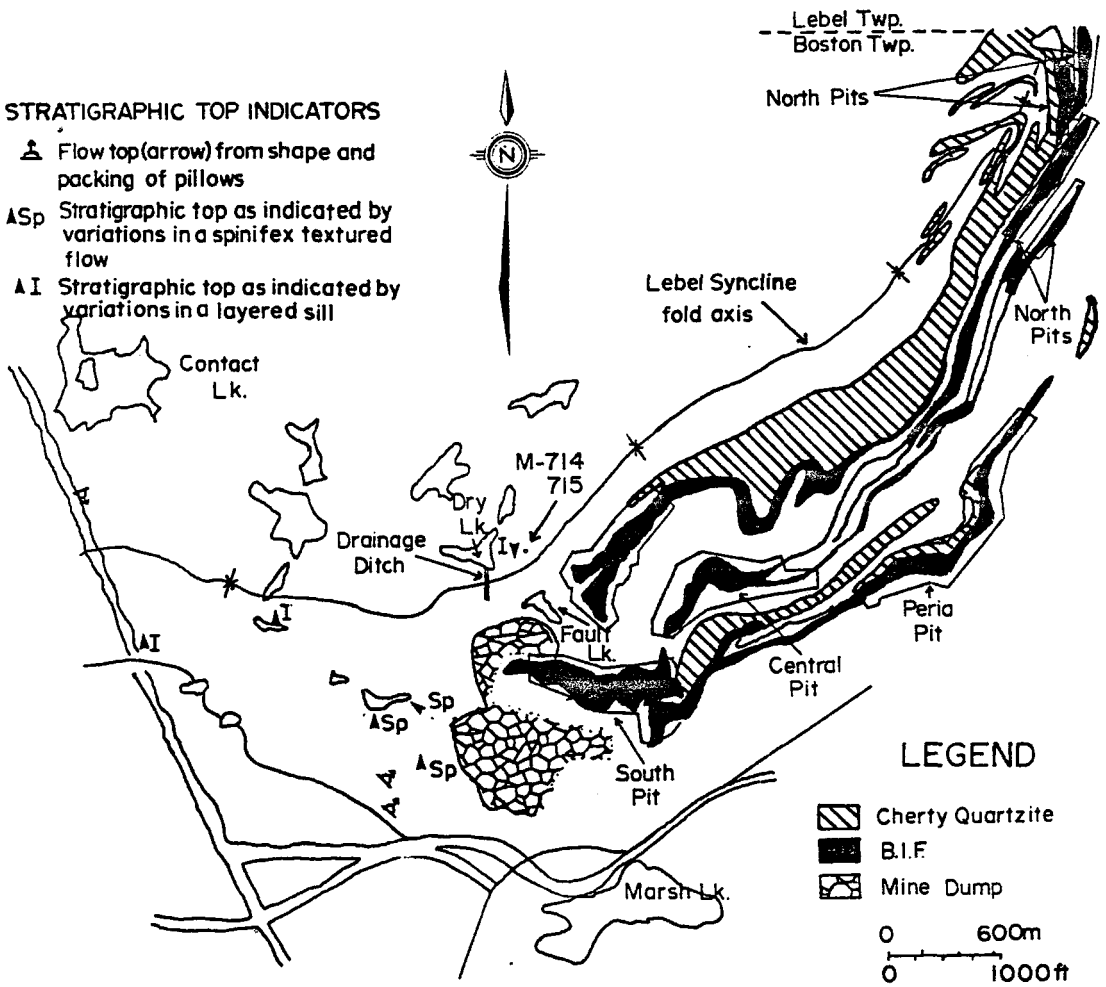

FIGURE 3-17: Projection of the Lebel Syncline fold axis southwest into the thesis map area from the Lebel-Boston Township boundary.

Lake and has a low MgO komatiitic andesite with a strongly epidotized flow-top breccia on its west wall. The altered flow-top can be followed through a number of tight synclinal and anticlinal structures on the north-south trending ditch face. No photographs are available but figure 3-18 adequately depicts the structure. This location is roughly between the komatiitic basalts at Dry and Fault Lakes whose similarity was previously noted and may represent the location of the fold axis.

On the northwest trending power line in the western part of the thesis map area, determinations on relatively undeformed pillows indicate tops are to the south. To the south on the same power line and near Finger Lake (figure 3-17), the stratigraphic variation of the phases of a differentiated sill indicate that tops are to the north. As outcrops between the two locations on the power line are sparse, the location of the synclinal axis cannot be constrained very closely. The location of the fold axis between the power line and Dry Lake is also approximate and positioned parallel to the outline of the peridotite-gabbro and gabbro sills. The location of top determinations made by the writer south of Beaver Lake are shown in figure 3-17. There are many top determinations in pillowed Catherine Group basalts south of the map area which indicate that tops are to the north (Lawton, 1957).

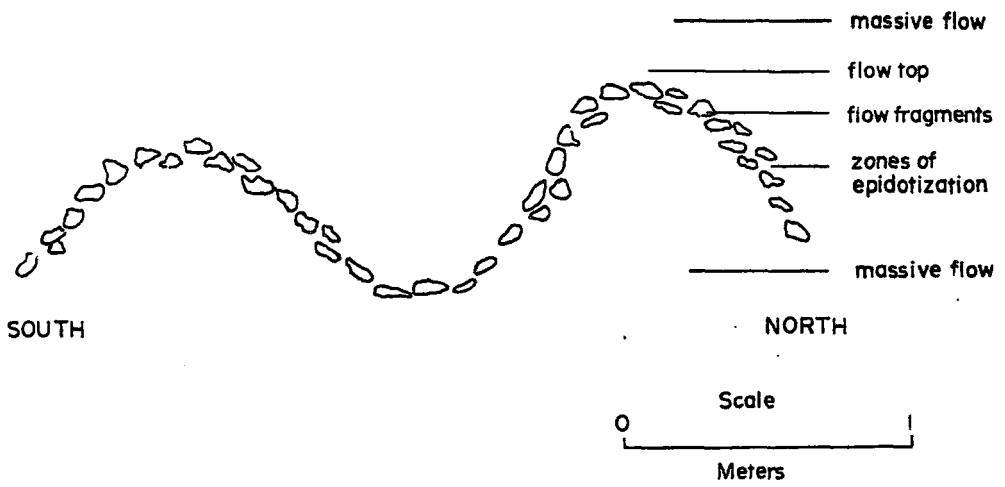

FIGURE 3-18: Sketch of a tightly folded komatiitic andesite as seen along the face of a north-trending drainage ditch south of Dry Lake. The folding is made obvious through the epidotized flowtop breccia.

3-13 Metamorphic Facies Distribution

The southern part of the thesis map area, (south of Beaver Lake and the South Pit) has been metamorphosed to the greenschist facies (Figure 3-19). The hornblende hornfels is found to the north and is recognized by the presence of hornblende in thin sections. Garnet occurs in both facies.

The majority of the rocks in both facies have unoriented texture. The exception is fine grained, biotite and/or sericite bearing sediments in which the micas show preferential orientation parallel to bedding.

Lithologies within 200 meters of the Lebel Stock/country rock contact near Far Lake (figure 3-19) contain certain hornfels textures not seen further south. Hornblende is randomly oriented and very coarse grained in the Contact Gabbro. Magnetite is coarse grained in massive iron formation xenoliths within the gabbro. Primary bedding has been destroyed. In clastic sediments south of the Contact Gabbro, sericite is coarse grained and randomly oriented. This contrasts with the fine grained, well foliated sericite which is characteristic of sediments on the south limb of the Lebel Syncline.

3-14 Lineaments (Joints), Faults and Shear zones

Many linear valleys found within the map area are probably the result of deep weathering and erosion of weak fractured zones. Most are clearly visible as lineaments on

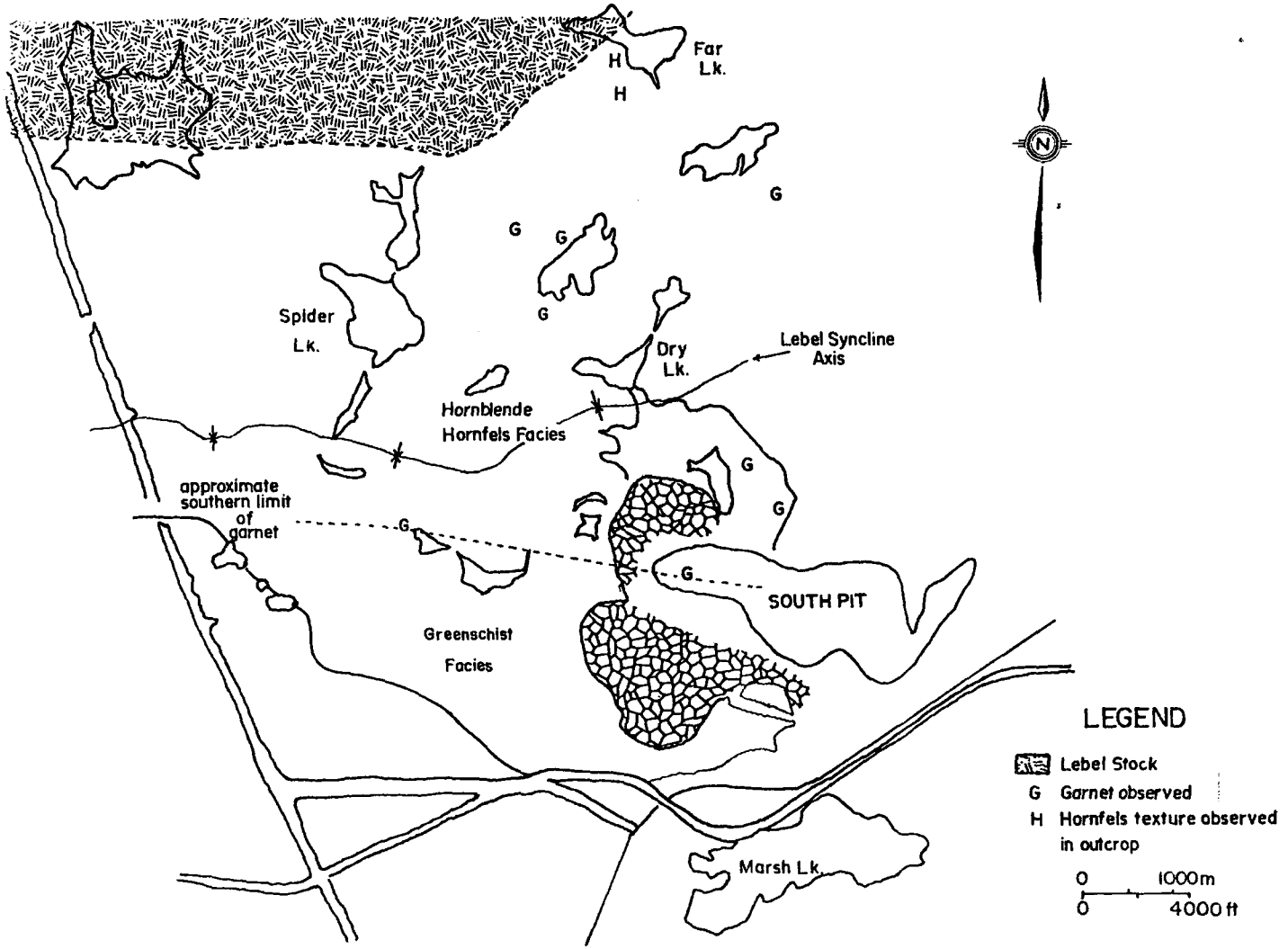

FIGURE 3-19: Outline of metamorphic facies and distribution of garnet.

air photos 78-1-40-114 and 78-1-40-115 (figure 1-5). Figure 3-20 shows their distribution and orientation. These lineaments do not offset the strata and are thus likely joints rather than faults.

There are four prominent directions for these lineaments as shown in figure 3-20. These are 50-55°west of north, 25°east of north, less than 10°south or north of east and very close to north-south. Figure 3-20 shows that changes in direction can occur. Only one zone which passes beneath the dump site west of the South Pit can be traced entirely across the thesis map area.

The majority of the lineaments are oblique to folded strata and likely post-date folding. North-south trending lineaments at Contact Lake cut across the Lebel Stock/country rock contact and thus developed at a very late stage.

There are five localities in the map area (figure 3-20) where displacement of strata can be attributed to faulting. The amount of displacement at these localities is unknown but is believed to be small.

Shear zones are marked south and southwest of the South Pit in figure 3-20. Rocks within these zones are often altered (epidotized, carbonatized). Quartz veinlets and syenite dykes are locally abundant. The shear zones clearly pre-date alkalic igneous activity. The shear zones cut across warped strata south and southwest of the South

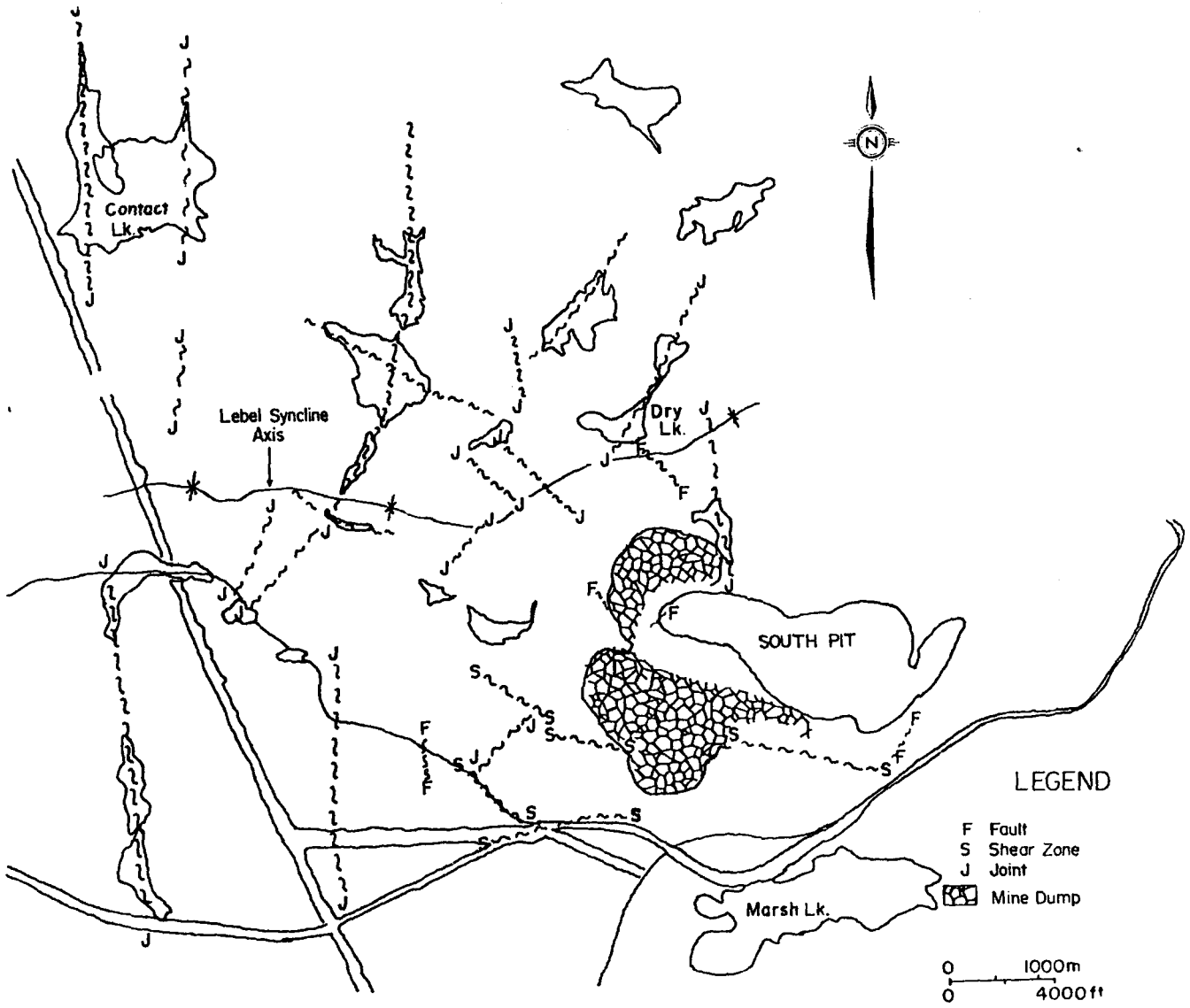

FIGURE 3-20: Location of faults (F), joints (J) and shear zones (S) in the map area. The major lineaments in the map area appear to be joints.

Pit indicating that they post-date much of the folding.

Chapter 4

Field Characteristics, Petrography and Geochemistry of Volcanic Rocks

4-1 Introduction

In this section, the field characteristics and petrography of each volcanic rock type are discussed, and major and trace element abundances for each type are compared to representative volcanics from other Archean terranes. Differences between komatiitic volcanics within the thesis map area are highlighted as are differences between komatiitic and non-komatiitic suites. The chemical variations within the komatiitic suite are discussed separately and are compared to those in other Archean terranes.

The thesis map area has been metamorphosed to at least the greenschist facies and then intruded by dykes, veins and veinlets of syenite, biotite lamprophyre and feldspar porphyry. The development of the hornblende hornfels facies may have been synchronous with or pre-dated some of these intrusions. Nevertheless, post-greenschist epidote, silica and carbonate zones of variable intensity are spatially associated with the dykes. Plate 4-1 shows a strongly carbonatized volcanic as an example. Bearing this

PLATE 4-1 Strongly carbonatized high MgO komatiitic basalt outcropping very near sample locality M-177 (map 1) south of the South Pit in Sequence 4. The beige weathering veinlets and domains are the carbonate (CB). The carbonate-free basalt is labelled B.

in mind, it is easy to understand how the rocks run the risk of alteration such that their chemistry fails to reflect original igneous chemistry.

To minimize the effect of post-igneous alteration, the samples used for petrographic and geochemical study are those void of quartz, epidote or carbonate veinlets or zones. Thus essentially all of the mineralogy in the samples studied is attributed to the greenschist metamorphic event or to the combined greenschist and hornblende hornfels metamorphism. The majority of the major elements and all of the trace elements reflect those of the igneous parent. This will be elaborated on further as the chapter proceeds.

4-2 Komatiites

Komatiites are found at the base of all of the komatiitic sequences. This rock type is easily distinguished from intrusive peridotite by polyhedral jointing (plate 4-2) as seen in the field. The polyhedrons become smaller towards the flow top in each flow. Polyhedral jointing forms during cooling of the flow (Arndt et al., 1979). Arndt et al. (1977) point out that it superficially resembles a breccia but differs from flow and tectonic breccias in that the polyhedra are not displaced with respect to one another.

Spinifex textured komatiites are found in the fourth, fifth and seventh sequences. Plate 4-3 shows this

PLATE 4-2 Polygonally jointed komatiite. The joints weather recessively. The flow is at or near the base of sequence 7 south of Beaver Lake between sample localities M-56 and M-57 (map 1).

PLATE 4-3 Random oriented books of spinifex in komatiite in the fifth sequence between sample localities M-174 and M-150 (map 1) below the South Pit.

texture as seen immediately south of the South Pit. Randomly orientated books of bladed antigorite with magnetite completely pseudomorph primary bladed olivine. The spinifex texture is formed by the rapid crystallization of liquid devoid of olivine phenocrysts. Spinifex textures are found at or near the top of the flows . Figure 4-1 shows the variation in textures within spinifex textured flows as documented on well exposed flows in Munro Township by Arndt et al. (1977). Similar variations were observed in spinifex bearing flows in the fourth, fifth and seventh sequences. Plate 4-3 is from the A2 zone in type A flow. Flow type C without spinifex textures is more common in the map area. Plate 4-2 represents flow type C.

Komatiites weather chocolate brown, light green or dark green colours. In hand specimen, they are fine grained, black, light grey or light green in colour and are magnetic. Flow thicknesses were observed to be from 1.5 to 3 meters on a few well exposed outcrops. This thickness is consistent with that observed for better exposed komatiite flows in Munro Township (Arndt et al., 1977).

In komatiites, the silicate mineralogy and silicate mineral abundances varies with the MgO content. Komatiites with very high MgO abundances such as M-231 (MgO = 32.83%) shown in plate 4-4 are rich in antigorite and Mg-rich chlorite. In plate 4-4 these two minerals completely pseudomorph primary tabular olivine phenocrysts. Light

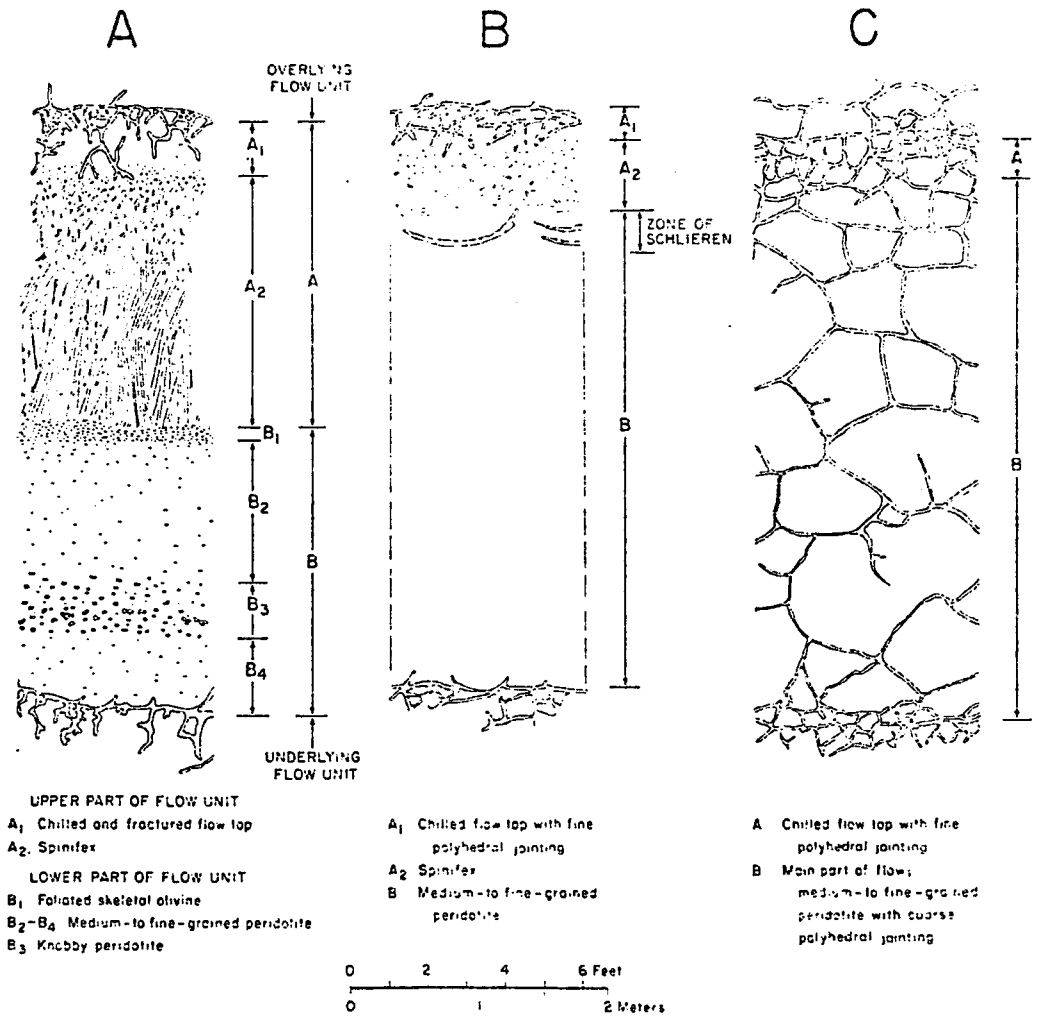

FIGURE 4-1: Diagrammatic sections through three types of komatiite flows.
A. a flow with an upper spinifex zones.
B. a flow with limited spinifex texture.
C. a flow without spinifex texture.
(from Arndt et al., 1977)

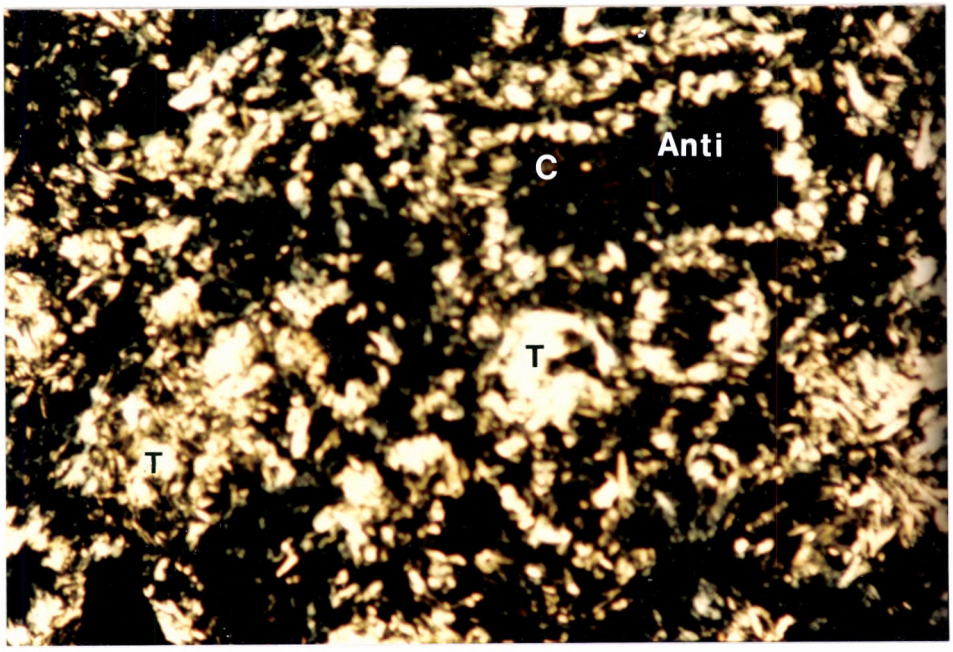

PLATE 4-4 Olivine phenocrysts are completely replaced by antigorite (Anti) and chlorite (C). Tremolite (T) is interstitial to the phenocrysts. The section is from M-231 near or at the base of sequence 7, immediately west of the mine site. The section is comprised of 60% phenocrysts. Polarized light, X63. The field of view is 1.0 x 1.5 mm.

coloured tremolite forms a boundary around the phenocrysts while interstitial material is antigorite and tremolite. Very fine grained disseminated chromite and magnetite which are not visible in plate 4-4 together make up 5% of M-231.

Komatiites with lower MgO abundances such as M-103 from a massive flow in the seventh sequence (MgO=23.05%) and shown in plate 4-5 are composed largely of tremolite with lesser chlorite. In M-103, the tremolite is acicular and completely pseudomorphs primary pyroxene, likely augite. The matrix is composed of chlorite and tremolite. Very fine grained disseminated opaque minerals which are not visible in plate 4-5 make up 2% of M-103.

The compositions of the komatiites from the thesis map area (major elements plus Cr, Ni, Co and V) fall within the range of reported representative compositions of komatiites from other Archean terranes (table 4-1).

4-3 High MgO Komatiitic Basalts

High MgO komatiitic basalts are invariably polygonally jointed and are commonly massive. The consistent low weathering of the joints gives outcrops a rugged texture (plate 4-6) distinguishing them from massive intrusive pyroxenite and most low MgO komatiitic basalts and andesites. Spinifex-bearing high MgO komatiitic basalts shown in plate 4-7 are found in the second, third, fifth, seventh and eighth sequences and are more common than

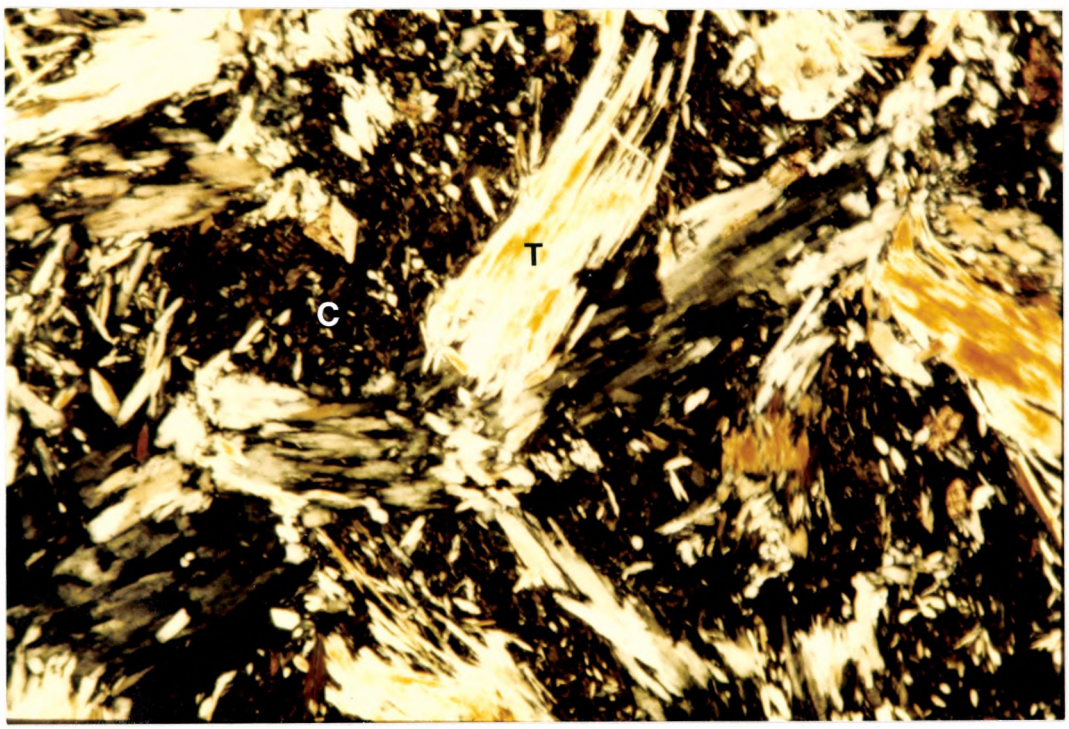

PLATE 4-5 Tabular grains of tremolite (T) in a finer grained groundmass of chlorite (C) and tremolite (T). The chlorite is the Mg-rich variety, having anomalous brown interference colours. Polarized light, x63. The field of view is 1.0 x 1.5 mm.

Table 4-1 (notes)

Chemical analyses of thesis map area komatiites and komatiites from other Archean terranes.

Location

1. Thesis map area
2. Munro Township, Ontario
3. Lamotte Township, Quebec
4. Finland
5. Barberton Belt, South Africa
6. Zimbabwe, Rhodesia
7. Yilgarn Block, Western Australia
8. Pilbara Block, Western Australia

References

8, SA-2048, P9-120, P9-187: (Arndt et al., 1977)
75D222, 75D173, 75D113, 75D042: (Gelinas, 1979a)
S3, S833, S829: (Jahn et al., 1980)
49J: (Sun and Nesbitt, 1978)
331/783, SG3, 331/784: (Nesbitt et al., 1979)
NG152, NG7631, NG7625: (Nisbet et al., 1977)
06, 98, 153, 180: (Naldrett and Turner, 1977)
15-AB (average of five samples)(Glickson and Hickman, 1981)
14AB (average of four samples)(Glickson and Hickman, 1981)

N.B. Major element compositions in this and all tables in this text are given as wt.% and are normalized to 100% on an anhydrous basis. Cr, Ni, Co and V abundances are in ppm. In table 4-1 the samples are divided into four groups based on MgO content.

A: MgO contents are between 32 and 35 %
B: MgO contents are between 26 and 28 %
C: MgO contents are between 21 and 25 %
D. MgO contents are greater than 18 % and up to 20 %

X-ray fluorescence analysis at McMaster University measures total iron which is reported here as Fe_2O_3. Major element composition listings in the literature include FeO, or FeO and Fe_2O_3 or Fe_2O_3. For comparative purposes, FeO and (FeO and Fe_2O_3) literature abundances were converted to Fe_2O_3. Literature major element compositions were then normalized to 100 %. Those derived from this study are given as such.

This conversion of data was accomplished using a program written by Steve Davies at McMaster University. The conversion, FeO to Fe_2O_3 is based on the equation

$$Fe_2O_3 = (FeO)\left(\frac{69}{78}\right),$$

In Fe_2O_3, Fe constitutes 69 % by weight. In FeO, it constitutes 78 % by weight.

Table 4-1

Chemical analyses of thesis komatiites and representative komatiites from other Archean terranes.

(A)

Sample #	1 M-231	2 8	3 75D222	4 S3	5 49J	6 NG152	7 106	8 15-AB
SiO_2	43.92	44.9		41.83	45.42	47.15	42.73	46.77
Al_2O_3	6.18	5.3		3.70	3.68	5.15	4.51	4.53
Fe_2O_3	12.00	10.4		16.96	12.25	9.90	12.79	8.67
MgO	32.83	33.6		32.85	32.30	32.25	33.47	34.85
CaO	4.32	5.0		3.80	5.30	5.12	5.72	4.48
Na_2O	0.05	0.35		0.11	0.44	0.20	0.29	0.30
K_2O	0.03	0.08		0.13	0.17	0.03	0.04	0.02
TiO_2	0.34	0.19		0.34	0.20	0.22	0.22	0.20
MnO	0.27	0.18		0.25	0.22	0.14	0.24	0.15
P_2O_5	0.07	-		0.03	0.02	0.01	-	0.03
Total	100.00	100.00		100.00	100.00	100.17	100.01	100.00
Cr	2478		3200	5879		3005	3400	1322
Ni	2200			1485		1622		1435
Co	135			106		126		92
V	115			97				

Table 4-1 (continued)

(B)

Sample #	M-141	SA-2048	75D173	S833	331/783	NG7631	98	14-AB
SiO_2	43.92	45.81	47.97	47.23	46.78	47.87	47.83	45.05
Al_2O_3	7.19	7.38	6.98	6.77	4.46	6.80	6.42	5.04
Fe_2O_3	13.39	11.75	9.51	11.77	13.73	10.33	11.71	14.96
MgO	26.80	26.05	27.51	26.33	26.73	27.18	26.83	27.74
CaO	7.97	7.66	7.32	7.11	7.36	6.37	6.59	6.09
Na_2O	0.05	0.83	0.20	0.12	0.28	0.20	0.10	0.05
K_2O	0.03	0.06	0.00	0.09	0.01	0.69	0.02	0.02
TiO_2	0.42	0.27	0.39	0.29	0.42	0.33	0.31	0.71
MnO	0.22	0.21	0.11	0.19	0.20	0.19	0.18	0.27
P_2O_5	0.02	-	0.01	0.12	0.04	0.03	-	0.06
Total	100.01	99.99	99.88	100.02	100.00	99.99	99.99	99.99
Cr	3212	4100	4000	2343	2942	2857	4300	3721
Ni	1594	1700	-	1133	1229	1300	1364	1771
Co	125	-	-	95	-	127	111	112
V	127	-	-	153	137			173

Table 4-1 (continued)
(C)

	1	1	1	1	2	3	4	5	6	7
Sample	M-227	M-56	M-44	M-103	P9-120	75D113	S829	SG3	NG7625	153
SiO_2	42.88	48.93	42.87	46.84	43.64	49.31	45.67	48.78	50.61	49.36
Al_2O_3	9.31	6.81	7.50	8.04	9.27	8.13	9.99	6.63	6.63	6.25
Fe_2O_3	14.26	10.86	13.48	12.53	13.54	8.34	13.73	13.25	10.71	13.60
MgO	23.74	23.15	23.01	23.05	23.48	22.76	21.26	21.06	24.41	21.02
CaO	8.87	9.49	12.25	8.74	9.29	9.91	8.29	9.18	6.60	8.75
Na_2O	0.05	0.05	0.05	0.05	0.12	0.67	0.22	0.35	0.20	0.12
K_2O	0.04	0.11	0.04	0.05	0.01	0.03	0.05	0.04	0.22	0.02
TiO_2	0.57	0.36	0.40	0.48	0.44	0.59	0.53	0.36	0.36	0.63
MnO	0.28	0.21	0.30	0.15	0.21	0.19	0.20	0.29	0.21	0.25
P_2O_5	0.01	0.03	0.09	0.08	-	0.06	0.06	0.06	0.04	-
Total	100.01	100.00	99.99	100.01	100.00	99.99	100.00	100.00	99.99	100.00
Cr	3496	2212	3291	2760	3272	3500	2645	4860	3288	3400
Ni	861	876	1838	1300	980	1100	793	1150	1389	1073
Co	132	96	133	81	109	-	108	-	135	125
V	172	105	142	129	-	-	212	162	-	-

Table 4-1 (continued)
(D)

Sample	M-650	M-202	P9-187	75D042	331/784	180
SiO_2	47.50	46.81	47.85	51.29	49.74	49.06
Al_2O_3	8.69	8.59	9.83	9.70	5.22	9.59
Fe_2O_3	11.96	12.33	13.88	8.59	14.65	12.61
MgO	19.06	19.60	18.47	19.82	19.63	19.31
CaO	11.09	11.59	8.02	8.51	9.62	7.22
Na_2O	0.05	0.05	0.69	1.27	0.38	1.41
K_2O	0.95	0.08	0.04	0.05	0.02	0.04
TiO_2	0.44	0.48	0.49	0.60	0.50	0.51
MnO	0.25	0.36	0.22	0.12	0.18	0.24
P_2O_5	0.01	0.11	0.05	0.05	0.05	-
Total	100.00	100.00	100.00	100.00	99.99	99.99
Cr	2295	4017	1902	2500	2591	3600
Ni	961	1125	487		1066	
Co	115	128	--		--	
V	130	139	184		162	

PLATE 4-6 Polygonally jointed high MgO komatiitic basalt at Dry Lake 20 meters north of sample locality M-290 (map 1) on the north limb of the Lebel Syncline. The jointing is accentuated here by low weathering and locally by carbonate fill.

PLATE 4-7 Spinifex textured high MgO komatiitic basalt in the fifth sequence southeast of Beaver Lake at sample locality M-232 (map 1). The light weathering lithology near the top of the photo is a syenite dyke. The long axis of the actinolite blades in the basalt are orientated perpendicular to the local strike.

spinifex-bearing komatiites. Locally, high MgO komatiitic basalts are pillowed.

High MgO komatiitic basalts weather dark green to light green as seen in plates 4-6 and 4-7, respectively. The light green weathering varieties resemble some komatiites.

In hand specimen, these basalts are usually fine grained, dark green to light green and usually are not magnetic. In the massive polygonally jointed flows, 60 to 80 % light green to colourless tremolite-actinolite are randomly orientated in a groundmass largely of fine grained tremolite-actinolite and clinozoisite. The amphibole is darker in colour in the lower MgO members of this group, probably reflecting increased abundances of iron in the amphibole structure. The coarser amphibole is both tabular and acicular in form while the fine grained amphibole is acicular. Clinozoisite is acicular or occurs in very fine grained masses. Fine grained Mg-rich chlorite, occurs in aggregates 0.5 mm in diameter in some samples and never exceeds 10 % of the sample. Plate 4-8 is a sample showing amphibole, clinozoisite and chlorite. Fine grained euhedral biotite and sericite crosscut amphibole-clinozoisite grain boundaries and do not exceed 1 % in abundance. Fine grained euhedral to subhedral chromite is disseminated in clinozoisite.

In spinifex textured flows, parallel acicular

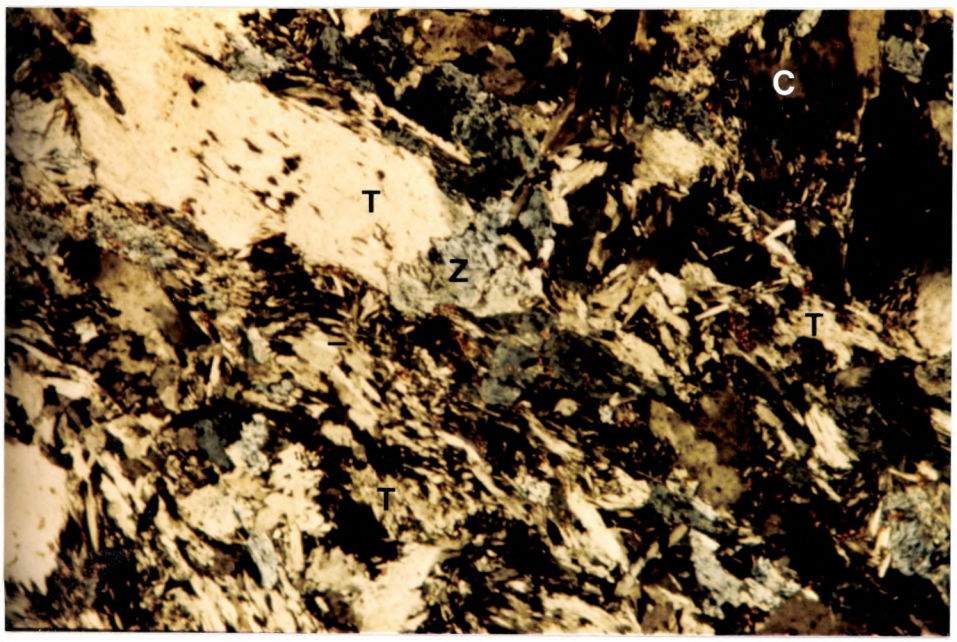

PLATE 4-8 Tabular coarse tremolite (T) with finer grained clinozoisite (Z), magnesium-rich chlorite (C) and acicular tremolite (T) in M-116. This is from sequence 3 immediately north of the Adams Mine road west of the mine site. Polarized light, x63. Field of view 1.0 x 1.5 mm.

needles of tremolite-actinolite up to 10 cm in length occur with very fine grained interstitial clinozoisite as in M-134 or with very fine grained albite as in M-232.

The high MgO komatiitic basalts in the map area are similar in composition to those from other areas noted in table 4-2 with the exception that: (1) the map area rocks almost invariably have higher K_2O abundances than those from the other areas. (2) certain high MgO komatiitic basalts with MgO abundances less than 14 % (M-116, M-213 and M-238) have anomalously high Cr, Ni and Co abundances not found in the other areas considered for comparison. The Cr, Ni and Co abundances in the three samples noted above are greater than many of the analyzed komatiites and higher than other high MgO komatiitic basalts with greater MgO abundances.

Cr content can be linked to chromite abundances. M-29 for instance has approximately 2 % chromite and 4712 ppm Cr. M-232 on the other hand has approximately 0.5 % chromite and 1219 ppm Cr.

Both M-29 with 1368 ppm Ni and M-232 with 458 ppm Ni have trace amounts of sulphides. Most of this is pyrite with lesser amounts of pyrrhotite and chalcopyrite. Neither sample is magnetic.

The anomalously high K_2O abundances in the basalts can be linked to the presence of minor amounts (1 %) of biotite and sericite. These minerals are rare in basalts from the other localities reviewed.

Table 4-2 (notes)

Chemical analyses of thesis map area high MgO komatiitic basalts and those from other Archean terranes.

Locations

1. Thesis map area
2. Munro Township, Ontario
3. Destor Township, Quebec
4. Finland
5. Barberton Belt, South Africa
6. Zimbabwe, Rhodesia
7. Yilgarn Block, Western Australia
8. Pilbara Block, Western Australia

References

P9-223, P9-226: (Arndt and Nesbitt, 1982)
75D128, 75D039, 75D015, 75D017: (Gelinas, 1979b)
S831, SU3: (Jahn et al., 1980)
NG120, BL32, NG34: (Nisbet et al., 1977)
331/779: (Nesbitt et al., 1979)
55, 159: (Naldrett and Turner, 1977)
331/337: (Sun and Nesbitt, 1978)

N.B. The samples are divided into three groups based on MgO content:

A: MgO contents are greater than 16 % and up to 18 %
B: MgO contents are greater than 14 % and up to 16 %
C: MgO contents are greater than 12 % and up to 14 %

Sample	1 M-163	1 M-59	1 M-98
SiO_2	49.20	47.47	48.06
Al_2O_3	9.85	10.84	9.71
Fe_2O_3	9.41	12.86	11.73
MgO	16.57	17.24	16.38
CaO	12.18	9.47	11.62
Na_2O	0.63	0.05	1.34
K_2O	0.75	1.24	0.35
TiO_2	0.60	0.57	0.53
MnO	0.21	0.26	0.22
P_2O_5	0.60	0.00	0.05
Total	100.00	100.00	99.99
Cr	1131	1550	2413
Ni	511	593	688
Co	81	103	95
V	114	168	154

Table 4-2
(A)

2	3	4	5	6	7	8
	75D128			NG120	55	331/337
	52.83			50.10	49.06	51.87
	9.57			10.90	9.74	9.94
	7.89			11.59	12.65	10.64
	17.27			17.99	17.81	16.51
	10.38			7.63	8.72	9.07
	1.32			0.85	1.18	0.98
	0.00			0.02	0.06	0.34
	0.58			0.64	0.52	0.39
	0.12			0.20	0.24	0.23
	0.04			0.05	-	0.04
	100.00			100.00	99.98	100.01
	2800			706	3100	
				200	581	
				97	108	

Table 4-2 (continued)

Sample	M-55	M-26	M-272	P9-223	75D039 (B)	S831	331/779	BL32	159
SiO_2	48.39	49.55	49.89	50.32	53.73	49.29	53.94	53.63	46.63
Al_2O_3	10.28	7.86	7.97	8.42	1.24	11.37	4.44	11.45	11.81
Fe_2O_3	12.57	12.88	14.21	11.82	7.68	11.44	11.16	9.19	12.00
MgO	15.05	15.56	14.40	14.77	15.67	15.72	15.02	14.50	15.19
CaO	10.70	12.33	12.18	13.62	9.06	9.61	12.77	10.24	12.96
Na_2O	1.45	0.68	0.42	0.31	2.64	1.70	1.90	0.07	0.34
K_2O	0.62	0.28	0.26	0.03	0.04	0.05	0.05	0.01	0.35
TiO_2	0.57	0.44	0.31	0.42	0.72	0.55	0.50	0.65	0.48
MnO	0.24	0.31	0.37	0.24	0.16	0.18	0.18	0.18	0.24
P_2O_5	0.12	0.12	0.00	0.04	0.06	0.07	0.04	0.06	-
Total	99.99	100.01	100.01	99.99	101.00	99.98	100.00	99.98	100.00
Cr	1859	2636	2391	2058	2600	2067	2304		3400
Ni	366	950	1109	461	800	622	421		549
Co	70	84	120	-	-	85	-		108
V	179	121	118	160	-	225	174		-

Table 4-2 (continued)

(C)

Sample	1 M-134	1 M-116	1 M-127	1 M-213	1 M-238	2 P9226	3 75D015	3 75D017	4 SU3	6 NG34
SiO_2	50.39	49.45	49.42	50.64	45.55	51.07	51.50	52.68	49.49	52.83
Al_2O_3	11.54	11.01	12.42	8.04	13.26	12.20	12.25	12.93	11.49	10.67
Fe_2O_3	12.43	10.66	12.20	12.86	15.63	11.60	9.93	10.23	12.05	10.29
MgO	12.59	14.24	12.29	13.89	13.30	12.20	13.71	13.64	13.52	13.35
CaO	9.02	11.81	9.58	12.00	8.92	8.52	8.75	8.86	11.52	9.91
Na_2O	2.18	0.98	2.90	0.83	0.98	3.39	2.84	0.60	0.90	2.11
K_2O	1.97	0.82	0.12	0.93	1.07	0.09	0.08	0.03	0.34	0.06
TiO_2	0.57	0.60	0.71	0.42	0.81	0.67	0.70	0.78	0.42	0.56
MnO	0.21	0.29	0.22	0.31	0.46	0.19	0.18	0.15	0.24	0.18
P_2O_5	0.00	0.13	0.15	0.08	0.03	0.07	0.05	0.08	0.05	0.04
Total	99.90	99.99	100.01	100.00	100.01	100.00	99.99	99.98	100.00	100.00
Cr	1029	4642	1709	3173	3174	1089	1500	2400	1198	
Ni	287	1228	390	1958	1216	285	--	--	211	
Co	79	84	66	166	140	--	--	--	55	
V	173	167	212	128	243	237	--	--	223	

4-4 Low MgO Komatiitic Basalts

In the field, low MgO komatiitic basalts are best distinguished from high MgO komatiitic basalts by the absence of a rugged, weathered surface caused by recessive weathering of polygonal joints. These basalts are commonly but not always smoother weathering. Approximately 70 % of these basalts are polygonally jointed. The jointing shows up best when accentuated by quartz veins or syenite dykelets. Locally, polygonal jointing is observed to grade upwards into a flow top breccia. Many basalts are pillowed and variolitic (plate 4-9).

Low MgO komatiitic basalts weather to a medium to dark green colour. In hand specimen, they are black to dark grey and are commonly fine grained. These basalts are not as hard as low MgO komatiitic andesites but it is sometimes difficult to discriminate between the two in the field.

Low MgO komatiitic basalts consist of 50 to 60 % actinolite, 0 to 30 % clinozoisite, 20 to 45 % albite, up to 2 % chromite, up to 1 % sericite and trace amounts of epidote, and sulphide. Texturally, the basalts can be divided into two groups, these are:

(1) acicular pyroxene basalt.

(2) pyroxene phyric basalt.

One should bear in mind that all original pyroxene has been replaced by actinolite. Basalts regarded as pyroxene phyric have tabular actinolite in addition to acicular actinolite.

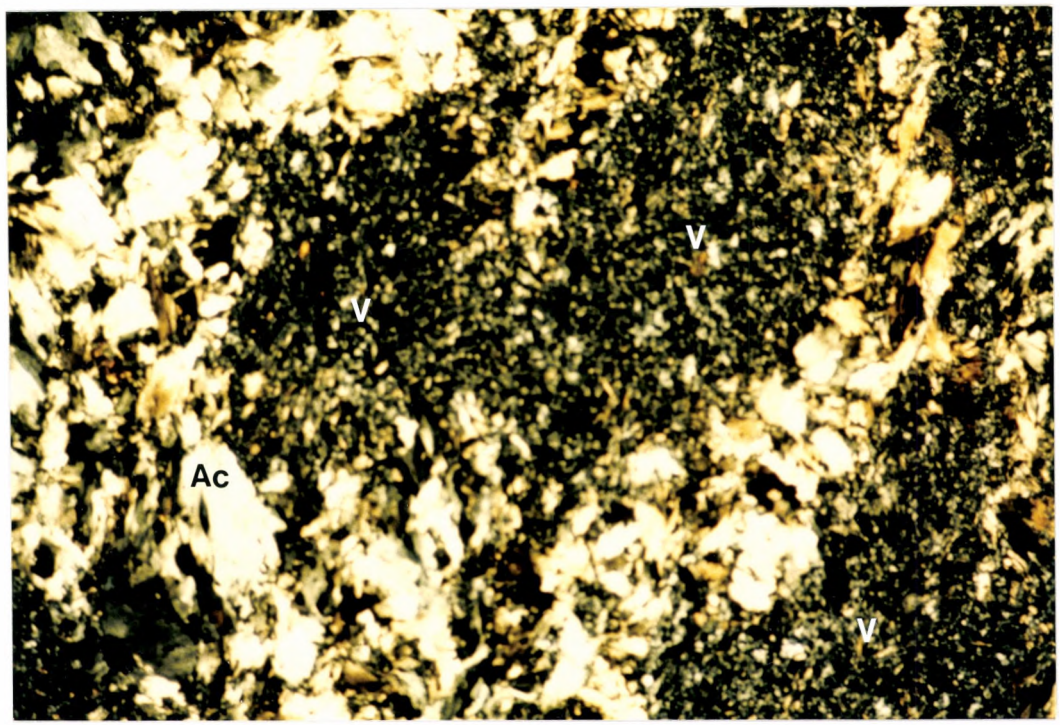

PLATE 4-9 Variolites (V) comprised of quartz and albite are separated by thin zones of actinolite (Ac) in M-2, (map 1) a basalt from sequence 4 west of the mine site. Polarized light, x25. Field of view 2.5 x 4.0 mm.

Actinolite is hosted by albite and clinozoisite. Acicular pyroxene types have acicular actinolite only, either randomly orientated or with grains arranged parallel to one another (spinifex texture). Actinolite is hosted by a groundmass of albite. Clinozoisite is absent. Where actinolite needles are widely spaced, the white weathering of the albite-rich groundmass gives the outcrop a gabbroic appearance (plate 4-10).

As can be seen in table 4-3, six of nine analyzed low MgO komatiitic basalts from the south limb of the Lebel Syncline have uniquely high Cr, Ni and Co abundances when compared to those in other Archean terranes. Low MgO komatiitic basalts are found on the north limb. M-298 and M-280 from the Dry Lake area do not have the unusual high Cr, Ni and Co abundances.

M-69 with 3105 ppm Cr and 850 ppm Ni has approximately 2 % chromite and trace amounts of sulphide. M-298 with 603 ppm Cr and 152 ppm Ni has trace amounts of chromite and sulphide. The sulphide in both samples is mostly pyrite with little visible pyrrhotite.

4-5 Low MgO Komatiitic Andesites

Low MgO komatiitic andesites overlie high or low MgO komatiitic basalts or komatiites on the south limb of the Lebel Syncline west of the mine site. Shown in plates 4-11 and 4-12 are polygonally jointed andesite flows which

PLATE 4-10 Acicular actinolite orientated parallel to one another and perpendicular to the local strike. The abundant white weathering albite-rich matrix gives the outcrop a gabbroic look. This texture is found at Dry Lake and at North Lake on the north limb of the Lebel Syncline. Sample M-298 was taken from the outcrop shown here.

Table 4-3 (notes)

Chemical analyses of thesis map area low MgO komatiitic basalts and those from other Archean terranes.

Locations

1. Thesis map area
2. Munro Township, Ontario
3. Destor Township, Quebec
4. Finland
5. Barberton Belt, South Africa
6. Zimbabwe, Rhodesia
7. Yilgarn Block, Western Australia
8. Pilbara Block, Western Australia

References

P9-178, P9-179, P9-180: (Arndt and Nesbitt, 1982)
75D012: (Gelinas, 1979b)
S252, S261: (Jahn et al., 1980)
331/780, LV4: (Nesbitt et al., 1979)
NG133, BL22, BL26: (Nisbet et al., 1977)
162, 154, 139: (Naldrett and Turner, 1977)
7-NSB (Average of six): (Glikson and Hickman, 1981)
11-CB (Average of six): (Glikson and Hickman, 1981)

N/B. The samples are divided into three groups based on MgO content:

A: MgO contents are greater than 10 % and up to 12 %
B: MgO contents are between 8 and 10 %
C: MgO contents are less than 8 %

Table 4-3
(A)

Sample	1 M-298	1 M-177	1 M-436	1 M-404	1 M-160	2 P9178	3 75D012	4	5 331/780	6 NG133	7 139	8 Z-NSB
SiO_2	50.39	51.27	50.05	50.62	53.00	50.14	53.91		53.17	54.34	50.99	53.23
Al_2O_3	13.05	11.65	11.09	13.48	10.10	13.09	13.52		8.18	11.24	11.74	12.08
Fe_2O_3	12.76	12.28	13.91	9.40	9.80	12.79	7.58		11.93	10.69	12.40	9.33
MgO	10.43	11.27	10.84	11.81	11.04	10.44	11.66		11.87	11.62	11.06	11.90
CaO	8.76	10.02	10.36	8.73	10.84	10.26	8.35		11.58	8.74	10.35	11.27
Na_2O	2.30	2.23	2.38	3.49	2.01	2.05	3.85		2.30	2.58	2.58	0.81
K_2O	1.43	0.10	0.32	1.49	1.49	0.04	0.01		0.04	0.02	0.11	0.39
TiO_2	0.66	0.61	0.59	0.75	0.82	0.66	0.84		0.67	0.56	0.57	0.64
MnO	0.17	0.46	0.40	0.17	0.20	0.19	0.23		0.19	0.19	0.20	0.23
P_2O_5	0.06	0.10	0.06	0.04	0.71	0.06	0.05		0.07	0.03	-	0.11
Total	100.00	99.99	100.00	99.98	100.01	100.00	100.00		100.00	100.01	100.00	99.99
Cr	603	5932	2958	881	527	1060	4000		904		1200	875
Ni	152	1334	2124	194	106	162			138		199	216
Co	81	193	168	89	59						87	51
V	205	192	182	205	173	251			238		-	264

Table 4-3 continued
(B)

Sample	1 M-117	1 M-143	1 M-47	1	2 P9-179	3	4 S252	5 LV4	6 BL22	7 154	8 11-CB
SiO_2	51.05	51.02	52.73		51.07		47.51	51.07	50.80	51.55	51.08
Al_2O_3	15.09	12.99	11.91		13.18		15.38	14.42	15.88	15.14	15.19
Fe_2O_3	9.15	13.51	13.04		12.57		12.98	10.98	10.35	9.25	9.13
MgO	9.59	8.95	8.69		9.47		10.01	8.94	8.47	9.60	10.15
CaO	10.03	9.66	11.04		10.51		10.62	9.48	12.34	11.55	10.82
Na_2O	2.07	2.13	1.16		2.16		2.08	2.10	1.04	2.05	2.37
K_2O	2.00	0.76	0.36		0.12		0.34	2.14	0.11	0.19	0.47
TiO_2	0.82	0.61	0.61		0.67		0.77	0.61	0.77	0.51	0.59
MnO	0.16	0.34	0.33		0.19		0.22	0.20	0.17	0.16	0.20
P_2O_5	0.04	0.03	0.13		0.06		0.10	0.06	0.06	-	0.06
Total	100.00	100.00	100.00		100.00		100.01	100.00	99.99	100.00	100.00
Cr	329	3476	2847		833		325	330		800	697
Ni	152	1386	885		124		212	160		158	177
Co	92	194	134				56			72	
V	221	190	178		256		281	255			

Table 4-3 (continued)
(C)

Sample	1 M-199	1 M-97	1 M-280	2 P9-180	4 S261	6 BL26	7 162
SiO_2	53.24	52.56	52.75	50.71	48.44	53.13	50.61
Al_2O_3	14.18	14.97	13.56	13.92	15.93	15.14	14.88
Fe_2O_3	11.75	11.31	13.63	13.98	13.05	10.62	13.67
MgO	7.52	7.18	6.51	7.27	8.04	7.10	7.30
CaO	9.91	6.18	8.73	9.42	12.20	10.34	9.88
Na_2O	0.96	4.41	2.53	3.56	1.11	2.37	2.32
K_2O	1.39	2.32	0.71	0.09	0.06	0.15	0.14
TiO_2	0.72	0.78	0.79	0.75	0.86	0.87	0.96
MnO	0.24	0.20	0.54	0.23	0.20	0.19	0.24
P_2O_5	0.10	0.08	0.26	0.07	0.09	0.07	-
Total	100.01	99.99	100.00	100.81	99.98	99.98	100.00
Cr	3022	1666	355	173	325	1046	210
Ni	946	381	181	68	168	191	140
Co	139	106	49		73	94	81
V	216	245	126		264		

PLATE 4-11 Polygonally jointed low MgO komatiitic andesite from the sixth sequence west of the mine site at sample locality M-578 (map 1). This texture was visible here only because fresh moss was stripped from the outcrop. The otherwise dried moss which cannot be scraped from the outcrop gives the outcrop a massive appearance. As viewed here, the andesite could easily be confused from a high MgO komatiitic basalt or a komatiite. This was frequently done during the first two weeks of mapping.

PLATE 4-12 Polygonally jointed low MgO komatiitic andesite from the sixth sequence near sample locality M-115 (map 1). The wide spacing between some polyhedra is due to the low weathering of an orange weathering carbonate which has filled the joints and replaced some adjoining rock.


RICOH

resemble high MgO komatiitic basalts on outcrop. Plate 4-13 shows the more common smooth weathering flow with thin joints which are not recessively weathered. The jointing is sometimes accentuated by quartz. These flows resemble low MgO komatiitic basalts on outcrop. Other komatiitic andesites are massive, fine to medium grained. Many outcrops observed on the north limb resemble flows shown in plate 4-13 and are hard and thus were mapped as komatiitic andesite. On the shores of Spider Lake, pillowed low MgO komatiitic andesites weather light green and resemble high Al_2O_3 komatiitic basalts and andesites.

Komatiitic andesites are composed of 40 to 60 % actinolite, 0 to 45 % clinozoisite, 10 to 50 % albite, up to 2 % chromite, up to 1 % sericite and trace amounts of epidote and sulphide.

On the basis of textures, komatiitic andesites are subdivided into three groups (1) pyroxene phyric (2) acicular pyroxene and (3) plagioclase phyric flows. Shown in plates 4-14 and 4-15 are examples of 2 and 1 respectively. The acicular pyroxene in plate 4-14 contains parallel actinolite up to 2 cm in length in a groundmass of fine grained acicular actinolite and a fine grained mosaic of anhedral albite. Actinolite in acicular pyroxene types is also randomly orientated, as is shown in plate 4-15. Compared to low MgO komatiitic basalts with similar textures, the andesites generally have less actinolite and more albite.

PLATE 4-13 Polygonally jointed low MgO komatiitic andesite from the sixth sequence near sample locality M-47. The thin joints weather white.

PLATE 4-14 Acicular actinolite (Ac) in a groundmass of polygonal albite (A). The actinolite is preferentially orientated in one direction - perpendicular to local strike. The section is from M-578 from the sixth sequence. Polarized light, x63. Field of view is 1.0 x 1.5 mm.

PLATE 4-15 Tabular coarse actinolite (Ac) in a groundmass of acicular actinolite and albite. The section is from M-220 at the top of sequence 3 south of the South Pit on the mine site. Polarized light, x63. Field of view is 1.0 x 1.5 mm.

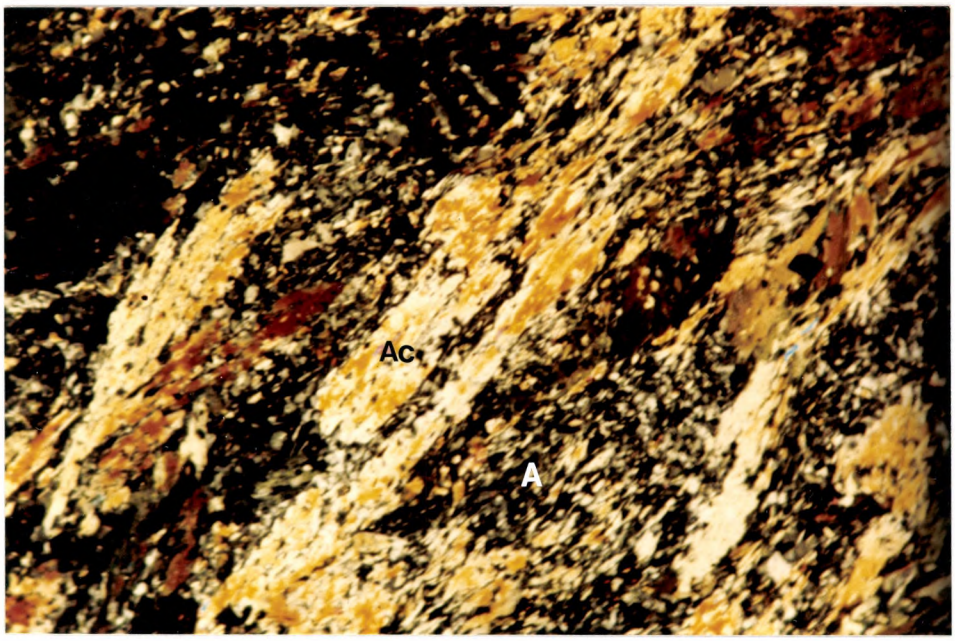
Ac
A

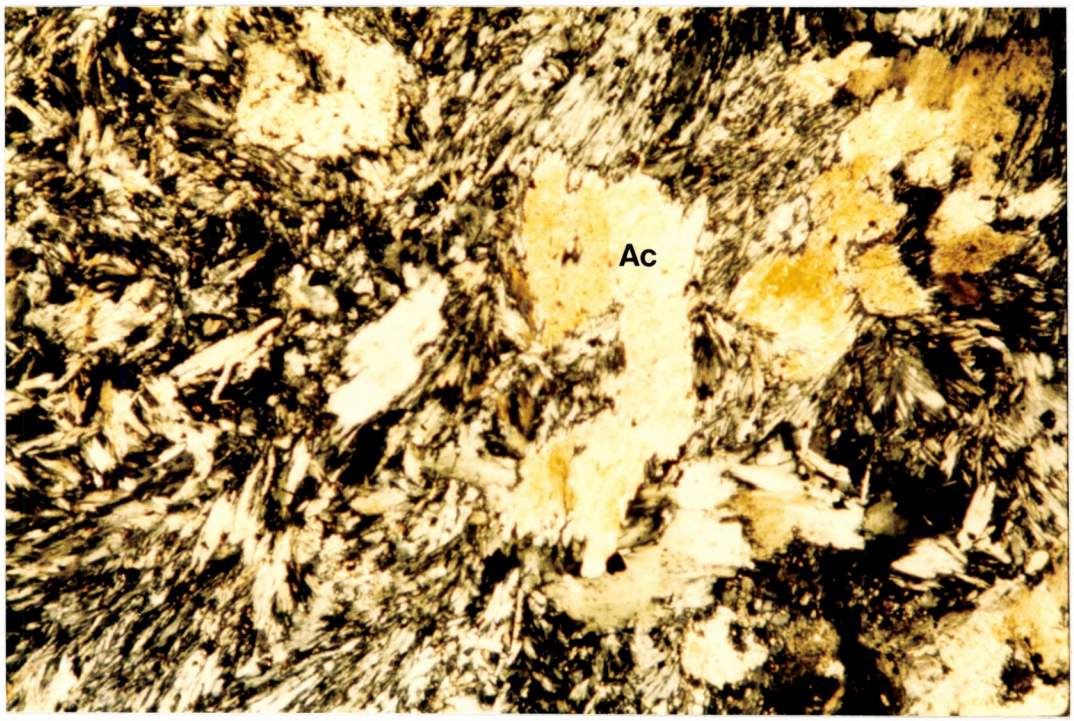
Ac

Plate 4-15 shows an example of pyroxene phyric andesite. Tabular, lathlike actinolite 0.5 mm in length makes up 5 % of the rock and is set in a fine groundmass of acicular actinolite and albite. In other andesites with this texture, albite is the only groundmass material. In plagioclase phyric flows such a M-1, stubby, high relief clinozoisite pseudomorphs presumably after plagioclase rest in an optically continuous groundmass of actinolite.

The analyzed low MgO komatiitic andesites from the south limb of the Lebel Syncline have high Cr abundances. As seen in table 4-4, all but sample M-73 have Cr abundances > 1000 ppm. Analyzed low MgO komatiitic andesites from the north limb (M-395, M-330, M-612 and M-280) have lower Cr abundances, less than 600 ppm. The Cr-rich andesites invariably have higher Ni and Co and lower Al_2O_3 abundances than the andesites with less than 600 ppm Cr (table 4-4).

Chromite in the Cr-rich andesites shows variable relationships with the silicate minerals. In M-3, it shows no preference, occurring in acicular actinolite, in the albite groundmass and on actinolite-albite grain boundaries (plate 4-16). In M-220, chromite is most abundant in the acicular actinolite-rich matrix and is uncommon in the coarser actinolite phenocrysts (plate 4-17). In M-43, chromite is found almost exclusively in the albite-rich groundmass (plate 4-18). Chromite most commmonly occurs as disseminated, very fine grained, (0.01 to 0.02 mm) euhedral

Table 4-4 (notes)

Chemical analyses of thesis map area low MgO komatiitic andesites and those from other Archean terranes.

locations: 1. Thesis map area
3. Destor Township, Quebec
5. Barberton Belt, South Africa
6. Zimbabwe, Rhodesia
7. Yilgarn Block, Western Australia

References:
75D132, 75D018, (Gelinas, 1979b)
331/338, 331/339, (Nesbitt et al., 1979)
NG198, NG159, (Nisbet et al., 1977)

N.B.: The samples are divided into four groups based on MgO content.
A: MgO contents are greater than 10 % and up to 12 %
B: MgO contents are greater than 8 % and up to 10 %
C: MgO contents are between 6 and 8 %
D: MgO contents are less than 6 %

Table 4-4

Chemical analyses of thesis map area low MgO komatiitic andesites and representative andesites from other Archean terranes

(A)

	1	3	3	5
Sample Number	M-70	75D132	75D018	331/339
SiO_2	57.08	58.00	54.92	54.79
Al_2O_3	9.45	12.71	12.19	11.93
Fe_2O_3	11.59	6.77	8.07	10.64
MgO	11.29	11.43	11.40	11.72
CaO	7.89	7.29	9.06	7.52
Na_2O	1.65	3.07	3.54	2.72
K_2O	0.26	0.00	0.00	0.70
TiO_2	0.46	0.62	0.69	0.39
MnO	0.26	0.08	0.11	0.19
P_2O_5	0.07	0.04	0.03	0.02
Total	100.00	100.00	100.01	99.99
Cr	4551	3400	2300	
Ni	1675			
Co	110			
V	168			

(B)

	1	1	1	1	6	6
Sample Number	M-220	M-218	M-76	M-107	NG198	NG159
SiO_2	55.79	59.66	58.12	58.13	59.13	55.28
Al_2O_3	13.14	10.84	11.85	11.19	10.75	12.98
Fe_2O_3	10.49	10.60	9.71	10.85	8.02	9.28
MgO	7.99	8.19	8.81	7.99	8.53	8.23
CaO	6.36	6.85	8.38	9.66	9.28	9.60
Na_2O	4.97	2.85	1.95	0.87	3.54	3.57
K_2O	0.05	0.12	0.33	0.45	0.01	0.17
TiO_2	0.75	0.52	0.62	0.57	0.54	0.61
MnO	0.35	0.33	0.16	0.23	0.14	0.20
P_2O_5	0.11	0.02	0.08	0.08	0.05	0.07
Total	100.00	100.00	100.00	100.00	99.99	100.00
Cr	5312	5718	3539	3481		
Ni	1780	1909	945	1148		
Co	195	269	82	96		
V	239	192	208	202		

Table 4-4 (continued)

Chemical analysis of thesis map area low MgO komatiitic andesites and representative andesites from other Archean terranes

				(C)			
	1	1	1	1	1	1	1
Sample Number	M-1	M-3	M-124	M-578	M-269	M-340	M-612
SiO_2	57.37	61.97	55.95	57.33	56.76	57.12	57.72
Al_2O_3	12.43	11.97	12.17	14.49	12.53	12.37	14.72
Fe_2O_3	9.10	7.53	11.31	8.16	10.56	10.58	8.33
MgO	6.54	6.74	7.06	6.00	7.51	7.88	7.07
CaO	12.44	6.35	10.55	8.74	9.53	9.04	7.42
Na_2O	0.89	4.38	0.94	3.68	1.90	2.06	3.27
K_2O	0.24	0.08	0.87	0.62	0.35	0.10	0.46
TiO_2	0.65	0.67	0.67	0.68	0.63	0.61	0.71
MnO	0.24	0.22	0.32	0.24	0.21	0.23	0.14
P_2O_5	0.09	0.09	0.16	0.06	0.02	0.00	0.16
Total	100.00	100.00	100.00	100.00	100.00	100.00	100.00
Cr	2433	4596	2517	1202	3146	3255	268
Ni	611	1043	603	303	1134	1032	143
Co	67	96	70	112	192	175	63
V	196	215	214	228	193	195	119

				(D)		
	1	1	1	1	1	1
Sample Number	M-126	M-11	M-106	M-395	M-330	M-73
SiO_2	56.48	55.45	59.62	55.78	58.37	58.12
Al_2O_3	14.79	14.88	13.38	15.66	15.38	14.95
Fe_2O_3	9.80	9.54	9.12	8.65	8.88	9.71
MgO	5.71	5.31	4.87	5.78	4.73	4.70
CaO	9.34	8.35	8.88	9.67	6.90	6.57
Na_2O	2.05	5.00	2.68	2.98	3.65	2.29
K_2O	0.76	0.31	0.60	0.07	0.94	2.36
TiO_2	0.79	0.81	0.66	0.89	0.76	0.81
MnO	0.22	0.26	0.21	0.30	0.26	0.24
P_2O_5	0.05	0.09	0.13	0.20	0.13	0.26
Total	100.00	100.00	100.00	100.00	100.00	100.00
Cr	2463	1068	2976	560	333	407
Ni	805	203	708	195	142	58
Co	139	57	165	75	74	47
V	214	248	206	154	127	130

PLATE 4-16 Chromite grains clustered with actinolite (Ac) and albite (A) in M-3 from sequence 4. Plain transmitted light, x63. Field of view is 1.0 x 1.5 mm.

PLATE 4-17 Very fine disseminations of chromite hosted by actinolite (Ac) in M-220 from the top of sequence 3. Plain transmitted light, x63. Field of view is 1.0 x 1.5 mm.

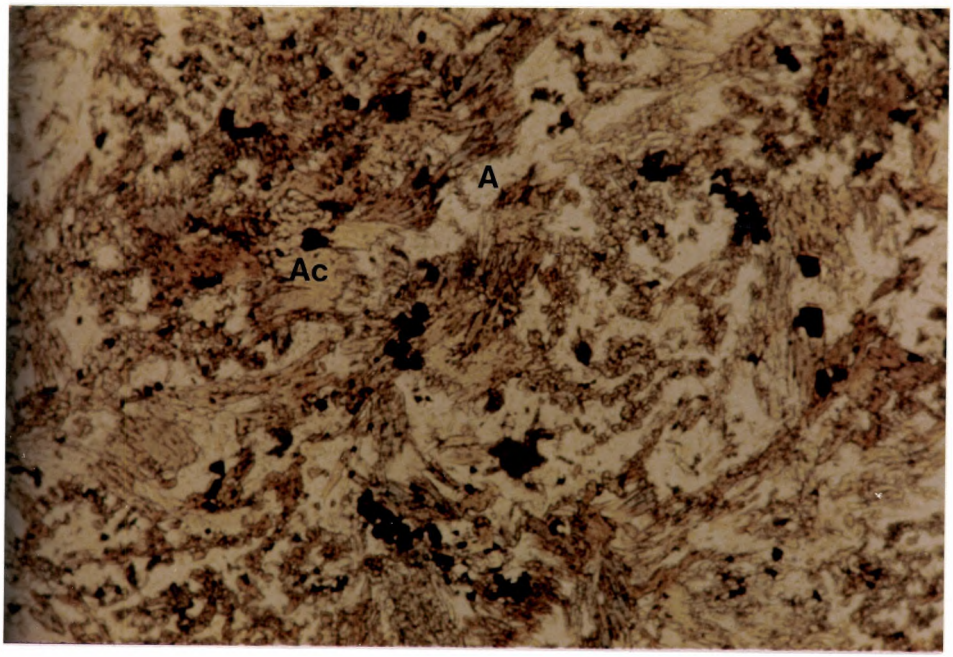
A
Ac

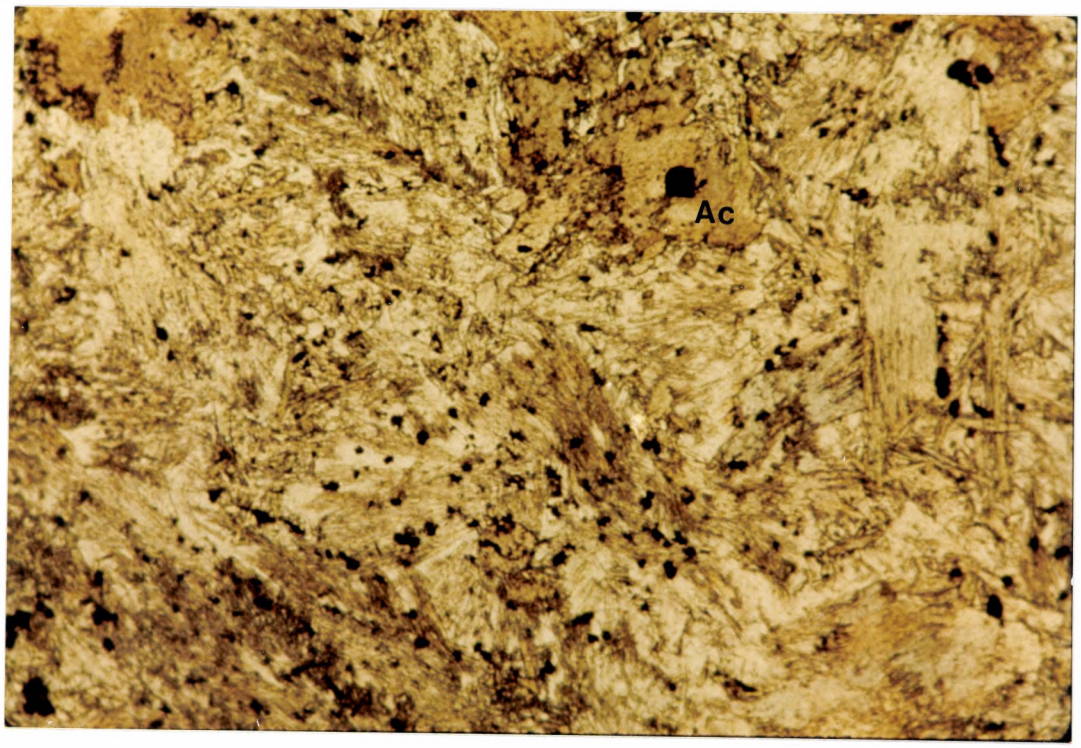
Ac

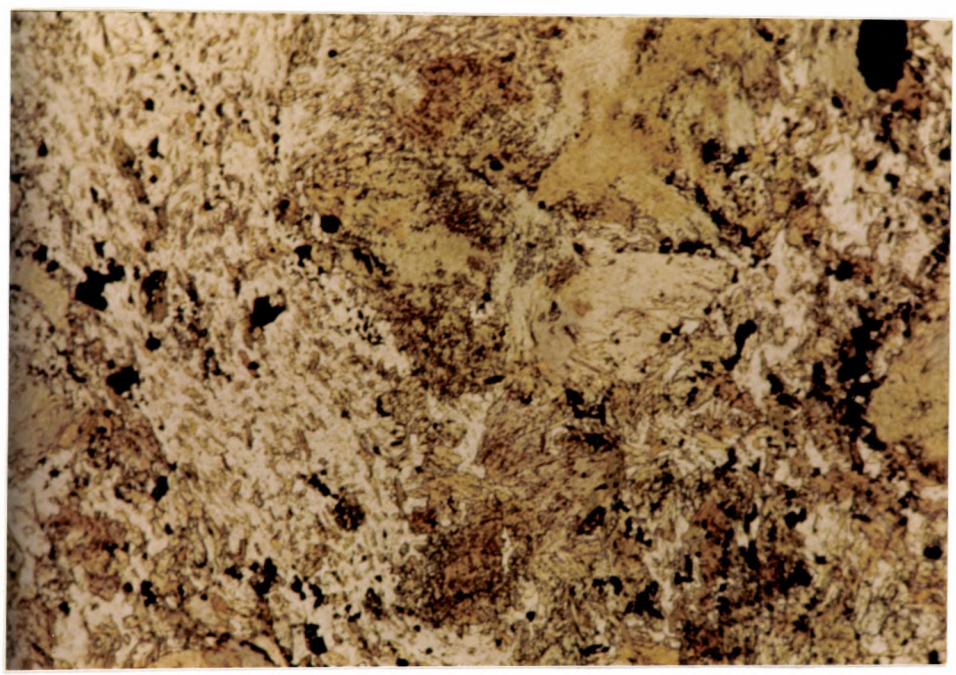

PLATE 4-18 Chromite concentrated in the albite-rich matrix in M-43 from sequence 4, plain transmitted light x63. Field of view is 1.0 x 1.5 mm.

to anhedral grains. Locally, chromite clusters make aggregates up to 0.05 mm in diameter which are in contact with both actinolite and albite.

Fine grained, anhedral pyrite is present in trace amounts and occurs either in contact with chromite or in contact with silicates. The textures and spatial relationships chromite and sulphide show with the silicates in these andesites resembles those observed in the low MgO komatiitic basalts.

The Cr, Ni and Co abundances in the south limb low MgO komatiitic andesites are similar to those in most analyzed low MgO komatiitic basalts from the south limb but greater than most analyzed high MgO komatiitic basalts and komatiites. This is seen in table 4-5.

High SiO_2, low MgO volcanics of komatiitic affinity have been reported in the literature from:

(1) Destor Township, Quebec, (Gelinas, 1979b)

(2) Munro Township, Ontario, (Arndt et al., 1977)

(3) Belingwe, Zimbabwe, (Nisbet et al., 1977)

(4) Pilbara Block, Whim Creek Group, (Sun and Nesbitt, 1978)

(5) Finnish greenstone belts (Auvray et al., 1982, Jahn et al., 1980)

The high SiO_2 (SiO_2>54%), low MgO (MgO<12%) volcanics are referred to as andesitic komatiites by Arndt et al. (1977) and Gelinas (1979b). In both localities, they

Table 4-5

Comparison of the chemical compositions of a representative low MgO komatiitic andesite, basalt, high MgO komatiitic basalt and komatiite from the south limb of the Lebel Syncline.

	Low MgO komatiitic andesite	Low MgO komatiitic basalt	High MgO komatiitic basalt	komatiite
Sample	M-220	M-413	M-26	M-56
SiO_2	55.79	51.02	49.55	48.93
Al_2O_3	13.14	12.99	7.86	6.81
Fe_2O_3	10.49	13.51	12.88	10.86
MgO	7.99	8.95	15.56	23.15
CaO	6.36	9.66	12.33	9.49
Na_2O	4.97	2.13	0.68	0.05
K_2O	0.05	0.76	0.28	0.11
TiO_2	0.75	0.61	0.44	0.36
MnO	0.35	0.34	0.31	0.21
P_2O_5	0.11	0.03	0.12	0.03
Total	100.00	100.00	100.00	100.00
Cr	5312	3476	2636	2295
Ni	1780	1386	950	961
Co	195	194	84	115
V	239	190	121	130

are minor in abundance relative to associated basalts and komatiites. Nesbitt et al. (1977) refer to high SiO_2 volcanics at Belingwe as basaltic andesites and andesites. They note that these flows are not abundant and occur with the more abundant basalts which are interlayered with and show complete gradations from komatiites. Sun and Nesbitt (1978) give major element compositions of andesites in a table of komatiites and komatiitic volcanics. Jahn et al (1980) show three analyses of volcanics in the komatiitic series from Finnish greenstone belts with SiO_2 > 54 % in TiO_2 versus SiO_2 variation diagram. Auvray et al (1982) note that a komatiite series in Finnish greenstone belts covers the entire range of composition from ultramafic cumulates to andesites (SiO_2 approximately equal to 55 %, MgO approximately equal to 4 %). Sun and Nesbitt (1978), Jahn et al. (1980) and Auvray et al. (1982) do not state the relative abundances of the andesites to basalts (komatiitic) and komatiites. However, they do not appear to be abundant in these areas, as they are referred to only briefly.

The low MgO komatiitic andesites in the map area are similar in terms of major element compositions to the andesites shown in table 4-4. High Cr, Ni and Co komatiitic volcanics are reported only from the komatiitic andesites in Destor Township (Gelinas, 1979b).

4-6 Low Al_2O_3 Komatiitic Dacites

Two samples, M-31 and M-115 are regarded as low Al_2O_3 komatiitic dacites. Their locations are shown on map 1 and their chemical compositions are shown in table 4-6.

M-31 was taken near the top of sequence 3 which is dominated volumetrically by low MgO komatiitic andesites. In the field, M-31 was mapped as a low MgO komatiitic andesite. It has vague polygonal jointing. M-31 consists essentially of a mat of very fine grained, acicular actinolite (45 %) and albite (55 %). Petrographically it resembles M-220, a low MgO komatiitic andesite, which outcrops 400 meters along strike to the east.

M-115 is taken near the top of sequence 8 near Beaver Lake (figure 3-12). Sequence 8 is comprised of komatiites, komatiitic basalts and andesites. The jointing in M-115 weathers low, making the outcrop resemble some high MgO komatiitic basalts. The outcrop was mapped as a low MgO komatiitic basalt. M-115 is regarded as a plagioclase phyric flow, resembling the basalts in sequence 8. It contains 15 % clinozoisite, 40 % albite and 45 % actinolite.

Both M-115 and M-31 have high Cr abundances, 3735 ppm and 4286 ppm, respectively, and are part of sequences with this feature (See appendix A). Both have approximately 2 % chromite. Comparing M-31 to komatiitic andesites in sequence 3 (see appendix A), the dacite has higher SiO_2 and low Al_2O_3, Fe_2O_3, MgO and CaO abundances.

Table 4-6

Major element, Cr, Ni, Co and V abundances for low Al_2O_3 komatiitic dacites

	M-31	M-115
SiO_2	65.61	63.71
Al_2O_3	10.69	10.13
Fe_2O_3	8.66	7.55
MgO	4.96	7.72
CaO	5.99	6.88
Na_2O	2.33	2.85
K_2O	0.93	0.39
TiO_2	0.55	0.49
MnO	0.20	0.22
P_2O_5	0.08	0.07
Total	100.00	100.00
Cr	4286	3735
Ni	799	927
Co	312	73
V	149	180

Low Al_2O_3 komatiitic dacites are a small component (volumetrically) of the volcanic pile.

4-7 High Al_2O_3 Komatiitic Basalts and Andesites

High Al_2O_3 komatiitic basalts and andesites are abundant on the mine site in the eastern part of the map area. They are rare west and northwest of the mine site. In map area NB-1, they are the predominate volcanic lithology (maps 3,4) . They are present in map area NB-2 where they overlie low MgO komatiitic basalts which in turn overlie komatiites. Immediately south of the South Pit, and in two locations west of the mine site they abruptly overlie high MgO komatiitic basalts and komatiite.

All of the high Al_2O_3 basalts and andesites in the thesis map area appear to be flows as evidenced by pillow selvages. The flows weather beige, white to light green (plate 4-19), are invariably very fine grained and are light to dark grey in colour on their fresh surfaces. They are not polygonally jointed nor do they have spinifex textures. In outcrop and in hand specimen, they can resemble some low MgO komatiitic andesites as previously noted in section 4-5.

They are composed of 50 to 70 % randomly orientated tabular to acicular actinolite (0.1 mm in length) in a very fine grained albite groundmass (plate 4-20). Very fine grained opaque minerals occur in both the amphibole and albite and make up to 0.5 % of the samples studied.

PLATE 4-19 Pillowed high Al_2O_3 komatiitic basalt observed at sample locality M-182 immediately north of the South Pit. The pillow selvages are 1 to 3 cm thick and weather a dark, rusty brown, in contrast to the beige weathering interior.

PLATE 4-20 Fine grained high Al_2O_3 komatiitic basalt (M-174) from the fifth sequence at the southeast edge of the South Pit. Polarized light, 25x. Field of view is 2.5 x 4.0 mm.

The major element composition and Cr, Ni, Co and V abundances are given in table 4-7 for three high Al_2O_3 komatiitic basalts and two high Al_2O_3 komatiitic andesites from the thesis map area. These volcanics have greater than 17 % Al_2O_3, less than 6 % MgO, less than 500 ppm Cr and variable K_2O abundances.

The two high Al_2O_3 komatiitic andesites differ sharply from representative low MgO komatiitic andesites in that they are significantly lower in MgO, Cr and Ni (table 4-8). The average TiO_2 content for the five analyzed Al_2O_3 rich samples in table 4-7 is 0.59 % which is lower than the average TiO_2 contents of ten low MgO komatiitic basalts (0.71 %) and eighteen low MgO komatiitic andesites (0.68 %).

Some low MgO komatiitic andesites (M-330, M-395 and M-73) which can be mistaken for high Al_2O_3 komatiitic andesites in the field have similar low Cr and Ni abundances (table 4-8) characteristic of the high Al_2O_3 volcanics. In particular, both have low Cr and Ni abundances.

The high Al_2O_3 komatiitic basalts and andesites in the map area resemble calc-alkalic basalts and andesites from the Blake River Group of cycle II north of Kirkland Lake and the average calc-alkalic basalts and andesites from the Superior Province in terms of most major elements. Representative samples from the thesis area and averages from Jolly (1975) and Goodwin (1977) are compared in table 4-9. The thesis map area samples are notably higher in MgO,

Table 4-7

Major element, Cr, Ni, Co and V abundances for high Al_2O_3 komatiitic basalts and andesites

	High Al_2O_3 komatiitic basalt			High Al_2O_3 komatiitic andesite	
	M-302	M-105	M-185	M-174	M-353
SiO_2	48.48	52.80	53.24	54.31	56.02
Al_2O_3	18.51	18.42	17.17	18.16	17.32
Fe_2O_3	10.29	7.17	11.93	11.22	9.68
MgO	5.43	3.28	3.93	3.43	2.26
CaO	12.53	11.38	9.29	7.40	10.03
Na_2O	3.30	2.66	2.02	2.19	1.56
K_2O	0.46	3.27	0.88	2.16	2.28
TiO_2	0.62	0.58	0.56	0.63	0.58
MnO	0.30	0.23	0.36	0.48	0.26
P_2O_5	0.06	0.19	0.02	0.02	0.01
Total	100.00	100.00	100.00	100.00	100.00
Cr	422	410	214	422	405
Ni	84	25	67	123	45
Co	88	27	56	115	66
V	255	194	48	256	200

Table 4-8

Comparison of the major element, Cr, Ni, Co and V contents between representative low MgO komatiitic andesites and the two analyzed high Al_2O_3 komatiitic andesites.

	low MgO komatiitic andesites				high Al_2O_3 komatiitic andesites	
	M-395	M-330	M-220	M-1	M-174	M-353
SiO_2	55.78	58.37	55.79	57.37	54.31	56.02
Al_2O_3	15.66	15.38	13.14	12.43	18.16	17.32
Fe_2O_3	8.65	8.88	10.49	9.10	11.22	9.68
MgO	5.79	4.73	7.99	6.54	3.43	2.26
CaO	9.67	6.90	6.36	12.44	7.40	10.03
Na_2O	2.98	3.65	4.97	0.89	2.19	1.56
K_2O	0.07	0.94	0.05	0.24	2.16	2.28
TiO_2	0.89	0.76	0.75	0.65	0.63	0.58
MnO	0.30	0.26	0.35	0.24	0.48	0.26
P_2O_3	0.20	0.13	0.11	0.09	0.02	0.01
Total	100.00	100.00	100.00	100.00	100.00	100.00
Cr	520	333	5312	2433	422	405
Ni	195	142	1718	611	123	45
Co	75	74	195	67	115	66
V	154	127	239	196	256	200

N.B. M-395 and M-330 are representative of analyzed low MgO komatiitic andesites on the north limb of the Lebel Syncline. M-220 and M-1 are representative of analyzed low MgO komatiitic andesites on the south limb. M-220 and M-1 are from sequence 3. M-174 is from sequence 5.

Table 4-9

Comparison of the major element, Cr, Ni and Co contents of high Al_2O_3 komatiitic volcanics and calc-alkalic volcanics.

	1	2	3	4	5	6	7	8	9
SiO_2	49.23	53.07	48.48	52.90	53.24	54.31	59.64	57.59	56.02
Al_2O_3	18.13	17.73	18.51	17.80	17.17	18.16	16.86	16.54	17.32
Fe_2O_3	10.21	9.33	10.29	9.64	11.93	11.22	6.91	8.45	9.68
MgO	5.70	6.16	5.43	5.65	3.93	3.43	4.43	4.29	2.26
CaO	10.84	8.66	12.53	7.88	9.29	7.40	5.92	7.02	10.03
Na_2O	3.87	3.03	3.30	4.09	2.02	2.19	4.00	4.21	1.56
K_2O	0.59	0.57	0.46	0.71	0.88	2.16	1.03	0.84	2.28
TiO_2	1.28	1.05	0.62	1.20	0.56	0.63	0.85	0.96	0.58
MnO	0.15	0.20	0.30	0.13	0.36	0.48	0.21	0.11	0.26
P_2O_5		0.19	0.06	-	0.02	0.02	0.15		0.01
Total	99.99	100.00	100.00	99.99	100.00	100.00	99.99	100.00	100.00
Cr	108	176	422	95	214	422	105		405
Ni	170	131	45	155	67	123	112		45
Co		34	66		56	115	27		66

1. Average of 8 Basalts, Blake River Group (Jolly, 1975).
2. Average of 180 Basalts, Superior Province (Goodwin, 1977).
3. M-302, thesis map area.
4. Average of 28 Basaltic Andesites, Blake River Group (Jolly, 1975).
5. M-185, thesis map area.
6. M-174, thesis map area.
7. Average of 386 Andesites, Superior Province, (Goodwin, 1977).
8. Average of 15 Andesites, Blake River Group (Jolly, 1975).
9. M-353, thesis map area.

N.B. The basalts, basaltic andesites and andesites above are designated as calc-alkaline following Irvine and Baragar, (1971).

K_2O and Cr and lower in TiO_2.

It is not possible to compare the thesis map area high Al_2O_3 komatiitic volcanics to others found in a similar geological association with komatiites. This relationship is not observed elsewhere in the Archean to the author's knowledge. High Al_2O_3 volcanics referred to as calc-alkalic are spatially associated with komatiitic volcanics but not in the manner (komatiites overlain by less magnesium-rich flows) observed in the Adams Mine site.

Viljoen et al. (1982) report that quartz-sericite felsic tuffs of calc-alkalic affinity are intercalated with komatiites and komatiitic basalts in the Barberton Belt in South Africa. However, these rocks may be sedimentary but if volcanic, then they are likely distal and perhaps contemporaneous but not necessarily related to the komatiites in one volcanic sequence. Barley et al. (1984) report that in the Warrawonna Group in the Pilbara Block of western Australia, tholeiitic lava sequences are intercalated and interfinger with calc-alkalic volcanics. Minor amounts of komatiitic volcanics are locally associated with the tholeiites. Although Barley considers the tholeiites and komatiites to be partly contemporaneous with calc-alkalic volcanism, there is no mention of stratigraphic relationships such as those found in the Larder Lake Group.

4-8 High Fe_2O_3, Al_2O_3 Komatiitic Basalt

Immediately north of the South Pit, pillowed high Fe_2O_3, Al_2O_3 komatiitic basalt is characterized by very fine grain size, black colour on fresh surfaces, and is magnetic. Due to poor exposure, it was not established whether this lithology overlies, underlies or is intercalated with high Al_2O_3 komatiitic basalt in this locality. However, Norbert Blum (personal communication) has observed that this rock type stratigraphically overlies the high Al_2O_3 flows south of the Peria Pit.

Petrographically, the high Fe_2O_3, Al_2O_3 komatiitic basalt (M-197) resembles M-174, a high Al_2O_3 komatiitic andesite except that M-197 has 1 to 2 % opaque minerals (magnetite) versus 0.5 % in M-174. The higher magnetite content in M-197 is expressed in the major element chemistry in that the high Fe_2O_3, Al_2O_3 komatiitic basalt has very high, distinctive and unique Fe_2O_3 abundances when compared to the high Al_2O_3 komatiitic basalt (table 4-10). However, other than Fe_2O_3, M-197 resembles the three high Al_2O_3 komatiitic basalt samples in table 4-10 in terms of major element, Cr and Ni contents. In particular, M-197 has very low MgO, TiO_2, Cr and Ni contents and high Al_2O_3 contents which are characteristic of the high Al_2O_3 komatiitic basalt.

Volcanic rocks as rich in Fe_2O_3 as the Adams Mine area high Fe_2O_3, Al_2O_3 komatiitic volcanics are not common

Table 4-10

Comparison of the major element, Cr, Ni, Co and V abundances for the one high Fe_2O_3, Al_2O_3 komatiitic basalt and the three high Al_2O_3 komatiitic basalts analyzed from the thesis area.

	High Fe_2O_3, Al_2O_3 komatiitic basalt	High Al_2O_3 komatiitic basalt		
	M-197	M-302	M-105	M-185
SiO_2	48.50	48.48	52.80	53.84
Al_2O_3	16.76	18.51	18.42	17.17
Fe_2O_3	18.50	10.29	7.17	11.93
MgO	4.24	5.43	3.28	3.93
CaO	9.81	12.53	11.38	9.29
Na_2O	0.51	3.30	2.66	2.02
K_2O	0.59	0.46	3.27	0.88
TiO_2	0.55	0.62	0.58	0.56
MnO	0.54	0.30	0.23	0.36
P_2O_5	0.00	0.06	0.19	0.02
Total	100.00	100.00	100.00	100.00
Cr	443	422	410	214
Ni	136	84	25	67
Co	116	88	27	56
V	220	255	194	48

in Archean and younger terranes. Jensen (1978b) reports a few very iron-rich tholeiitic basalts from the Kinojevis Group north of Kirkland Lake. These are intercalated with iron-rich tholeiitic basalts with lower Fe_2O_3 abundances and magnesium-rich tholeiitic basalts as defined by the Jensen Cation Plot. Volcanic flows referred to as ferrobasalts have been reported from the Galapagos Spreading Center (Byerly et al., 1976) and from the Spiess Ridge segment of the Southwest Indian Ridge (Le Roex et al., 1982). At the Galapagos Center, the ferrobasalts are associated with chemically diverse volcanic rocks including rhyodacites and andesites which is what is found in the map area.

In table 4-11, the major element compositions of the iron-rich volcanics from the Kinojevis Group and from the Galapagos Spreading Center are compared to the composition of M-197 from the thesis map area. M-197 is much higher in Al_2O_3 and lower in MgO, TiO_2 and Na_2O than those from the other two localities.

4-9 High Al_2O_3 Komatiitic Dacites

M-260 is classified as a high Al_2O_3 komatiitic dacite with 63.40 % SiO_2 and 16.43 % Al_2O_3 (table 4-12). It is a massive, light grey, very fine grained, hard rock and may be tuffaceous. The unit from which M-260 was taken lies on the north side of the South Pit where it overlies B.I.F.. This B.I.F. stratigraphically overlies high Al_2O_3 komatiitic

Table 4-11

Major element composition of a Fe_2O_3, Al_2O_3 rich komatiitic basalt from the map area and Fe-rich volcanics from the Kinojevis Group and from the Galapagos Spreading Centre.

	High Fe_2O_3, Al_2O_3 komatiitic basalt	Iron-rich tholeiitic basalts		Ferrobasalt
	M-197	TH20	TH23	P00071N2
SiO_2	48.52	48.35	49.54	49.69
Al_2O_3	16.77	13.34	14.36	11.35
Fe_2O_3	18.51	18.26	18.23	18.60
MgO	4.24	6.36	8.23	4.30
CaO	9.81	6.05	6.78	9.27
Na_2O	0.46	4.08	2.39	2.54
K_2O	0.59	1.08	0.07	0.19
TiO_2	0.55	2.47	2.40	3.74
MnO	0.54	0.00	0.00	0.31
P_2O_5	0.01	0.00	0.00	-
Total	100.00	100.00	99.99	99.99

M-197 is from immediately north of the South Pit.
TH20 and TH23 are from the Kinojevis Group (Jensen, 1978b) and were classified using the Jensen Cation Plot.
P00071N2 is from the Galapagos Spreading Centre (Byerly et al., 1976). The term ferrobasalt is from Byerly et al. (1976)

Table 4-12

Major element, Cr, Ni, Co and V abundances for the high Al_2O_3 komatiitic dacite

	M-260
SiO_2	63.40
Al_2O_3	16.43
Fe_2O_3	7.90
MgO	2.73
CaO	1.31
Na_2O3	1.07
K_2O	3.91
TiO_2	0.72
MnO	0.13
P_2O_5	0.41
Total	100.00
Cr	108
Ni	88
Co	26
V	94

basalts and andesites. High Al_2O_3 komatiitic dacite is overlain by high Al_2O_3 komatiitic basalt and/or andesite and resembles thin units (20 meters thick) intercalated with B.I.F. in the Central Pit.

M-260 has the lowest Cr and Ni abundances of any sampled volcanic in the thesis map area. Its TiO_2 abundance (0.72 %) is slightly higher than those of high Al_2O_3 komatiitic basalts and andesites which have a narrow range of 0.56 to 0.63 % TiO_2. This TiO_2 content matches the average TiO_2 contents of ten low MgO komatiitic basalts (0.71 %).

4-10 Assessment of Post-Igneous Modification

In the introduction to this section, it was pointed out that the chemical composition of volcanics in the map area largely reflect the original igneous compositions. This can be shown in part by plotting the abundances of each of the elements versus MgO. This is done for all of the komatiitic volcanic samples and is shown in figures 4-2(a-g) and 4-3(a-d). It is seen that with decreasing MgO, the abundances of Al_2O_3, TiO_2 and SiO_2 show sharp and well defined increases. Fe_2O_3 is relatively constant over the range in MgO between 13 and 32 %. Below 13 %, Fe_2O_3 decreases. CaO abundances increase gradually with increasing MgO reaching a peak at MgO level of 13 to 16 %,

FIGURE 4-2 a to g. Variation diagrams of major oxides versus MgO for komatiites and komatiitic volcanics.

a) TiO_2 vs. MgO

b) Al_2O_3 vs. MgO

c) SiO_2 vs. MgO

d) CaO vs. MgO

e) Na_2O vs. MgO

f) K_2O vs. MgO

g) Fe_2O_3 vs. MgO

▽ Komatiite

△ High MgO komatiitic basalt

▲ High MgO komatiitic andesite

□ Low MgO komatiitic basalt

■ Low MgO komatiitic andesite

◪ Low Al_2O_3 komatiitic dacite

o High Al_2O_3 komatiitic basalt and andesite

● High Al_2O_3 komatiitic dacite

× High Fe_2O_3, Al_2O_3 komatiitic basalt

(symbols are identical for Figure 4-3 a to d)

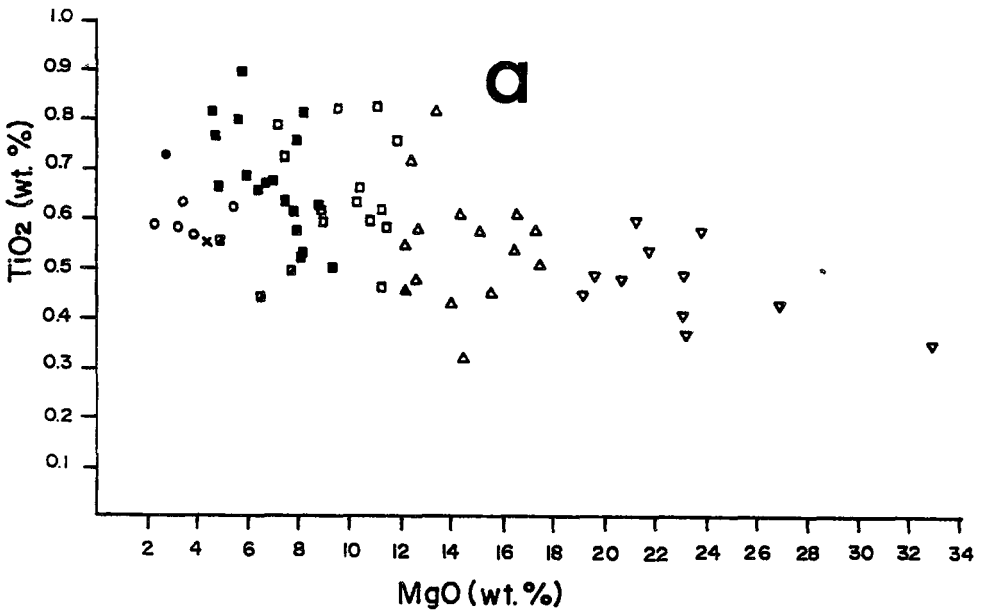
a
TiO2 (wt. %)
1.0
0.9
0.8
0.7
0.6
0.5
0.4
0.3
0.2
0.1
2 4 6 8 10 12 14 16 18 20 22 24 26 28 30 32 34
MgO (wt. %)

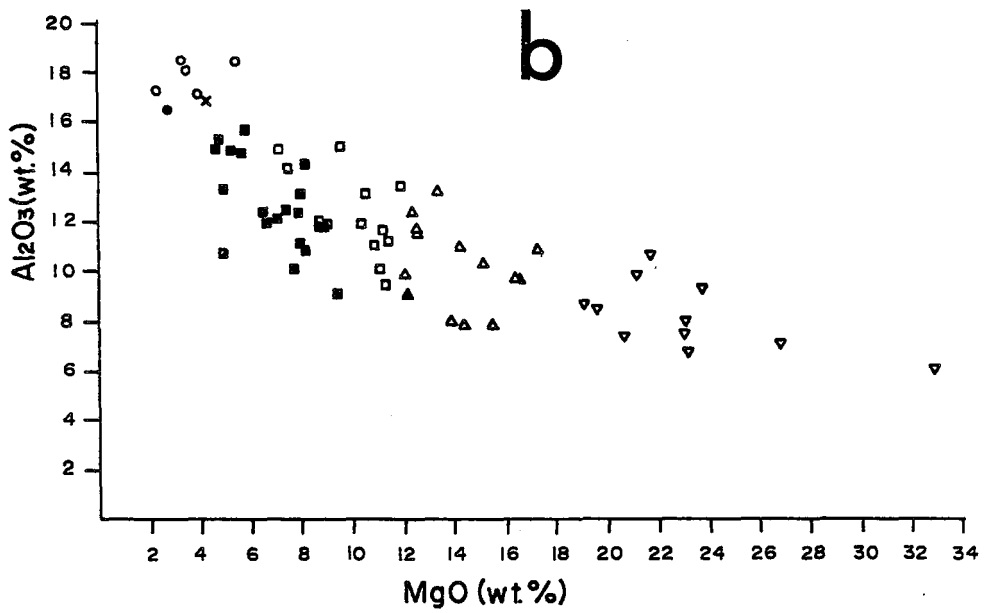
b
Al2O3(wt.%)
20
18
16
14
12
10
8
6
4
2
2 4 6 8 10 12 14 16 18 20 22 24 26 28 30 32 34
MgO (wt.%)

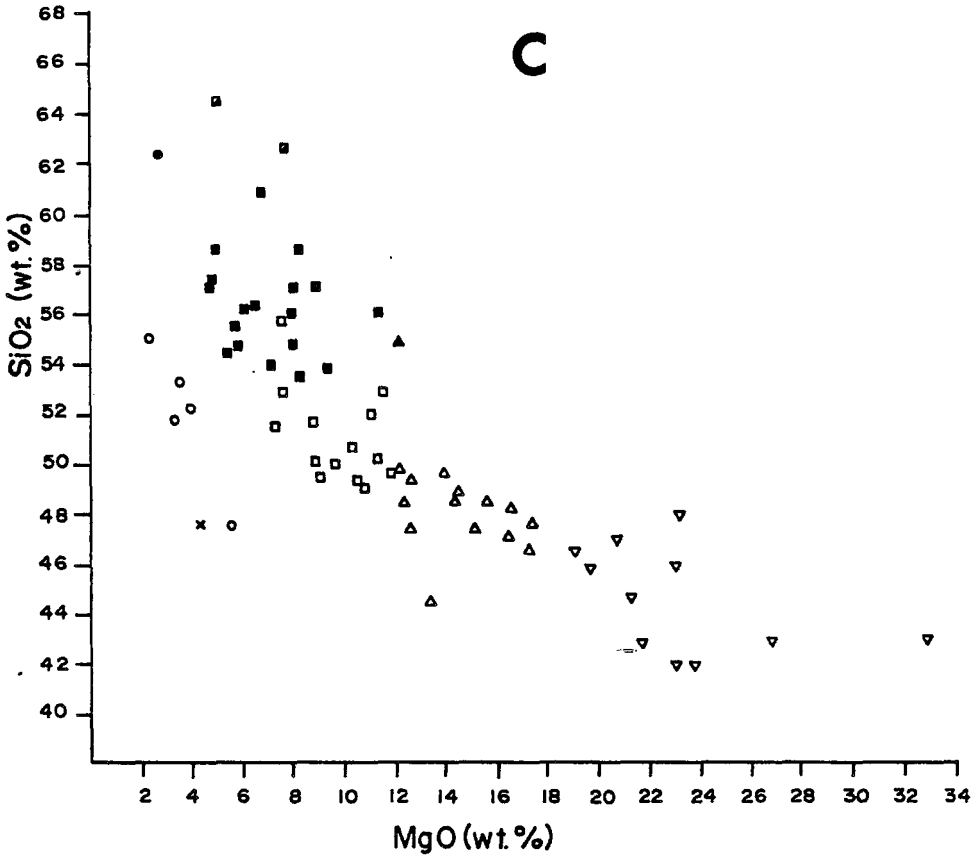
c
SiO2 (wt.%)
MgO (wt.%)

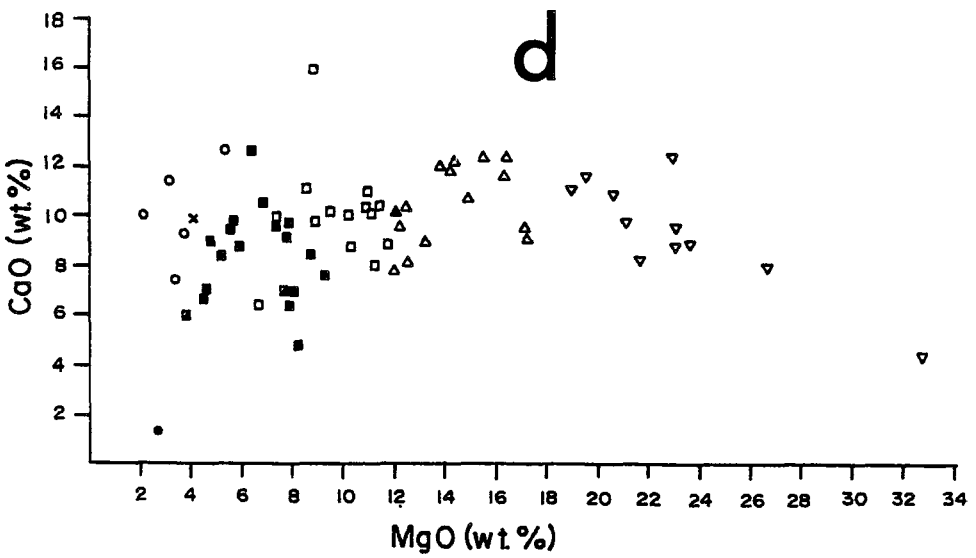
d
CaO (wt.%)
MgO (wt.%)

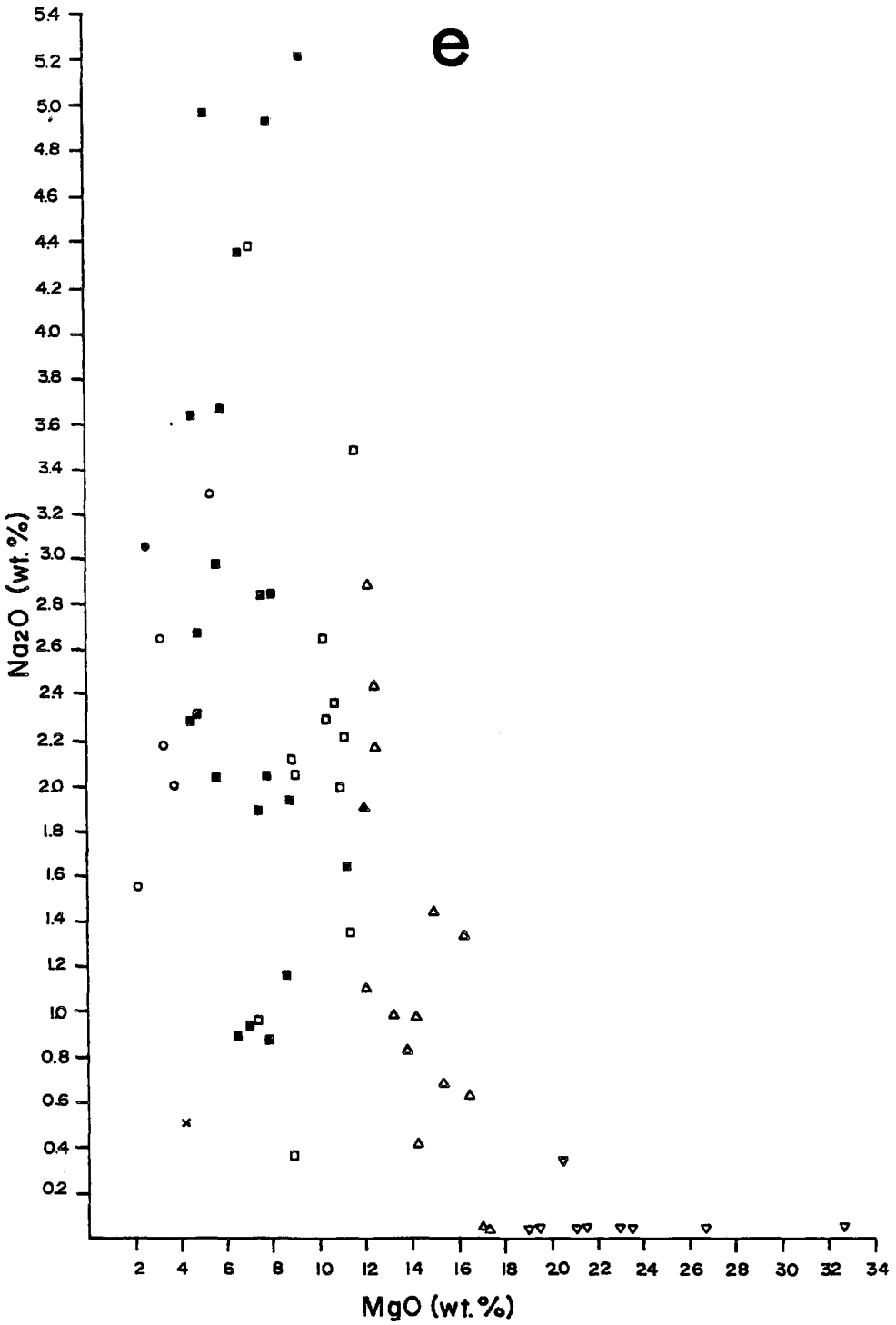
e
Na2O (wt.%)
MgO (wt.%)
5.4
5.2
5.0
4.8
4.6
4.4
4.2
4.0
3.8
3.6
3.4
3.2
3.0
2.8
2.6
2.4
2.2
2.0
1.8
1.6
1.4
1.2
1.0
0.8
0.6
0.4
0.2
2
4
6
8
10
12
14
16
18
20
22
24
26
28
30
32
34

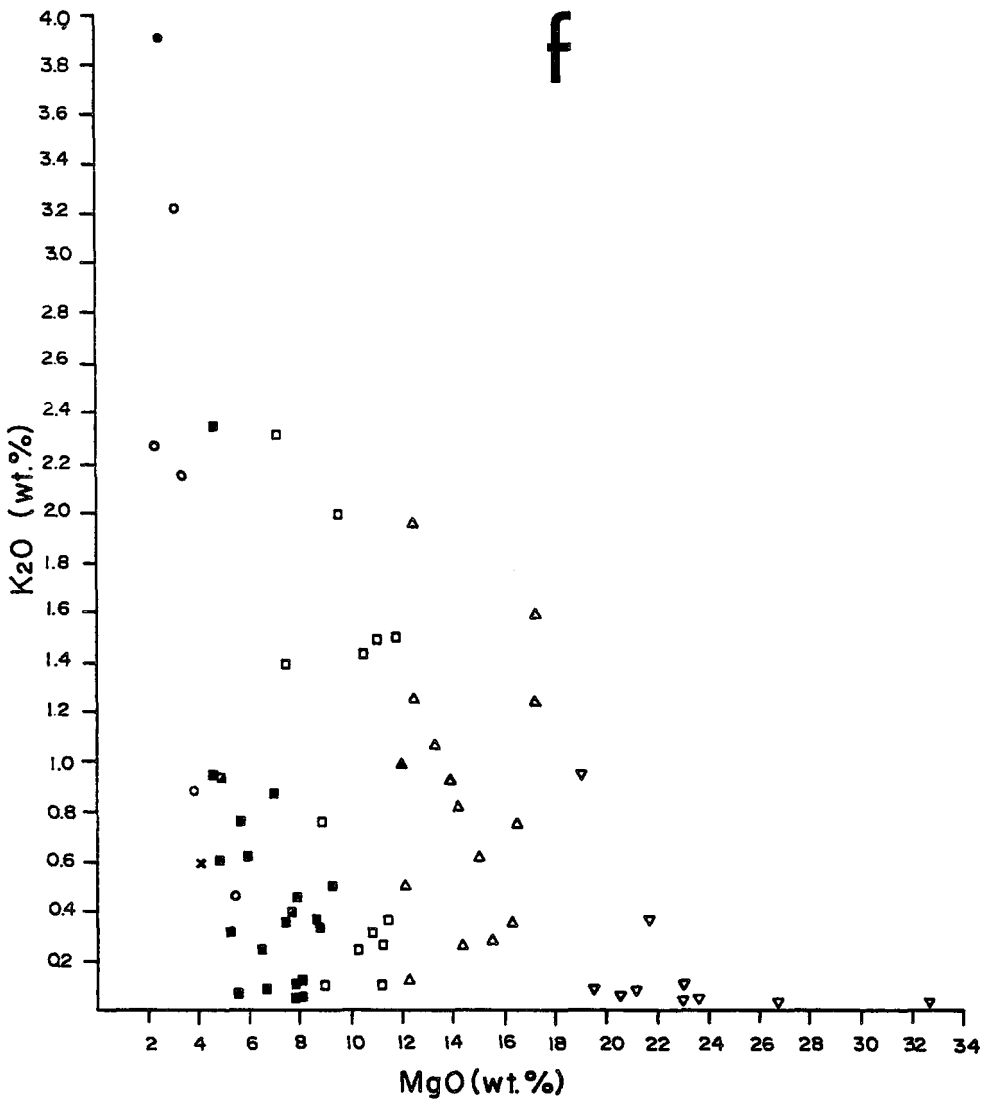
f
K2O (wt.%)
MgO (wt.%)
4.0
3.8
3.6
3.4
3.2
3.0
2.8
2.6
2.4
2.2
2.0
1.8
1.6
1.4
1.2
1.0
0.8
0.6
0.4
0.2
2
4
6
8
10
12
14
16
18
20
22
24
26
28
30
32
34

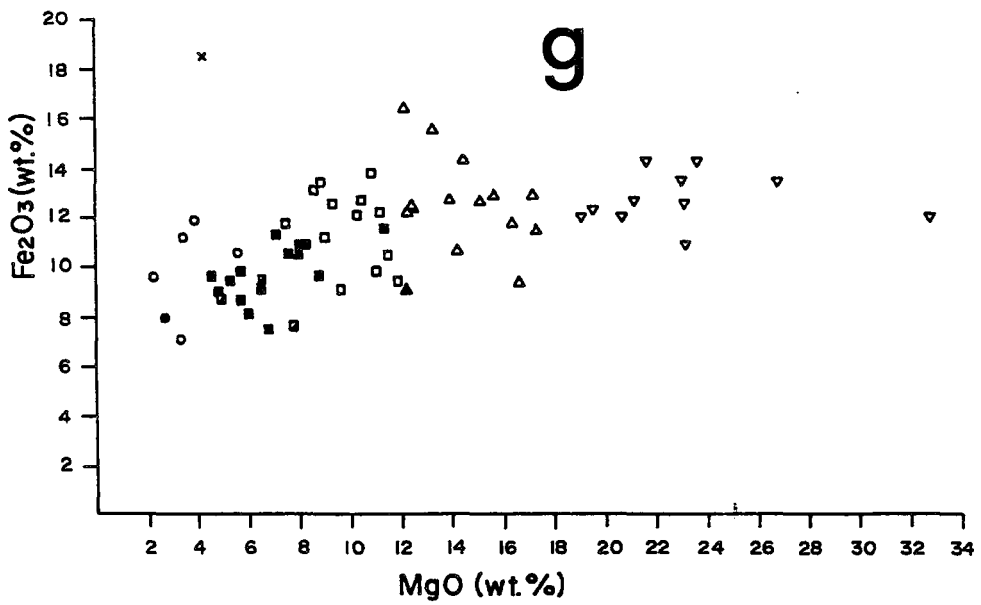
g
Fe2O3(wt.%)
MgO (wt.%)
20
18
16
14
12
10
8
6
4
2
2 4 6 8 10 12 14 16 18 20 22 24 26 28 30 32 34

FIGURE 4-3 a-d Variation diagrams of Cr, Ni, Co, and V versus MgO.

a) Cr vs. MgO

b) Ni vs. MgO

c) Co vs. MgO

d) V vs. MgO

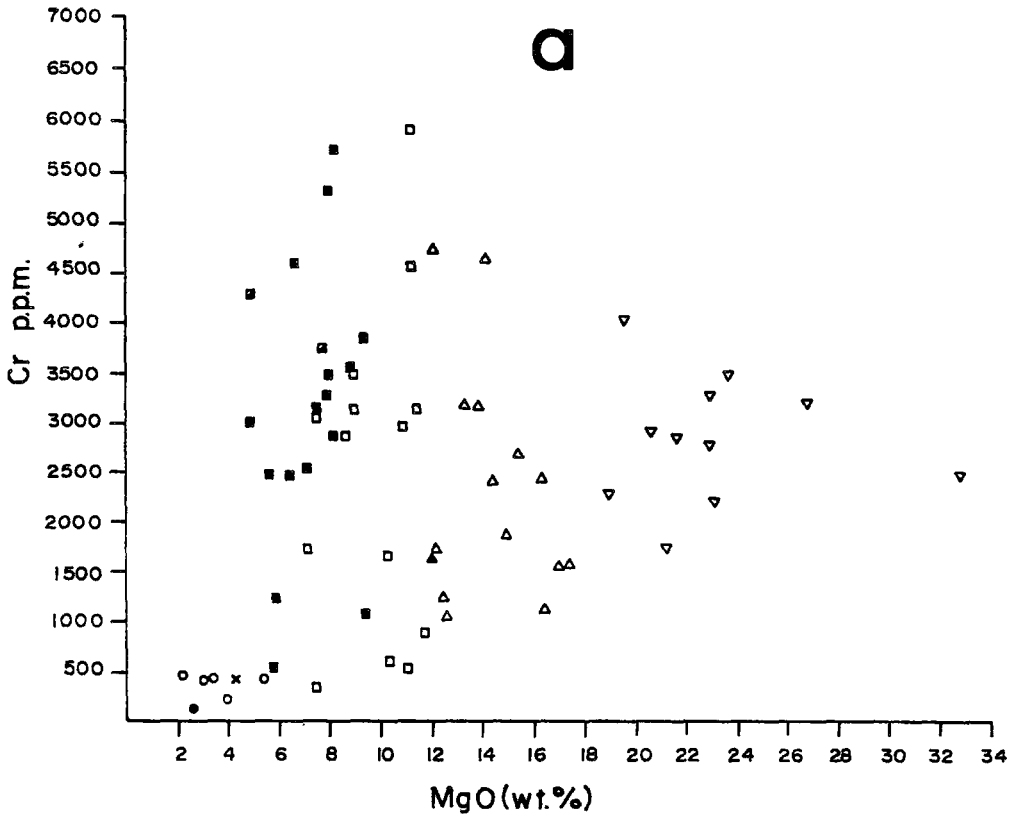
a
Cr p.p.m.
7000
6500
6000
5500
5000
4500
4000
3500
3000
2500
2000
1500
1000
500
2 4 6 8 10 12 14 16 18 20 22 24 26 28 30 32 34
MgO (wt.%)

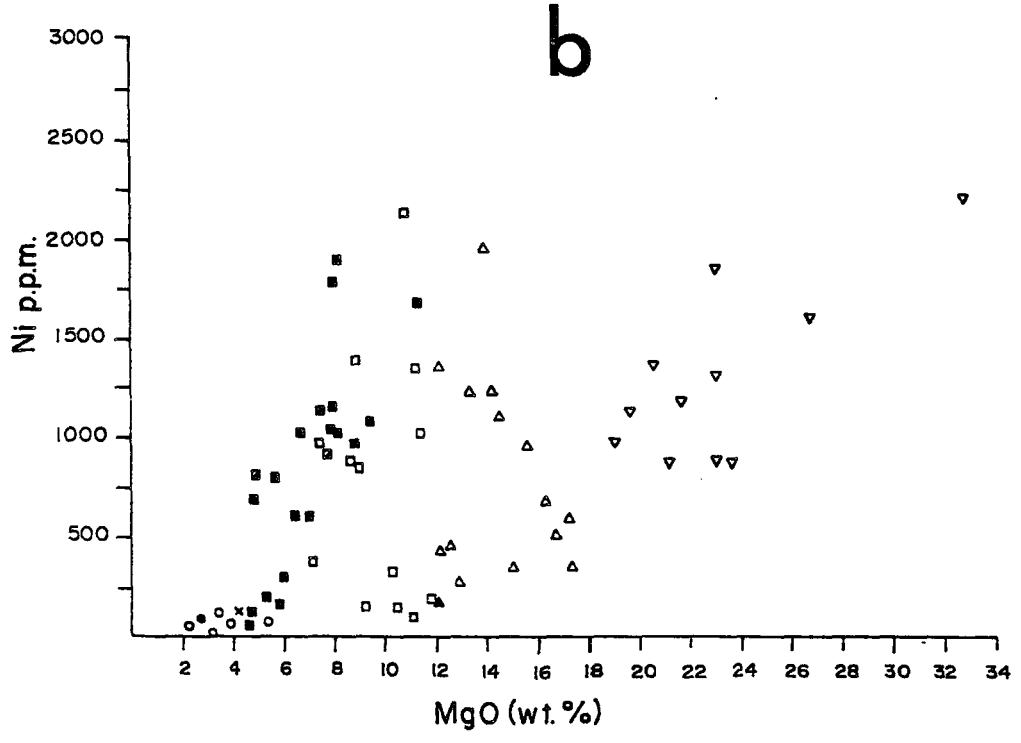
b
Ni p.p.m.
3000
2500
2000
1500
1000
500
2 4 6 8 10 12 14 16 18 20 22 24 26 28 30 32 34
MgO (wt.%)

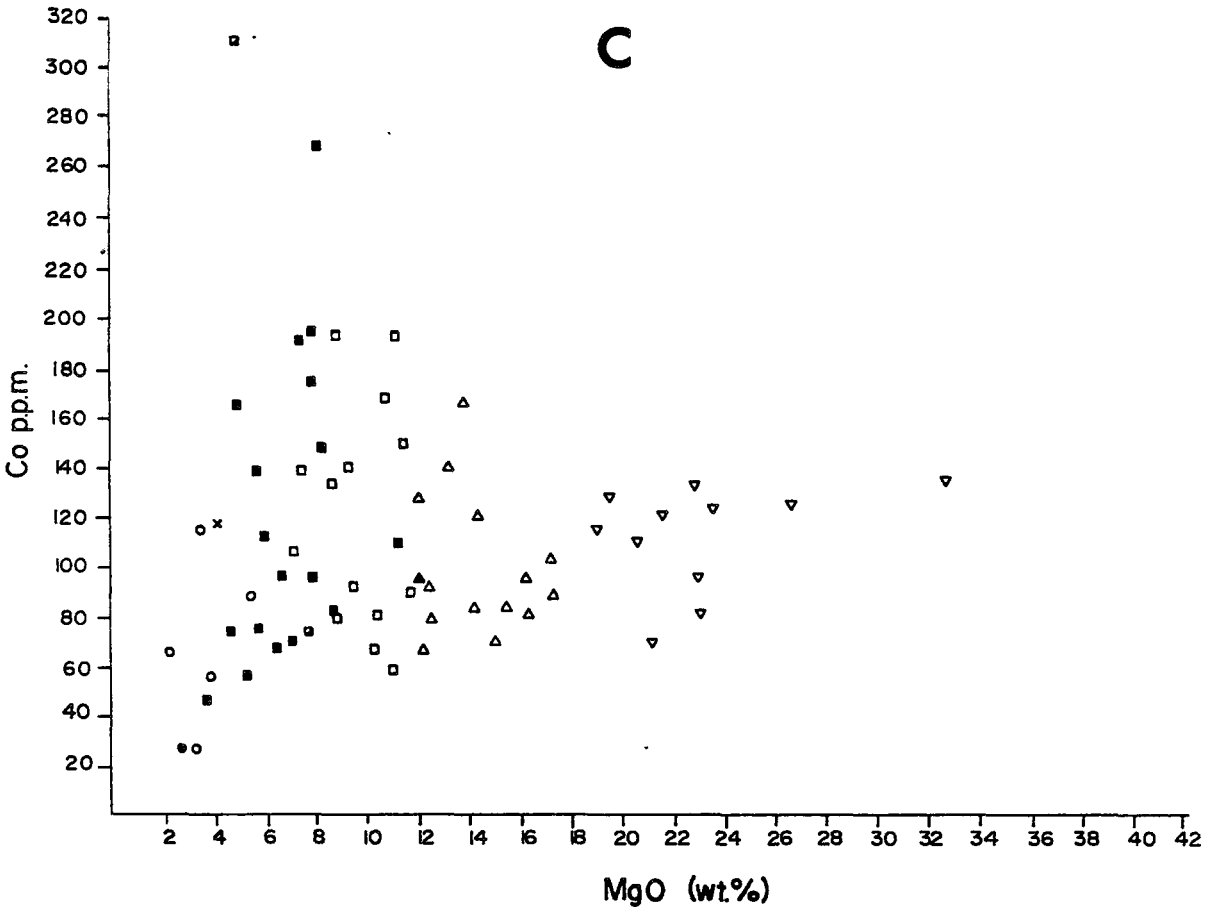
c
Co p.p.m.
320
300
280
260
240
220
200
180
160
140
120
100
80
60
40
20
2 4 6 8 10 12 14 16 18 20 22 24 26 28 30 32 34 36 38 40 42
MgO (wt.%)

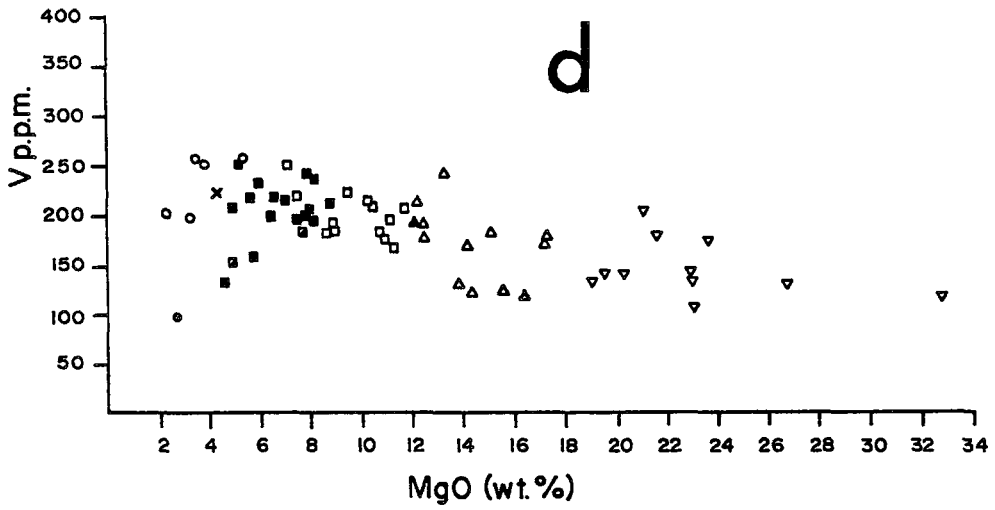
d
V p.p.m.
400
350
300
250
200
150
100
50
2 4 6 8 10 12 14 16 18 20 22 24 26 28 30 32 34
MgO (wt.%)

after which CaO decreases. There is a greater scatter in the data for both the Na_2O versus MgO and K_2O versus MgO plots for all volcanics except komatiites.

In the V versus MgO plot, there is a general gradual increase in V with decreasing MgO. Scatter in the plot exists at low MgO abundances. Ni abundances decrease with a corresponding fall in MgO from 34 % to 16 %. There is great scatter at lower MgO abundances. Co abundances decrease with a decrease from 34 % to 15 % MgO. There is greater scatter at lower MgO abundances. The Cr versus MgO variation diagram shows scatter for samples with less than 16 % MgO. Cr abundances decrease in flows ranging from 24 to 16 % MgO.

The systematic variation shown by SiO_2, TiO_2, Al_2O_3, CaO, Fe_2O_3, and V through a wide range of MgO suggests that weathering, metamorphism and post-metamorphic alteration did not greatly change the original abundances of these elements. These variations most likely then reflect igneous processes. The scatter associated with Na_2O and K_2O clearly indicates alteration. The conclusions reached here for the major elements are similar to those reached by Nisbet et al. (1977) who used the same type of variation diagrams for komatiitic sequences from Belingwe, Rhodesia.

The patterns shown by Cr, Ni and Co versus MgO are believed to be igneous. This suggestion is discussed further in section 4-14 and in chapter 8.

4-11 Potassic Alteration

The anomalously high K_2O abundances in the high and low MgO komatiitic basalts can be linked to minor amounts of biotite and sericite. These minerals are believed to be secondary, formed during post-greenschist metamorphic alteration as they replace greenschist metamorphic grade minerals. This is shown in plate 4-21, a thin section from M-298, a low MgO komatiitic basalt with 1.43% K_2O and approximately 1 % biotite. Here, biotite cuts across coexisting albite grain boundaries and replaces parts of actinolite grains. Sample M-298, like all others, was selected in the field as representative of unaltered rock. The causes of potassic alteration are discussed in section 9-6.

4-12 Explanation for Scatter in the Na_2O Versus MgO Variation Diagrams

The wide variation in Na_2O abundances in komatiitic basalts and andesites can be related to variations in the amounts of albite relative to clinozoisite. This is best seen by comparing M-1 to M-3 and M-124 to M-578. M-1 and M-3 have roughly similar major element compositions apart from Na_2O and CaO as do M-124 and M-578 (table 4-13). M-124 and M-1 are plagioclase phyric with clinozoisite pseudomorphs of plagioclase phenocrysts in an actinolite-clinozoisite bearing groundmass. Albite occurs in minor amounts only.

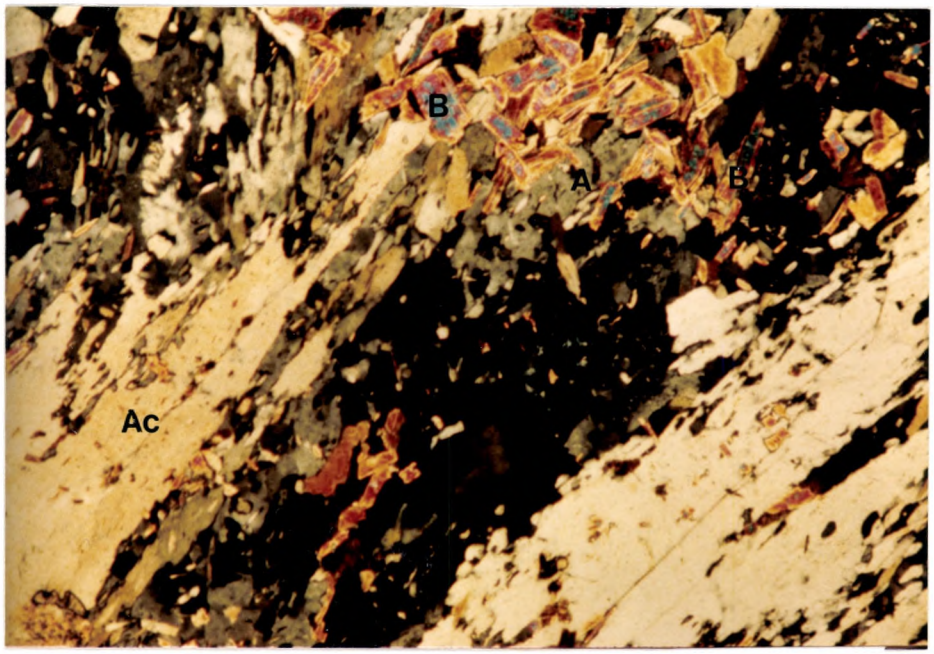

PLATE 4-21 Biotite (B) lathes replace acicular actinolite (Ac) at the top of the photo. Less obvious is biotite (B) cutting across albite (A) grain boundaries near the upper right hand side of the photo. M-298 is from the north side of Dry Lake. Polarized light, x63. Field of view is 1.0 x 1.5 mm.

Table 4-13

Comparison of major element compositions of M-1 to M-3 and M-124 to M-578

	M-1	M-3	M-124	M-578
SiO_2	57.37	61.97	55.95	57.33
Al_2O_3	12.43	11.97	12.17	14.49
Fe_2O_3	9.10	7.53	11.31	8.16
MgO	6.54	6.74	7.06	6.00
CaO	12.44	6.35	10.55	8.74
Na_2O	0.89	4.38	0.94	3.68
K_2O	0.24	0.08	0.87	0.62
TiO_2	0.65	0.67	0.67	0.68
MnO	0.24	0.22	0.32	0.24
P_2O_5	0.09	0.09	0.16	0.06
Total	100.00	100.00	100.00	100.00

N.B. M-1 is from sequence 3. M-3 and M-124 are from sequence 4. M-578 is from sequence 6.

Na_2O abundances are low while CaO abundances are high relative to M-578 and M-3 where acicular actinolite is hosted in an albite-rich groundmass.

Albitization of the groundmass in M-3 and M-578 during metamorphism clearly involves gain in Na as the original igneous groundmass would have consisted of a more calcic plagioclase. Formation of clinozoisite during metamorphism likely resulted in the loss of Na as clinozoisite does not host Na in its structure.

It would seem that the character of feldspar alteration is a function of the original igneous texture. In the examples used above, it is those samples with acicular amphibole crystals which have the albite groundmass. Acicular crystal structures reflect rapid cooling (Arndt and Fleet, 1979). The samples with coarse clinozoisite and actinolite pseudomorphs likely reflect slower cooling conditions. Perhaps albitization prefers glassy material which would likely be associated with rapid cooling. This is in contrast to Binns et al. (1982) who propose that glass would be chloritized, involving Na loss while more crystalline feldspars would become albitized.

4-13 A Brief Discussion on Scatter in the Cr, Ni and Co Versus MgO Variation Diagrams

The patterns found in these three variation diagrams (figures 4-3a-c) are not attributable to metamorphism or alteration. Most of the Cr in the volcanic flows is likely

concentrated in chromite which is not seen to be a late addition (cross-cutting relationships) in thin sections. The high Cr abundances in many komatiitic basalts and andesite thus likely represent primary igneous abundances.

Ni and Co in the komatiitic volcanics were likely originally incorporated into igneous olivine, pyroxene, pyrite and pyrrhotite. The Ni and Co now present in the samples may be contained in metamorphic antigorite and actinolite and in primary pyrite and pyrrhotite. There is no petrographic evidence for addition of a Ni-Co bearing phase such as pyrrhotite to Ni and Co-rich basalts and andesites. The Ni and Co abundances given in this study thus likely represent primary igneous abundances.

The patterns shown by Cr, Ni and Co versus MgO variation diagrams thus reflect original igneous trends. A tentative explanation for these patterns will be given in chapter 8.

4-14 Sequence 1 Volcanics

Sequence 1, including intercalated sediments is 150 meters thick where not structurally thickened and is laterally continuous across the thesis map area. Gabbroic flows mapped by earlier workers (Lawton, 1957; Hewitt, 1949; Abraham, 1950) as directly overlying the Skead Group in neighbouring Skead and McElroy Townships to the southeast are in all likelihood a part of sequence 1.

Sequence 1 is characterized largely by massive, tholeiitic and calc-alkalic basaltic flows. Locally near the top of the sequence, pillowed basaltic flows are observed. Flow tops were recognized by their fine grained nature and sometimes brecciated appearance. Flow thicknesses are not known with any degree of certainty but many may be greater than 5 to 10 meters in thickness. This estimate represents the size of many outcrops on which a flow top is not recognized. However it should be pointed out that flow tops with thin chilled margins are easily missed.

Most of the basalts weather to yield a salt and pepper texture, and are medium grained. They appear equigranular in hand specimen and can be confused with intrusive gabbro.

In thin section, they are seen to be amphibole phyric. Forty to 50 % randomly orientated actinolite which range in size from 0.5 to 2 mm are set in a finer grained clinozoisite-rich matrix with minor albite. The clinozoisite is commonly microgranular but locally occurs as euhedral lathes. Opaque minerals occur in irregular shaped aggregates (0.01 mm in diameter) associated with actinolite and albite. The opaque minerals make up 0.5 % to 1.0 % of the basalts.

Locally the basalts are characterized by a distinctive acicular actinolite texture. Actinolite needles

2 mm to 2 cm in length are either randomly orientated or arranged parallel to one another (plate 4-22) perpendicular to local strike in a fine grained groundmass of albite and clinozoisite. The randomly orientated form was more commonly observed.

Due to poor exposure and the difficulty in finding flow contacts, most localities where this texture was observed could not be related to proximity to flow tops. However all may be analogous to one outcrop found south of the South Pit where the relationship between fine grained flow top, randomly orientated acicular amphibole texture, preferentially orientated acicular amphibole texture and massive medium grained (amphibole phyric) texture is established. This is outlined in figure 4-4.

Similar skeletal features were observed in the upper parts of tholeiitic flows from the Kinojevis Group studied by Pearce and Birkett (1974). The textures and the stratigraphic variation documented in figure 4-4 are also comparable to that seen in komatiites, high and low MgO komatiitic basalts and low MgO komatiitic andesites in the map area.

The major elements and Cr, Ni Co, and V abundances for five basalt flows are shown in table 4-14. Samples M-162 and M-516 which are richer in Fe_2O_3 than M-225, M-208 and M-204, plot in the tholeiitic field on the Jensen Cation Plot (figure 4-5). M-225, M-208 and M-204 plot in the calc-

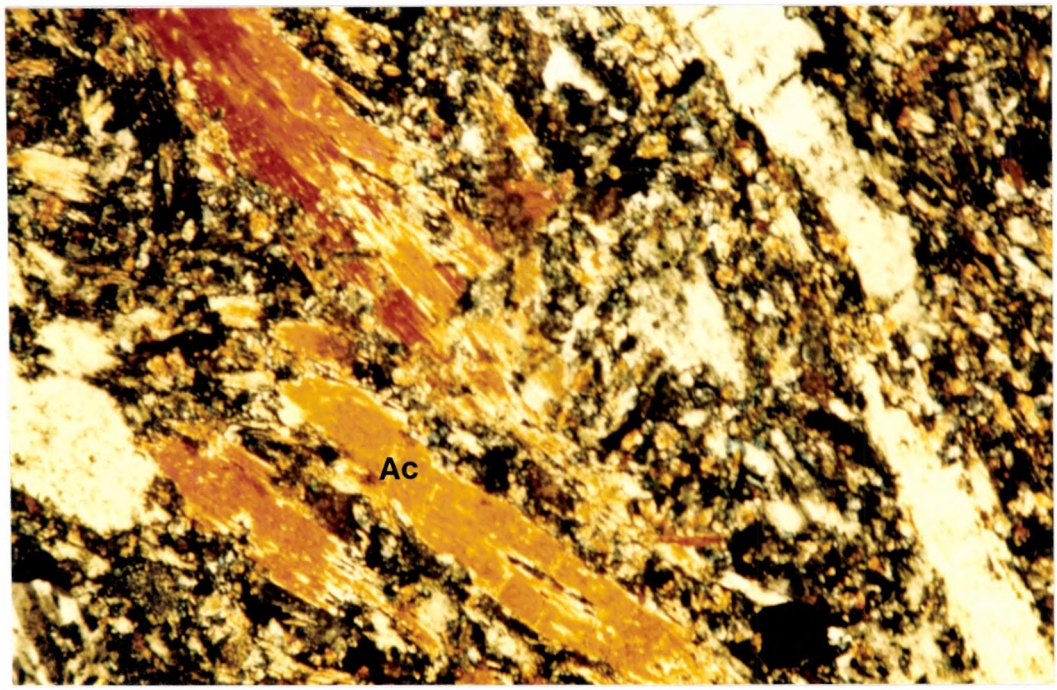

PLATE 4-22 Acicular actinolite (Ac) orientated parallel to one another and perpendicular to the flow top in a calc-alkalic basalt at the top of sequence 1. The section is from M-85 along the railroad tracks north of Marsh Lake (map 1). Polarized light, x63. Field of view is 1.0 x 1.5 mm.

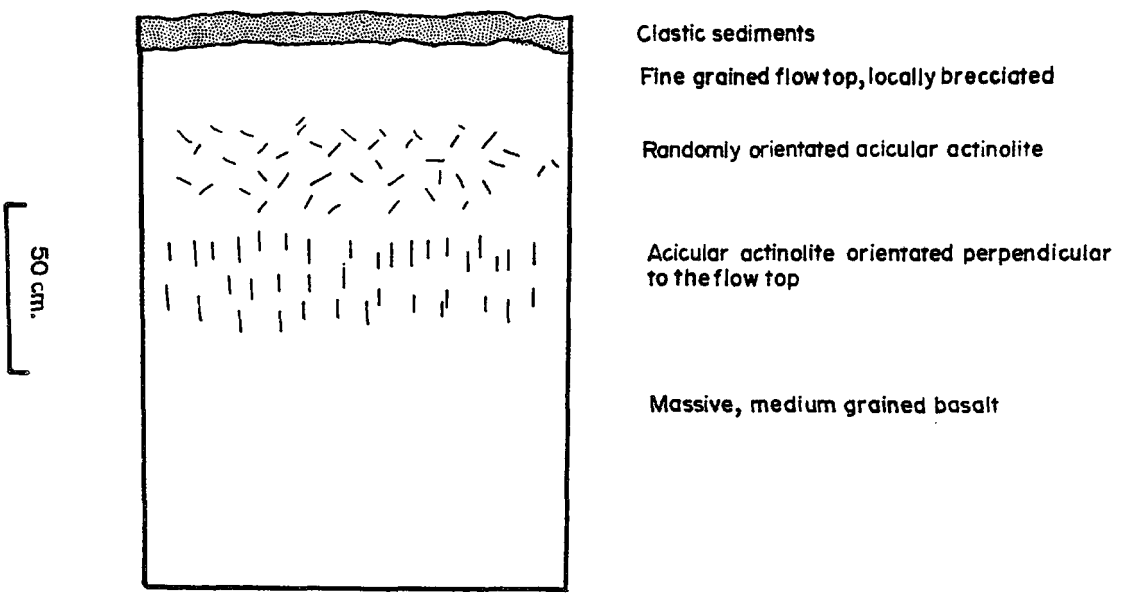

FIGURE 4-4 Generalized section of a calc-alkalic basalt exposed on the south side of the railroad tracks at M-85 (map 1). The base of the flow was not observed and the thickness of the flow is not known.

Table 4-14

Major element Cr, Ni, Co and V abundances for sequence 1 basalts

	M-162	M-516	M-225	M-204	M-208
SiO_2	49.84	49.77	52.84	53.84	52.48
Al_2O_3	12.74	15.57	15.53	14.89	14.80
Fe_2O_3	14.53	12.22	9.79	9.39	9.22
MgO	7.62	8.84	6.54	6.40	7.57
CaO	10.38	7.36	9.25	10.49	11.08
Na_2O	3.28	3.06	4.37	3.23	3.53
K_2O	0.36	2.04	0.50	0.61	0.32
TiO_2	0.92	0.83	0.92	0.85	0.78
MnO	0.25	0.24	0.17	0.14	0.14
P_2O_5	0.08	0.08	0.09	0.15	0.08
Total	100.00	100.00	100.00	100.00	100.00
Cr	451	173	224	338	466
Ni	75	75	114	69	96
Co	34	56	114	87	79
V	207	191	228	205	203

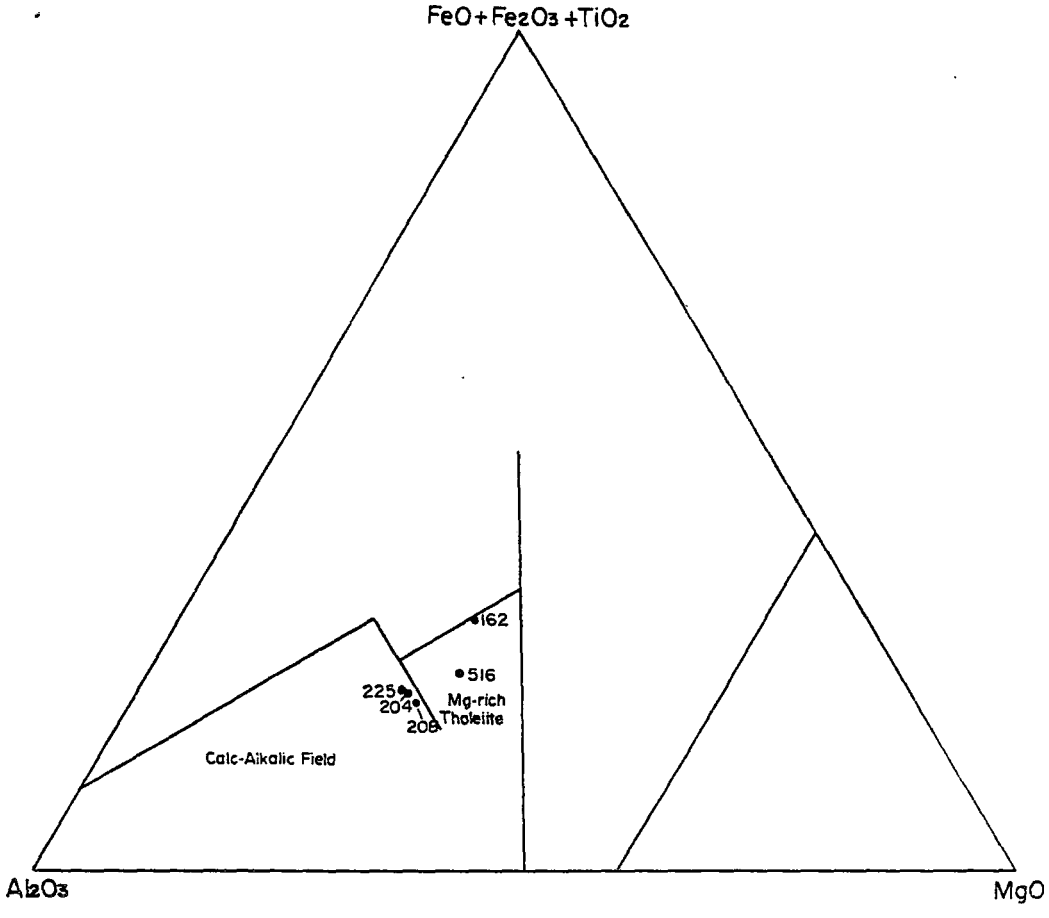

FIGURE 4-5 Plots of sequence 1 basalts on the Jensen Cation Plot.

alkalic field and are the stratigraphically highest flows in sequence 1.

The tholeiitic basalts resemble high iron basalts from the Kinojevis Group (table 4-15) in terms of major oxide composition while the calc-alkalic basalts have lower Al_2O_3 and TiO_2 and higher CaO abundances than representative calc-alkalic basalts and basaltic andesites from the Blake River Group, and calc-alkalic basalts from the Superior Province (table 4-16).

4-15 Comparison of Sequence 1 Basalts and Komatiitic Volcanics

Sequence 1 basalts can generally be discriminated from overlying komatiitic basalts on TiO_2 versus MgO and TiO_2 versus SiO_2 variation diagrams shown in figures 4-6a and 4-6b respectively. Sequence 1 flows generally plot higher than the komatiitic basalts, being richer in TiO_2 at given MgO and SiO_2 abundances.

The calc-alkalic basalts resemble some low MgO komatiitic basalts in major element composition as seen in table 4-17 but almost invariably have lower Cr, Ni and Co abundances than komatiitic basalts.

Five sequence 1 basalt samples average 300 ppm Cr and 86 ppm Ni. These values are similar to the averages of the three analyzed high Al_2O_3 komatiitic basalts (349 ppm Cr and 59 ppm Ni) but well below the averages of eleven low MgO komatiitic basalts (2,054 ppm Cr and 713 ppm Ni).

Table 4-15

Comparison of the major element compositions of sequence 1 tholeiitic basalts with those of tholeiitic basalts from the Kinojevis Group.

	M-162	M-516	1	2	3
SiO_2	53.84	49.77	46.95	51.10	50.84
Al_2O_3	14.89	15.57	14.41	13.30	15.05
Fe_2O_3	9.39	12.22	13.57	15.00	13.89
MgO	6.40	8.84	8.12	5.92	5.48
CaO	10.49	7.36	13.39	8.60	8.98
Na_2O	3.23	3.06	1.99	3.90	2.84
K_2O	0.61	2.04	0.23	0.25	0.38
TiO_2	0.85	0.83	0.93	1.20	2.29
MnO	0.14	0.24	0.22	0.28	0.26
P_2O_5	0.15	0.08	0.19	-	-
Total	99.99	100.01	100.00	100.00	100.01

1. Representative high iron basalt (Pearce and Birkett, 1974) from Thackeray Township, northeastern Ontario.

2. Representative tholeiite basalt, Munro Township, northeastern Ontario (Arndt et al., 1977). Munro Township lies within the Kinojevis Group.

3. Representative tholeiite basalt (Jolly, 1975) from the Kinojevis Group.

Jolly (1975) defines a basalt as a rock with 46 to 50 % SiO_2. Jolly considers tholeiites to be those fractionates which at some stage of the mafic end members display significant non-enrichment.

Pearce and Birkett define a high-iron basalt as having greater than 12 % FeO. Thackeray Township lies within the Kinojevis Group.

Table 4-16

Comparison of the major element compositions of sequence 1 calc-alkalic basalts with calc-alkalic basalts from the Supeior Province.

	M-204	M-208	M-225	1	2	3
SiO_2	53.84	52.48	52.84	52.90	53.07	52.54
Al_2O_3	14.89	14.80	15.53	17.80	17.73	16.19
Fe_2O_3	9.39	9.22	9.79	9.64	9.33	11.02
MgO	6.40	7.57	6.54	5.65	6.16	7.54
CaO	10.49	11.08	9.25	7.88	8.66	7.67
Na_2O	3.23	3.53	4.37	4.09	3.04	3.34
K_2O	0.61	0.32	0.50	0.71	0.57	0.37
TiO_2	0.85	0.78	0.92	1.20	1.05	1.18
MnO	0.14	0.14	0.17	0.13	0.20	-
P_2O_5	0.15	0.08	0.09	-	0.19	0.13
Total	99.99	100.00	100.00	100.00	100.00	99.98

1. Basaltic Andesite, Blake River Group (Jolly, 1975).

2. Superior Province calc-alkalic basalt (Goodwin, 1977).

3. DuFault calc-alkalic basalt (Gelinas et al., 1977).

Jolly (1975) defines a basaltic andesite as having 50 to 55 % SiO_2. Calc-alkalic volcanics are considered to be those that display continual iron-depletion during fractionation.

Gelinas et al. (1977) subdivide volcanic rocks into the tholeiitic and calc-alkalic associations on the A.F.M. diagram (Irvine and Baragar, 1971).

Goodwin (1977) classifies volcanic rocks according to the Barth-Niggli cation norm (Irvine and Baragar, 1971).

FIGURE 4-6a Variation diagram of TiO_2 versus MgO for komatiitic basalts and andesites and sequence 1 basalts.

● komatiitic volcanics
▲ sequence 1 basalts

FIGURE 4-6b Variation diagram of TiO_2 versus SiO_2 for komatiitic basalts and andesites and sequence 1 basalts.

● komatiitic volcanics
▲ sequence 1 basalts

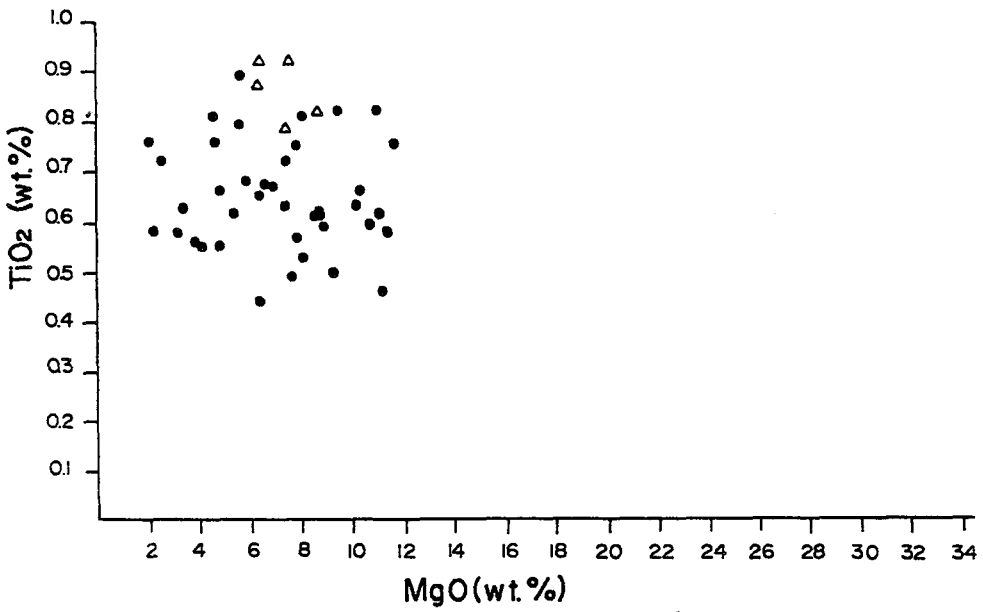
TiO2 (wt.%)
1.0
0.9
0.8
0.7
0.6
0.5
0.4
0.3
0.2
0.1
2 4 6 8 10 12 14 16 18 20 22 24 26 28 30 32 34
MgO(wt.%)

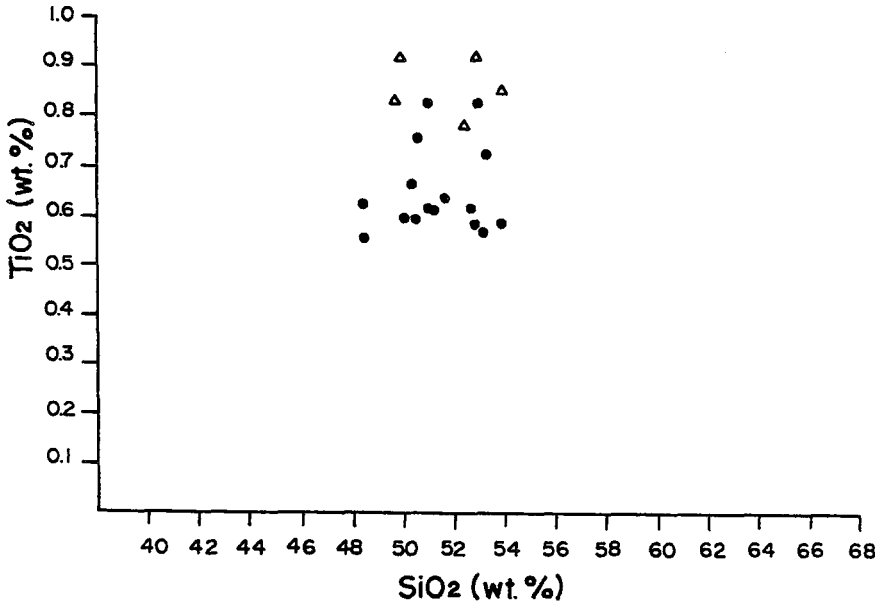
TiO2 (wt.%)
1.0
0.9
0.8
0.7
0.6
0.5
0.4
0.3
0.2
0.1
40 42 44 46 48 50 52 54 56 58 60 62 64 66 68
SiO2 (wt.%)

Table 4-17

Comparison of major element, Cr, Ni, Co and V contents between sequence 1 calc-alkalic basalts and two low MgO komatiitic basalts.

	calc-alkalic basalts			low MgO komatiitic tholeiites	
	M-208	M-204	M-225	M-117	M-97
SiO_2	52.48	53.84	52.84	51.05	52.56
Al_2O_3	14.80	14.89	15.53	15.09	14.97
Fe_2O_3	9.22	9.39	9.79	9.15	11.31
MgO	7.57	6.40	6.54	9.59	7.18
CaO	11.08	10.49	9.25	10.03	6.18
Na_2O	3.53	3.23	4.37	2.07	4.41
K_2O	0.32	0.61	0.50	2.00	2.32
TiO_2	0.78	0.85	0.92	0.82	0.78
MnO	0.14	0.14	0.17	0.16	0.20
P_2O_5	0.08	0.15	0.09	0.04	0.08
Total	100.00	100.00	100.00	100.00	100.00
Cr	466	338	224	329	1666
Ni	96	69	114	152	381
Co	79	87	114	92	106
V	203	205	228	221	245

N.B. M-117 is from sequence 3. M-97 is from sequence 6.

Sequence I basalts are not polygonally jointed as are most komatiitic volcanics. They locally show preferentially orientated acicular amphibole near few tops similar to that observed in komatiitic volcanics with amphiboles and in komatiites with antigorite.

Some fine to medium grained low MgO komatiitic basalts which are not polygonally jointed, such as those at Dry and North Lakes resemble sequence 1 basalts in the field.

4-16 Characterization of Komatiites and Komatiitic Volcanics by C.I.P.W. Norms

The C.I.P.W. norms for komatiites and komatiitic volcanics are given in table C-1 in appendix C. The following observations can be made.

1) Only M-260, a high Al_2O_3 komatiitic dacite is corundum normative. This is the only sample that is not diopside normative.
2) All komatiitic andesites and dacites are quartz normative.
3) Some low MgO and high Al_2O_3 komatiitic basalts are quartz normative.
4) Nepheline is reported from only five norms, M-44 (komatiite), M-404 and M-97 (low MgO komatiitic basalts) and M-302 and M-105 (high Al_2O_3 komatiitic basalts).
5) Olivine occurs in the norms of the komatiites and the

komatiitic basalts.

6) Hypersthene occurs in all but four norms.

The presence of nepheline in the five norms likely indicates potassic alteration. The presence of corundum in M-260, a high Al_2O_3 komatiitic dacite likely reflects the low CaO and high Al_2O_3 abundances which are not believed to be the result of alteration. The presence of corundum in basalts would indicate peraluminous compositions due to depletion of CaO (Gelinas et al., 1977). The presence of hypersthene in the norms reflects a subalkalic character.

4-17 Characterization of Sequence 1 Basalts by C.I.P.W. Norms

From table C-1 in appendix C, the following observations can be made:

1) All five samples are diopside and hypersthene normative.
2) None are nepheline normative.
3) M-225 is corundum normative.
4) M-204 which is quartz normative is not olivine normative. The other four are olivine normative.

It is not known why M-225 is corundum normative. Quartz normative M-204 has 53.84% SiO_2 and is close to being an andesite (on the basis of SiO_2 abundance).

4-18 Summary

1. The composition of many of the volcanic rocks

preserved in the Adams Mine area is clearly different from the composition of volcanics found in other Archean terranes and this is highlighted by:

(a) the presence of high Cr, Ni and Co abundances in low MgO komatiitic basalts, andesites and in low Al_2O_3 dacites. In figures 4-7a-h, trace element versus MgO variation diagrams for Finnish komatiites and komatiitic volcanics are compared to those for the thesis area rocks. The variation diagrams for the Finnish rocks typifies the trends for the three elements versus MgO in most Archean terranes and contrasts greatly with the variation diagrams from the study area.

(b) the presence of high Al_2O_3 volcanics which can be linked stratigraphically to the komatiites in the manner here observed. High Al_2O_3 volcanics do not have high Cr, Ni and Co abundances.

(c) the presence of high Fe_2O_3, Al_2O_3 volcanics which can be linked stratigraphically to komatiites.

2. Variation diagrams indicate that abundances of SiO_2, Al_2O_3, TiO_2, MgO, CaO, Fe_2O_3 and V in komatiites and komatiitic volcanics have not been significantly effected by metamorphism and alteration and that Na_2O and K_2O have been. There is no petrographic evidence to suggest mobility of Cr, Ni and Co during metamorphism and alteration.

FIGURE 4-7 Variation diagrams of
a) Cr versus MgO
c) Ni versus MgO
e) Co versus MgO
g) V versus MgO
for komatiites and komatiitic volcanics from
o Kukmo greenstone belt
□ Suomussalini greenstone belt
Δ Tipasjarvi greenstone belt
from Auvray et al. (1982)

Variation diagrams of
b) Cr versus MgO
d) Ni versus MgO
f) Co versus MgO
h) V versus MgO
for komatiites and komatiitic volcanics from the thesis map area. The symbols for komatiites and komatiitic volcanic lithologies are similar to those in figure 4-3a-d.

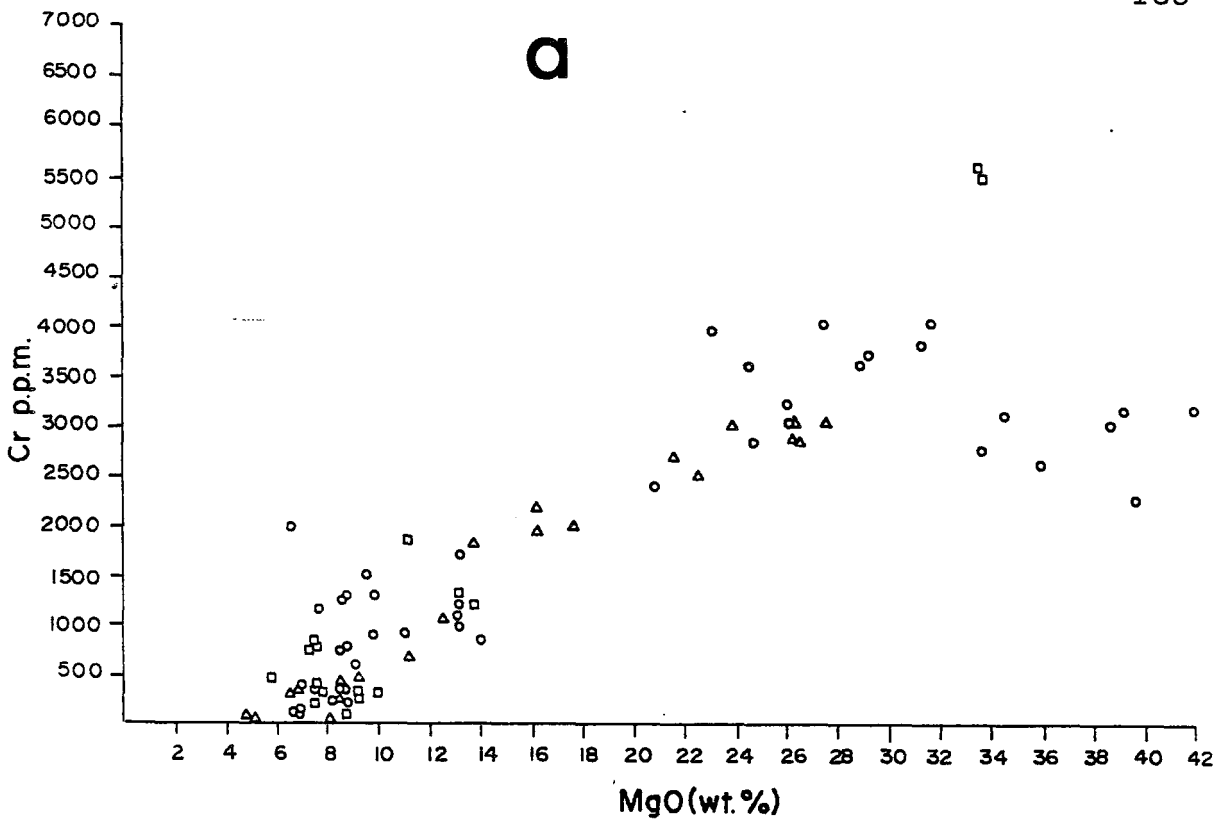
a
Cr p.p.m.
7000
6500
6000
5500
5000
4500
4000
3500
3000
2500
2000
1500
1000
500
2 4 6 8 10 12 14 16 18 20 22 24 26 28 30 32 34 36 38 40 42
MgO(wt.%)

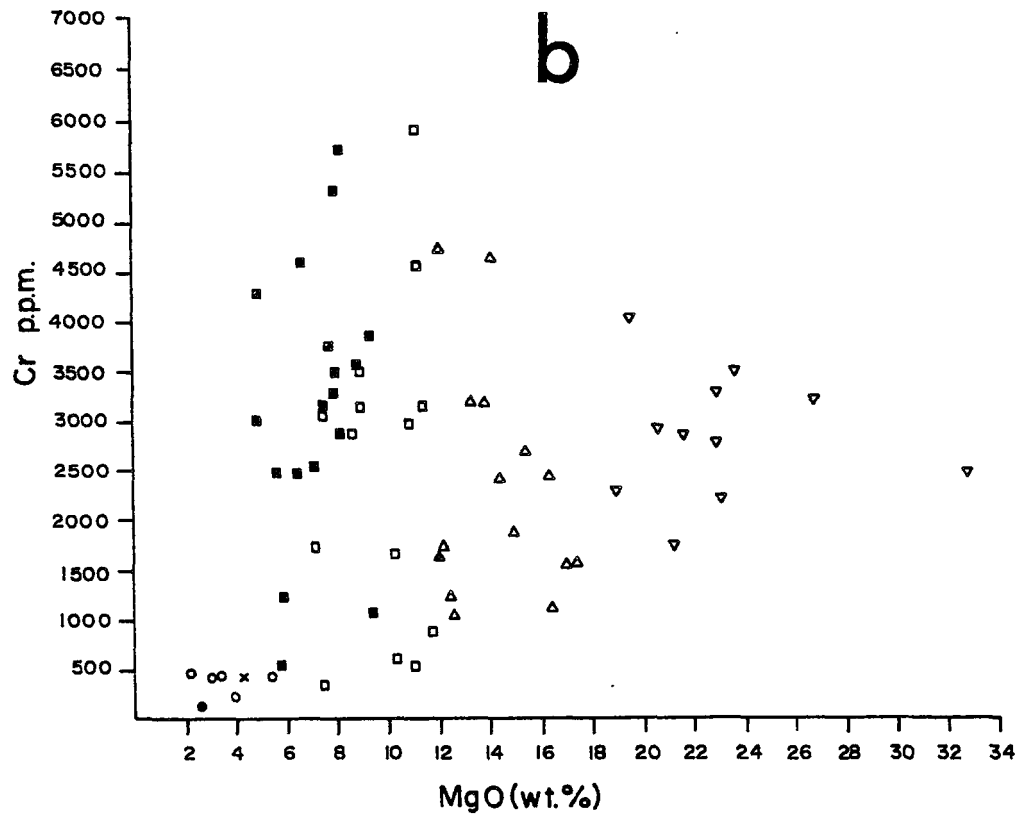
b
Cr p.p.m.
7000
6500
6000
5500
5000
4500
4000
3500
3000
2500
2000
1500
1000
500
2 4 6 8 10 12 14 16 18 20 22 24 26 28 30 32 34
MgO(wt.%)

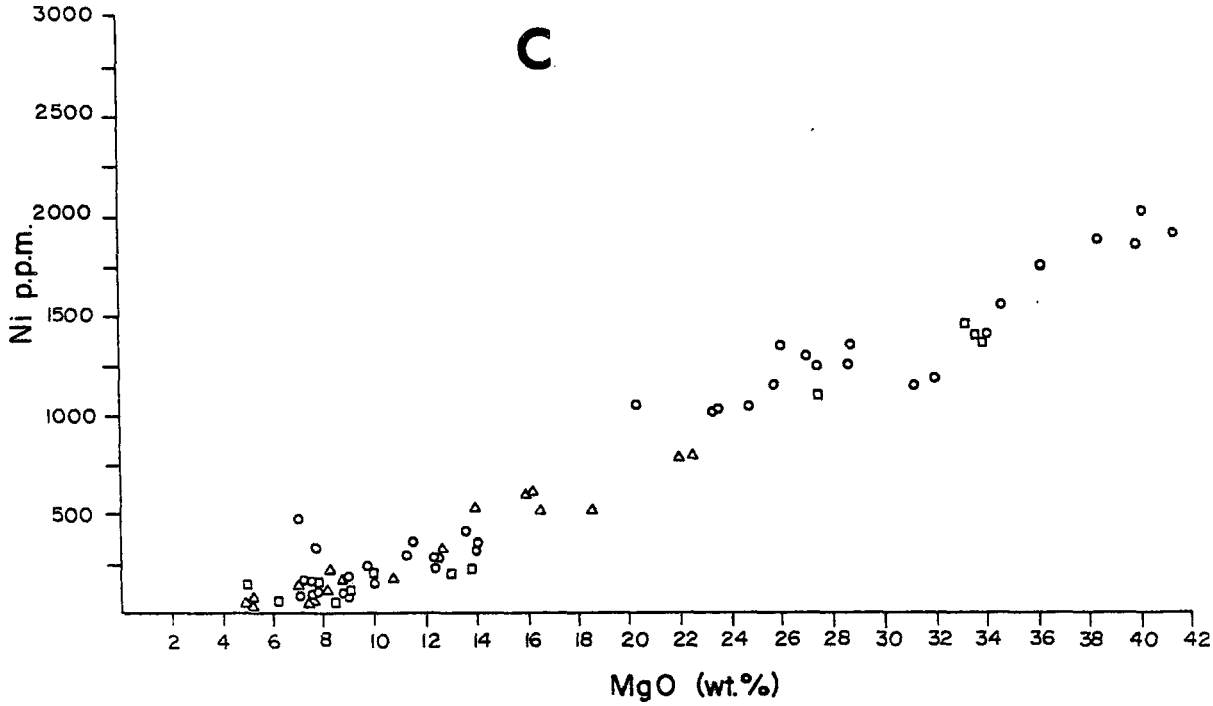
c
Ni p.p.m.
3000
2500
2000
1500
1000
500
2 4 6 8 10 12 14 16 18 20 22 24 26 28 30 32 34 36 38 40 42
MgO (wt.%)

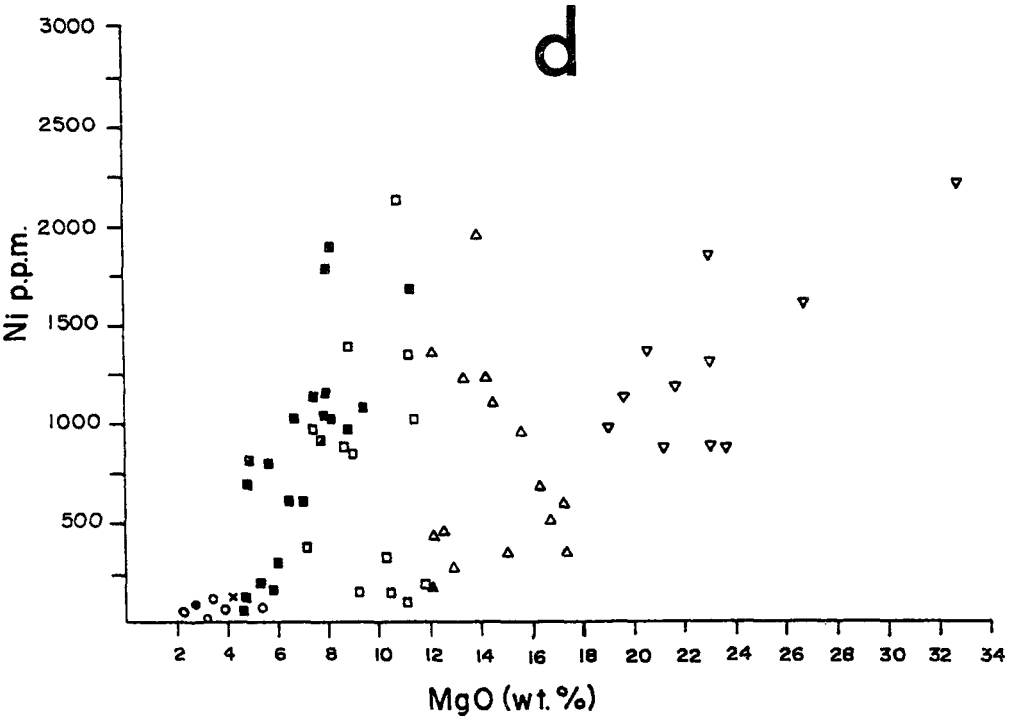
d
Ni p.p.m.
3000
2500
2000
1500
1000
500
2 4 6 8 10 12 14 16 18 20 22 24 26 28 30 32 34
MgO (wt.%)

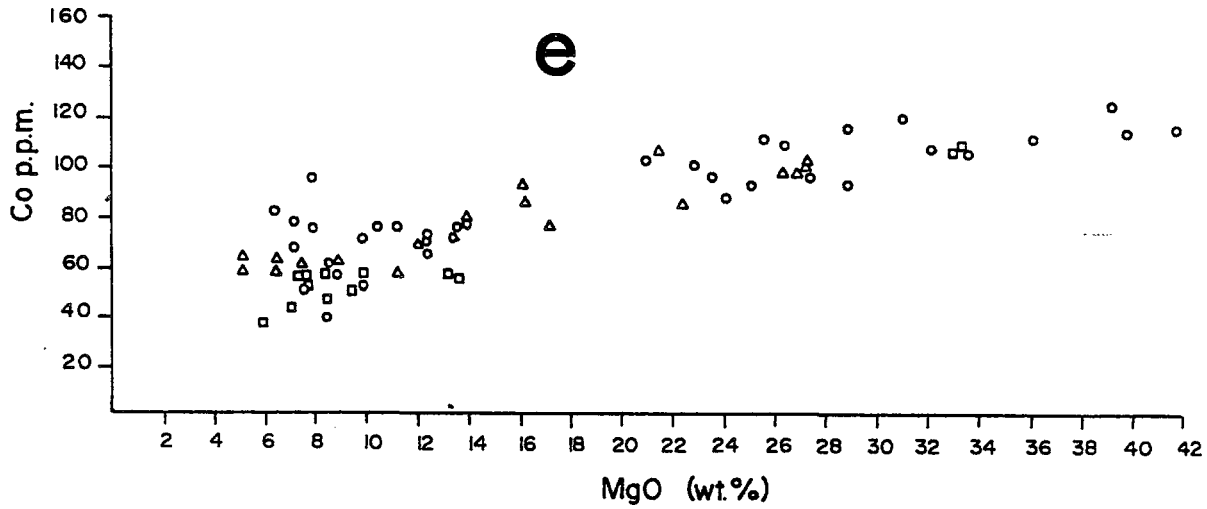
e
Co p.p.m.
160
140
120
100
80
60
40
20
2 4 6 8 10 12 14 16 18 20 22 24 26 28 30 32 34 36 38 40 42
MgO (wt.%)

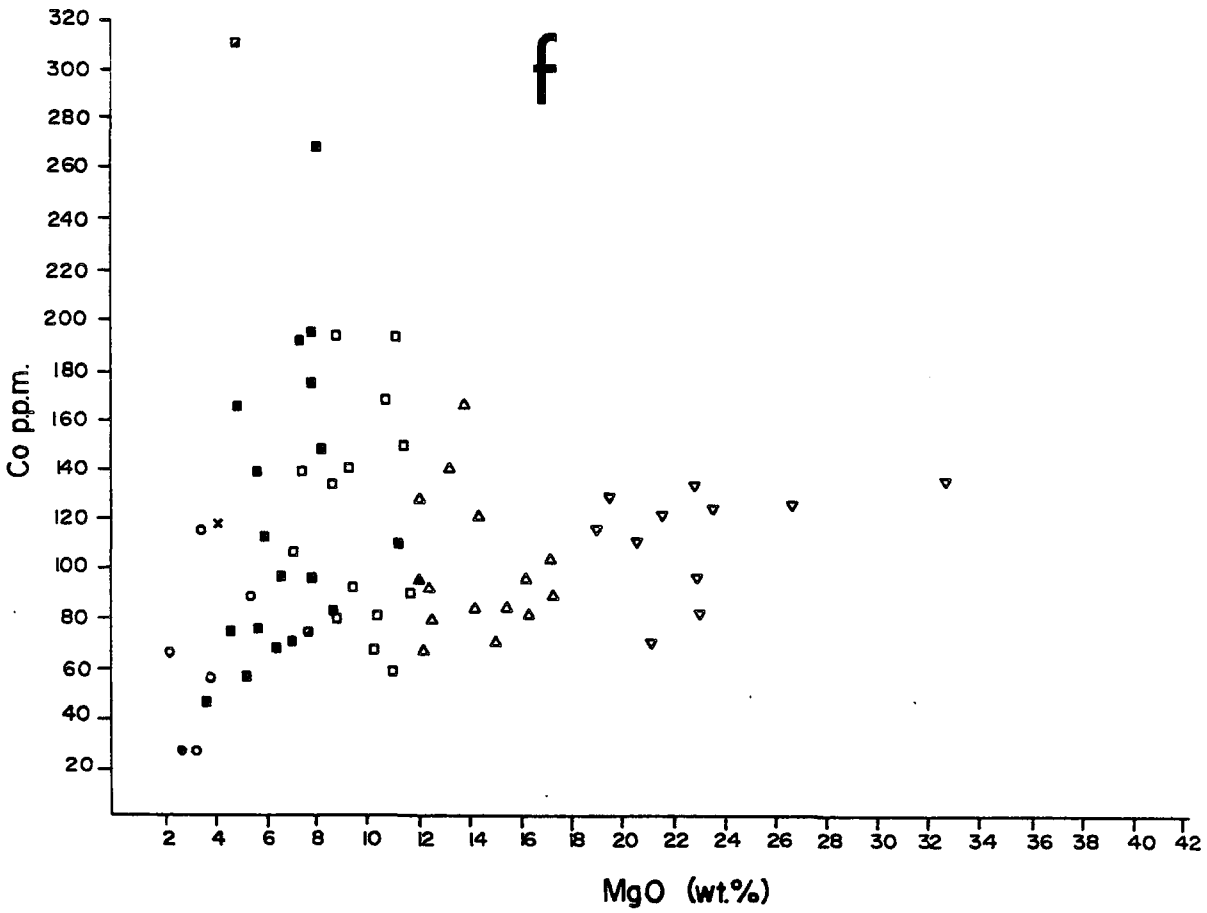
f
Co p.p.m.
320
300
280
260
240
220
200
180
160
140
120
100
80
60
40
20
2 4 6 8 10 12 14 16 18 20 22 24 26 28 30 32 34 36 38 40 42
MgO (wt.%)

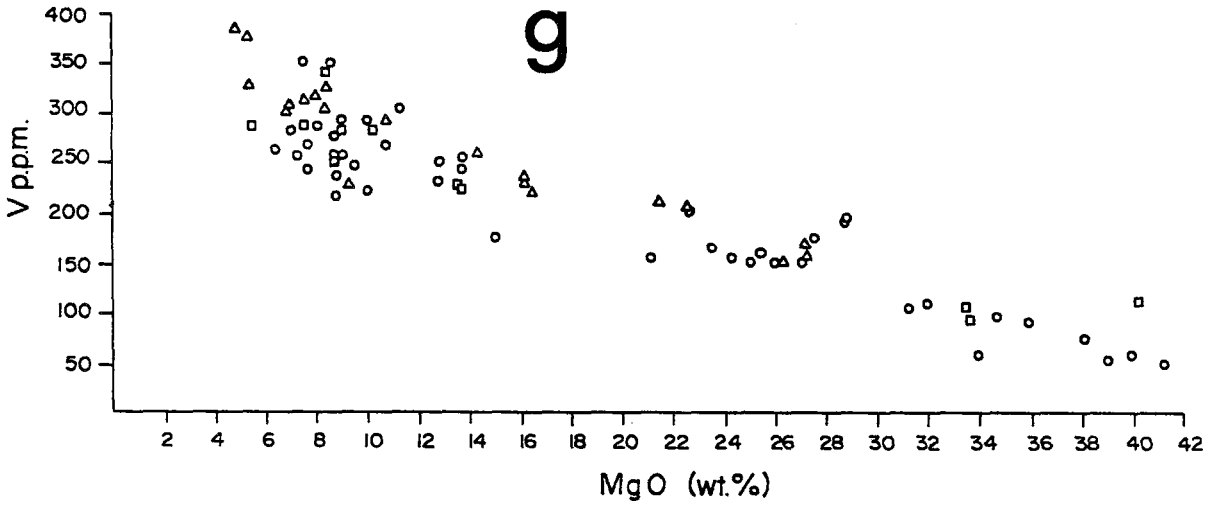
g
V p.p.m.
400
350
300
250
200
150
100
50
2 4 6 8 10 12 14 16 18 20 22 24 26 28 30 32 34 36 38 40 42
MgO (wt.%)

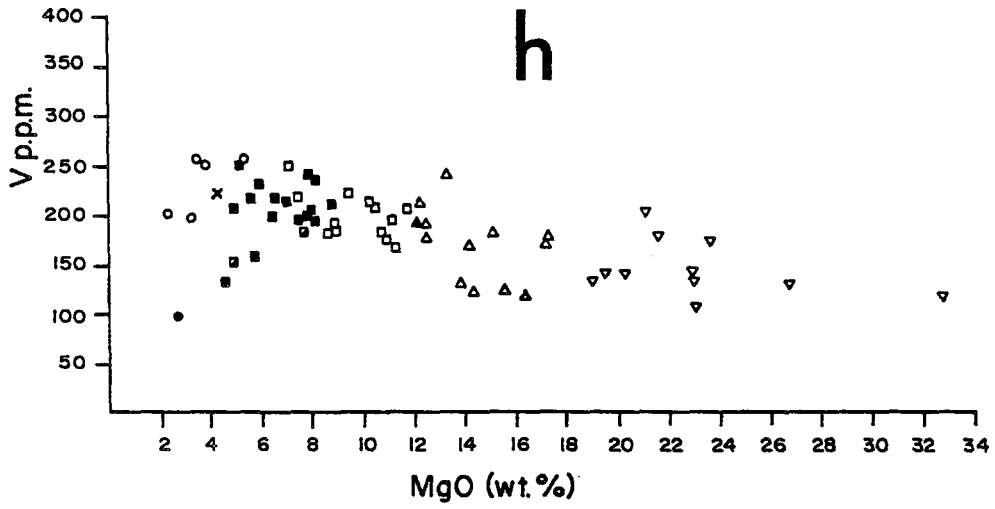
h
V p.p.m.
400
350
300
250
200
150
100
50
2 4 6 8 10 12 14 16 18 20 22 24 26 28 30 32 34
MgO (wt.%)

3. High and low MgO komatiitic basalts are anomalously rich in K_2O when compared to those from other Archean terranes. The high K_2O contents in these rocks are likely attributed to a late potassic alteration event in the thesis map area.

4. Sequence 1 is composed of tholeiitic and calc-alkalic volcanic flows. These have on average higher TiO_2 abundances than komatiitic basalts for any given SiO_2 or MgO abundance. There are no ultramafic or high MgO flows in sequence 1.

Chapter 5

Geology and Petrography of Sedimentary Rocks

5-1 Introduction

There are sixteen separate stratigraphic levels in the map area where sediments are found, ten on the south limb of the Lebel Syncline and six on the north limb. These sedimentary units are outlined roughly in figure 5-1 and in more detail in map 6. They range in exposed thickness from 0.5 meters to 120 meters. Many of these units show a lithological variability along strike which was not fully documented in this study due to lack of mapping time and the relatively poor exposure. In regard to the second point, the majority of the outcrops are located in the bush where they are invariably lichen covered, hard, flat and often rusty weathering. This masks sedimentary structures and prevents easy breaking of hand specimens. Sedimentary lithologies found in the map area are indicated in table 5-1.

The sandstones examined petrographically have been classified according to a classification given by Pettijohn (1975) using the diagrams shown in figure 5-2a and b. The thin sections examined were not point counted. Abundances of quartz, feldspar, rock fragments and matrix shown in

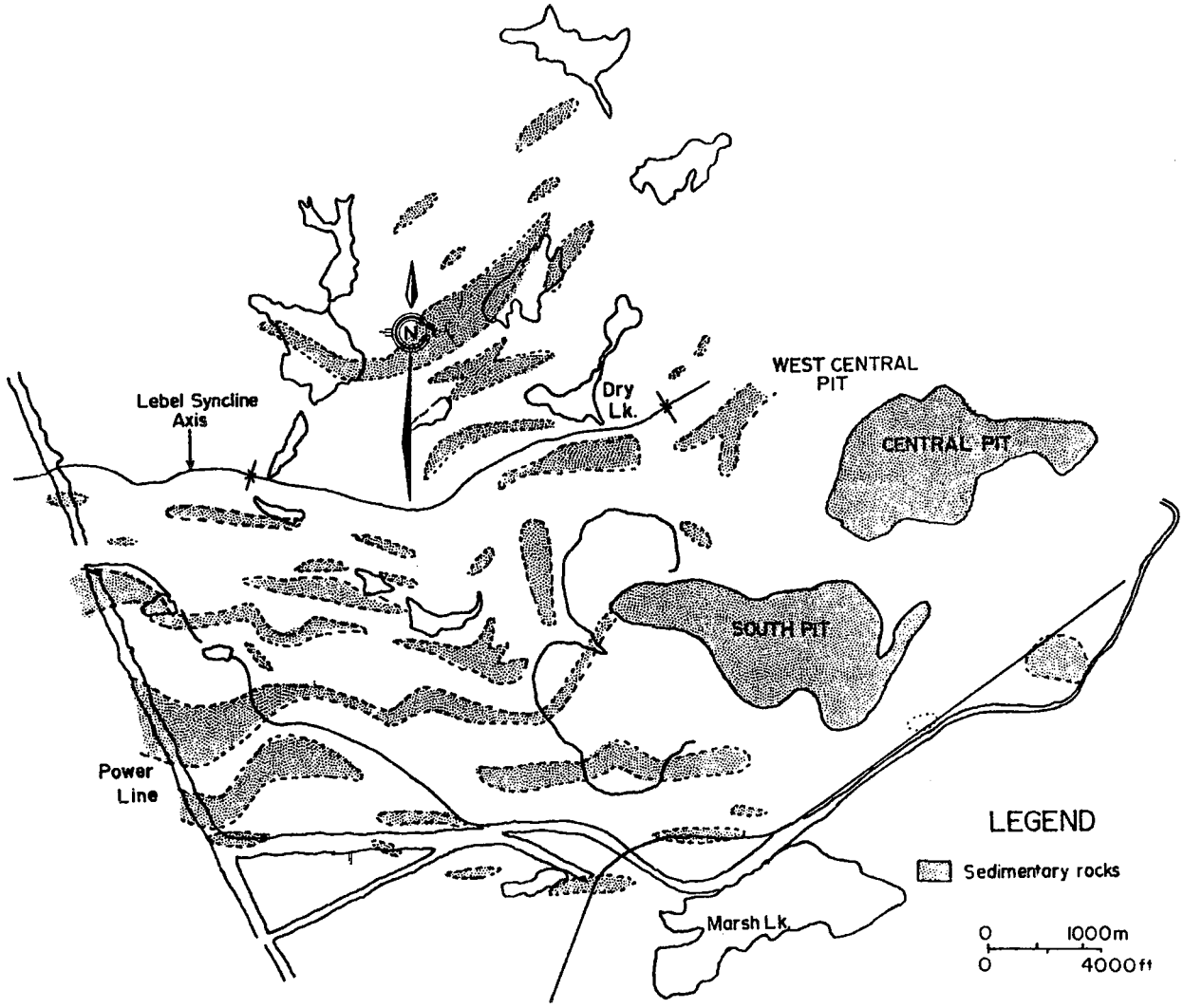

FIGURE 5-1 Outline of sedimentary units found in the map area.

Table 5-1

Sedimentary lithologies in the Map Area

Sandstone, Massive Appearing (mainly lithic arenites)
Sandstone and or siltstone, thinly laminated
Granule Conglomerate
Pebble Conglomerate
Cobble Conglomerate
Banded Iron Formation (oxide facies)
Chert
Carbonaceous Sediment/Chert
Argillite

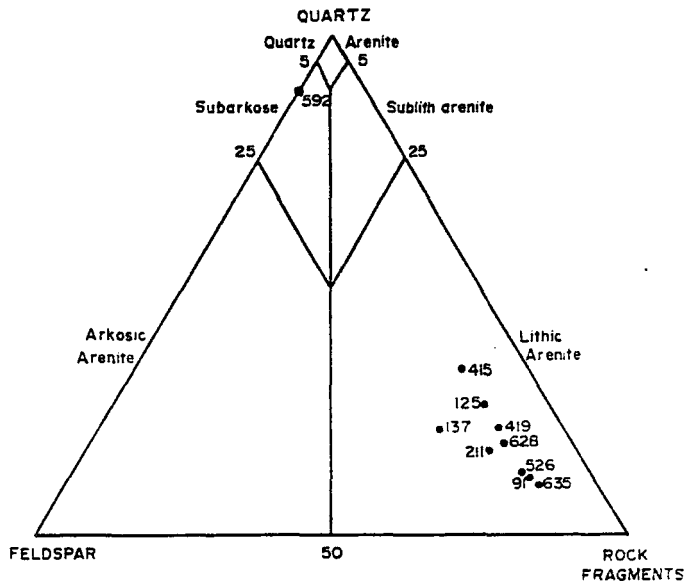

FIGURE 5-2a Classification of sandstones with 15 % or less matrix from Pettijohn (1975).

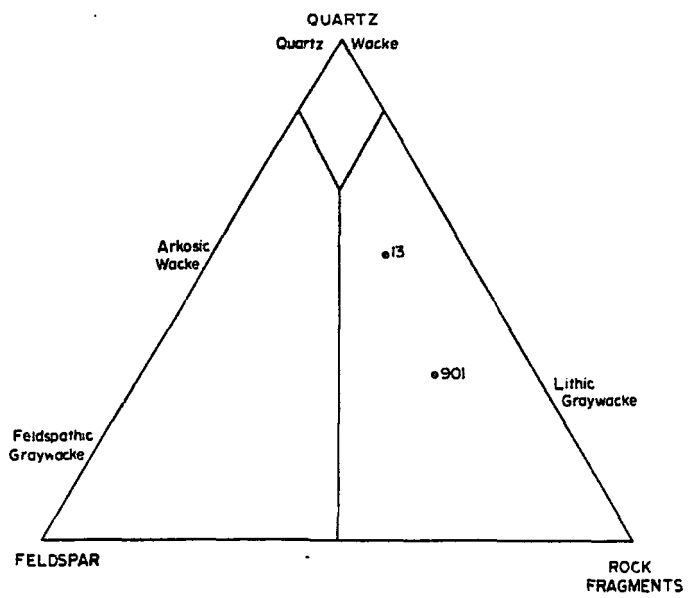

FIGURE 5-2b Classification of sandstones with greater than 15 % matrix from Pettijohn (1975).

table 5-2 were estimated visually. Feldspars were distinguished from quartz by treating the thin sections with sodium cobaltinitrite, BaCl and K-rhodizonate solutions, using a method of Houghton (1980). K-feldspar stains yellow, plagioclase stains pink. The location of samples in figures 5-2a and b are shown in map 1.

Sandstones identified from hand specimen only are referred to mainly by their color and hardness. Where more than about 25 % of the grains are coarser than sand size - pebble sized for instance - the sample was referred to as a pebble conglomerate after Williams, Turner and Gilbert (1954). Pebbly sandstones have less than 25 % pebble sized grains. The Udden-Wentworth scale shown in figure 5-3 was used to define grain sizes in thin section and in the field. Metamorphism and deformation have resulted in the recrystallization of sedimentary rock constituents but it is believed that grain sizes have not been significantly readjusted beyond a 200 meter zone adjacent to the Lebel Stock.

Field classification of strata based on thickness is after Ingram (1954)(table 5-3). Metamorphism and deformation have not destroyed sedimentary features such as this except adjacent to the Lebel Stock.

Chert was recognized in the field by its hard and extremely fine-grained appearance. It can best be distinguished from very fine grained quartz-rich sandstones

Table 5-2

Estimated percentages of quartz, feldspar, rock fragments and matrix in twelve map area sedimentary rock samples.

Sample Number	Quartz	Feldspar	Rock Fragments	Matrix
M-91	9	22	70	9
M-592	80	11	--	9
M-13	40	10	20	30
M-125	25	9	60	6
M-137	20	10	55	5
M-211	16	10	65	4
M-415	30	10	50	10
M-419	21	4	65	10
M-901	18	12	30	40
M-635	11	9	80	--
M-526	11	10	65	14
M-628	16	11	60	13

N.B. 95 % of feldspars in all sections are plagioclase.

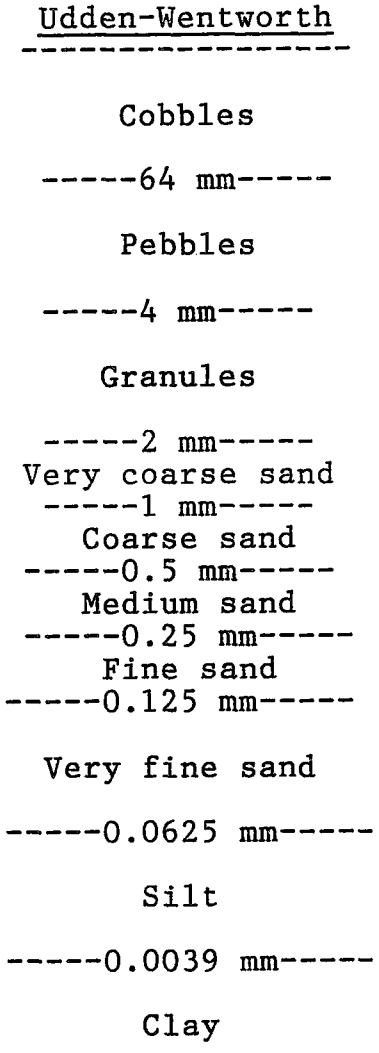

FIGURE 5-3 The Udden-Wentworth size grade scale taken from Blatt, Middleton and Murray (1980).

Table 5-3

Classification of stratification based on thickness after Ingram (1954)

Beds	very thick bedded	100 cm.
	thick bedded	30 cm.
	medium bedded	10 cm.
	thin bedded	3 cm.
	very thin bedded	1 cm.
Laminae	thick laminae	0.3 cm.
	thin laminae	

by the absence of a recognizable clastic component in hand specimen. However, some outcrops mapped as chert may quite conceivably be very fine grained recrystallized quartz-rich siltstones. This problem is highlighted in a study by La Tour et al. (1984) on interlayered feldspathic quartzite and quartzite in the mine site, both of which look the same in hand specimen. The former are interpreted as rhyolitic volcaniclastic sediments; the latter, a chemically deposited chert. If this interpretation is correct, then the field classification of some sedimentary rocks west and north of the mine site simply as cherts may be an oversimplification.

Black chert which has 1 to 10% very fine grained disseminated graphite or amorphous carbon is referred to as carbonaceous chert. Soft, black, carbon and/or graphite rich samples are referred to as carbonaceous sediments. Soft, well cleaved dark grey sediments are called argillite. These contain 30 % or more micaceous minerals.

5-2 Sediments Intercalated with Sequence 1

The stratigraphically lowermost sediment is an ungraded cobble conglomerate which is well exposed on clean outcrops beside the railroad tracks (sample locality M-518, figure 5-4). The conglomerate has an outcrop strike length of 200 meters and a maximum exposed thickness of 15 meters. In plate 5-1, it is seen that the conglomerate is composed of 50 % subrounded to subangular white weathering, medium

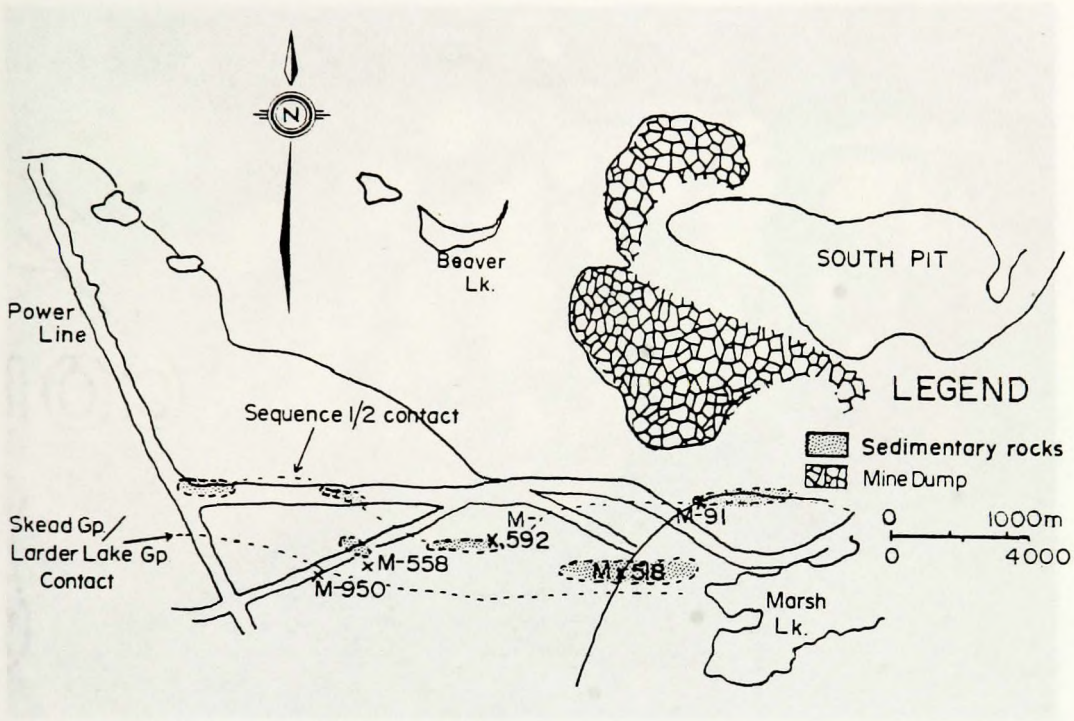

FIGURE 5-4 Outline of sedimentary units intercalated with sequence 1 and found along the sequence 1/2 contact. M-518, 558, 950 and 91 are locations of outcrops which are referred to in the text.

PLATE 5-1 Subrounded to subangular white weathering granodioritic clasts in a green weathering groundmass at M-518. The local strike direction is parallel to the right edge of the photograph.

grained granodiorite clasts, 0.5 mm to 20 cm in length. These clasts are supported in a light green weathering fine grained matrix. The clasts are composed of 20 % euhedral hornblende with a grain size averaging between 0.2 to 0.5 mm in size, 15 % clinozoisite and 20 to 30 % quartz with average grain sizes of 0.2 mm and 30 to 40 % very fine grained untwinned feldspar. The matrix is shown in plate 5-2 and is composed of 90 % fine grained hornblende and 10 % fine grained feldspar. Locally, rounded medium grained diorite clasts up to 2 cm in diameter are found in the conglomerate. The long axis of the granodiorite clasts as exposed on a flat outcrop is parallel to the strike of the stratigraphy.

Fine grained massive, siliceous, white sandstones and thinly laminated white and grey chert occur near the top of sequence 1 north of sample locality M-558 (figure 5-4). They have an exposed thickness of four meters. The sandstone underlies the chert.

The contact between sequence 1 and the underlying Skead Group is best exposed along the Adams Mine road in the western part of the map area. The Skead Group here is represented by a massive feldspar porphyry rock, possibly a flow and thinly laminated tuff. A tuff sample (M-950) is composed of 15 to 20 % euhedral to subhedral clinozoisite with grain sizes averaging 0.1 mm in a very fine grained groundmass of quartz and clinozoisite. This assemblage

PLATE 5-2 The groundmass to the granodiorite clasts is dominated by hornblende and albite. Polarized light, x63. The field of view is 1.0 x 1.5 mm.

resembles the crystal tuff described by Abraham (1950) which, along with porphyritic lavas, make up the majority of the unit later named the Skead Group by Ridler (1969). Massive porphyritic and non-porphyritic flows and laminated tuffs similar to that at the Adams Mine road cut were observed at several locations to the east near or at the Skead Group/Larder Lake Group contact. These limited field observations suggest that sedimentary rocks are absent along the contact. This is consistent with regional mapping (Lawton, 1957; Abraham, 1950; Jensen, 1979).

5-3 Sediments Found at the Sequence 1-2 Interface

Thinly laminated chert shown in plate 5-3 overlies and/or underlies massive fine grained siliceous white sandstones along the boundary between sequences 1 and 2. This unit is approximately 2 to 5 meters in thickness.

Sample M-91, a lithic arenite taken along the railroad tracks, contains 15 % euhedral clinozoisite laths with an average grain size of 0.5 mm and 70 % felsic volcanic rock fragments which average 0.2 mm in diameter. Quartz arenite (sample M-592) contains 10 % subrounded to subangular monocrystalline quartz clasts (0.5 mm in diameter) in a very fine grained quartz-rich framework.

5-4 Sediments Found at the Sequence 2-3 Interface

This sedimentary unit can be traced from M-137 east

PLATE 5-3 A flat, smooth weathering outcrop of finely laminated chert at the interface between sequence 1 and 2 near M-592 (figure 5-4). The strike is 090 and the dip vertical.

to M-160, a distance of approximately 400 meters (figure 5-5). Massive sandstones at M-211 south of the South Pit in the mine site are at roughly the same stratigraphic position and may be stratigraphically correlative with these rocks.

The sediments, where best exposed at M-125, are approximately 20 meters thick and consist mainly of a massive appearing, rusty, low weathering, sandstone which is underlain by a well cleaved argillite. M-125 is a lithic arenite composed of 60 % subangular clasts of felsic volcanics (0.1 to 0.3 mm in diameter), 10 % monocrystalline, subrounded quartz clasts (0.1 to 0.2 mm in diameter) in a fine grained framework consisting largely of quartz with lesser feldspar and sericite as is shown in plate 5-4. The felsic volcanic clasts are poikilitic with numerous randomly oriented sericite inclusions. The argillite (M-130) has a similar composition to the framework of the associated arenites with 70 % quartz and feldspar and 30 % very fine grained sericite. The sericite imparts a foliation parallel to lithological contacts. Lithic arenites at M-137 and M-211 also contain minor amounts of subangular polycrystalline quartz clasts, likely recrystallized chert and subangular and angular pyrite clasts in addition to the major clast type (felsic volcanics).

5-5 Sediments Underlying Sequence 4 and or 5 and Overlying Sequence 3

Sediments which overlie the third volcanic sequence

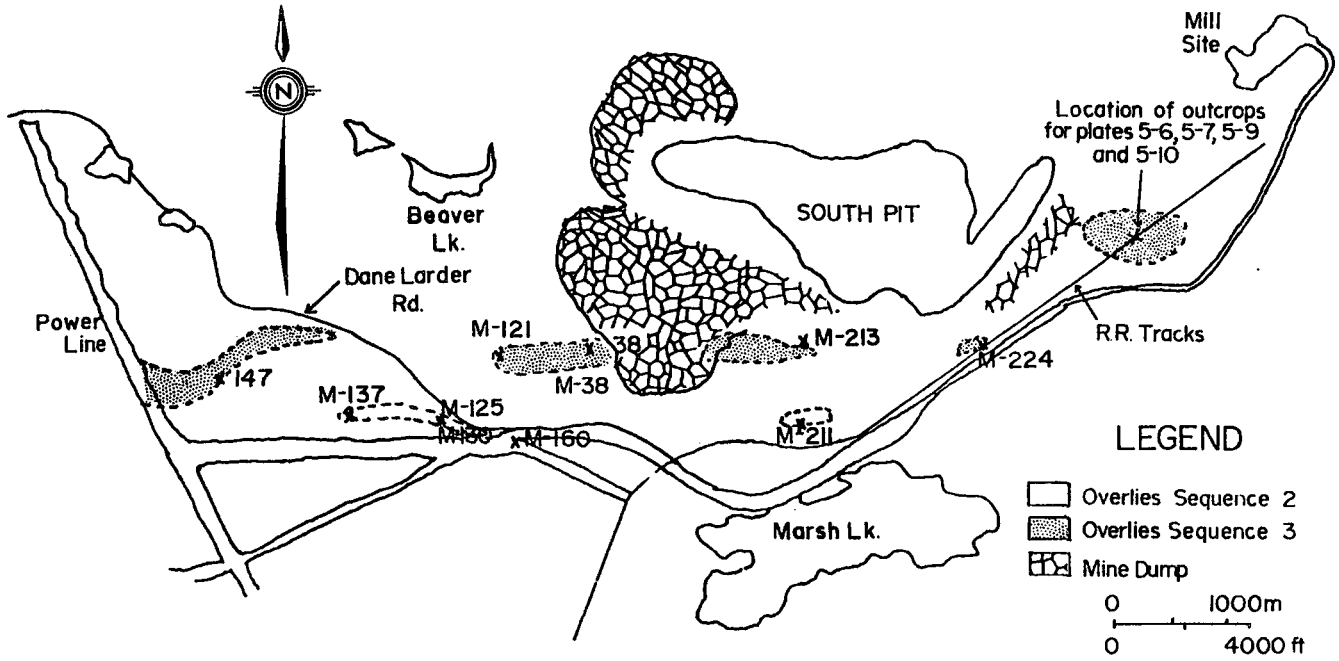

FIGURE 5-5 Outline of the sedimentary units overlying sequences 2 and 3.

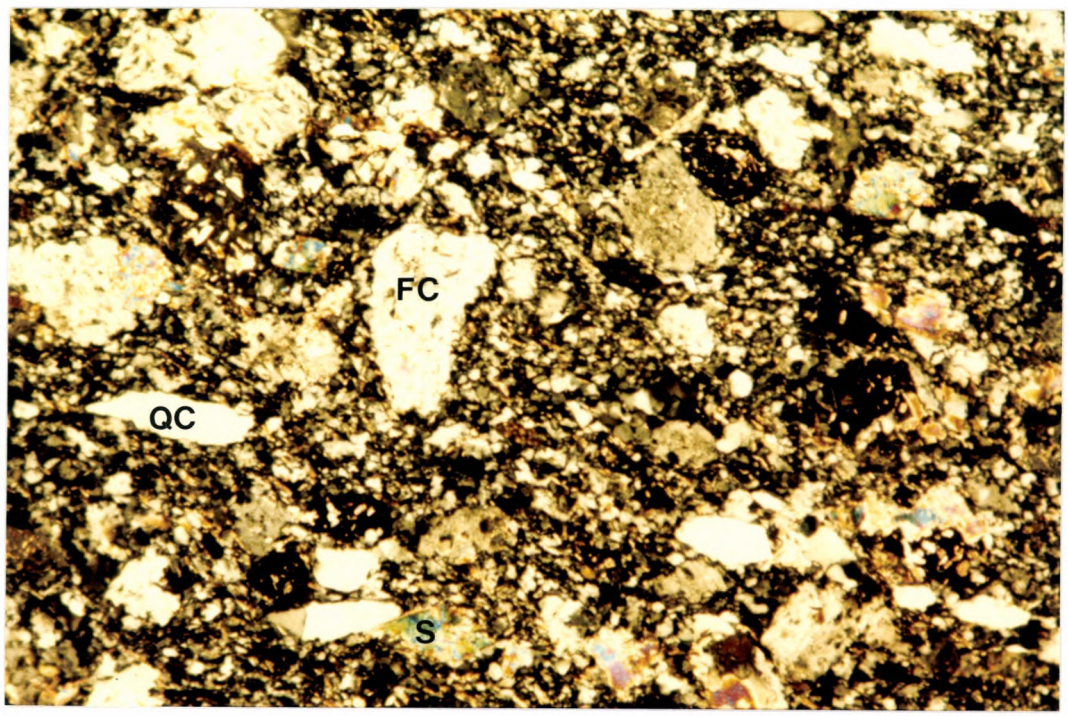

PLATE 5-4 Sublithic arenite (M-125). Clear are the subangular felsic clasts (F.C.), the clean monocrystalline quartz clasts (Q.C.), and the brownish framework comprised dominantly of quartz. The high birefringence grains are sericite (S). Polarized light, x63. The field of view is 1.0 x 1.5 mm.

(figure 5-5) are the best exposed sediments in the map area aside from B.I.F.. Numerous well exposed outcrops are found along the railroad tracks and mine roads in the mine site and along the northwest trending power line in the western side of the thesis map area. These sedimentary rocks consist of a number of separate areas of outcrops which are roughly time equivalent, as suggested by their consistent stratigraphic relationship to the volcanics. Conglomerates are abundant in this interval.

Ungraded pebble conglomerate exposed near M-213 is shown in plate 5-5. This conglomerate consists of 60 % angular to subangular chert and argillite clasts which are supported in a quartz dominated matrix. It has an exposed thickness of 25 meters. From M-38 to M-121 (figure 5-5), pebble conglomerates are spatially associated with laminated argillite, carbonaceous sediment, chert, and medium grained massive sandstones. The pebble conglomerate contains either subangular volcanic clasts (felsic and mafic) or angular argillite clasts. M-13, a sandstone from this locality which was examined petrographically is a lithic greywacke (table 5-2). The rock fragments are felsic volcanics.

The most westerly part of this unit that was mapped directly underlies sequence 5. Near the Dane-Larder road, it contains scattered outcrops of hard, rusty weathering, dark grey or white siliceous sandstone, chert and carbonaceous sediments. Further west, ungraded pebble and

PLATE 5-5 An outcrop of pebble conglomerate exposed near M-213 south of the South Pit which is representative of the abundant conglomerate exposure in this vicinity.

cobble conglomerates are present. The conglomerate at M-147 contains angular chert clasts while along the power line, angular B.I.F. clasts predominate. Both conglomerates have a siliceous, white to grey, cherty matrix. The long axes of the blocky chert clasts at M-147 parallels local strike.

East of M-213 to south of the mill, ungraded cobble and pebble conglomerate is the predominant sedimentary rock type. The conglomerates here are subdivided into three types based on clast type.

Type I: mostly cobble conglomerate, minor pebble conglomerate, with angular to subangular white siliceous sandstone and chert clasts supported in a rusty weathering felsic matrix (plate 5-6).

Type II: cobble and pebble conglomerates with angular to subangular, white and light green chert, feldspar porphyry, fine grained felsic to intermediate volcanic, mafic volcanic and massive pyrite clasts (plate 5-7). The clasts are supported in a dark green to grey, fine grained siliceous matrix which consists of variable fine to very fine grained quartz and actinolite with felsic clasts up to 0.5 mm (plate 5-8).

Type III: clast supported, cobble conglomerate with angular mafic and ultramafic clasts, locally spinifex bearing (plate 5-9).

At two locations within type III conglomerates, units approximately 1 meter thick consist of medium to fine

PLATE 5-6 Type I conglomerate exposed south of the mill at the railroad tracks (figure 5-5). The large white clast below the camera lens cover is chert.

PLATE 5-7 Type II conglomerate as exposed on a blasted outcrop along the railroad tracks south of the mill (figure 5-5). Visible clasts include feldspar porphyry (F.P.), chert (C.) and rhyolite (R.). The long axes of the clasts exposed on this nearly vertical face parallel the local strike.

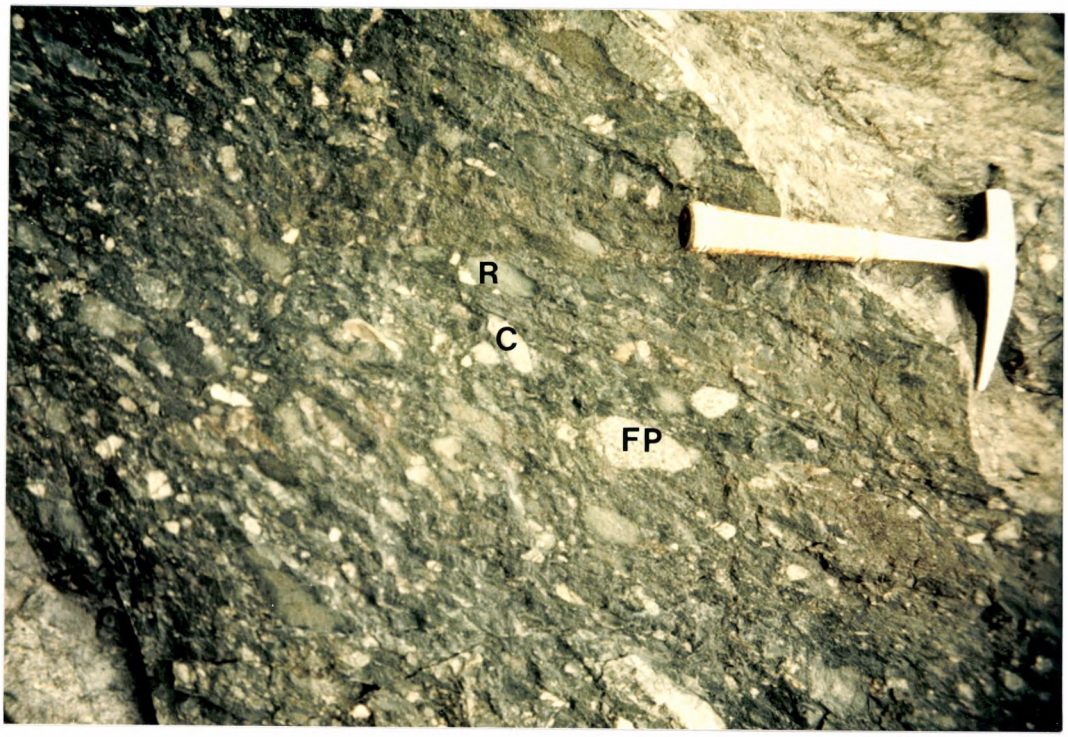
R
C
FP

PLATE 5-8 Sample M-224, Type II conglomerate. The hard, dark green matrix is comprised of subangular felsic clasts (F.C.), actinolite (A.C.), quartz (Q) and sericite (S). Polarized light, x63. Field of view is 1.0 x 1.5 mm.

PLATE 5-9 Type II conglomerate as exposed at the railroad tracks south of the mill. Most of the clasts seen here are angular, elongate, komatiitic basaltic (the pencil points to the one such clast). They show a preferred orientation with this long axis, as exposed on this vertical section, parallel to the local strike. Occasional white clasts are chert. The conglomerate here is clast supported.

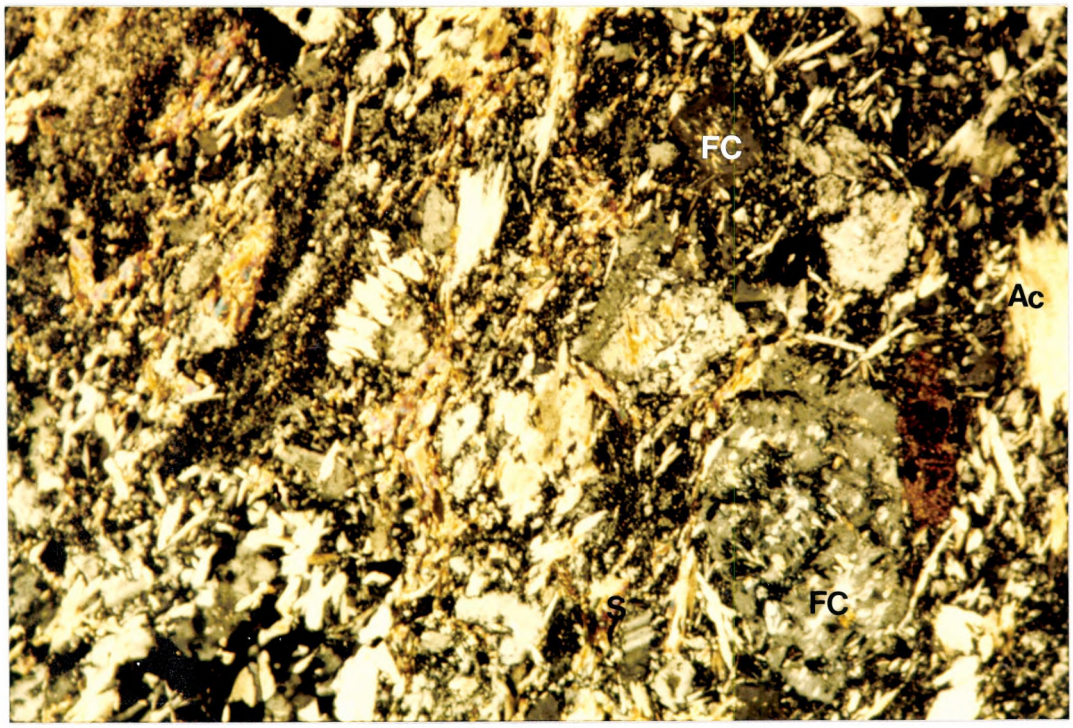
FC
Ac
S
FC

grained sandstone which fines upwards to siltstone and chert (plate 5-10). These units have sharp contacts with the conglomerates.

5-6 Sediments Overlying Sequence 5

Sediments overlying sequence 5 (figure 5-6) west of the mine site occupy the same stratigraphic interval as the iron formations in the South and Peria Pits. The iron formations in the pits and west of the mine site are thinly laminated to thinly bedded with chert and magnetite layers 0.1 to 5 cm thick (plate 5-11). The quartz and magnetite in these layers is fine to very fine grained. Locally actinolite-rich layers (70 % fine grained actinolite and 30 % very fine grained quartz and albite) and grunerite-bearing layers (20 % fine grained grunerite and 80 % very fine grained quartz) are interbedded with the two. Fine grained euhedral pyrite forms up to 10 % of the actinolite-rich layers. The actinolite-rich layers are referred to as mafic tuff in map 3.

B.I.F. in the South Pit is approximately 50 meters thick and is underlain by a massive grey chert 5 to 15 meters in thickness. West of the mine site, where B.I.F. is a minor lithology relative to the more abundant chert and clastic sediments, B.I.F. has a maximum thickness of 10 meters. Locally the B.I.F. here is split into two horizons by high Al_2O_3 komatiitic andesite flows. B.I.F. is a

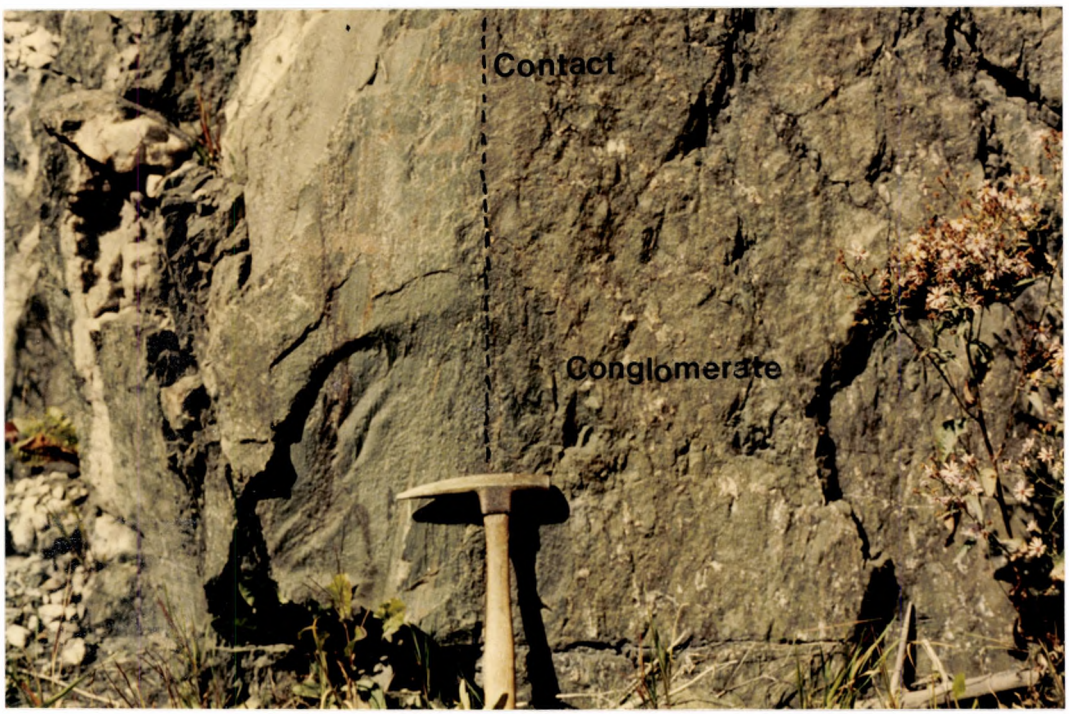

PLATE 5-10 The light grey, smooth weathering unit on the left side of this photo is 1 meter thick and shows graded bedding. Medium grained sandstone grades to the right into very fine grained sandstone, siltstone and chert. The lower contact of this unit is not exposed. The upper contact shown in the middle of the photo is abrupt. At this contact, thinly laminated chert is overlain by green weathering type III conglomerate. This photo is of a vertical rock exposure and is approximately at right angles to local strike. The dip of the contact here is nearly vertical.

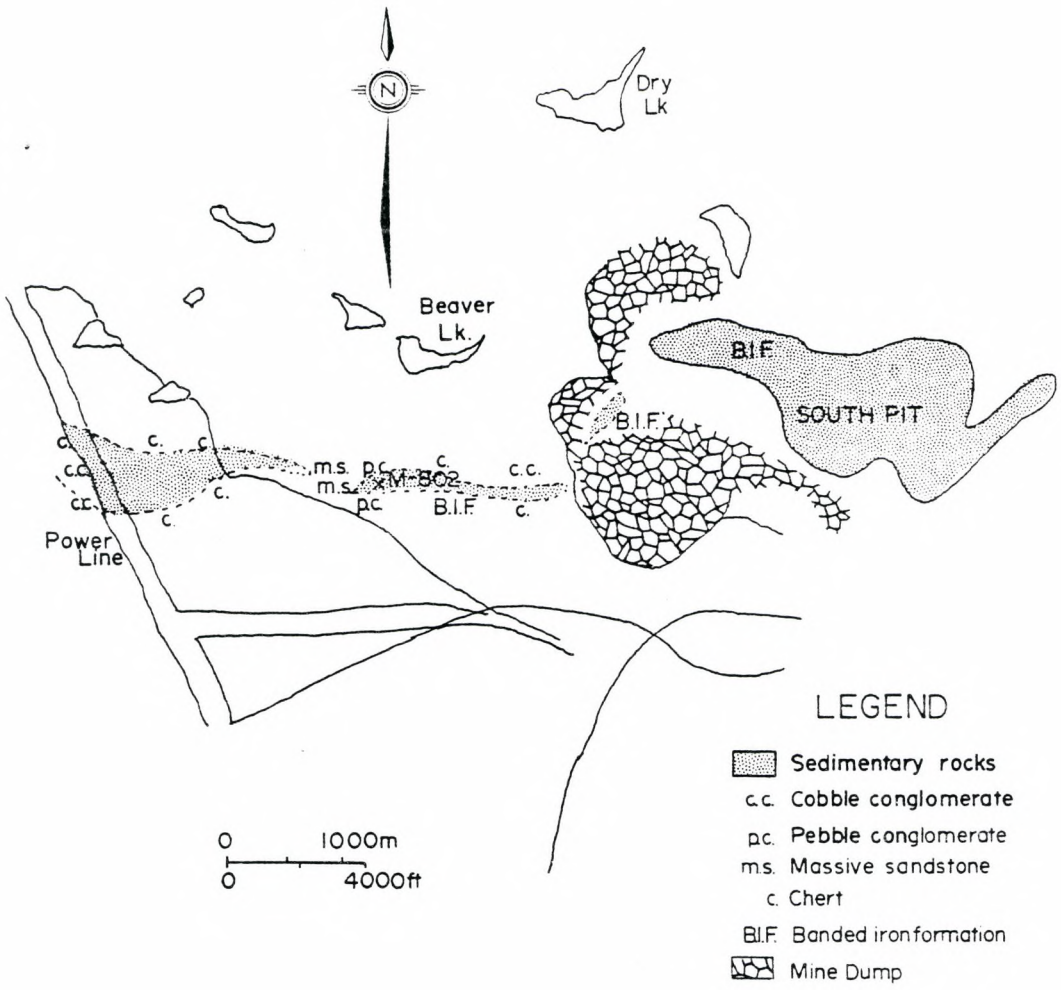

FIGURE 5-6 Outline of sedimentary rocks which overlie sequence 5.

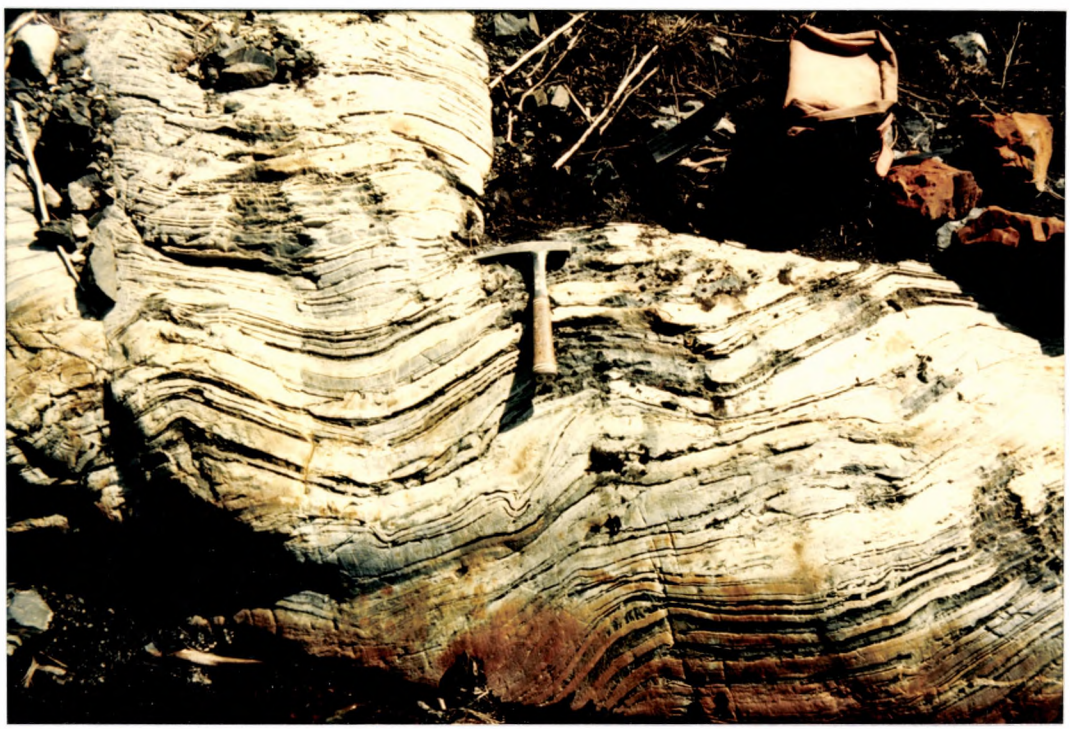

PLATE 5-11 Thinly bedded oxide facies banded iron formation from the stratigraphically lowest B.I.F. unit. This outcrop is located west of the mine site. The grey weathering layers are magnetite-rich whereas the white weathering layers are quartz-rich (chert). The slight undulation of the bedding is probably attributable to folding.

volumetrically minor lithology beneath the mine dump southwest of the South Pit. This is inferred from Lawton (1957) and McLeod (1952).

Massive and finely laminated chert overlies B.I.F. north of the Dane-Larder road and is interbedded with ungraded cobble conglomerate along the northwest trending power line and near the mine dump site. These conglomerates contain variable proportions of angular, blocky chert clasts in a cherty matrix. Pebble conglomerate is along strike from and locally underlies B.I.F. north of the Dane-Larder road. M-802, representative of this lithology contains 45 % subangular felsic volcanics and 20 % komatiitic basalt clasts up to 1.0 cm in diameter in a matrix of fine grained felsic clasts and very fine grained quartz. Massive, medium grained sandstone found near M-802 appears to resemble the conglomerates in composition.

The sedimentary unit overlying sequence 5 appears to be thickest (100 meters) between the northwest trending power line and the Dane-Larder road where it is folded around the south end of the Power Line Gabbro.

5-7 Sediments Overlying Sequence 7

This sedimentary unit is likely the lateral equivalent to B.I.F. at the Central Pit as noted in section 3-7. Very fine grained nonclastic sediments (B.I.F., chert, carbonaceous chert, argillite and carbonaceous sediment) are

dominant near and immediately east of the northwest trending power line, north of Dump Lake west of the mine dump and at Fault Lake (figure 5-7). Conglomerates are found south and east of Beaver Lake with massive chert with massive appearing fine to medium grained sandstones occupy the section west of Beaver Lake to east of the Dane-Larder road. B.I.F. occurs intermittently as a minor lithology with the sandstones.

The conglomerate southeast of Beaver Lake is characterized by subangular chert clasts while that east of Beaver Lake is dominated by angular komatiitic basalts clasts. Subrounded chert clasts are subordinate in abundance. Plate 5-12 shows a rare glimpse of clean outcrop of this second conglomerate type as exposed immediately west of Dump Lake. On lichen covered outcrop, this conglomerate is easily confused with a low MgO komatiitic basalt or andesite.

5-8 Sediments Intercalated With or Overlying Sequence 8

Sediments overlie and are locally intercalated with sequence 8. Clastic sediments predominate. B.I.F., chert and carbonaceous sediment are minor. The clastic sediments observed are lithic arenites (M-415, M-419 and M-901) and granule conglomerate. The coarsest, most abundant clasts in the arenites are angular to subangular felsic volcanic with fewer, finer grained subangular komatiitic basalt clasts.

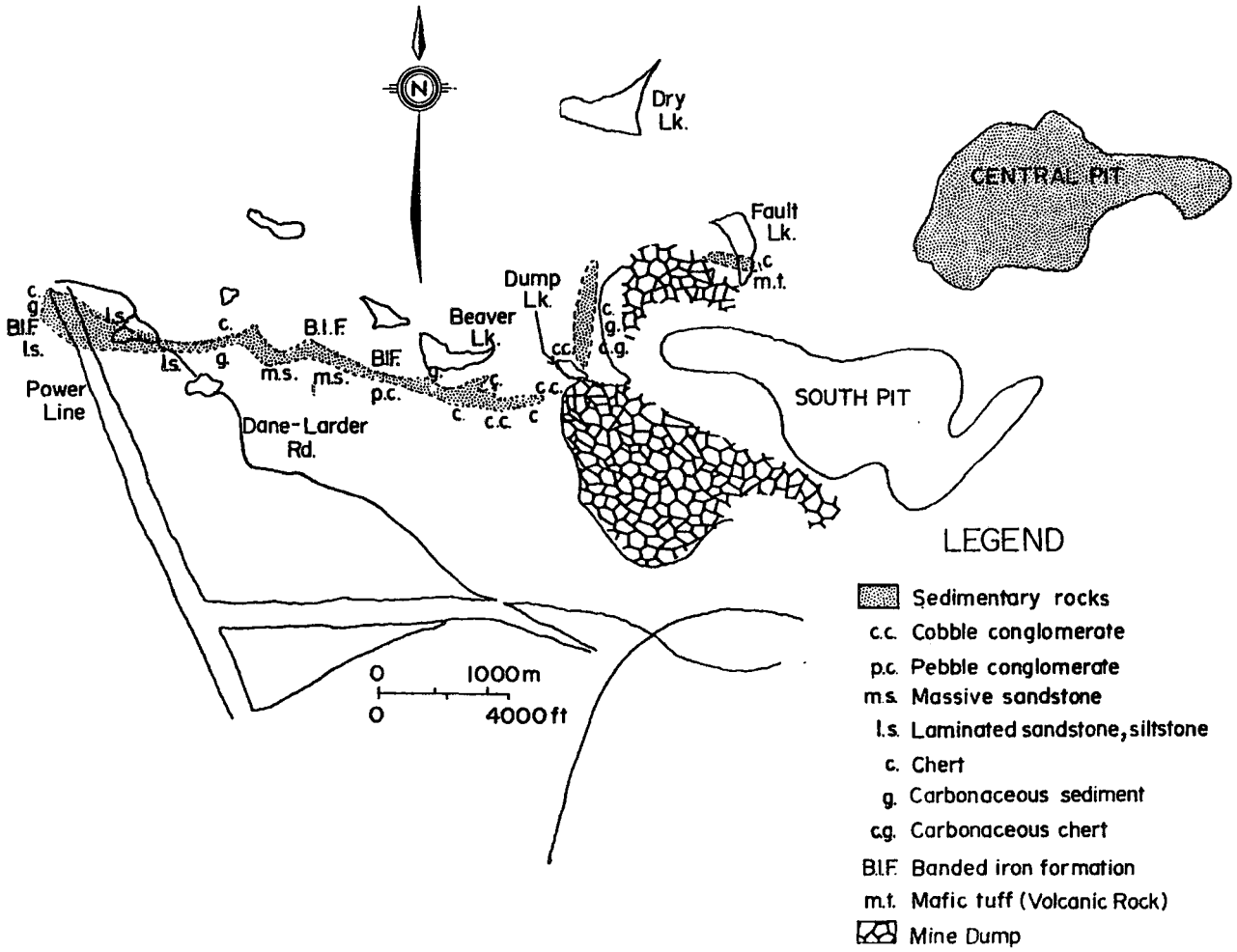

FIGURE 5-7 Outline of the sedimentary unit which overlies sequence 7.

PLATE 5-12 Angular komatiitic basalt clasts and subrounded white cherty clasts are set in a white weathering quartz-rich matrix. This photo is from the creek bed west of Dump Lake (figure 5-7). The sediment is bounded by sequences 7 and 8.

The framework consists largely of quartz and actinolite.

B.I.F. outcrops below and between the peridotite-gabbro and gabbroic sills stratigraphically above sequence 8 are regarded as the lateral equivalents to B.I.F. exposed in the West Central Pit. The reasoning for this was presented in section 3-7.

5-9 Sediments on the Northern Limb of the Lebel Syncline

As was stated previously, the northern limb has not been extensively mapped and as such the stratigraphy and structure could be better understood. However, sedimentary outcrops observed at several localities permitted the recognition of six separate stratigraphic units of variable thickness and lateral continuity. The six units are labelled as group 1 to 6 as shown in figure 5-8. Conductors picked up by a radem VLF-EM geophysical survey performed by A.C.A. Howe International Ltd. (MacMichael, 1981) are also shown in figure 5-8.

Group 1 sediments outcrop 100 to 200 meters south of the Lebel Stock and consist of carbonaceous sediment and a lithic arenite (M-628) compositionally similar to those such as M-125 underlying sequence 3 on the south limb. Sericite is coarse grained and randomly orientated in M-628. Group 1 sediments underlie komatiites and appear to be split up locally by a gabbroic sill. Carbonaceous sediments are expressed geophysically by conductor axes B and E. At Far

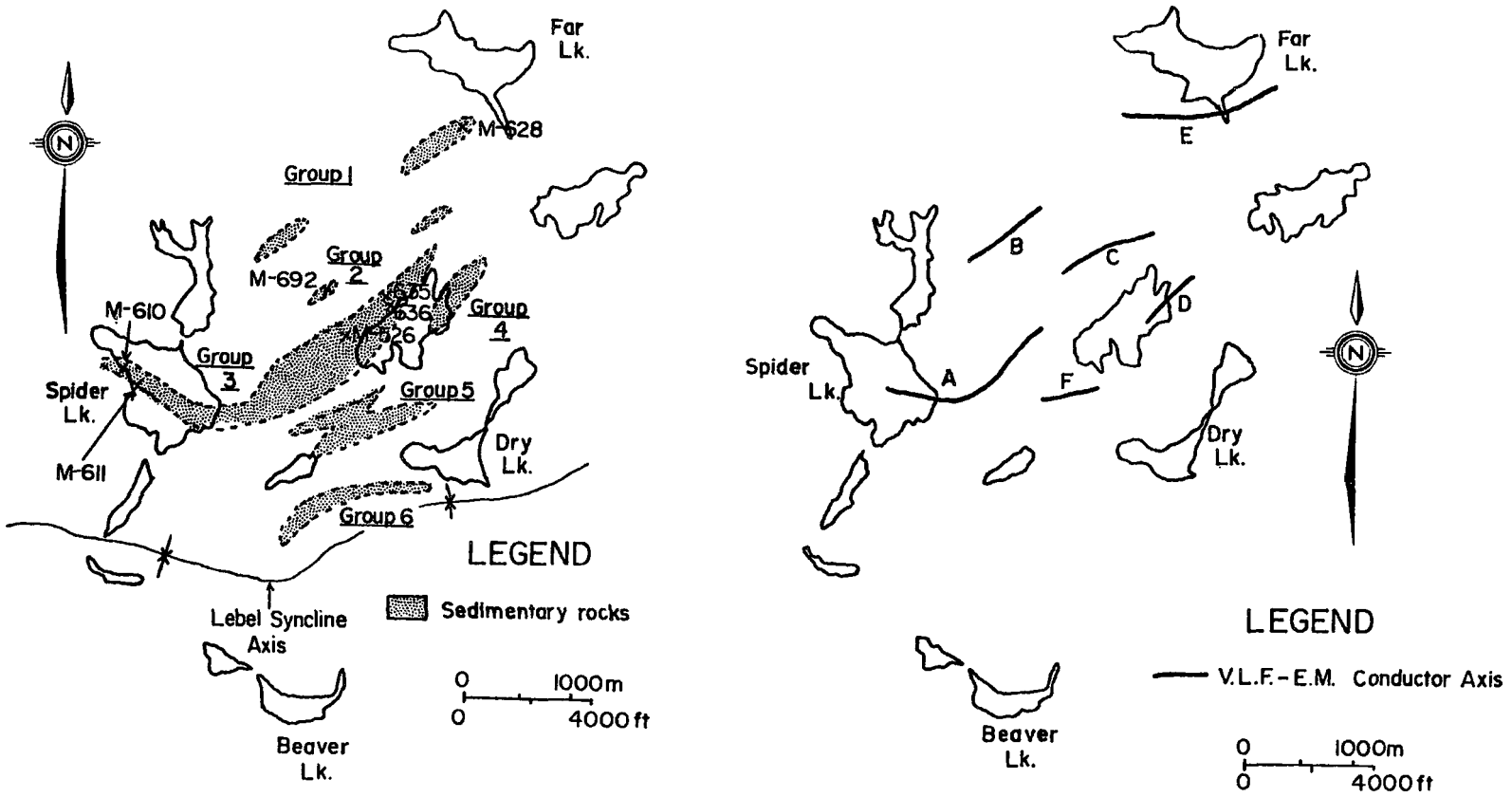

FIGURE 5-8 Outline of the six sedimentary units on the north limb of the Lebel Syncline and the radem V.L.F.-E.M. conductor axes outlined by A.C.A. Howe International Limited (MacMichael, 1981). The sample numbers are those referred to in section 5-9.

North Lake, the Contact Gabbro contains large xenoliths up to 10 meters in size consisting of coarse grained magnetite, presumably strongly recrystallized iron formation.

Group 2 sediments (pyrrhotitic chert and garnet-biotite-bearing argillite (M-691) are found south of the most northerly exposed komatiites. The sulphide bearing chert is expressed geophysically by conductor axis C which extends between the two end point outcrops which mark the group.

M-691 differs petrographically from argillite (M-130) from the south limb, in that it contains biotite and garnet instead of sericite as in M-130. Groups 1 and 2 sediments are not observed at, or immediately east of, Spider Lake where the Contact Gabbro outcrops.

Group 3 sediments make up the thickest and most laterally extensive unit in the mapped part of the north limb. This unit appears to be thickest (120 meters thick) along the north and west shores of North Lake where it is made up largely of hard, fine grained dark grey massive sandstones. Two samples M-526 and M-635 which were examined petrographically are lithic arenites which petrographically resemble those found low in the south limb stratigraphy. Felsic volcanics are the major rock fragment type in the arenites.

Lesser amounts of massive light grey, siliceous sandstone, ungraded cobble conglomerate, thinly laminated

chert, carbonaceous sediments and argillite occur here. The argillite as is seen in M-636 is biotite-bearing (plate 5-13). The conglomerate contains 25 to 30 % subangular, massive to banded, chert clasts in a white to rusty weathering, siliceous, very fine grained matrix (Plate 5-14). This conglomerate is laterally discontinuous in that it exposed along a strike length of 40 meters. It has a thickness of approximately 20 meters.

Carbonaceous sediments found along the northern and western limit of rock exposure between North and Spider Lakes likely produced the conductor axis A shown in figure 5-8. This axis is traced beneath Spider Lake and terminates near sediments exposed along the northwestern shoreline of Spider Lake, suggesting lateral continuity. The sediments observed there include finely laminated rock (M-611) with alternating quartz-rich and biotite-rich bands and granule conglomerate (M-610) containing stretched tremolite-rich (komatiitic basalt) clasts and rare felsic clasts in a fine grained quartz framework. Both these features were obvious in thin section but not in the outcrop.

Group 4 sediments underlie komatiites and are floored by intrusive sills. Carbonaceous sediments and pyritic chert are observed and expressed geophysically as conductor axis D which is of limited lateral extent (200 meters). Group 5 sediments form a relatively wide band (100 meters maximum thickness) immediately south and southwest of North Lake. This group consists largely of massive chert,

PLATE 5-13 A fine grained hard, black sedimentary rock (M-636) from Group 3 is comprised essentially of quartz and biotite. Polarized light, x63. Field of view, 1.0 x 1.5 mm.

PLATE 5-14 Conglomerate observed locally in Group III sediments west of North Lake. Clasts of B.I.F. and laminated chert have a positive relief in relation to their host groundmass.

with lesser argillite and carbonaceous sediments and is outlined by conductor F. Group 6 is found immediately north of the Lebel Syncline fold axis and consists of massive, dark grey, siliceous, fine grained sandstones and minor oxide facies B.I.F.. This group is interpretable as the folded lateral equivalent to the stratigraphically uppermost B.I.F. on the south limb of the Lebel Syncline.

5-10 Summary

1. There are sixteen sedimentary units in the map area. Ten are on the south limb of the Lebel Syncline, with six on the north limb.
2. These units usually occur below or above komatiitic volcanic units and commonly show lithology variations along strike.
3. On the mine site, chemical sediments are more abundant than clastic sediments. The opposite is true along strike west of the mine site.
4. Conglomerates are common and widespread on the south limb of the Lebel Syncline west of the mine site. They are observed locally on the north limb of the Lebel Syncline.
5. Lithic arenites with volcanic rock fragments are the most abundant sandstone examined petrographically.
6. Chemical sediments (chert, B.I.F., and carbonaceous sediments) are more abundant than are pelitic sediments (argillite).

Chapter 6

Interpretation of Sedimentary Rocks

6-1 Acceptance of a Deep Submarine Depositional Environment

The clastic, chemical and pelitic sediments in the thesis map area are intercalated with pillowed basaltic and andesitic flows throughout the succession on both limbs of the Lebel Syncline. This is clearly indicative of a persistent submarine environment during volcanism and sedimentation.

These flows are void of vesicularity, suggesting extrusion at considerable depth. Moore (1965) observes that tholeiitic, pillow basalt from the east rift zone of the Kilauea Volcano contains vesicles whose volume and size decrease systematically with depth. At depths of 800 meters, the basalts contain more than 10% vesicles with an average diameter of more than 0.5 mm (figure 6-1). At 4000 meters, vesicles are rare and are less than 0.1 mm in diameter. Similarly, Jones (1969) notes an increase in vesicularity with decreasing depth for the prevalent variety of pillow lava in Icelandic basaltic volcanoes. The non-vesicular nature of the komatiitic flows thus tends to rule out fluvial, coastal and subaerial depositional environments and points to a sedimentary depositional environment which is thousands of meters below the water/air interface.

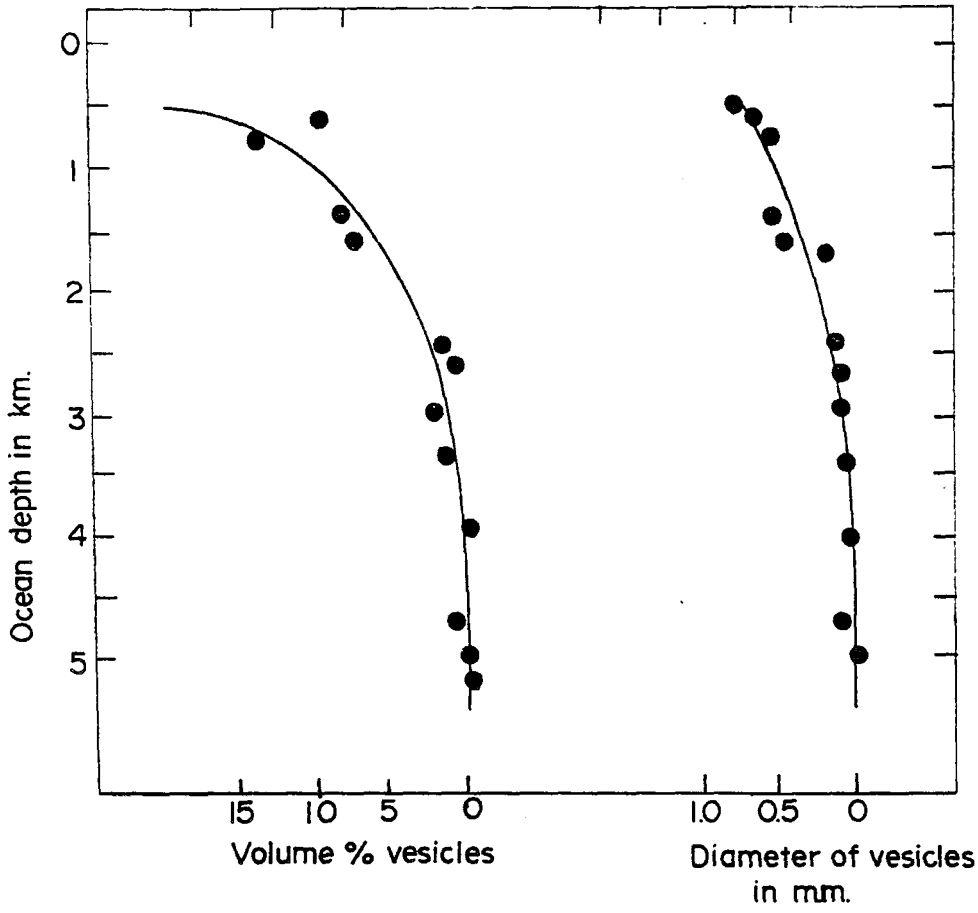

FIGURE 6-1 Change in volume % vesicles and average diameter of vesicles with depth for basalts of the east rift zone of Kilauea. From Moore (1965)

The widespread preservation of thinly laminated chemical sediments (B.I.F., chert, carbonaceous sediments) and pelitic sediments (argillite) is consistent with a deep submarine environment, one that is below storm wave base. Their presence reflects background sedimentation.

6-2 Recognition and Use of Sedimentary Structures and Textures

Sediment gravity flows can find their way into a deep submarine setting and one may suspect that the clastic sediments in the thesis map area record such an environment. Middleton and Hampton (1973) classify subaqueous sediment gravity flows into four ideal types depending on the mechanism of grain support. These are (1) turbidity currents (grains supported by fluid turbulence) (2) grain flows (grains supported by grain interaction) (3) liquefied sediment flows (grains supported by upward movement of intergranular fluid), (4) debris flow (grains supported by matrix strength).

Many clastic sediments deposited from a turbidity current have recognizable features imposed on the bed by the current, such as a sharp base with sole marks, graded bedding and Bouma divisions (Walker, 1979). The five divisions of an ideal Bouma sequence for turbidites (Bouma, 1962) are shown in figure 6-2. Walker (1979) points out that turbidites need not contain all five divisions and that massive ungraded sandstone and pebbly sandstones cannot be

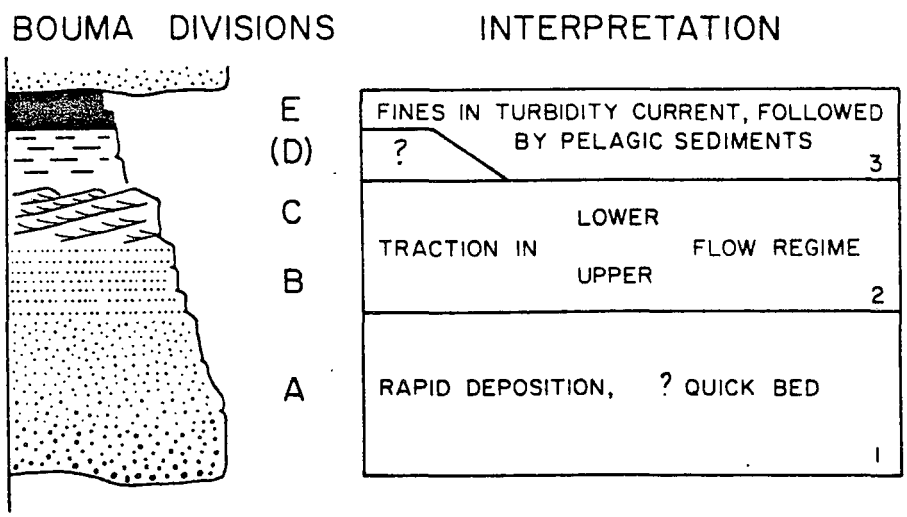

FIGURE 6-2 Five divisions of the Bouma model for turbidites: A - graded or massive sandstone. B - parallel laminated sandstone. C - ripple cross-laminated fine sandstone. D - faint parallel laminations of silt and mud, bracketed to emphasize that in weathered or tectonized outcrops it cannot be separated from E - pelitic division, partly deposited by the turbidity current, partly hemipelagic.

accounted for using the Bouma model.

The structures and vertical sequences to be expected in deposits from grain flows, liquefied flows and debris flows are shown in figure 6-3 from Middleton and Hampton (1973).

In the map area, most sedimentary structures and vertical sequences in fine to coarse grained sedimentary clastic rocks are very poorly exposed. As such, it was commonly not possible to recognize a turbidite by graded bedding for instance and it was impossible to definitely recognize deposits from liquefied sediment flows or grain flows by the structures shown in figure 6-3 (fluid escape pipe, dish structures, etc.). However, some observations and interpretations are possible. These are

1) a deposit from a turbidity current is recognized southwest of the mill site (plate 5-10) on the basis of graded bedding. Sandstone grades from medium to fine grained (bottom to top) and is overlain by a laminated cherty sediment. The sandstone represents Bouma's division A while the cherty rock likely falls into Bouma's division B and or D.
2) Ungraded, poorly sorted cobble and pebble conglomerate found at various stratigraphic levels on the south limb and locally on the north limb of the Lebel Syncline have the sedimentological characteristics of debris flows shown in figure 6-3.

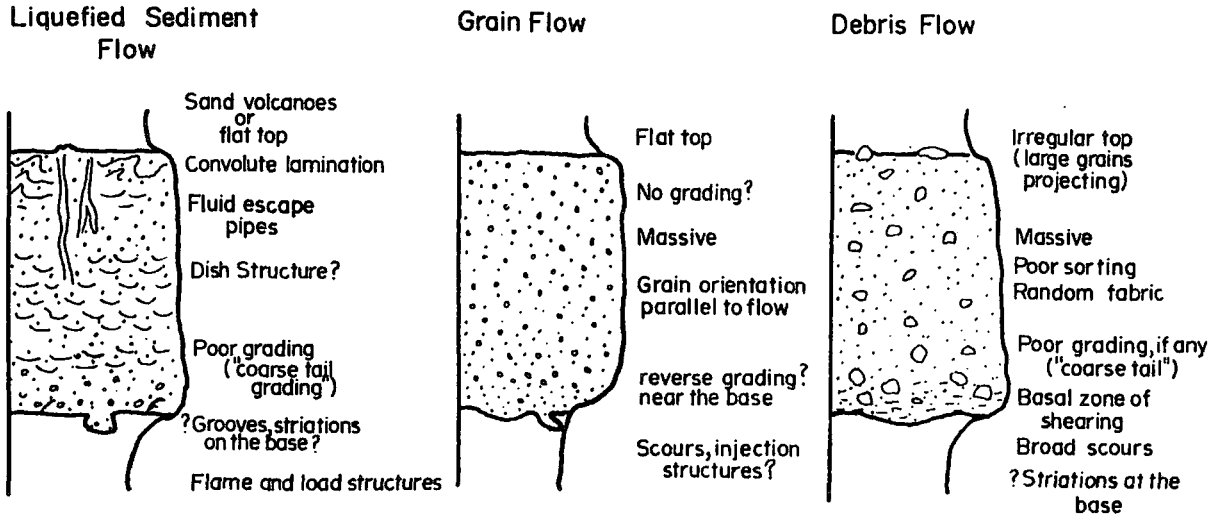

FIGURE 6-3 Sequence of structures in hypothetical single-mechanism deposits from Middleton and Hampton (1973).

3) Thinly laminated sandstone found throughout the thesis map area may be deposits from a turbidity current and may belong to divisions B, D, and E of the Bouma model (figure 6-2).
4) Sandstones which are massive in hand specimen may be part of a massive or graded bed. The inability to make this distinction prevents one from determining in the field the flow mechanism (turbidity, grain or liquefied) responsible for sediment transportation. The sandstones may have been deposited from any one of the three.
5) Chert, argillite, B.I.F. and carbonaceous sediment record background sedimentation between sediment gravity flow activity, temporally and spatially.

6-3 Relating Sedimentary Rocks Directly Underlying Sequence 5 to the McElroy Formation

Hyde (1978) considered clastic sedimentary rocks of the McElroy Formation outlined in figure 6-4 to be deposits from turbidity currents and debris flows. Hyde's (1978) interpretations are summarized in table 6-1.

Sedimentary rocks directly underlying sequence 5 in the thesis map area are regarded as the westward extension of the McElroy Formation for reasons discussed in section 3-9. On this basis, the following conclusions are drawn. The ungraded conglomerates found at five locations at this stratigraphic level fall into Hyde's sub-facies F-2. Well-exposed turbidites observed southwest of the mill site fall

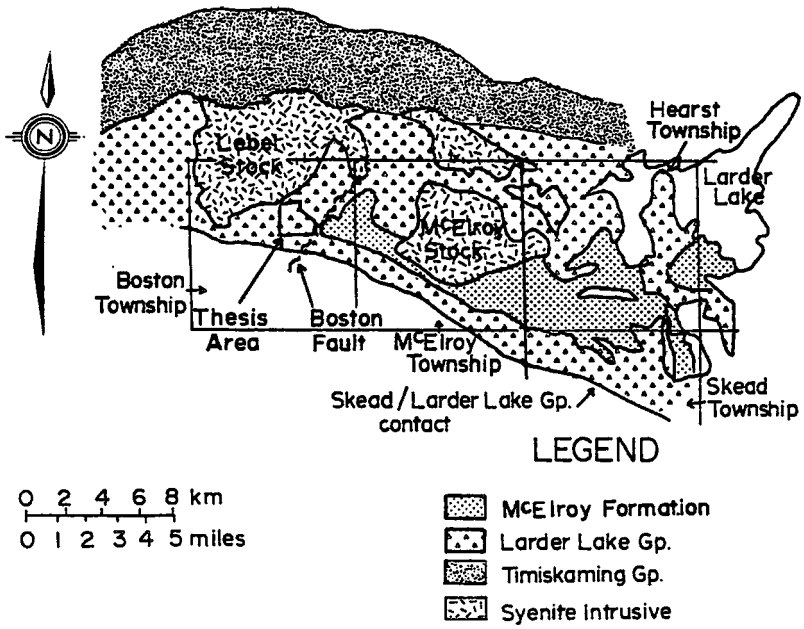

FIGURE 6-4 Outline of the McElroy Formation which is part of the Larder Lake Group.

TABLE 6-1

A Summary of Hyde's (1978) work for the McElroy Formation

Facies E - thin to very thick-bedded, graded, fine-coarse sandstones interpreted as proximal turbidites. They are interbedded with argillites.

Facies F - conglomerates associated with Facies E turbidites.

Sub-facies F-1 - Granule-pebble conglomerates with graded bedding interpreted as having been deposited from gravel-laden turbidity currents.

Sub-facies F-2 - Pebble-cobble conglomerates without graded bedding interpreted as emplaced by a debris flow mechanism.

Facies G - laminated sandstone, siltstone, and argillite interpreted as deposition from turbidity current flow on levees and interchannel areas of submarine fan.

Facies H - iron formation associated with sedimentary rocks; formed in a quiet-water sedimentary environment below storm wave base.

into Facies E. Chert and carbonaceous sediments are consistent with Facies H, and thinly laminated sandstones are consistent with Facies G. It is likely that F-1 conglomerates occur at this and other stratigraphic levels in the thesis map area.

6-4 Application of a Submarine Fan Environmental Model

The consistent preservation of thinly laminated chemical sediments and the absence of vesicles in the pillowed basaltic flows in the thesis map area point to a quiet and deep depositional environment as noted in section 6-1. Using present day morphological terms, this type of environment would include the continental rise (made up of coalescing submarine fans) and an abyssal plain (Walker, 1979). Turbidites and associated coarse clastics are most abundant in large submarine fans (Walker, 1979). The abyssal plains are considered to be composed of thin-bedded turbidites.

A submarine fan environment model from Walker (1978b) is shown in figure 6-5 and can be used to help make the following observations:

(1) The cobble and pebble conglomerates point to the bottom of the feeder channel and the foot of the slope as the most likely depositional environment.

(2) The presence of debris flows throughout the south limb stratigraphy points to a depositional environment

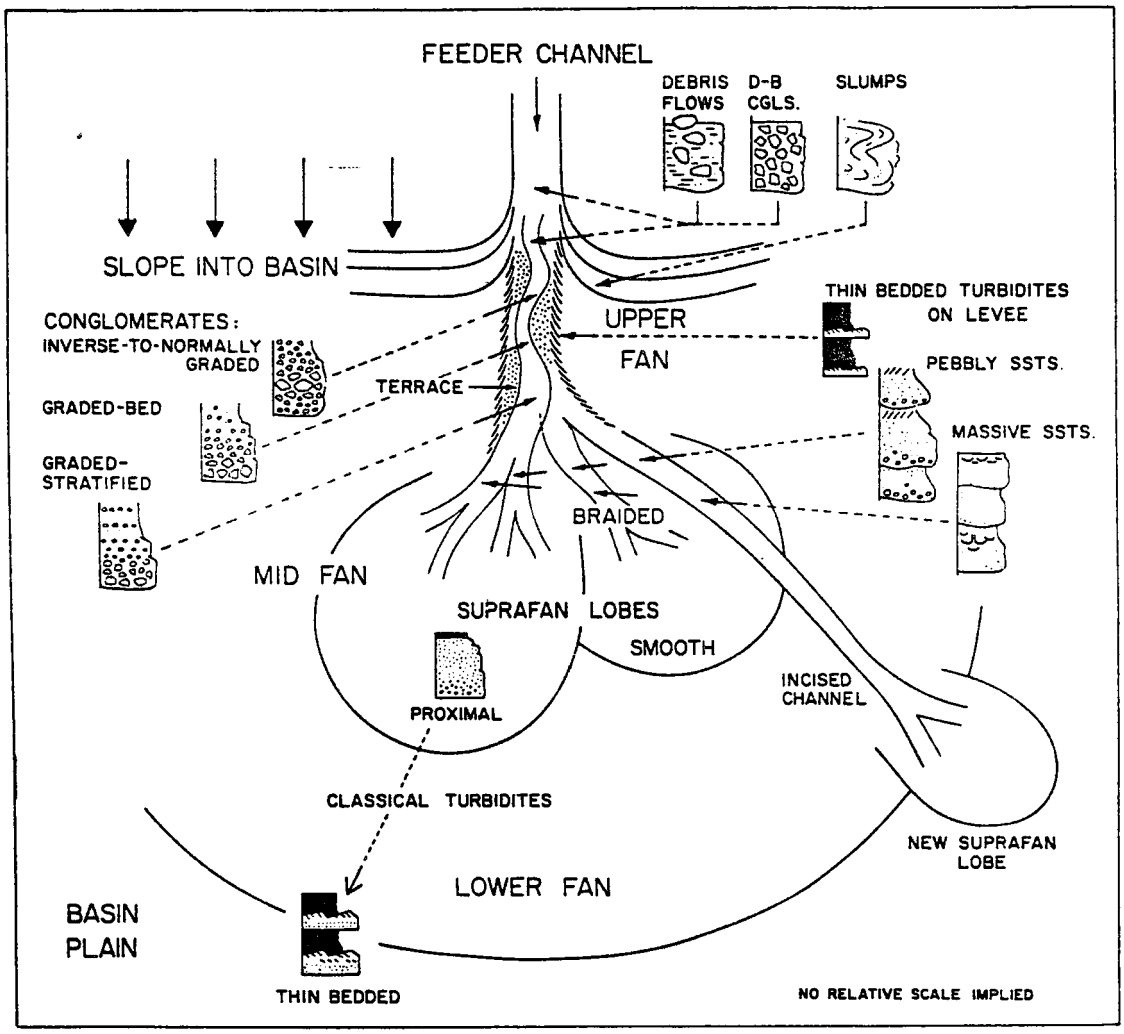

FIGURE 6-5 Submarine fan environmental model from Walker (1978b).

proximal to source throughout volcanism.

(3) The absence of abundant debris flows on the north limb does not necessarily indicate a depositional environment more distal from the source than that envisaged for the south limb. A similar situation is observed north-northeast of the South Pit on the south limb of the Lebel Syncline. Here B.I.F. is the major sedimentary type and is locally intercalated with minor amounts of conglomerate. The B.I.F. is along strike from abundant conglomerate west of the mine site. B.I.F. here is part of a proximal depositional environment.

(4) Conglomerates dominated by one of five different clast types are found at one stratigraphic level below the stratigraphically lowest B.I.F. on the south limb. This suggests practically contemporaneous deposition from many feeder channels and local sources.

Conglomerates in the thesis map area are in general dominated by one or two clast lithologies, indicative of local sources. This is also characteristic of the McElroy Formation. Hewitt (1949) reports that in Skead Township which is outlined in figure 6-4, the pebble assemblage in conglomerates is restricted to diorite, greenstone, rhyolite or rhyolite porphyry with one rock type usually predominating. Abraham (1950) similarly cites numerous examples of conglomerates dominated by one or two clast types in

McElroy Township.

In Quebec, conglomerates in the Bellecombe gneiss belt are comprised of argillite and quartzite. Those with B.I.F. clasts are rare (Dimroth et al., 1982).

(5) Finely laminated, very fine grained sandstones along strike from debris flows such as is found overlying the seventh sequence may be thinly bedded turbidites in low areas behind channel levees.

(6) Medium grained sandstones which are massive in hand specimen may be part of a massive or a graded bed. However, they do not appear to be thinly bedded (3 to 10 cm thick) and thus are not characteristic of the distal turbidites or those found in levees as is shown in figure 6-5. Although the outcrops are heavily weathered, it is expected that thin beds would have been noticed had they been present.

These massive appearing sandstones which are found on both limbs of the syncline may be either (1) channel deposits of massive sandstones (2) proximal turbidites deposited in the channel near the slope.

6-5 Provenance

Most of the conglomerates contain clasts similar to rock types found in the Larder Lake Group. In particular, komatiite, chert, argillite and sandstone clasts found in

conglomerates below the South Pit represent lithologies observed lower in the stratigraphy. It is most likely that these clasts were derived from the laterally equivalent lithologies in the lowest parts of the Larder Lake Group stratigraphy closer to, or on the slope of a topographic high. The fact that the Larder Lake Group clasts are angular is consistent with this interpretation. It is unlikely that there was sufficient time prior to deposition for clasts of Larder Lake Group lithologies to be rounded by abrasion.

Two conglomerates contain clasts foreign to the Larder Lake Group. In one south of the Adams Mine road, predominantly granodiorite clasts, and few diorite clasts occur in a hornblende-rich matrix. A source comprised of intermediate plutonic and mafic extrusive or intrusive rocks is indicated. The other is conglomerate exposed near the mill which carries rhyolite, chert, feldspar porphyry, greenstone and massive sulphide clasts.

Chert, massive sulphide, rhyolite and feldspar porphyry are rock types which form part of the Skead Group of cycle I (Jensen, 1979). Basalt is found in the underlying Catherine Group (Jensen, 1979). A topographically higher, lateral equivalent to the upper parts of cycle I in the Adams Mine area may have been the source area for the clasts in the conglomerate near the mill.

Medium-grained granodiorite is absent in cycle I but is characteristic of the plutons which are basement to cycle I in Quebec northeast of the thesis area. The granodiorite clasts in the conglomerate south of the Adams Mine road may have been derived from similar basement rocks exposed in the Adams Mine area during formation of the Larder Lake Group. The subrounded to subangular clasts at sample locality M-518 have experienced a greater degree of abrasion than has the more angular clasts representing cycle I and the Larder Lake Group. This is consistent with the basement interpretation for the granodiorite clasts.

Fine grained, quartz-rich clastic sediments below the stratigraphically lowest B.I.F. are part of a regionally extensive quartz-rich sedimentary unit to the east known as the McElroy Formation in Ontario, and the Bellecombe gneiss belt in Quebec (figure 6-6). The presence of felsic volcanic clasts in these sediments is evidence of a felsic volcanic source. However, Walker and Pettijohn (1971) have shown that felsic volcanic rocks are not important sources of quartz in regionally extensive quartz-rich turbidites whereas exposed and weathered, intermediate plutonic rocks are. The fine grained quartz-rich clastic sediments in the map area are probably derived from a mixed volcanic/plutonic source. The felsic volcanic clasts are likely from the Skead Group while the abundant quartz may be from the older plutonic basement.

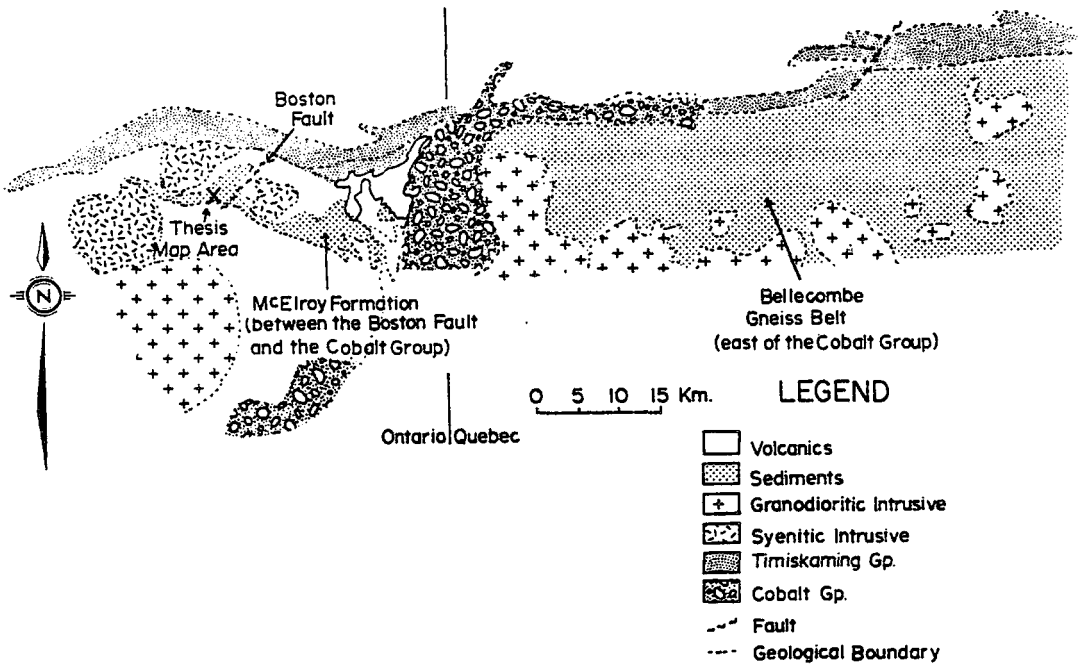

FIGURE 6-6 Geological map emphasizing the location of the McElroy Formation and the Bellecombe gneiss belt.

Conglomerates with clasts representing the Larder Lake, Skead and Catherine Groups also have a mixed source. Their quartz-rich matrix materials reflect the plutonic source.

Gariepy et al. (1984) have dated twenty-six separate detrital zircon grains from the Pontiac Group by the U-Pb method. Their results show that two age components were present in the source area.

(1) a 2700-2725 Ma old component.

(2) a 2940 Ma old component.

The younger component has an age which is consistent with the age of 2,710±2 Ma given by Nunes and Jensen (1980) for the Hunter Mine Group near the top of cycle I. The Skead Group is considered to be the same age as the Hunter Mine Group (Jensen, 1983). The older age component may apply to:

(1) the granodiorite and diorite clasts in conglomerates intercalated with sequence 1.

(2) the quartz which is abundant in fine grained clastic sediments and in conglomerates in the map area.

6-6 Paleocurrents

Walker (1978) suggested that the Superior Province in the Archean is better regarded as a large depositional area with relatively small landmasses developed in it rather than as a craton with basins developed in it. In this

context, the extensive sedimentary package which is comprised of sediments in the map area, the McElroy Formation and the Pontiac Group are regarded as deposits in one depositional area.

The landmass or landmasses were likely situated east and northeast of the Adams Mine site. Paleocurrent measurements (Hyde, 1978) in neighbouring McElroy Township indicate west and southwest paleoflow directions. Measurements by Goulet (1978) in Quebec indicate a source to the north for the Pontiac Group.

Chapter 7

Geology, Petrography and Geochemistry of Intrusive Rocks

7-1 Introduction

In this section the major types of intrusions which include:

1) peridotite sills
2) peridotite-gabbro sills and gabbroic sills
3) discordant gabbro bodies
4) syenite, biotite lamprophyre and feldspar porphyry dykes
5) diabase dykes

will be discussed. These intrusions are shown together in map 5.

7-2 Peridotite Sills

Peridotite sills shown in figure 7-1 are massive, orange to light green weathering conformable units. They are not abundant in the thesis map area or in adjacent NB-1 and NB-2 map areas.

On the south limb of the Lebel Syncline, a sill which overlies B.I.F. at the South Pit and the stratigraphically lowest B.I.F. west of the mine site averages 10 meters in thickness and has an outcrop strike

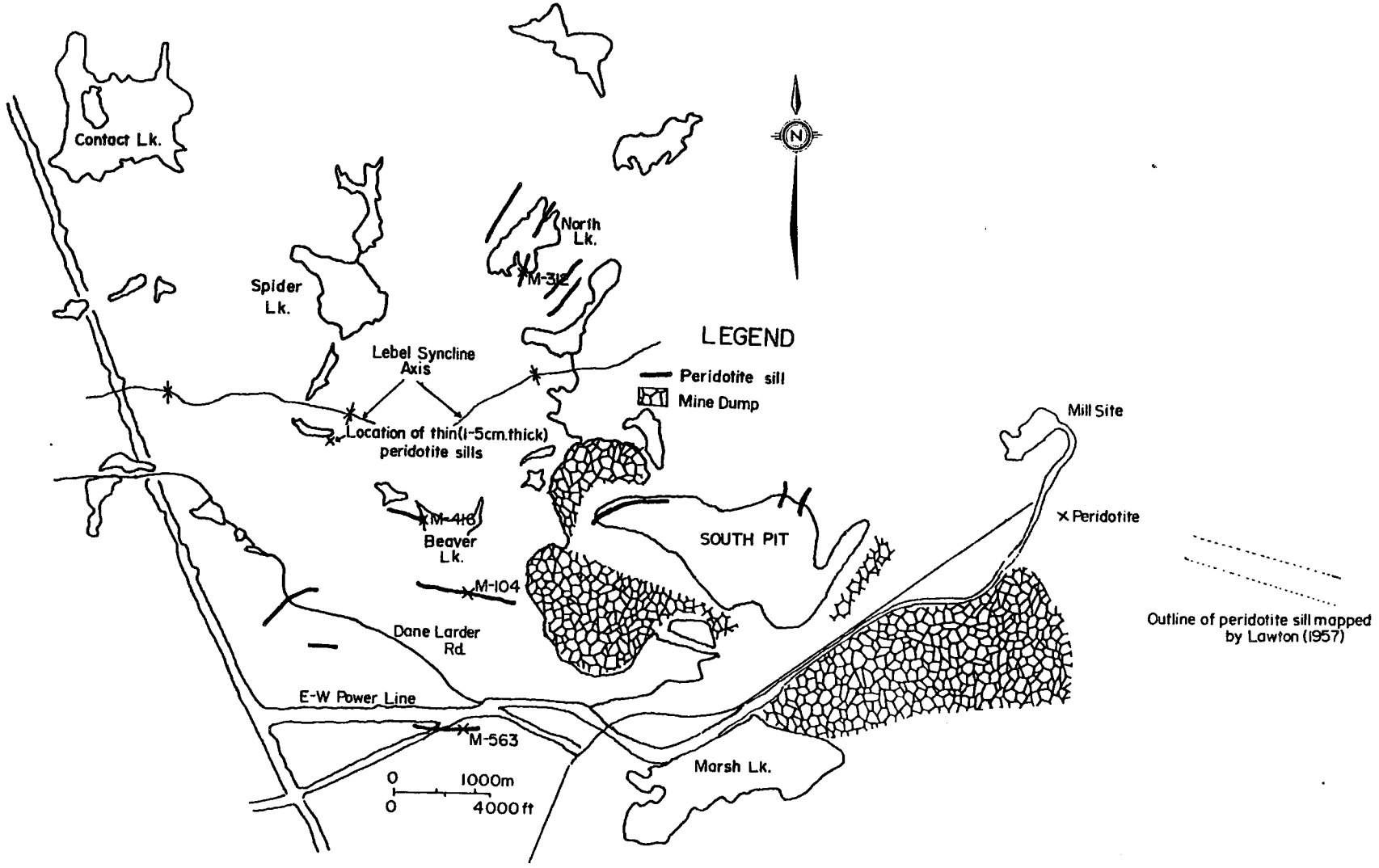

FIGURE 7-1 Location of peridotite sills in the map area.

length of approximately 1 km. The length of this sill is the greatest observed for a peridotite sill in the map area. This peridotite sill locally grades up into pyroxenite and gabbro. Several thin (1-5 cm) peridotite sills intrude B.I.F. below Finger Lake and lie between thicker layered peridotite-gabbro sills. Sills up to 10 meters in thickness intrude sequence 8 west of Beaver Lake. Outcrops of peridotite south of the Dane-Larder road in mixed sediments and south of the east-west trending power line near the base of sequence 2 may form portions of sills which are not laterally traceable owing to poor exposure. Peridotite found south of the mill site near map area NB-2 is likely part of a thick peridotite sill (200 meters thick) (Abraham, 1950) found below the McElroy Formation in eastern Boston Township and in neighbouring McElroy Township. Several peridotite sills of unknown thickness lie between group 3 sediments and Dry Lake on the north limb of the Lebel Syncline.

The sills are medium to fine grained, black and magnetic. Chilled margins are cherty in appearance and light grey in colour. The sills consist of 60 to 70 % antigorite, 10 to 20 % chlorite, 20 to 30 % tremolite and 5 % opaque minerals (chromite and magnetite).

The major elements and Cr, Ni, Co and V for M-104, M-416 and M-563, samples from three peridotite sills are compared to M-231, M-233 and M-141 respectively, which

represent komatiites with similar MgO abundances (table 7-1). The three sills shown in figure 7-1 have consistently lower Al_2O_3, TiO_2 and Fe_2O_3 abundances than the komatiites.

M-312 from a sill on the south side of North Lake (figure 7-1) has the highest MgO and Cr contents (table 7-2) for an analyzed sample from the map area. It is the richest in antigorite (80 %) and opaque minerals (6 to 7 %) of any intrusive rock examined petrographically.

7-3 Layered Peridotite-Gabbro Sills and Gabbroic Sills

Four sills are found on the south limb of the Lebel Syncline while seven or possibly more occur on the north limb. Figure 7-2 gives a general outline of the locations and extent of the sills. Gabbro is the most abundant phase in all of these sills. The microgabbroic phase is locally observed overlying the gabbro phase or is along strike from the gabbro phase, presumably where a sill thins.

Figure 7-3 is a stratigraphic section of a sill found along the northwest trending power line immediately north of the old Dane-Larder road. This location is indicated in map 5. The order of stratigraphy from bottom to top is peridotite, pyroxenite, gabbro and microgabbro. The pyroxenite phase is thinnest (2 meters) while the gabbroic phase is the thickest (30 meters). Although not directly observed because of incomplete exposure, the transition from phase to phase appears sharp. Not all of

Table 7-1 Comparison of major element, Cr, Ni, Co and V contents of three peridotite sills with three komatiites with similar MgO abundances

	komatiite	sill	komatiite	sill	komatiite	sill
	M-233	M-416	M-231	M-104	M-141	M-563
SiO_2	47.94	47.04	43.92	46.27	43.92	48.49
Al_2O_3	7.41	4.50	6.18	4.19	7.19	6.26
Fe_2O_3	12.00	10.84	12.00	9.89	13.37	11.62
MgO	20.63	21.75	32.83	33.76	26.80	25.76
CaO	10.84	15.41	4.32	5.34	7.97	7.24
Na_2O	0.35	0.05	0.05	0.05	0.05	0.05
K_2O	0.06	0.09	0.03	0.04	0.03	0.11
TiO_2	0.47	0.08	0.34	0.25	0.42	0.24
MnO	0.20	0.21	0.27	0.13	0.22	0.23
P_2O_5	0.10	0.03	0.07	0.07	0.02	0.01
Total	100.00	100.00	100.00	100.00	100.00	100.00
Cr	2916	1915	2478	2616	3296	2205
Ni	1369	1436	2200	1759	1074	880
Co	110	110	135	99	140	102
V	137	61	115	72	156	114

Table 7-2

Major element, Cr, Ni, Co and V contents of M-312

SiO_2	42.02
Al_2O_3	3.13
Fe_2O_3	12.32
MgO	41.79
CaO	0.26
Na_2O	0.05
K_2O	0.09
TiO_2	0.15
MnO	0.17
P_2O_5	0.01
Total	100.00
Cr	6374
Ni	1879
Co	200
V	57

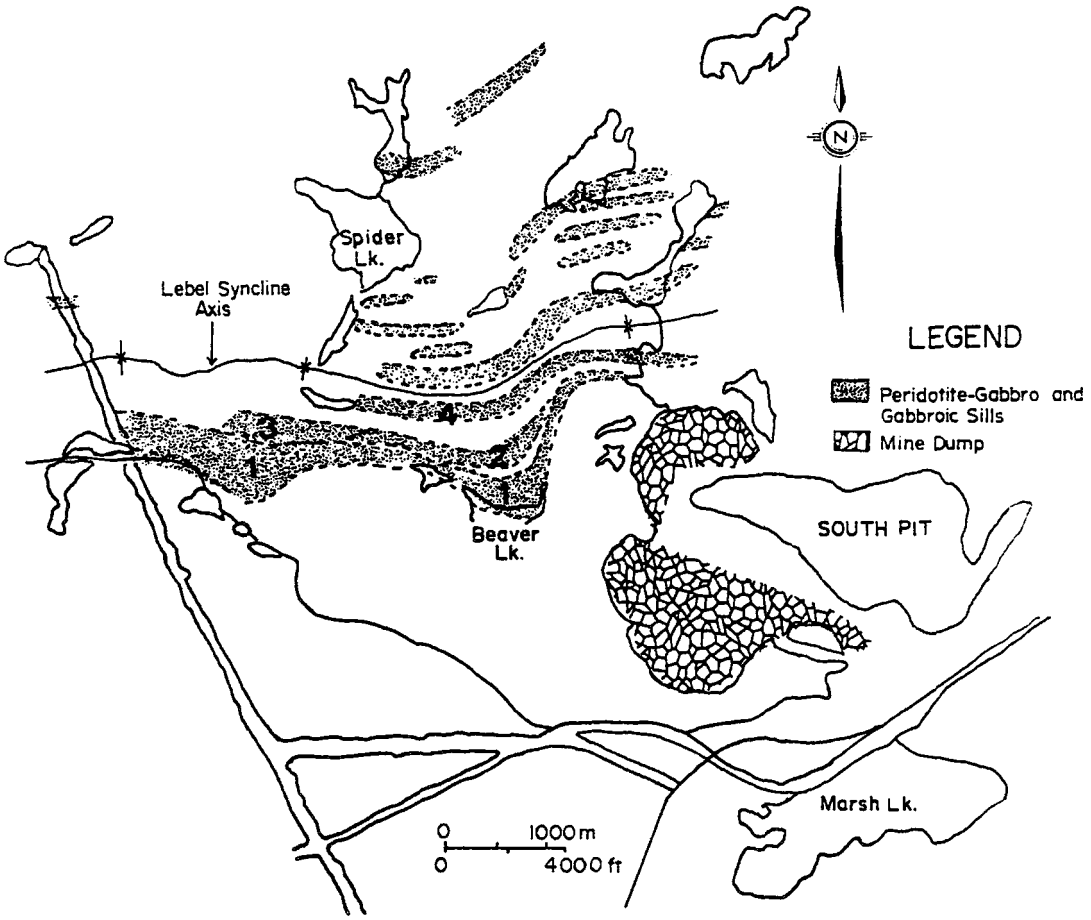

FIGURE 7-2 Outline of peridotite-gabbro and gabbroic sills in the thesis map area. The four sills on the south limb of the Lebel Syncline are numbered 1,2,3 and 4 based on stratigraphic position with "1" being the lowest and "4" the highest. These sills are also numbered on map 5.

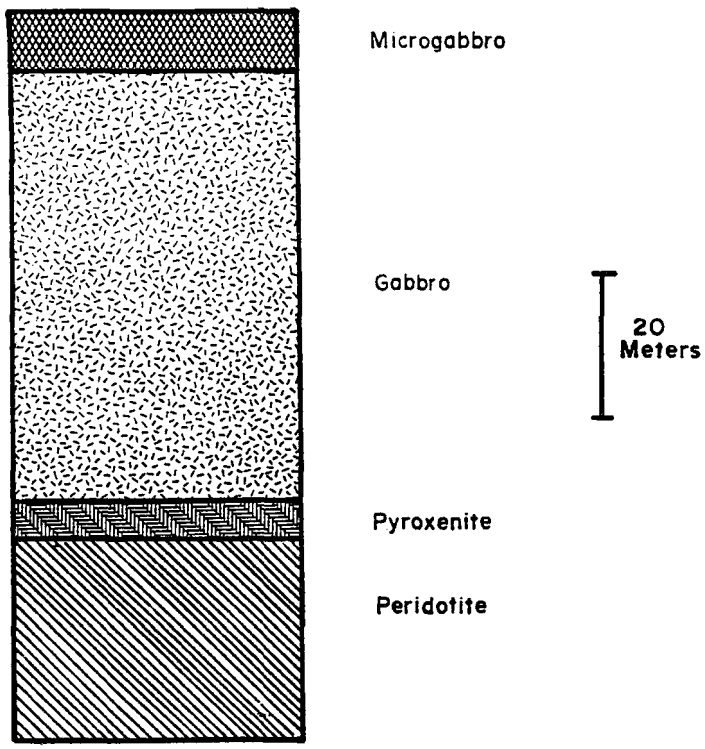

FIGURE 7-3 Schematic stratigraphic section through a layered peridotite-gabbro sill which is exposed on the west side of the map area. At this locality the sill is approximately 95 meters thick. Layered peridotite-gabbro and gabbroic sills range in thickness from 20 to 120 meters and average 40 to 50 meters in thickness.

the phases are present along the observed lateral extent of this sill. To the east, the peridotite and then the pyroxenite phases disappear (map 5).

The peridotite phase is massive, chocolate-brown weathering, fine to coarse grained, black on fresh surface and magnetic. It is comprised of 60 to 70 % antigorite, 10 to 20 % chlorite, 20 to 30 % tremolite and up to 5 % magnetite and chromite. It shows cumulate textures. Primary igneous mineralogy was undoubtedly olivine with lesser pyroxene and chromite. The pyroxenitic phase is fine to medium grained and has a dark green weathered and fresh surface. It shows cumulus textures with 70 to 90 % actinolite, 10 to 30 % interstitial albite and 0.5 to 2 % very fine grained disseminated opaque minerals.

The gabbroic phase is massive, medium grained and commonly weathers white (plate 7-1) or to a mottled black and white texture. As best seen in the sill just north of Beaver Lake, gabbroic rocks lower in the stratigraphy have a salt and pepper texture on fresh surface, not unlike their weathered surfaces, and are non-magnetic. Those higher in the stratigraphy of this sill are magnetic and are black on fresh surfaces.

In hand specimen both gabbros look equigranular. However, the stratigraphically higher gabbros are pyroxene-plagioclase phyric while the lower ones are pyroxene-phyric. Plagioclase has been completely pseudomorphed by

PLATE 7-1 White smooth weathering, massive gabbro exposed on the north side of Beaver Lake between sample localities M-111 and M-114 in map 1 and in figure 7-4.

clinozoisite while actinolite and hornblende presumably replaces pyroxene. Plagioclase-pyroxene phyric gabbros have greater abundances of magnetite, up to 3 % as opposed to 0.5 % or less in pyroxene phyric gabbros. Microgabbro is either plagioclase phyric or is equigranular and contains 2 to 3 % opaque minerals, 50 % amphiboles, 15 to 50 % albite and up to 30 % clinozoisite.

Twenty-two intrusive samples were analyzed for the major elements and the same trace elements determined for the volcanics. The sample locations are shown in figure 7-4. Fourteen samples are from the south limb while eight are from the north limb. Fifteen were taken from gabbroic or microgabbroic phases.

On the Jensen Cation Plot (figure 7-5), most of the gabbroic samples fall in the tholeiitic basalt field. Those that plot in the iron-rich tholeiitic basalt field are black, magnetic and plagioclase-pyroxene phyric samples. Those that are non-magnetic and lighter coloured in hand specimen usually plot in Jensen's magnesium-rich tholeiitic basalt and calc-alkalic basalt field. It should be pointed out that the Jensen Cation Plot is used here for descriptive purposes only.

The averages of gabbros plotting in the iron-rich tholeiitic basalt field are compared to those plotting in the magnesium-rich tholeiitic basalt field in table 7-3. The latter two are richer in MgO, Al_2O_3, Na_2O, Cr and Ni and

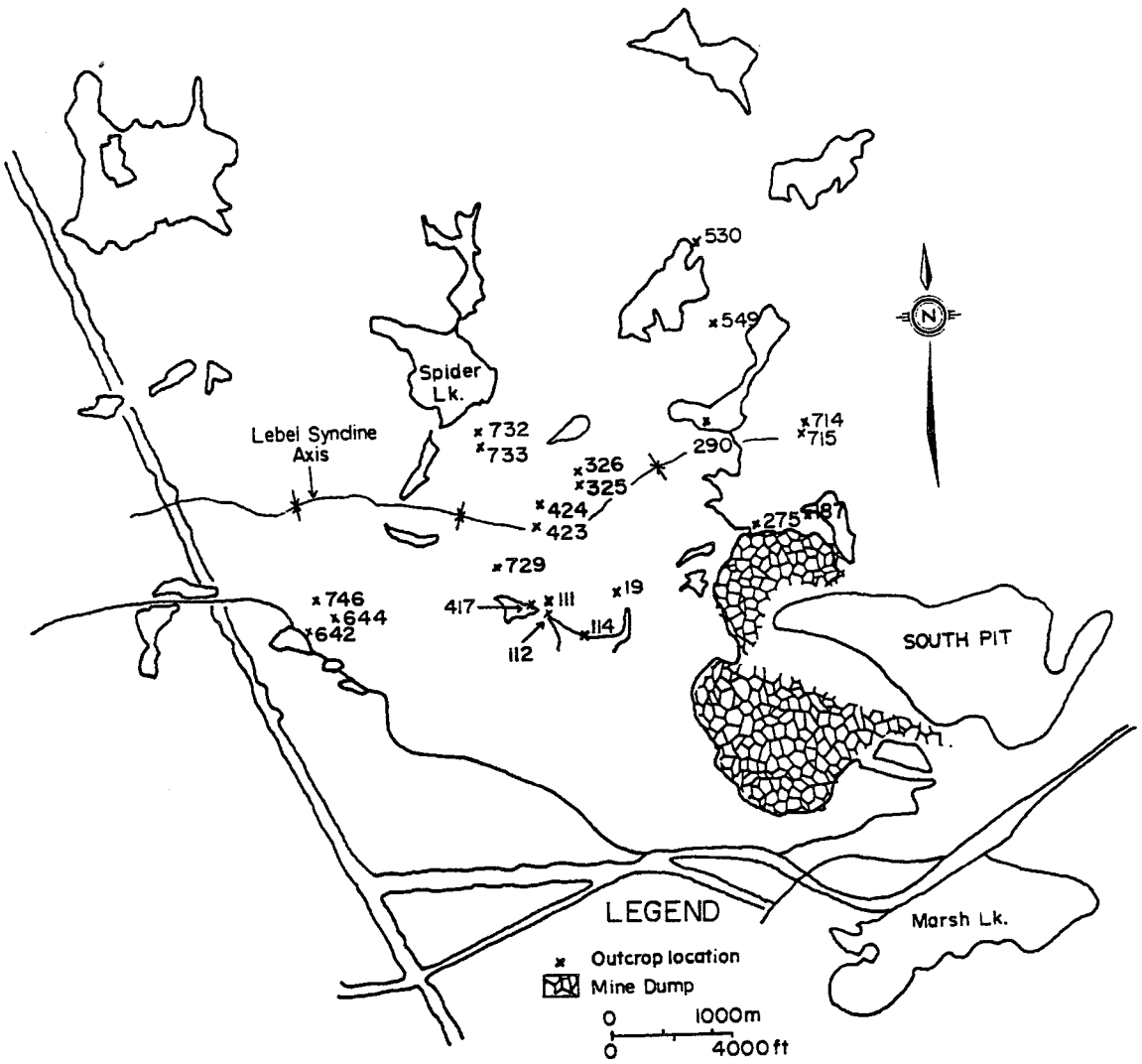

FIGURE 7-4 Location of analysed samples from the layered peridotite-gabbro and the gabbroic sills.

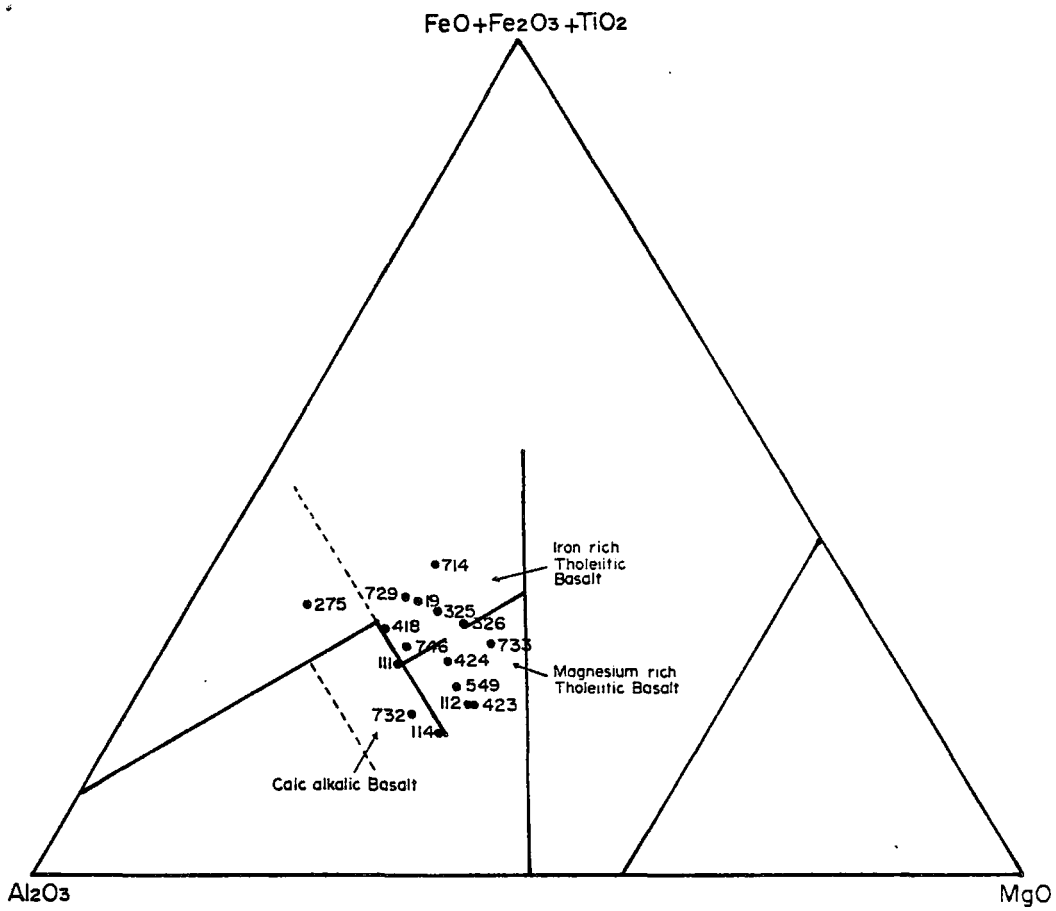

FIGURE 7-5 Plots of concordant gabbros on the Jensen Cation Plot.

● Gabbro

Table 7-3

Average major element, Cr, Ni, Co and V contents for concordant gabbros which plot in the tholeiitic and calc-alkalic basalt fields on the Jensen Cation Plot

	A	B	C
SiO_2	51.14	53.12	52.52
Al_2O_3	14.13	14.54	16.40
Fe_2O_3	15.07	11.26	10.00
MgO	5.86	8.38	7.32
CaO	8.29	7.32	8.97
Na_2O	2.90	3.43	3.49
K_2O	1.01	0.72	1.17
TiO_2	1.21	0.87	0.69
MnO	0.24	0.23	0.17
P_2O_5	0.14	0.11	0.12
Total	100.08	99.98	100.85
Cr	35	191	312
Ni	48	119	88
Co	84	76	65
V	345	225	199

A. Average of seven concordant gabbro samples which plot in the iron-rich tholeiitic basalt field on the Jensen Cation Plot.

B. Average of five concordant gabbro samples which plot in the magnesium-rich tholeiitic basalt field on the Jensen Cation Plot.

C. Average of three concordant gabbro samples which plot in the calc-alkalic basalt field on the Jensen Cation Plot.

poorer in TiO_2, CaO, Fe_2O_3, Co and V.

Two sets of analyses are given in table 7-4 to show the variation of oxides with stratigraphic height in two different sills. M-642, M-644, and M-746 are from the stratigraphically lowest sill on the south limb of the Lebel Syncline near the north-south trending power line while M-715 and M-714 are from the stratigraphically highest sill on the north limb near Dry Lake (figures 7-2 and 7-4). In the south limb sill, all elements show increasing concentration with stratigraphic height, except MgO, Cr, Ni and Co which decrease. M-714 is richer in all major elements except MgO and CaO as well as Cr, Ni and Co in comparison with M-715 in the north limb sill. Both sills show roughly similar elemental variations with stratigraphic height.

Pyroxenite generally resembles high MgO komatiitic basalts and some komatiites in major element composition as seen in the comparison in table 7-5. The three pyroxenite samples however have lower CaO and higher Al_2O_3 abundances than volcanics with similar MgO. Cr and Ni abundances are lower in the pyroxenites than in the high MgO komatiitic basalts.

There are no komatiitic volcanics in the thesis map area that have major element abundances which match those gabbros which plot in the iron-rich tholeiitic basalt field on the Jensen Cation Plot. Some gabbro samples such as M-112 which plot in the magnesium-rich tholeiitic basalt field

Table 7-4

Major element, Cr, Ni, Co and V contents for samples arranged from stratigraphic bottom to top from left to right.

	South limb sill			North limb sill	
	Peridotite M-642	Pyroxenite M-644	Gabbro M-746	Pyroxenite M-715	Gabbro M-714
SiO_2	45.07	47.57	54.33	45.73	51.41
Al_2O_3	4.68	12.73	14.33	11.33	13.14
Fe_2O_3	8.42	11.75	11.71	13.98	17.53
MgO	40.22	16.47	5.62	19.96	5.79
CaO	1.14	6.85	8.58	7.59	6.75
Na_2O	0.05	2.56	2.80	0.05	2.34
K_2O	0.13	0.43	1.19	0.68	1.09
TiO_2	0.13	0.48	1.09	0.42	1.58
MnO	0.13	0.13	0.26	0.22	0.24
P_2O_5	0.03	0.03	0.09	0.04	0.12
Total	100.00	100.00	100.00	100.00	100.00
Cr	2586	583	87	1381	8
Ni	811	240	63	437	15
Co	133	108	67	113	85
V	102	194	327	141	459

Table 7-5

Comparison of the major element, Cr, Ni, Co and V contents of intrusive pyroxenite samples to high MgO komatiitic basalts with approximately similar MgO abundances. The asterisk (*) over the sample number indicates a volcanic flow sample.

		*	*			*	*	*
	M-715	M-650	M-202	M-290	M-644	M-98	M-163	M-59
SiO_2	45.73	47.50	46.81	47.00	45.57	48.06	49.20	47.47
Al_2O_3	11.33	8.69	8.59	11.71	12.73	9.71	9.85	10.84
Fe_2O_3	13.98	11.96	12.33	14.26	11.75	11.33	9.41	12.86
MgO	19.96	19.06	19.60	16.84	16.47	16.38	16.57	17.24
CaO	7.56	11.09	11.59	7.31	6.85	11.62	12.18	9.47
Na_2O	0.05	0.05	0.05	1.87	2.56	1.34	0.64	0.05
K_2O	0.68	0.95	0.08	0.07	1.43	0.35	0.75	1.24
TiO_2	0.42	0.44	0.48	0.63	0.48	0.53	0.60	0.57
MnO	0.22	0.25	0.36	0.26	0.13	0.22	0.21	0.26
P_2O_5	0.04	0.01	0.11	0.05	0.03	0.05	0.60	0.00
Total	100.00	100.00	100.00	100.00	100.00	100.00	100.00	100.00
Cr	1381	2295	4017	1282	583	2413	1131	1550
Ni	437	961	1125	408	240	688	511	593
Co	113	115	128	101	108	95	81	103
V	141	130	139	175	194	154	114	168

resemble low MgO komatiitic basalts in this respect as is seen in table 7-6.

In TiO_2 versus MgO and TiO_2 versus SiO_2 variation diagrams shown in figures 7-6a and 7-6b respectively, more than half of the gabbros plot above low MgO komatiitic basalts and andesites.

7-4 The South Pit Gabbro and Related Intrusions

The South Pit Gabbro is a medium grained massive discordant body which cuts through the entire south limb stratigraphy south and north of the South Pit (figure 7-7). It is thickest below the South Pit having dimensions estimated at 200 by 200 meters. Plate 7-2 shows this intrusive where it cuts iron formation at the west end of the pit. It contains abundant xenoliths of iron formation, peridotite and various volcanic types observed in sequence 5.

In the field, the South Pit gabbro is best distinguished from the other gabbroic rocks (sequence 1 basalts and mafic portions of the sills) on the fresh surface. This intrusive is characterized by a medium grained mosaic of anhedral, light and dark coloured grains which do not sharply contrast with each other in hand specimen as they often do in the other gabbroic rocks. However it should be pointed out that in hand specimen, the South Pit Gabbro sometimes resembles concordant gabbros

Table 7-6

Comparison of major element, Cr, Ni, Co and V contents of a gabbro with a low MgO komatiitic basalt from sequence 3.

	M-112 (Gabbro)	M-117 (Basalt)
SiO_2	52.92	51.05
Al_2O_3	14.62	15.09
Fe_2O_3	9.94	9.15
MgO	8.47	9.59
CaO	7.86	10.03
Na_2O	3.85	2.07
K_2O	1.30	2.00
TiO_2	0.68	0.82
MnO	0.19	0.16
P_2O_5	0.16	0.04
Total	100.00	100.00
Cr	118	329
Ni	222	152
Co	52	69
V	196	202

N.B. M-112 plots in the magnesium-rich tholeiite basalt field on the Jensen Cation Plot. M-117 is one of the few analyzed low MgO komatiitic basalts in the map area with Cr abundances less than 1000 ppm.

FIGURE 7-6a TiO_2 versus MgO variation diagram showing concordant gabbros and komatiitic basalts and andesites.

- ▫ gabbro
- ● komatiitic basalt or andesite

FIGURE 7-6b TiO_2 versus MgO variation diagram showing concordant gabbros and komatiitic basalts and andesites.

- ▫ gabbro
- ● komatiitic basalt or andesite

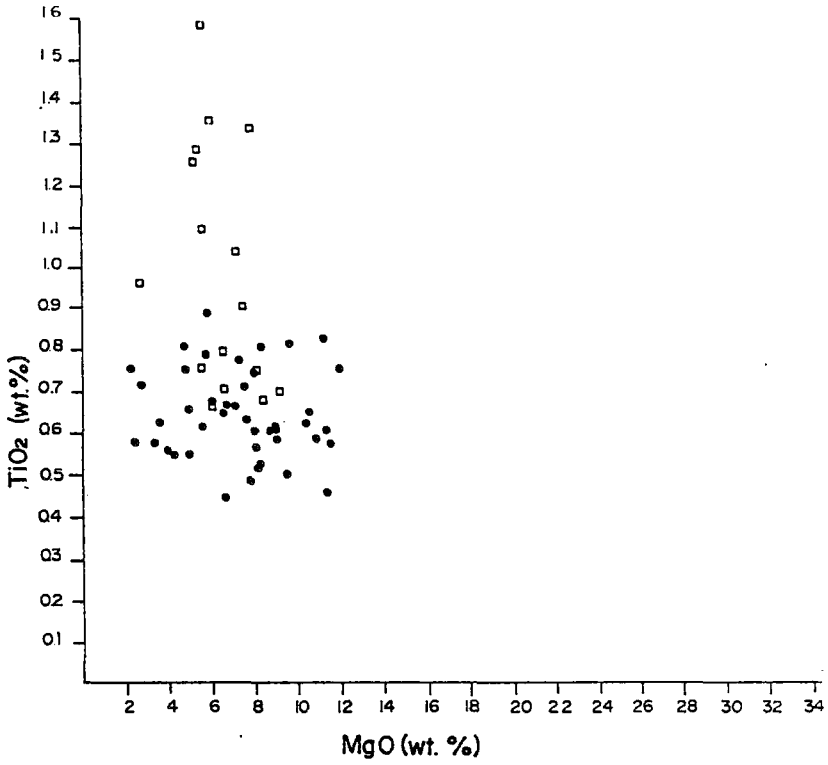
TiO2 (wt.%)
1.6
1.5
1.4
1.3
1.2
1.1
1.0
0.9
0.8
0.7
0.6
0.5
0.4
0.3
0.2
0.1
2 4 6 8 10 12 14 16 18 20 22 24 26 28 30 32 34
MgO (wt. %)

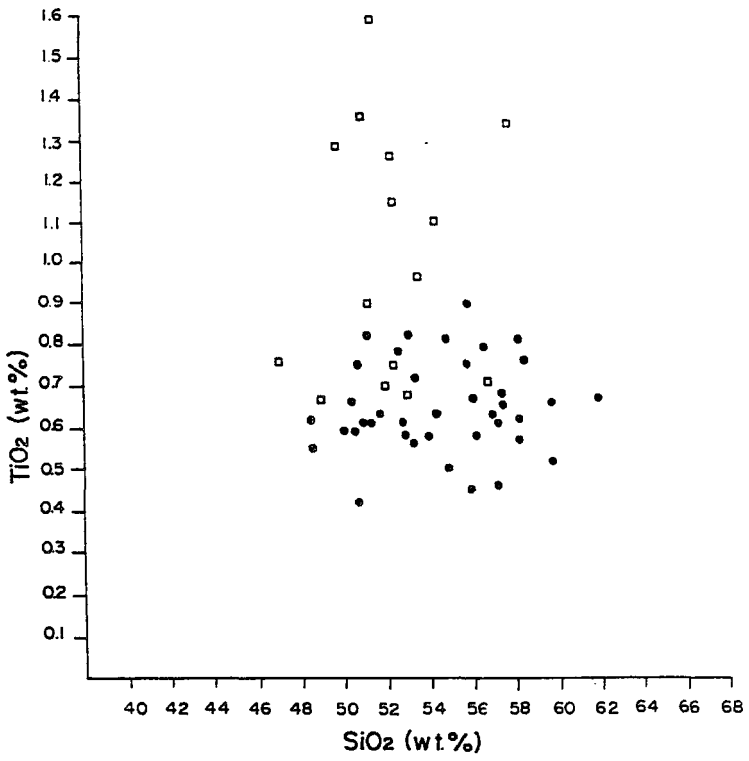
TiO2 (wt.%)
1.6
1.5
1.4
1.3
1.2
1.1
1.0
0.9
0.8
0.7
0.6
0.5
0.4
0.3
0.2
0.1
40 42 44 46 48 50 52 54 56 58 60 62 64 66 68
SiO2 (wt.%)

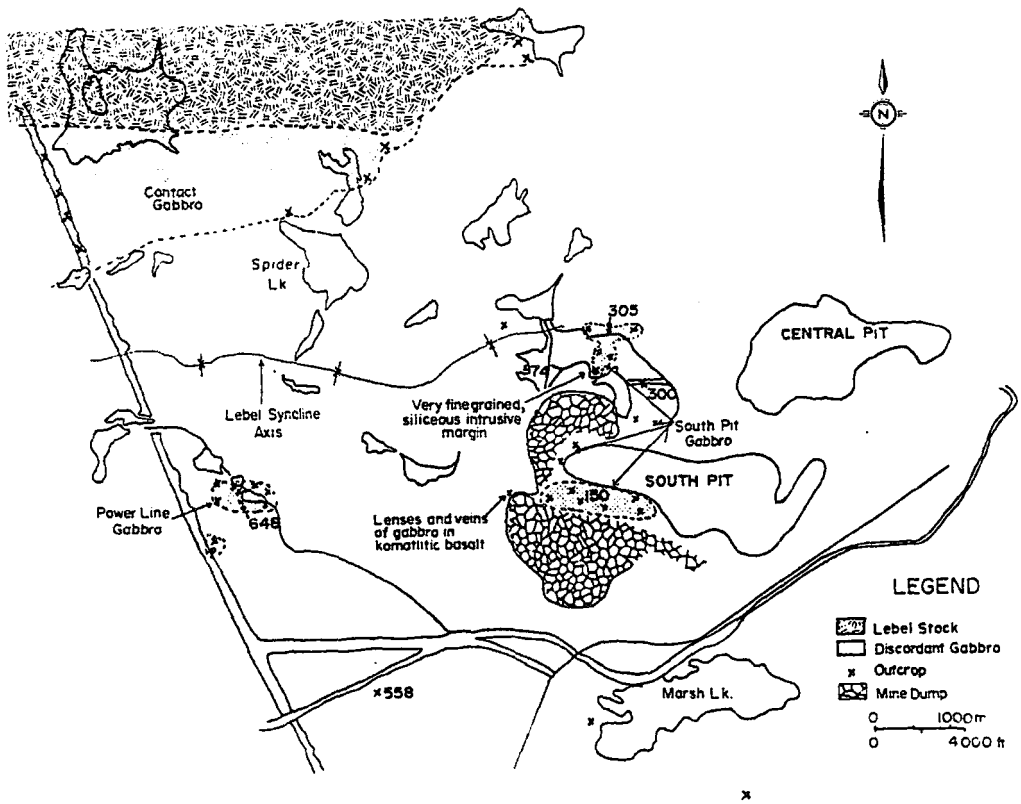

FIGURE 7-7 Location of gabbro outcrops considered as part of the discordant intrusives suite. Also plotted are the locations of analysed samples.

PLATE 7-2 Xenoliths of pillowed high Al_2O_3 komatiitic basalt and B.I.F. in the South Pit Gabbro where it cuts B.I.F. at the South Pit (near sample locality M-150). Concordant gabbros are not characterized by the presence of xenoliths.

which plot in the magnesium-rich tholeiitic basalt field on the Jensen Cation Plot.

The South Pit Gabbro is very fine grained and siliceous where found in one outcrop near its contact with the volcanics north of Fault Lake (figure 7-7). At another location south of Dump Lake, abundant medium grained gabbro occurs in small lenses averaging 10 x 20 cm in size and in veins averaging 3 cm in thickness which fill polygonal joints in high MgO komatiitic basalts. This exposure which is indicated in figure 7-7 marks a zone between komatiitic volcanics and the South Pit gabbro.

The South Pit Gabbro clearly post-dates the eight volcanic sequences on the south limb of the Lebel Syncline and pre-dates the tight folding in the South Pit. Its exact temporal relationship with the sills was not determined owing to poor exposure. However it does appear as though it cuts the sills southeast of Dry Lake in that the gabbroic phase of a sill is found both east and west of a series of South Pit Gabbro exposures.

The Power Line Gabbro described briefly in section 3-7 and the Contact Gabbro described in section 3-11 are considered to be related to the South Pit Gabbro. Both are shown in figure 7-7 and on map 5. This correlation is based on one or more of form and nature of occurrence, presence of xenoliths, hand specimen appearance, petrography and major and trace element chemistry. The Contact Gabbro appears to

truncate a gabbroic sill on the north limb of the Lebel Syncline (map 5) and thus post-dates sill emplacement as does the South Pit Gabbro. There are several outcrops shown in figure 7-7 which may be parts of smaller discordant gabbroic intrusions. The gabbros here resemble those in the three larger intrusions in hand specimen.

Both the South Pit Gabbro and the Power Line Gabbro can best be described petrographically as plagioclase phyric. Tabular outlines of clinozoisite and irregular, anhedral mosaics of albite are hosted by optically continuous actinolite. Plate 7-3 is of M-150, south of the South Pit. Clinozoisite makes up 40 %, albite 9 % and actinolite 50 % of M-150. Opaque minerals make up 1 % of M-150 and are concentrated in aggregates within actinolite.

Six samples from four different discordant intrusives were analyzed for the same major and trace elements as measured in the volcanics (table 7-7). The location of these samples is shown in figure 7-7. M-648 taken from the Power Line Gabbro is the richest in MgO. M-150, M-300 and M-305 taken from the South Pit Gabbro are remarkably consistent.

The average composition of the discordant gabbros is compared to those of the concordant gabbros and the high Al_2O_3 komatiitic basalts in table 7-8 to show the lower TiO_2 abundances of the discordant gabbros for relatively low MgO abundances (less than 10 %). Discordant gabbros plot in the

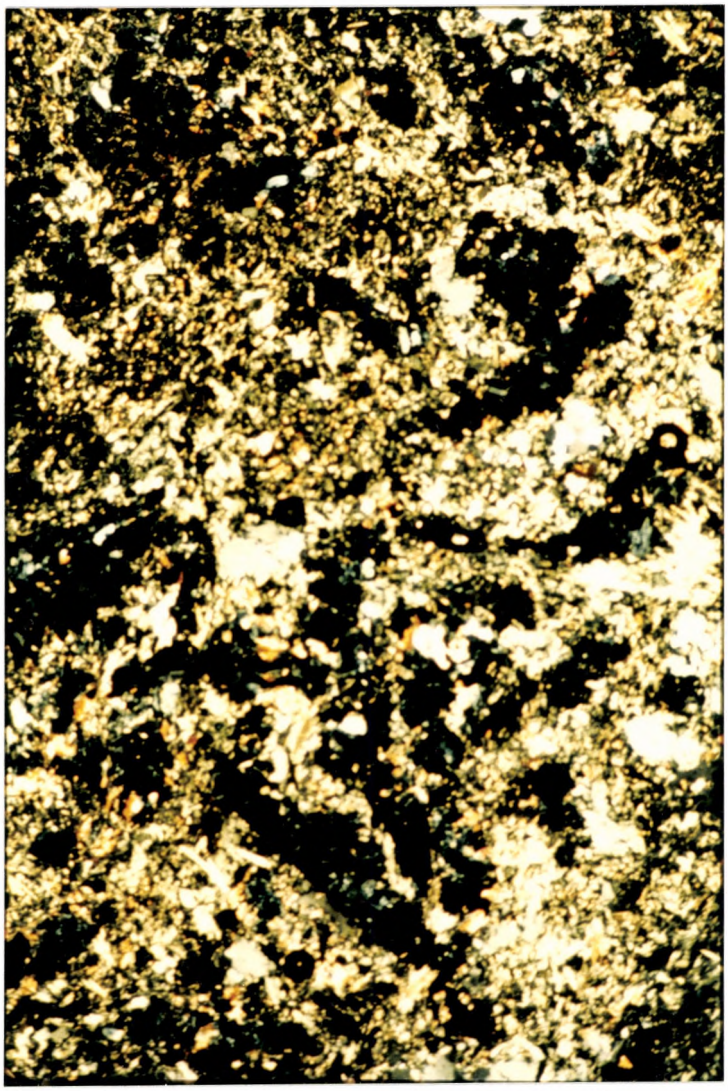

PLATE 7-3 The dark areas in M-150 represent clinozoisite pseudomorphs, probably after plagioclase. They rest in a background of actinolite, clinozoisite and albite. Polarized light, x 2.5. Field of view is 2.5 x 4.0 mm.

Table 7-7

Major element, Cr, Ni, Co and V contents of discordant type gabbroic intrusions

	M-150	M-300	M-305	M-74	M-648	M-558
SiO_2	51.85	51.60	52.00	53.40	47.35	52.26
Al_2O_3	15.47	15.96	15.37	15.47	16.03	16.90
Fe_2O_3	9.36	10.26	7.40	8.63	11.62	8.04
MgO	8.21	5.97	9.54	7.97	11.07	7.91
CaO	11.85	11.30	11.20	8.34	9.44	11.33
Na_2O	1.40	3.48	2.32	3.71	2.71	1.55
K_2O	1.12	0.73	1.66	1.55	1.07	1.28
TiO_2	0.46	0.39	0.36	0.55	0.33	0.55
MnO	0.18	0.29	0.15	0.23	0.34	0.16
P_2O_5	0.11	0.00	0.00	0.16	0.06	0.03
Total	100.00	100.00	100.00	100.00	100.00	100.00
Cr	589	371	833	293	460	665
Ni	115	59	117	90	68	122
Co	52	91	70	39	42	72
V	191	197	127	127	198	144

N.B.: M-150 is from the South Pit gabbro. M-300 and M-305 may be part of the same intrusion. M-648 is taken from the Power Line gabbro. M-558 is taken from an intrusion of unknown size south of the Adams Mine road. M-74 is from an intrusion of unknown size south of Dry Lake.

Table 7-8

Comparison of the average composition (major elements, Cr, Ni, Co and V) of the discordant gabbros with concordant gabbros and high Al_2O_3 komatiitic basalts

	A	B	C	D	E
SiO_2	51.41	51.14	53.12	52.52	51.51
Al_2O_3	15.87	14.13	14.51	16.40	18.03
Fe_2O_3	9.22	15.07	11.26	10.00	9.80
MgO	8.45	5.86	8.38	7.32	4.21
CaO	10.58	8.29	7.32	8.97	11.06
Na_2O	2.53	2.90	3.43	3.49	2.66
K_2O	1.24	1.01	0.72	1.17	1.54
TiO_2	0.44	1.21	0.87	0.69	0.59
MnO	0.23	0.24	0.23	0.17	0.30
P_2O_5	0.06	0.14	0.11	0.12	0.09
Total	100.10	99.99	99.96	100.85	99.79
Cr	535	35	191	312	349
Ni	95	48	119	88	59
Co	61	84	76	65	57
V	164	345	225	199	166

A. Average of six discordant gabbro samples.

B. Average of seven condordant gabbro samples which plot in the iron-rich tholeiitic basalt field on the Jensen Cation Plot.

C. Average of five concordant gabbro samples which plot in the magnesium-rich tholeiitic basalt field on the Jensen Cation Plot.

D. Average of three concordant gabbro samples which plot in the calc-alkalic basalt field on the Jensen Cation Plot.

E. Average of three high Al_2O_3 komatiitic basalts.

magnesium-rich tholeiitic basalt and calc-alkalic basalt fields on the Jensen Cation Plot (figure 7-8).

The average composition of the discordant gabbro most closely resembles the average composition of concordant gabbros plotting in the calc-alkalic basalt field (table 7-8).

7-5 Alkali-rich Dykes

Alkali-rich dykes are observed everywhere in the thesis map area. Three broadly defined types are recognized, based on hand specimen appearance.

1) syenite
2) biotite lamprophyre
3) feldspar porphyry.

Syenite can be further subdivided into three varieties: (1) a massive, fine grained, brick red variety, (2) a massive, fine to medium grained, white to light pink leucratic variety, (3) a massive, fine grained mafic variety. In the latter variety, mafic content ranges from 50 to 60 % so that the syenite resembles a gabbro in hand specimen. This variety was classified as mafic syenite in the field.

Plate 7-4 shows representative samples of alkali-rich dykes from the thesis map area. The lower left rock is from the Lebel Stock taken north of North Lake within 40 meters of its contact with the volcanics.

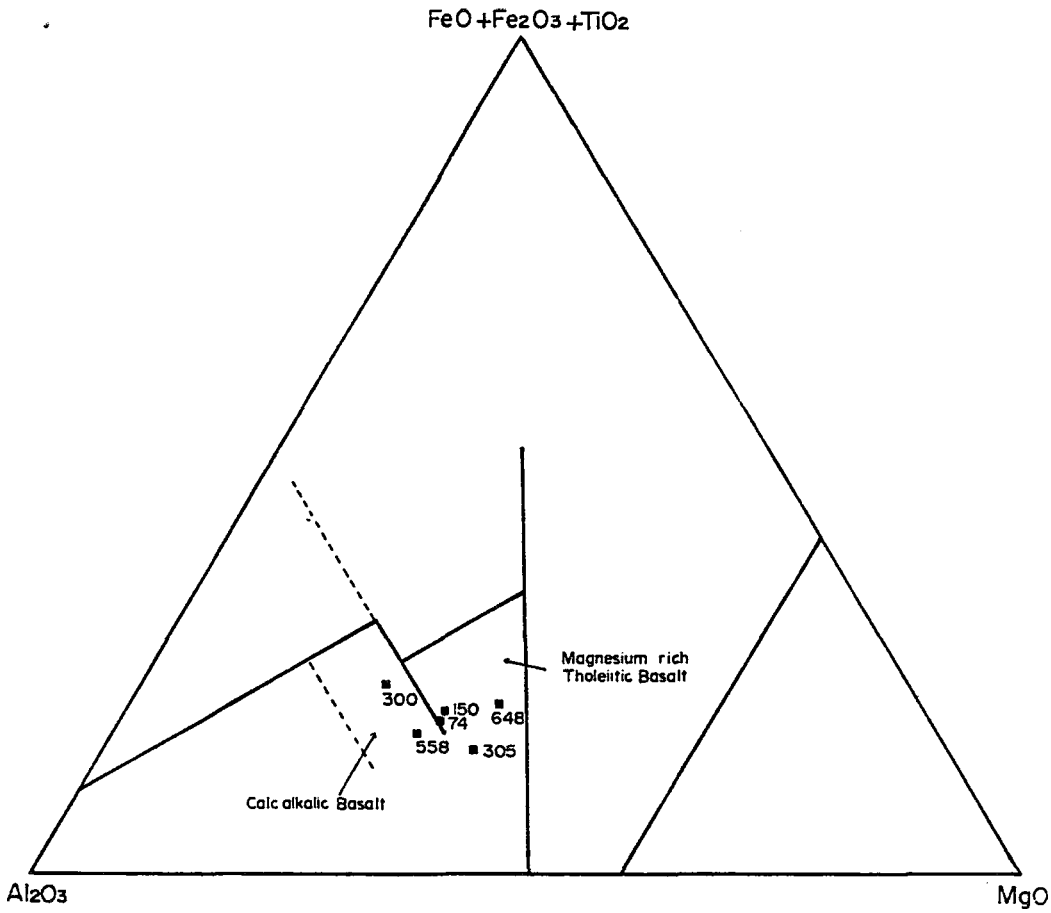

FIGURE 7-8 Plots of discordant gabbros on the Jensen Cation Plot.

■ Gabbro

PLATE 7-4 Representative samples of dyke lithogies in map area 1, 2, 3, 4, 6

1. Brick red, fine grained syenite
2. Light white, fine grained syenite
3. Quartz-feldspar porphyry
4. Quartz-feldspar porphyry
5. Syenite, the Lebel Stock
6. Biotite lamprophyre

Alkali-rich dykes range in width from 5 cm to 3 meters. Most are less than one meter wide. M-81 a leucratic syenite (plate 7-4) is fine grained and equigranular and contains 15 % hornblende, 70 % orthoclase and 5 % albite. Secondary chlorite and sericite are abundant as partial replacements of hornblende and feldspar respectively. M-685, the feldspar porphyry sample contains 40 % euhedral phenocrysts of albite, andesine and orthoclase which average 1 mm in length. The matrix is very fine grained and is comprised of feldspar with minor quartz and hornblende and has been extensively sericitized. Biotite lamprophyre has not been studied petrographically. However, the fine to medium grained biotite phenocrysts range in abundance from 5 to 15 %. The matrix is fine grained and dark grey to dark green.

M-641, from the Lebel Stock is medium grained and equigranular and is comprised of 75 % euhedral orthoclase, 5 % euhedral albite and 20 % euhedral green hornblende. Minor amounts of secondary sericite and chlorite are present. The weakly to non-metamorphosed character of M-641, M-8 and M-685 is in sharp contrast to their pervasively metamorphosed host lithologies.

Figure 7-9 shows the locations and trends of thirty-nine alkali-rich dykes and the locations of thirteen outcrops which are probably portions of alkali-rich dykes. Sixteen light-coloured syenitic dykes have variable trends.

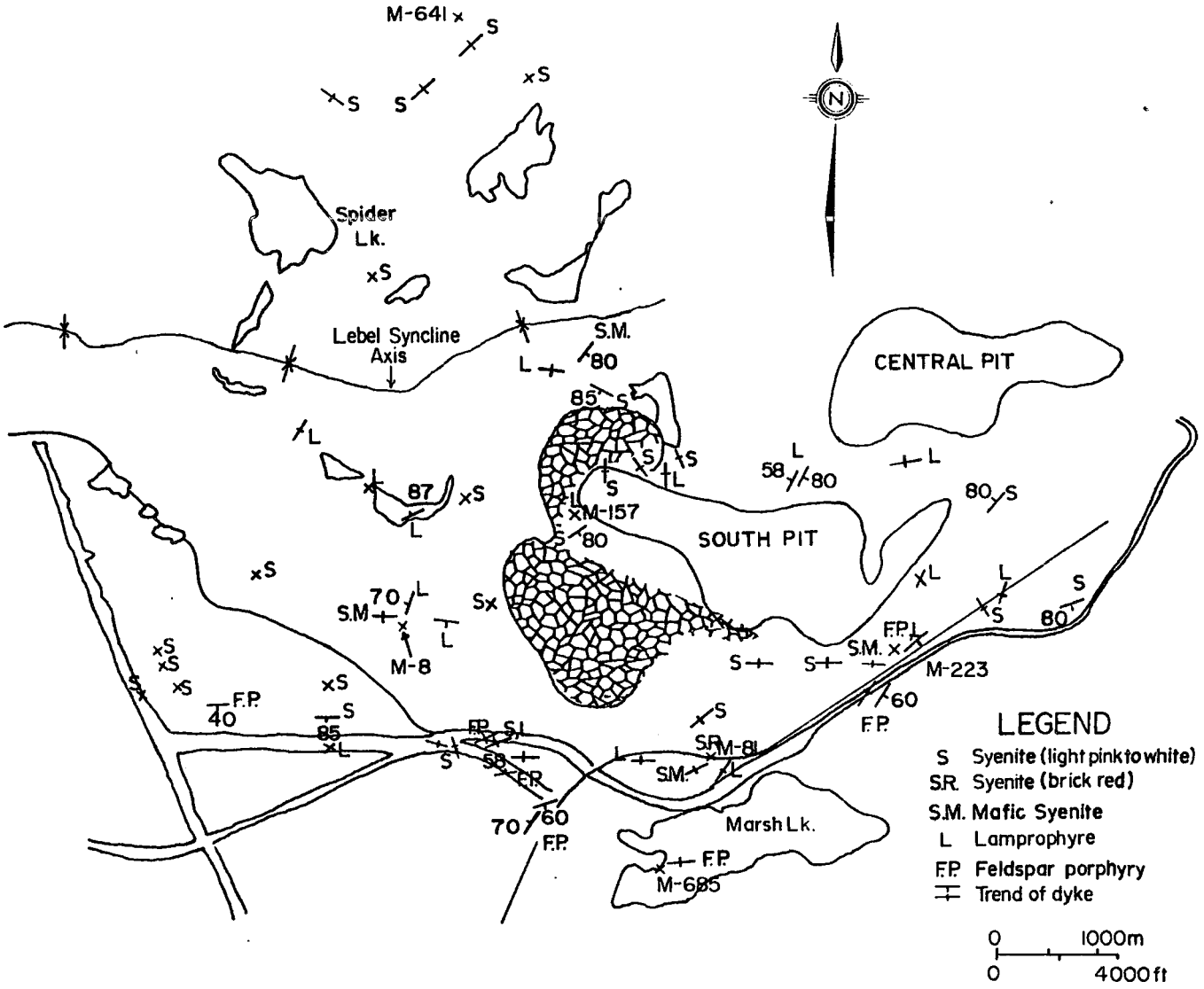

FIGURE 7-9 Location of alkalic dykes in the thesis map area.

Eleven outcrops are comprised of light-coloured syenite. This was the most abundant dyke lithology observed outside of the South Pit.

Fourteen biotite lamprophyre dykes have north-south through to east-west trends. Northwest trends were not observed. Six feldspar porphyry dykes have northeast-southwest and east-west trends. Five of these porphyry dykes are confined to a narrow northeast striking zone south and southeast of the South Pit.

Brick red syenite was observed at M-81 along the railroad tracks south of the South Pit (figure 7-9). Four mafic syenite dykes were observed, three with east-west trends, the other with a northeast-southwest trend.

Dubuc (1966a) made a detailed geological study of the South and Central Pits following stripping and recognized two generations of lamprophyre dykes - those with northeast-southwest trends and those with east-west trends. The former cut the latter. Few lamprophyre dykes with northwest trends were observed. Dubuc (1966a) notes that the lamprophyres cut syenite with a northwest-southeast pattern. Cross-cutting relationships observed by the author in the map area are as follows: feldspar porphyry cuts lamprophyre which in turn cuts syenite.

Figure 7-10 is a dyke map modified from Dubuc (1966b) and shows more than one hundred dykes cutting B.I.F. at the South Pit. Approximately 80 % of these dykes are

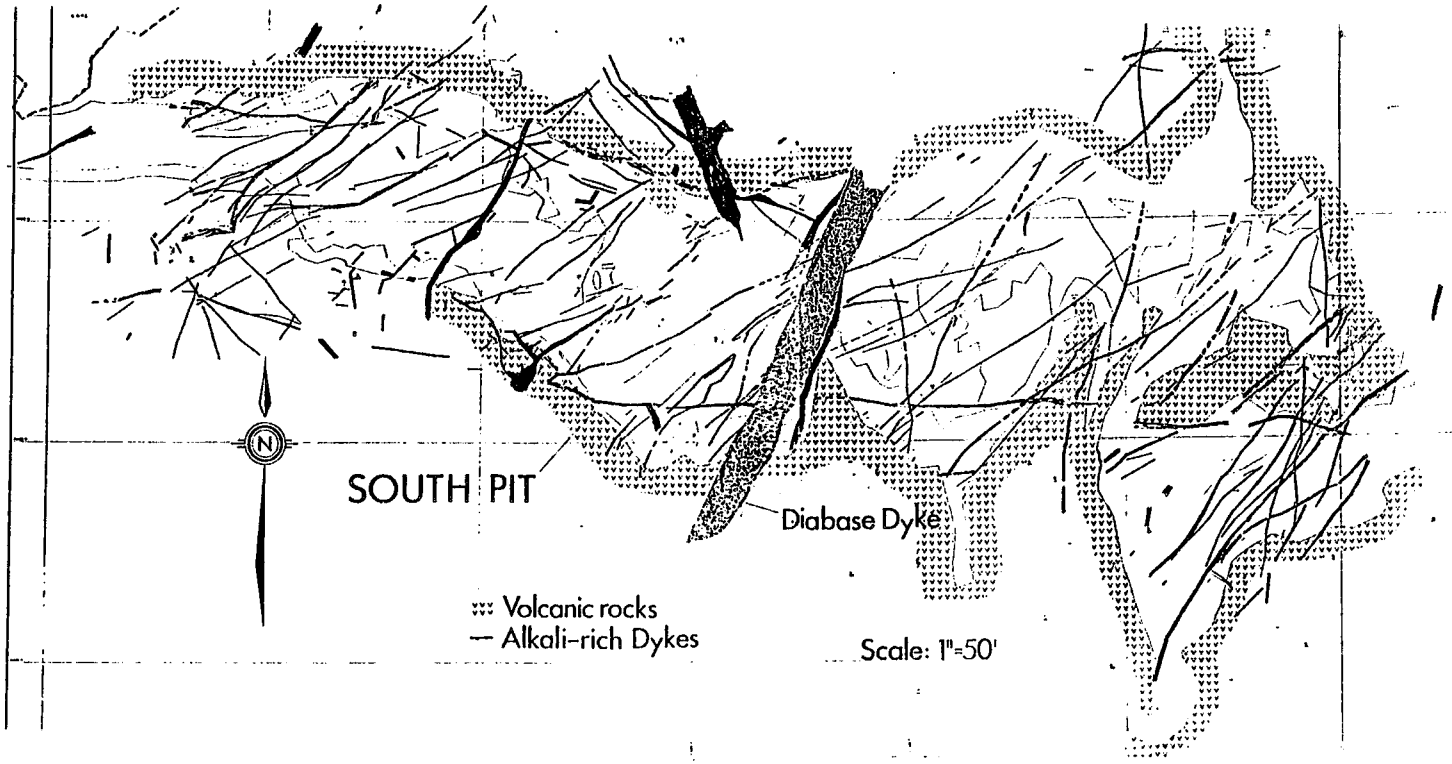

FIGURE 7-10 Outline of the South Pit and the alkalic dykes which cut it. Dubuc (1966b) originally distinguished lamprophyre from syenite on this map. These are not distinguished in this figure. The volcanic symbols, diabase dyke code and names were added by the author of this thesis.

lamprophyric, the rest are syenitic. This writer observed the light-coloured variety of syenite in the pit.

There are twice as many dykes observed within the South Pit than outside of it. This difference may be a function of differences in intensity of deformation. The South Pit B.I.F., being tightly folded (prior to alkali-dyke emplacement) may have experienced greater amounts of fold related fracturing than other parts of the map area. It is also possible that many dykes were missed outside of the South Pit owing to the poor exposure and that many lamprophyre dykes were missed because they are similar in appearance to many volcanic lithologies on the weathered outcrop surface.

The thesis map area dykes resemble others found throughout the Kirkland Lake area. Table 7-9 notes name, analysis and location for two syenite, one lamprophyre and one porphyritic syenite dyke samples in this area. Figure 7-11 shows their locations.

These dykes are richer in one or both of Na_2O and K_2O than the averages of analyzed volcanic and intrusive lithologies from the thesis map area. Analyses in table 7-9 can be compared to ten low MgO komatiitic basalts which average 2.34 % Na_2O and 1.09 % K_2O, eighteen low MgO komatiitic andesites which average 2.67 % Na_2O and 0.38 % K_2O and five high Al_2O_3 komatiitic volcanics which average 2.35 % Na_2O and 1.81 % K_2O. Six discordant gabbros average

Table 7-9

Major element abundances of alkalic intrusives from various localities in the Kirkland Lake area.

	1	2	3	4
SiO_2	59.90	52.13	44.80	67.38
Al_2O_3	19.83	13.64	17.85	15.63
Fe_2O_3	3.90	10.28	14.17	3.17
MgO	0.95	7.24	8.97	1.48
CaO	2.11	5.56	6.99	2.64
Na_2O	7.38	2.73	4.97	3.80
K_2O	4.96	6.82	0.09	5.28
TiO_2	0.66	0.85	1.77	0.36
MnO	0.08	0.14	0.22	0.08
P_2O_5	0.22	0.63	0.15	0.16
Total	99.99	100.02	99.98	99.98

1. Felsic syenite, Macassa Mine, (Kerrich and Watson, 1984).
2. Augite syenite, Macassa Mine, (Kerrich and Watson, 1984).
3. Lamprophyre, Highway 624 Band, Skead Township, (Jensen, 1978a).
4. Porphyritic syenite, Wright-Hargreaves Mine, (Kerrich and Watson, 1984).

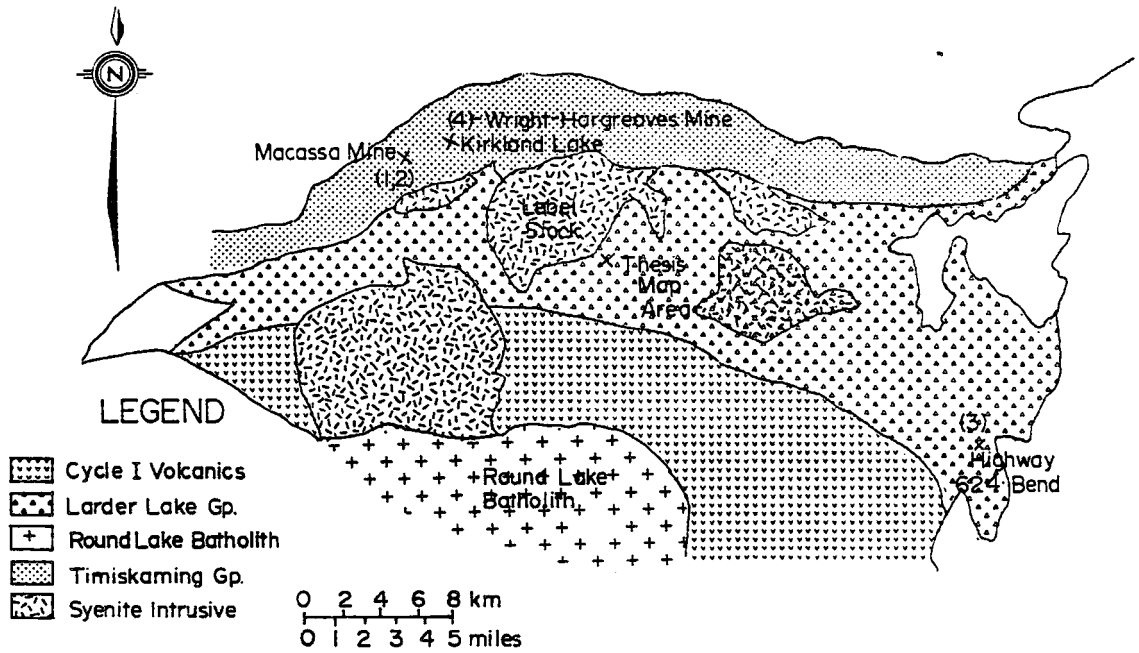

FIGURE 7-11 Location of alkalic intrusive samples cited in Table 7-9. Geology of the Kirkland Lake area is from Jensen (1980).

2.52 % Na_2O and 1.24 % K_2O while sixteen concordant gabbros average 3.19 % Na_2O and 0.93 % K_2O. Five sequence 1 basalts average 3.49 % Na_2O and 0.77 % K_2O.

7-6 Diabase Dykes

The two diabase dykes observed in the thesis map area mark the latest intrusive event. This is clear in the field where these dykes cut all lithologies including the feldspar porphyry dykes.

Both diabase dykes are vertical or near vertical dipping and are approximately 30 meters in width. The dyke which cuts the South Pit strikes 010° to 020° while the dyke which passes south of the South and Peria Pits and the mill has a strike of 070° (figure 7-12): The two cross near the Adams Mine road south of the South Pit. Both grade outwards from fine grained margins to medium grained centers and are easily recognized in the field in that 1) they weather a rusty brown colour, 2) they have not been visibly altered (no epidote veinlets, for example) and 3) they have a blocky appearance, attributable to two easily recognized joint sets which are roughly at right angles to each other. Plate 7-5 shows the more southerly dyke where it is exposed south of the South Pit.

The dykes have an ophitic texture with 40 % partially altered euhedral feldspar up to 3 mm in length enclosed by 58 % coarser anhedral clinopyroxene. The

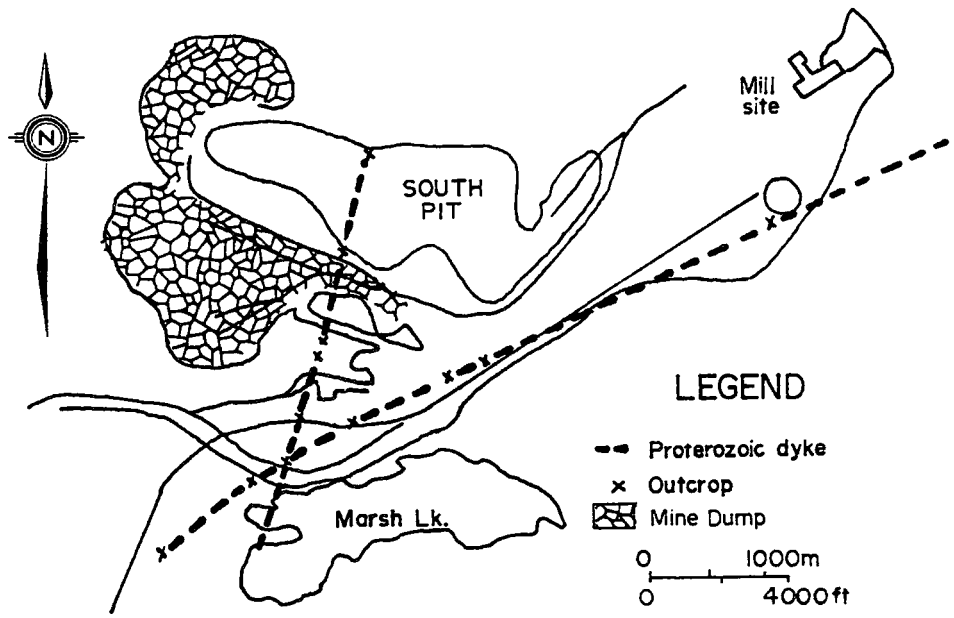

FIGURE 7-12 Location of the two diabase dykes as observed in the thesis map area. The two intersect near the Adams Mine road. The more northerly striking dyke cuts B.I.F. at the South Pit but is not observed north of it in the map area or in NB-1 map area. The same dyke is observed to the north in the Lebel Stock (Lawton, 1957). It apparently pinches out locally along its extent. The more easterly striking dyke strikes below the Peria Pit east of the map area (Lawton, 1957). On Lawton's 1957 map, the two dykes can be traced south into the Catherine Group of cycle I. These two dykes are the only ones of their kind mapped in Boston Township by Lawton (1957).

PLATE 7-5 Photograph of the more southerly diabase dyke where it cuts komatiites of sequence 5 near sample locality M-218. This is between the South Pit and the Adams Mine road.

feldspar is characterized by albite and carlsbad-albite twins. Using Michel-Levy's method, the feldspars are labradorite. Up to 50 % of some feldspars have been replaced by a very fine grained mat of prehnite and clinozoisite (plate 7-6). Clinopyroxene is locally altered to chlorite. Magnetite makes up 2 % of these intrusives, occurring in aggregates between pyroxene grains. Magnetite is abundant enough to impart a magnetic character to the dykes. Igneous hornblende is locally observed.

One diabase dyke sample, M-80 was analysed for major elements and Cr, Co, V, Ni. In table 7-10 it is seen that this sample and three representative concordant gabbros which plot in the iron-rich tholeiitic basalt field on the Jensen Cation Plot have similar chemistries. Their high Fe_2O_3 and TiO_2 abundances are distinctive relative to other igneous rock types in the map area..

It should be noted that thin, 20 to 50 cm wide mafic dykes locally observed throughout the map area are not related to the two diabase dykes. These mafic dykes which are fine grained and have variable strikes and dips, resemble low MgO komatiitic basalts and andesites in hand specimen. They are locally cut by syenitic veinlets or are epidotized and they are not observed to cut the concordant and discordant gabbros. These observations suggest that they are related to komatiitic volcanism.

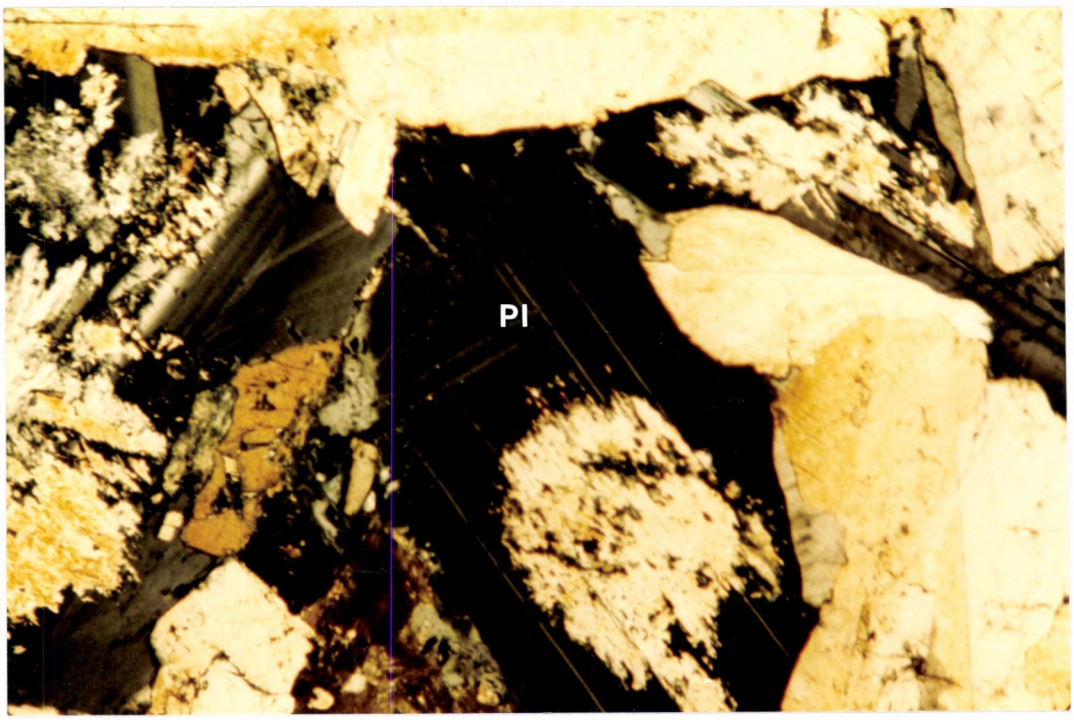

PLATE 7-6 Plagioclase (Pl) is only locally altered to a fine grained mosaic of prehnite and clinozoisite in M-80. Polarized light, x63. Field of view is 1.0 x 1.5 mm.

Table 7-10

Comparison of major elements and Cr, Ni, Co and V contents between the diabase dyke sample and three concordant gabbros which plot in the iron-rich tholeiitic basalt field on the Jensen Cation Plot.

	Diabase dyke	Concordant gabbros		
Sample	M-80	M-325	M-19	M-714
SiO_2	50.80	50.91	52.94	51.84
Al_2O_3	13.36	13.14	13.25	13.14
Fe_2O_3	14.45	14.83	14.99	17.53
MgO	7.03	6.08	5.25	5.79
CaO	9.67	8.71	9.70	6.75
Na_2O	2.34	3.75	2.44	2.34
K_2O	1.16	0.85	0.43	1.09
TiO_2	1.37	1.35	1.25	1.58
MnO	0.22	0.26	0.28	0.24
P_2O_5	0.21	0.13	0.16	0.12
Total	100.00	100.00	100.00	100.00
Cr	139	52	4	8
Ni	88	68	63	15
Co	65	86	80	85
V	261	302	297	459

Chapter 8

Petrogenesis of Igneous Rocks

8-1 Derivation of Ultramafic Liquids

Komatiites can be derived from ultramafic silicate liquids. As proof of this contention, Bickle (1982) sites the following evidence: phenocryst poor glassy flow tops with MgO abundances of 30 % in komatiites, relict olivines equilibrated with liquids with up to 30 % MgO and iron/magnesium variations in komatiitic suites. These variations cannot be explained by accumulation of olivine into liquids with less than 24 % MgO (Bickle, 1982).

Three models which account for the derivation of ultramafic liquids are briefly outlined below.

(1) High degrees of partial melting (up to 60 %) of a depleted mantle source; that is, one which had experienced a previous melting event, leaving refractory residuals and trapped liquid (Arndt, 1977). The residue may have been dunite or harzburgite. Arndt (1977) proposed this two step melting model because he believed that a liquid would not remain in contact with the residue until a very high degree of melting (60 %) was attained, if only a one stage event as proposed by Green et al. (1975), had occurred.

(2) Cox (1978) proposed a mechanical mixing model where

magmas initially formed in the mantle as crystal-rich mushes from which some liquid separates. As this mush rose, crystals dissolved to produce an ultramafic liquid.

(3) Bickle et al. (1977) proposed a two-stage process. Initial partial melting of a dunitic or harzburgitic residue in the mantle produced a magma with a MgO content of 24 %. This magma separated from the residue at depths near 100 km.. It then incorporated surrounding mantle, up to its own mass as it rose. The entrained solid was melted during rapid transport to the surface.

To determine which of these three models best accounts for the generation of the ultramafic liquids which eventually parented the komatiites in the Adams Mine area is beyond the scope of this thesis. However, for a detailed discussion of komatiite genesis, one should refer to Smith and Erlank's (1982) work on the Barberton komatiites.

8-2 Fractional Crystallization: Genesis of High MgO Komatiitic Basalts

In the seven komatiitic sequences observed on the south limb of the Lebel syncline, komatiites are found at the base of each sequence and are overlain by high MgO komatiitic basalts. This trend is consistent with fractional crystallization of olivine with or without pyroxene in a magma chamber for each of these sequences.

Residual liquids drawn from the magma chamber as fractional crystallization proceeds would be progressively poorer in magnesium.

The depletion in MgO in the residual liquid and the gradation from a komatiite to the overlying high MgO komatiitic basalts can be easily explained by the fractionation of a forsterite-rich olivine. In figures 8-1a and b, all volcanic samples analyzed from the seven komatiitic sequences on the south limb of the Lebel Syncline are plotted on the M.C.A. diagram. It is seen that samples with greater than 12 to 13 % MgO plot at or near the mid-section of the diagram, directly below the MgO apex. This reflects the importance of olivine fractionation on the composition of liquids with greater than 12 to 13 % MgO. In Munro Township, olivines are forsterite-rich in both komatiites (Fo, 84-95) and high MgO komatiitic basalts (Fo, 76-87) (Arndt et al., 1977).

The decrease in Cr abundances in flows ranging from 24 to 16 % MgO as seen in figure 8-2a is explained by the removal of Cr-spinel (chromite). Chromite exists as a liquidus phase in a co-tectic relationship with olivine (Irvine, 1975). In komatiites, chromite is generally rich in Cr_2O_3 averaging approximately 50 % (Naldrett and Smith, 1981). In Munro Township, chromite has Cr_2O_3 contents between 39.5 and 56.2 % (Arndt et al., 1977). Fractionation of olivine which is unusually rich in Cr_2O_3, as is observed

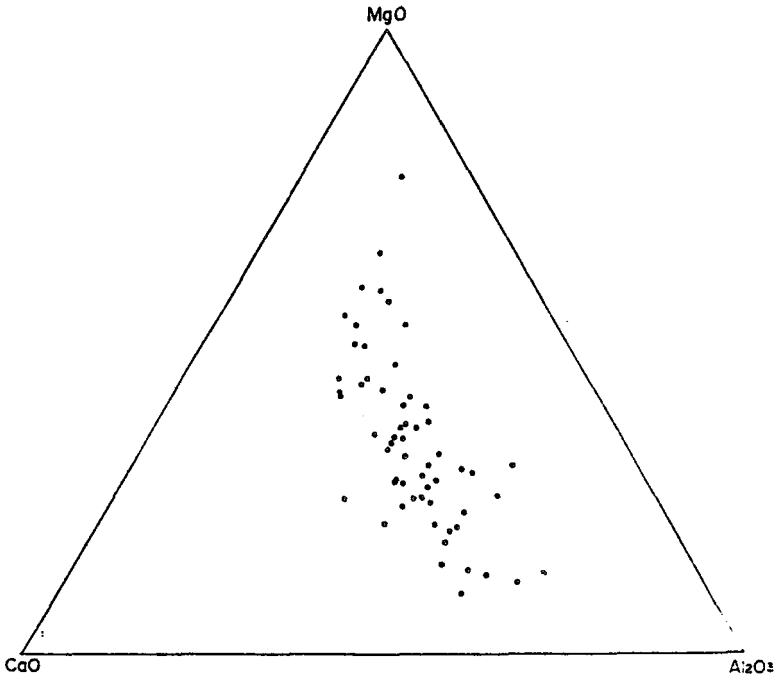

FIGURE 8-1a Plots of komatiite and komatiitic volcanic samples from the south limb of the Lebel Syncline in the map area on the M.C.A. diagram.

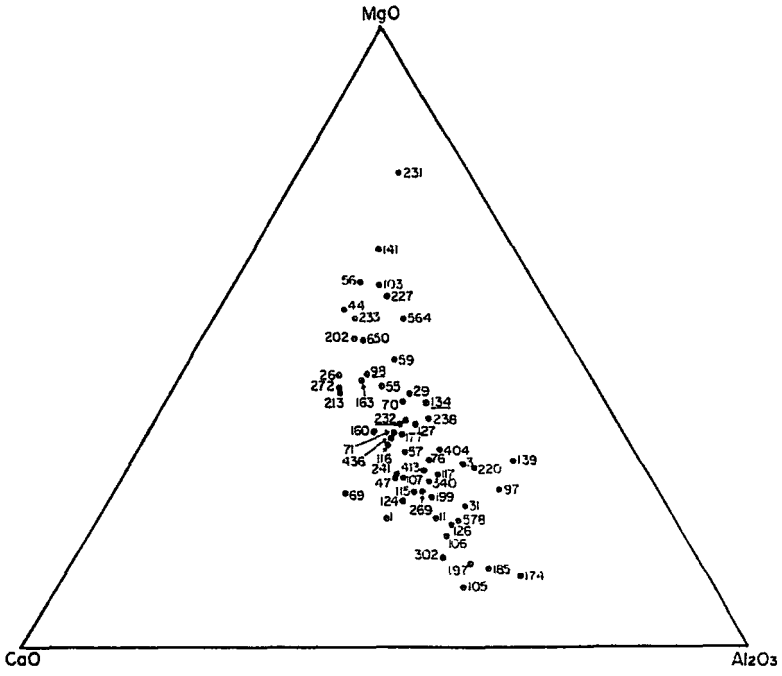

FIGURE 8-1b Plots of komatiite and komatiitic volcanic samples from the south limb of the Lebel Syncline in the map area on the M.C.A. diagram. Sample numbers are indicated. M-134 has 12.59% MgO. M-232 has 12.49% MgO. M-98 has 16.38% MgO.

FIGURE 8-2(a) Variation diagram of Cr versus MgO for komatiites and komatiitic volcanics from the thesis map area.

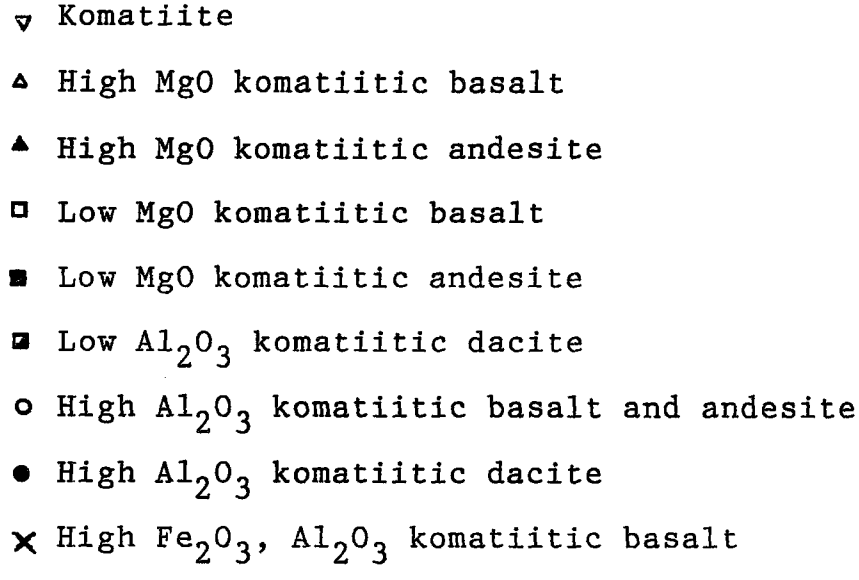

FIGURE 8-2(b) Variation diagram of Ni versus MgO for komatiites and komatiitic volcanics from the thesis map area.

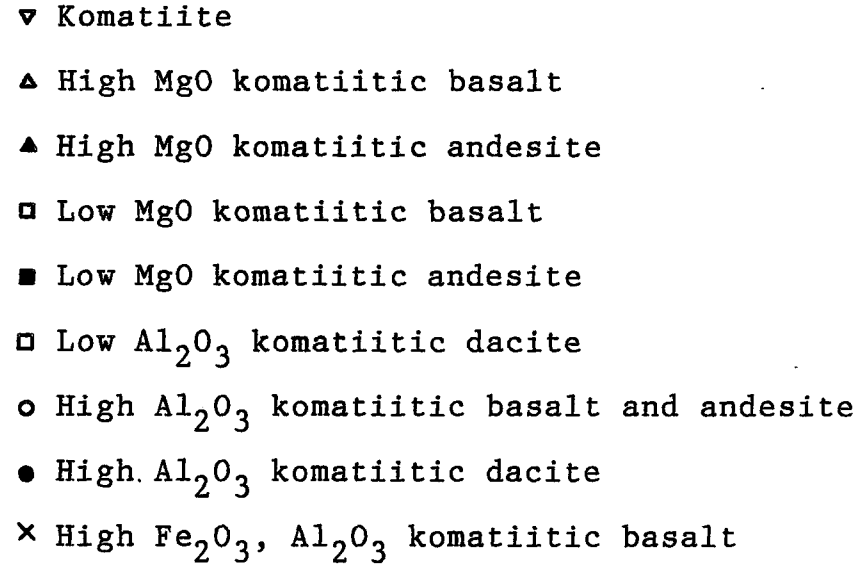

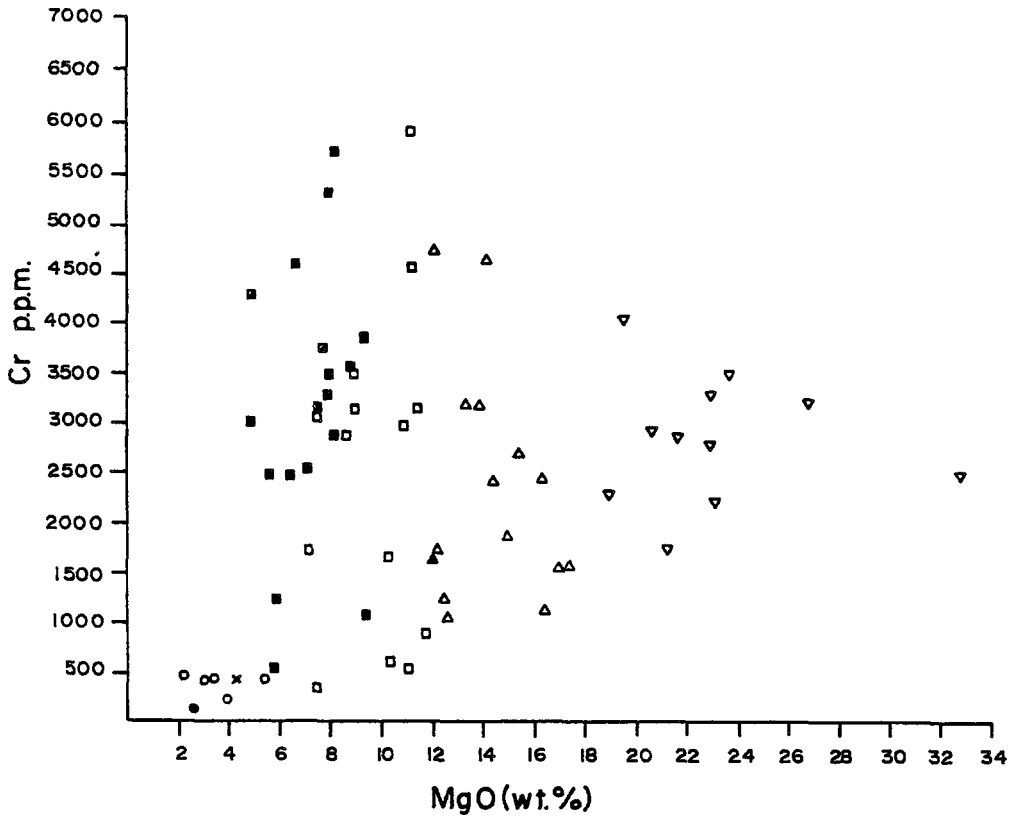
Cr p.p.m.
7000
6500
6000
5500
5000
4500
4000
3500
3000
2500
2000
1500
1000
500
2 4 6 8 10 12 14 16 18 20 22 24 26 28 30 32 34
MgO (wt.%)

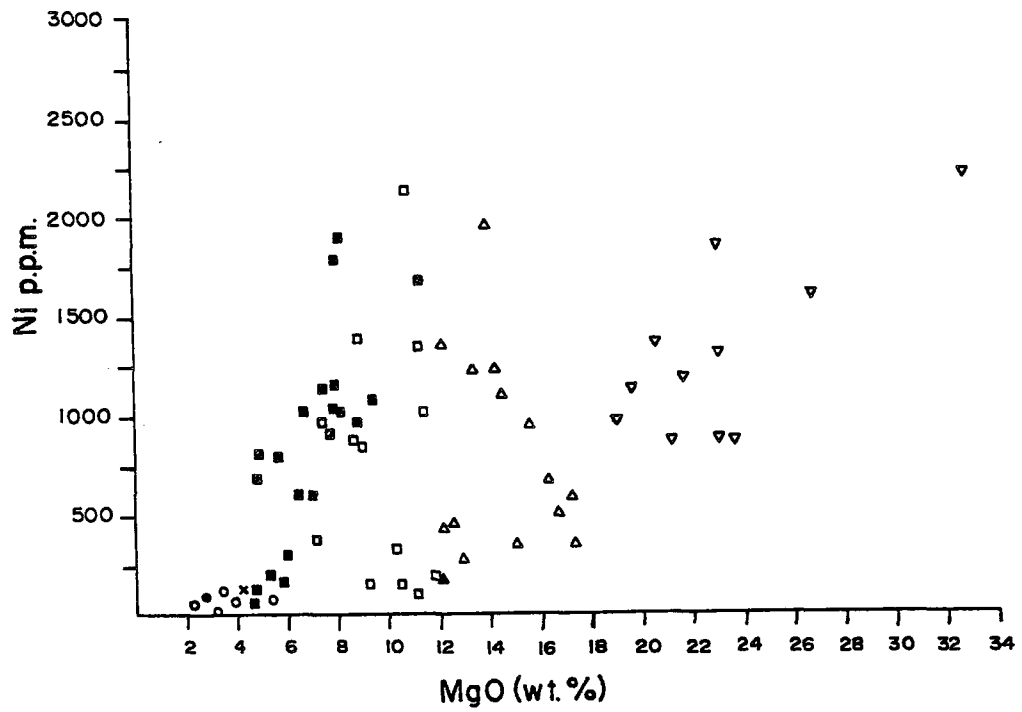
Ni p.p.m.
3000
2500
2000
1500
1000
500
2 4 6 8 10 12 14 16 18 20 22 24 26 28 30 32 34
MgO (wt.%)

in Munro Township (0.14 to 0.33 %)(Arndt et al., 1977), may also contribute to Cr depletion in a magma. The decrease in Ni abundances in flows with MgO abundances ranging from 24 % to 16 % shown in figure 8-2b is accounted for by preferential incorporation of Ni^{+2} into olivine (Taylor et al., 1969). The NiO content in Munro Township komatiites is high, ranging from 0.32 to 0.55 % and shows a rough positive correlation with forsterite content in olivine (Arndt et al., 1977).

Depletion of Ni in cooling komatiitic liquids might also be attributed to removal of Ni by a Ni-rich immiscible sulphide melt. However, this is not the case in the map area as komatiites which most reflect the primary melt contain only trace amounts of sulphides and in particular are poor in Cu (absence of chalcopyrite). Sulphur saturated ultramafic liquid would not have these characteristics. Unless sulphides and trace metals such as Cu were lost during alteration, metamorphism and deformation, the features noted above indicate that the Adams Mine komatiites and their parent ultramafic liquids were not sulphur saturated and the separation of a Ni-rich immiscible sulphide melt is not likely.

Other analyzed elements (SiO_2, Al_2O_3, CaO, TiO_2 and V) which have not been effected by alteration show increases in abundances through the MgO interval of 34 to 15 % because they are not major constituents of the two major

fractionating phases (olivine and chromite). Some Fe_2O_3 may be removed by olivine and chromite which explains its relative constancy in abundance over the interval in question.

8-3 Genesis of Cr and Ni-rich Low MgO komatiitic Basalts and Andesites

When liquid in the magma chamber reaches MgO abundances of 12 to 15 %, fractionation of pyroxene replaces that of both olivine and chromite. The sharp increase in Ni abundances in basalts of this MgO content indicates that olivine fractionation has ceased or was significantly reduced. This sharp increase is highlighted by comparing the Ni versus MgO variation diagram for the map area (figure 8-2b) with one from a typical Archean terrane (figure 8-3a).

The increase in Ni abundances is coupled with the divergence of data points on the A.M.C. diagram (figure 8-1) towards the $MgO-Al_2O_3$ join for samples with MgO less than 13 %. This second feature indicates that a phase was being removed which was richer in CaO than Al_2O_3. Clearly, a clinopyroxene is the prime candidate.

A comparison of figure 8-2a with 8-3b helps illustrate how Cr abundances increase sharply at MgO levels of less than 15 %. The coincidental sharp increase in Cr and Ni suggest that chromite precipitation ceased with olivine precipitation. This is consistent with Irvine's (1967) observation that chromite crystallization appears to

FIGURE 8-3(a) Variation diagram of Ni versus MgO for komatiites and komatiitic volcanics in the
o Kukmo greenstone belt
□ Suomussalini greenstone belt
△ Tipasjarvi greenstone belt
from Auvray et al. (1982)

FIGURE 8-3(b) Variation diagram of Cr versus MgO for komatiites and komatiitic volcanics in the
o Kukmo greenstone belt
□ Suomussalini greenstone belt
△ Tipasjarvi greenstone belt
from Auvray et al. (1982)

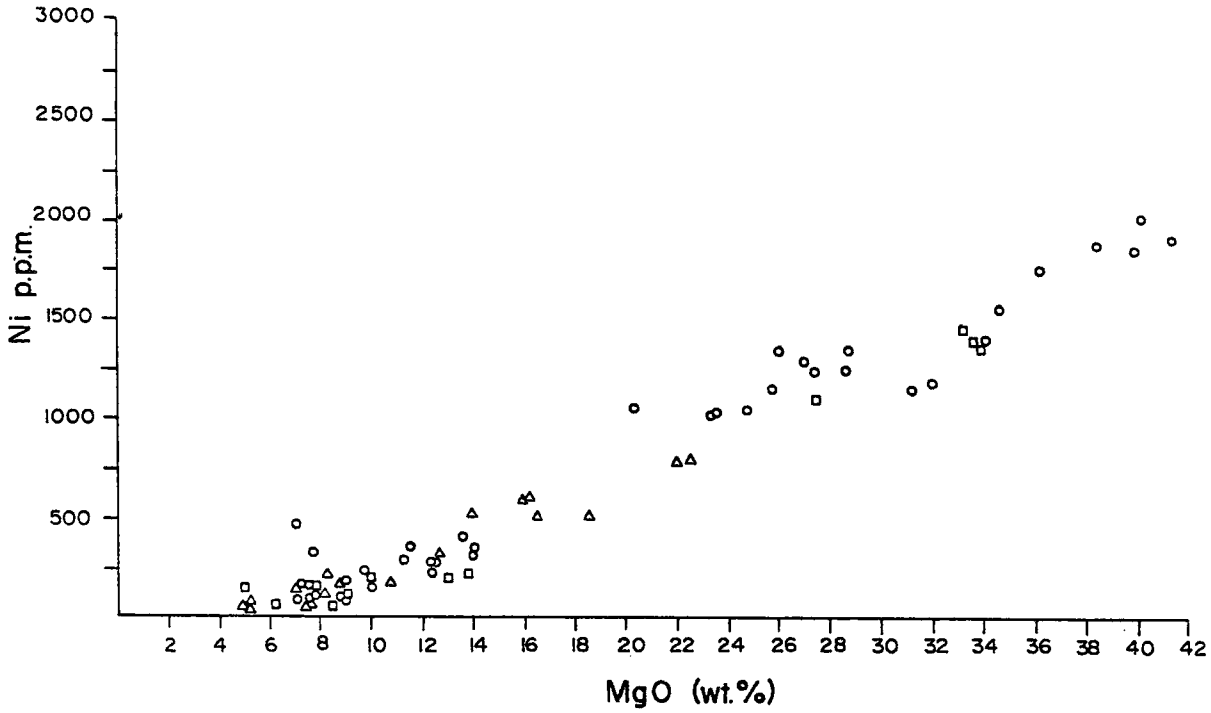
Ni p.p.m.
3000
2500
2000
1500
1000
500
2 4 6 8 10 12 14 16 18 20 22 24 26 28 30 32 34 36 38 40 42
MgO (wt.%)

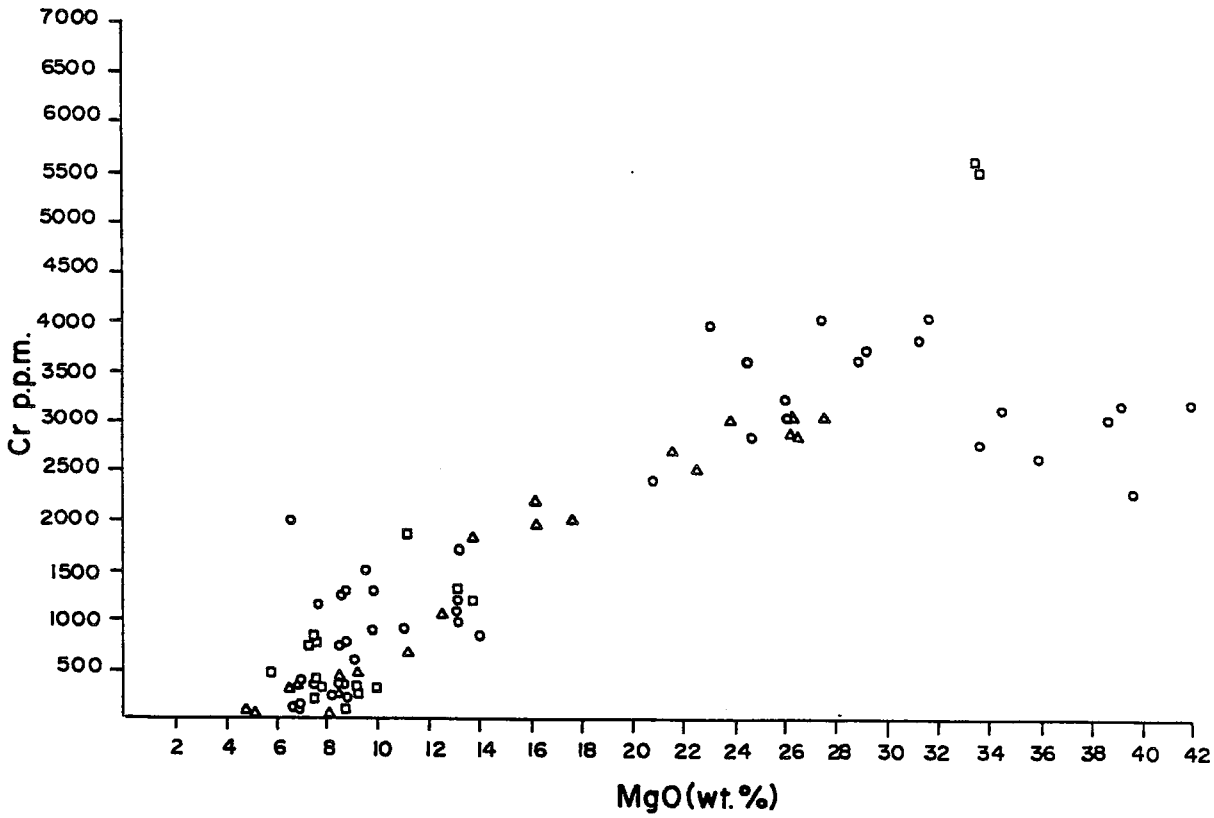
Cr p.p.m.
7000
6500
6000
5500
5000
4500
4000
3500
3000
2500
2000
1500
1000
500
2 4 6 8 10 12 14 16 18 20 22 24 26 28 30 32 34 36 38 40 42
MgO(wt.%)

stop owing to a peritectic reaction with clinopyroxene (diopsidic augite).

The rather abrupt change in fractionating phases at this point can be attributed to rapid cooling. Arndt and Fleet (1979) have demonstrated that pigeonite, followed by subcalcic augite crystallize from liquids which would have crystallized olivine, followed at lower temperatures by diopside under equilibrium crystallization.

It is not likely that the pyroxene would deplete the residual magma significantly in Cr. Pyroxenes formed under rapid cooling conditions have relatively low Cr_2O_3 abundances. Representative electron microprobe analyses of acicular pyroxenes grown under rapid cooling conditions from Munro Township komatiitic basalts are given in table 8-1. The cores of the pyroxenes are comprised of pigeonite with Cr_2O_3 contents of 0.63 and 0.76 %. Pigeonite cores make up 10 to 20 % of the volume of the pyroxene. The more voluminous augite mantles have Cr_2O_3 contents in the order of 0.23 to 0.16 %.

These Cr_2O_3 contents for augite are well below those of

1) 0.88 % Cr_2O_3 in augite from gabbros in southwest Africa (Hess, 1949).
2) 0.81 % Cr_2O_3 in slowly cooled augite in Fred's flow in Munro Township (Arndt et al., 1977).
3) 1.53 % Cr_2O_3 in a spinel lherzolite nodule in kimberlite

Table 8-1

Representative election microprobe analysis from pyroxenes in the Alexo Flow, a thick layered komatiitic flow, from Arndt and Fleet (1979).

	1	2	3	4	5
SiO_2	53.6	51.9	55.2	51.9	50.6
Al_2O_3	2.32	3.14	2.02	4.6	5.1
FeO_{Total}	9.7	7.6	9.4	7.7	8.4
MgO	26.7	18.3	28.9	17.8	17.6
CaO	6.76	17.8	4.02	17.3	17.0
Na_2O	n.d.	n.d.	0.04	0.14	n.d.
K_2O	n.d.	n.d.	n.d.	n.d.	n.d.
TiO_2	n.d.	n.d.	0.11	0.37	n.d.
MnO	n.d.	n.d.	0.26	0.25	n.d.
P_2O_5	n.d.	n.d.	n.d.		n.d.
Cr_2O_3	0.76	0.39	0.63	0.23	0.16
Total	99.84	99.13	100.58	100.29	98.86

1. Pigeonite from core of needle (Ax14) in pyroxene spinifex textured lava
2. Augite from centre of mantle surrounding pigeonite; composite needle (Ax14) in spinifex textured lava
3. Pigeonite from core of needle (Ax11d) in pyroxene spinifex-textured lava
4. Augite adjacent to pigeonite in composite needle (Ax11d)
5. Augite at margin of composite needle (Ax11d)

N.B. Ax14 and Ax11d are the sample numbers of two pyroxene needles. The Alexo Flow is in Dundonald Township in northeastern Ontario and lies within the Stoughton-Roquemaure Group.

from southeastern Australia (Ferguson and Sheraton, 1979).

Naldrett (1981) notes that skeletal pyroxenes in komatiitic lavas have unusually high total Al_2O_3 content and a high proportion of Al(Z=4) to Al(Z=6) which is attributed to disequilibrium crystallization consequent upon supercooling. This Al enrichment is important as it may help to explain the high SiO_2 abundances in low MgO komatiitic andesites. A higher proportion of Al in the tetrahedral position results in a lower proportion of Si there (Kushiro, 1960). The residual liquid is thereby enriched in SiO_2. Furthermore, Fleet and MacRae (1975) note that Al enrichment in the pyroxenes would tend to suppress the crystallization of plagioclase which in turn, would result in a residual melt further enriched in SiO_2.

The SiO_2 enrichment cannot be explained in terms of removal of iron-rich oxides under high oxygen pressures, leaving the residual liquid poorer in iron but enriched considerably in SiO_2, as proposed by Osborne (1959). Vanadium is compatible with magnetite so that removal of magnetite should result in depletion of V (Taylor et al., 1969). This is not observed for the map area samples.

There is a similarity in the V contents of the low MgO komatiitic andesites and basalts which severely restricts the amount of magnetite which could be removed from a basaltic magma to produce an andesite. The average V

content for nine analyzed low MgO komatiitic basalts is 198 ppm while that for fourteen analyzed low MgO komatiitic andesites is 195 ppm. Ignoring three low MgO komatiitic andesites with 154, 127 and 130 ppm V, eleven analyzed andesites average 211 ppm V.

8-4 Genesis of High Al_2O_3 Komatiitic Volcanics

High Al_2O_3 komatiitic volcanics stratigraphically overlie komatiites and high and low MgO komatiitic basalts and are considered to have been parented by an ultramafic liquid. The production of the high Al_2O_3 volcanics can be related to rapid cooling rates in a fractionating magma chamber.

Gibb (1974) points out that plagioclase nucleation in liquids varies with cooling rates. Under slow cooling rates in plutons, plagioclase will crystallize from basaltic liquids at liquidus temperatures (equilibration crystallization). At faster cooling rates, crystallization temperatures are lowered below that at which equilibrium conditions occur. It is this second scenario that is envisioned for the formation of the high Al_2O_3 volcanics. Nucleation of plagioclase is delayed allowing the residual liquid to be enriched in Al_2O_3. In map area NB-2, high Al_2O_3 komatiitic basalt overlies low MgO komatiitic basalt. Prior to Al_2O_3 enrichment, the residual liquid likely resembled the low MgO komatiitic basalts in composition.

The high Al_2O_3 abundances in the high Al_2O_3 volcanic rocks cannot be related to the presence of plagioclase phenocrysts as the flows are aphyric. The absence of plagioclase phenocrysts is consistent with delayed plagioclase formation in a magma chamber. Plagioclase formed there under slow cooling rates may have been extruded and manifested as phenocrysts in the flows.

It is unlikely that olivine and chromite ceased to crystallize and fractionate out in response to the rapid cooling rates as has been suggested for the Cr and Ni-rich volcanics. Three high Al_2O_3 komatiitic basalt average 349 ppm Cr and 59 ppm Ni while two high Al_2O_3 komatiitic andesites average 414 ppm Cr and 84 ppm Ni. High Al_2O_3 volcanics can thus be considered the products of fractional crystallization primarily of olivine, chromite and pyroxene from an ultramafic liquid.

High Al_2O_3 komatiitic volcanics and Cr and Ni-rich low MgO komatiitic volcanics do not occur together (one overlying the other for example) in any of the komatiitic sequences in the map area. This is consistent with differing fractionation schemes which may be the result of differing rates of rapid cooling.

8-5 Genesis of High Fe_2O_3, Al_2O_3 Komatiitic Basalt

Fe_2O_3-rich komatiitic basalts stratigraphically overlie the high Al_2O_3 komatiitic basalts below the Peria

Pit. They represent an extremely evolved member of the komatiitic suite which may have been derived by fractional crystallization of liquids whose composition once matched those of the high Al_2O_3 basalts. To show that a high Fe_2O_3-basalt can be derived from a high Al_2O_3 basalt reference is made to Byerly et al. (1976).

Byerly et al. (1976) conducted least squares modelling on the trend of major elements versus MgO for the strongly differentiated volcanics from the Galapagos Spreading Centre. This modelling indicated that removal of 40 % plagioclase, 26 % clinopyroxene and 8 % olivine from a liquid of composition A can produce one of composition 3 (table 8-2). In table 8-2, composition A resembles A-11, a high Al_2O_3 basalt from map area NB-2 while composition 3 resembles A-29, a high Fe_2O_3 basalt from map area NB-2. Both A-11 and A-29 are from the same group below the Peria Pit. A-29 overlies A-11.

Sample M-197, a high Fe_2O_3, Al_2O_3 komatiitic basalt shown in table 8-2 is from pillowed flows overlying the South Pit. This iron-rich flow differs from A-29 in that it has higher Al_2O_3 abundances. The higher Al_2O_3 level may reflect lower levels of plagioclase nucleation and fractionation than that indicated in Byerly et al.'s example.

M-197 has 443 ppm Cr and 136 ppm Ni. These low abundances are consistent with derivation of a high

Table 8-2

Comparison of Larder Lake Group Fe-rich komatiitic volcanics with Fe-rich volcanics from the Galapagos Spreading Centre

	Galapagos Spreading Centre		Map area NB-2		Thesis map area
	A	3	A-11	A-29	M-197
SiO_2	50.13	49.23	50.07	49.00	48.50
Al_2O_3	16.24	11.24	16.69	13.72	16.76
Fe_2O_3	9.02(FeO)	18.43(FeO)	11.25	19.07	18.50
MgO	8.43	4.26	7.65	4.94	4.24
CaO	12.50	9.18	11.02	10.10	9.81
Na_2O	2.20	2.52	1.23	0.90	0.51
K_2O	0.06	0.19	1.08	0.09	0.59
TiO_2	1.03	3.71	0.56	1.40	0.55
MnO			0.36	1.30	0.54
P_2O_5	0.07	0.31	0.04	0.14	0.00
Total	99.68	99.07	100.00	100.00	100.00
Cr			366	197	443
Ni			86	27	136
Co			66	101	116
V			206	333	220

Fe_2O_3,Al_2O_3 komatiitic volcanic from a magma which parented the high Al_2O_3 komatiitic volcanics. High Al_2O_3 komatiitic volcanics have similar Cr and Ni contents.

8-6 Additional Support for the Concept of Rapid Cooling in a Magma Chamber

Rapid cooling and the development of acicular crystal forms are normally associated with extrusives. However it is not unreasonable to suggest comparable textures may develop in a subsurface magma chamber as a result of rapid cooling. This author has observed two examples of rapid cooling in intrusive rocks. These are: 1) acicular amphibole crystals up to 5 cm in length in concordant gabbro in the thesis map area; 2) acicular hornblende crystals up to 5 cm in length in diorite dykes which cut Grenville Province paragneiss near Bancroft, Ontario.

Moreover, Scoates et al. (1986) observe megadendritic and harrisitic textures characterized respectively by skeletal crystals of pyroxene and olivine in peridotites of the Bird River Sill in Manitoba. They point out that this is consistent with crystallization from supercooled melts.

8-7 Genesis of Sequence 1 Basalts

Sequence 1 basalts which have been classified as tholeiitic and calc-alkalic with the Jensen Cation Plot may

have been derived by fractional crystallization from a magnesium-rich (MgO 12-18 %) parental magma which in turn was derived by lower degrees of partial melting of the mantle than required to produce an ultramafic liquid. It is unlikely that these basalts represent magmas produced directly from the mantle. In the molar FeO versus MgO diagram shown in figure 8-4, they plot outside the boundaries of a field which represents liquid compositions capable of co-existing with an upper mantle. A relatively magnesium-rich magma will plot within this field.

It is also possible that sequence 1 basalts were derived from partial melting of the crust. Oxygen and strontium isotope studies and/or R.E.E. studies would certainly indicate the nature of the source and clear up this uncertainty.

However, derivation of sequence 1 basalts from magnesium-rich mantle derived magma is consistent with their TiO_2 values which are higher than those of the komatiitic basalts (figures 4-6a,b) which were derived from ultramafic liquids. Higher TiO_2 abundances are expected from an evolved igneous rock whose parental magma was derived by a relatively low degree of mantle partial melting versus one derived from more extensive partial melting.

If sequence 1 basalts are mantle derived, then their relatively low MgO abundances (average 7.39 %) and their lack of olivine phenocrysts can be explained by fractional

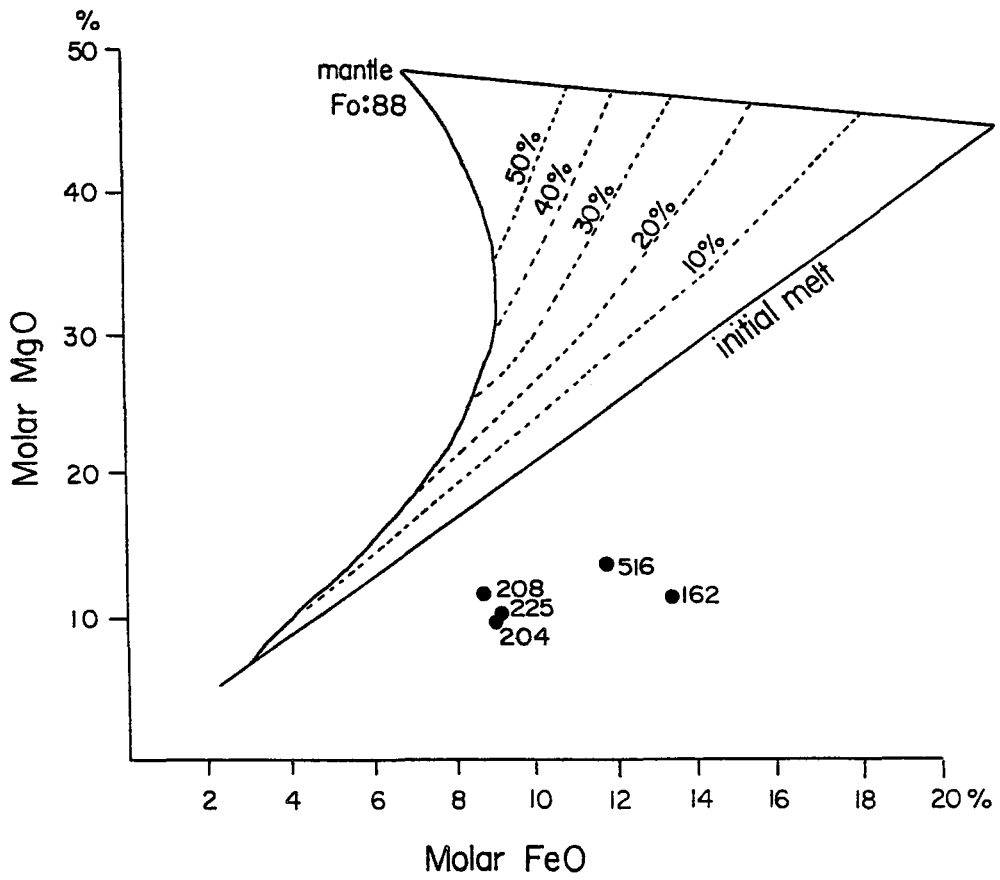

FIGURE 8-4 Tholeiites and calc-alkalic volcanics plotted on the MgO versus FeO plot ('Sail' diagram). The solid lines outline a field calculated by Hanson and Langmuir (1978) which encloses all liquid compositions that are capable of co-existing with an upper mantle of initial composition proposed by Carter (1970). The dashed lines indicate the percent of partial melting of the mantle of this composition.

crystallization of olivine in subvolcanic chambers.

Although the basalts are classified as tholeiitic and calc-alkalic, a tholeiitic trend (iron enrichment) or calc-alkalic trend (alkali enrichment) with stratigraphic height was not observed. An increase in alkali abundances with stratigraphic height might be difficult to establish due to metamorphism and alteration.

8-8 Relationship of the Peridotite, Peridotite-Gabbro and Gabbroic Sills to Volcanism

Arndt et al. (1979) point out that many of the layered peridotite-gabbro intrusions commonly found in areas of komatiitic volcanism are unrelated to the komatiitic lavas but have magmatic affinities with iron-rich tholeiitic volcanics, and that some layered sills are comagmatic with komatiitic volcanics. Arndt et al. (1977) note that layered sills of tholeiitic affinity have much more clinopyroxene-rich cumulates than olivine cumulates. Komatiitic examples on the other hand have a larger proportion of cumulus olivine, a smaller proportion of cumulus pyroxene and minor disseminated sulphide mineralization.

With this in mind, one might conclude that the peridotite sills which only locally have pyroxenitic or gabbroic phases are of komatiitic affinity. They may have developed by intrusion of ultramafic liquid or olivine crystal-liquid mush into the volcanic pile during extrusion of komatiites and komatiitic volcanics at slightly higher

crustal levels. The fact that peridotite sills are absent in the overlying non-komatiitic Kinojevis and Blake River Groups north of Kirkland Lake is consistent with this. On the other hand, the thicker more laterally extensive layered peridotite-gabbro and the gabbroic sills where pyroxene cumulates dominate would likely have a tholeiitic affinity.

Tholeiitic volcanics are found only at the base of the Larder Lake Group. Iron-rich and magnesium-rich tholeiitic basalts are however prevalent in the Kinojevis Group north of the Larder Lake Break. It is possible the sills in the map area are related to volcanism which accompanied the formation of the Kinojevis Group. This group conformably overlies the Larder Lake Group northwest of the Otto Stock (Jensen, 1983) but is best preserved north of Kirkland Lake.

The idea is appealing when one reviews the geology of Clifford and Ben Nevis Townships (Jensen, 1975), Melba and Bisley Townships (Jensen, 1972) and Thackeray, Elliot, Tannahill and Dokis Townships (Jensen, 1978b) which lie north of Kirkland Lake. The location of these townships is shown in figure 8-5. There, sills of gabbro capped by an upper quartz gabbro phase are up to 600 meters thick and 3 km in length and are hosted by tholeiitic basalts of the Kinojevis Group. They are not found in the overlying Blake River Group. The lithologies and dimensions of these sills are similar to many in the thesis map area.

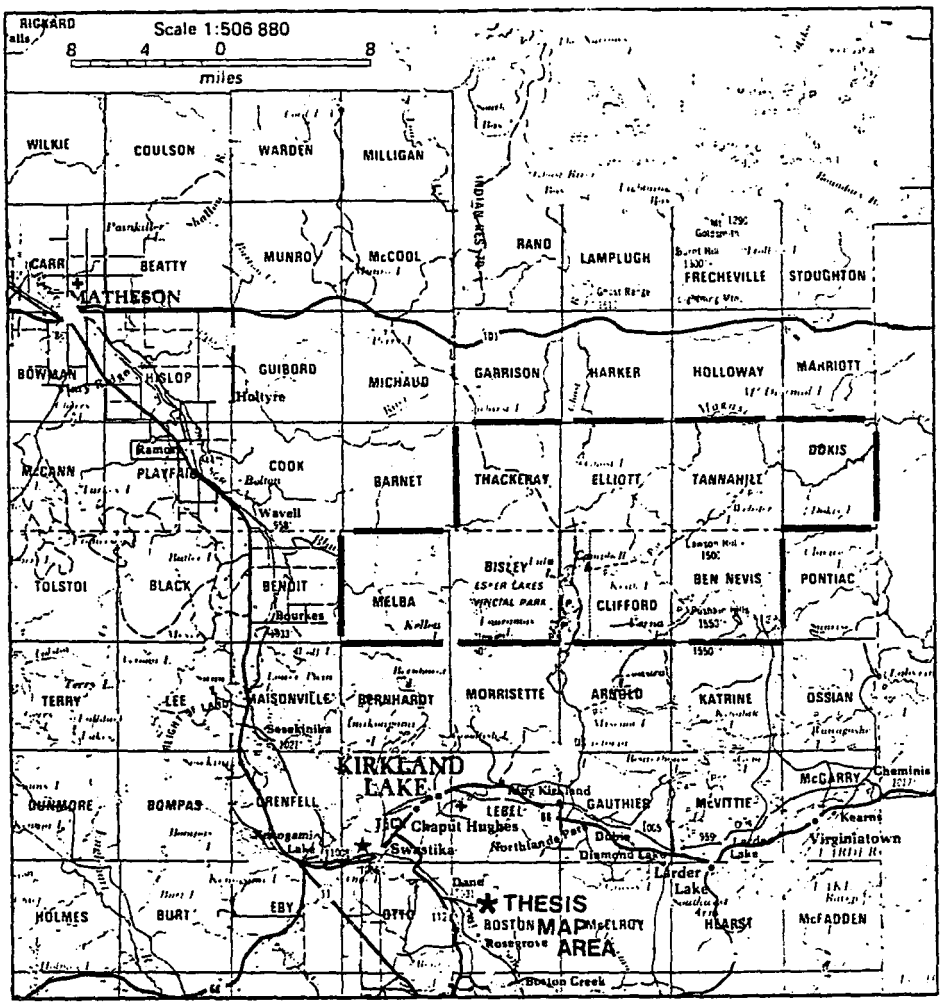

FIGURE 8-5 Townships mapped by Jensen (1972, 1975, 1978b) are outlined by thick dashed lines.

The major element compositions for Kinojevis Group volcanic flows in Jensen's (1978b) study area are compared to concordant gabbros in table 8-3. Jensen (1978b) does not give data for the intrusives. Clearly there is a strong similarity in the major element abundances of samples with similar MgO contents. Higher K_2O contents in the gabbros can be attributed to a late potassic alteration event which did not affect the map areas of Jensen (1978b).

On the basis of TiO_2 contents alone which have significant petrological implications as discussed in section 3-5, the concordant gabbros are more likely to be comagmatic with the tholeiitic volcanics of the Kinojevis Group than with the relatively TiO_2-poor volcanics of the Larder Lake Group.

In appendix A, seven of sixteen concordant gabbro and microgabbro samples have greater than 1.0 % TiO_2. Nine of sixteen samples have greater than or equal to 0.90 % TiO_2. These samples are considered to be fairly representative of the concordant gabbros in the map area. Only five of forty-four komatiitic volcanic samples with less than 12 % MgO have TiO_2 abundances greater than 0.80 %. All of these have less than 0.90 % TiO_2.

Jensen (1975) shows that four of eleven tholeiitic basalt samples from Clifford and Ben Nevis Townships with TiO_2 contents greater than 1.0 % while seven of eleven samples have greater than 0.90 % TiO_2. Jensen (1978b) shows

Table 8-3

Comparison of major element compositions of thesis map area concordant gabbros and Fe-rich tholeiites from the Kinojevis Group.

	TH3	M-729	TH5	M-423	TH8	M-549	TH11	M-112
SiO_2	51.40	49.83	49.22	51.62	51.76	52.58	51.48	53.58
Al_2O_3	14.99	14.85	17.85	17.17	16.52	14.40	15.97	14.75
Fe_2O_3	16.70	15.83	10.73	11.70	10.46	10.25	10.99	10.03
MgO	5.22	5.48	10.07	10.16	9.16	7.97	9.45	8.54
CaO	6.70	7.30	9.26	3.74	9.44	9.03	9.72	7.93
Na_2O	2.41	3.53	1.48	4.47	1.75	3.86	1.37	3.02
K_2O	0.43	1.33	0.65	0.10	0.18	0.77	0.14	1.31
TiO_2	2.14	1.29	0.75	0.73	0.73	0.75	0.89	0.69
MnO	0.00	0.30	0.00	0.21	0.00	0.33	0.00	0.19
P_2O_5	0.00	0.11	0.00	0.09	0.00	0.05	0.00	0.13
Total	99.99	99.90	100.01	99.99	100.00	99.99	100.01	100.17

N.B.: Thesis area intrusives are those with M before the sample number. Samples with TH are from Jensen (1978b). Jensen uses the Jensen Cation Plot to classify the volcanic rocks.

Table 8-3 (continued)

Comparison of major element compositions of some thesis map area concordant gabbros and iron-rich tholeiites from the Kinojevis Group.

	TH15	M-325	TH21	M-732	TH25	M-114
SiO_2	50.19	51.62	55.81	57.14	50.68	50.95
Al_2O_3	12.82	13.32	14.43	15.10	16.62	17.48
Fe_2O_3	15.73	15.04	9.84	8.07	11.56	9.10
MgO	6.32	6.16	6.64	6.65	9.64	9.03
CaO	7.26	8.84	7.57	8.35	8.36	4.35
Na_2O	4.70	2.40	3.53	2.25	2.17	6.79
K_2O	0.65	0.86	0.83	1.50	0.14	1.32
TiO_2	2.33	1.36	1.35	0.72	0.84	0.69
MnO	0.00	0.13	0.00	0.07	0.00	0.16
P_2O_5	0.00	0.26	0.00	0.15	0.00	0.13
Total	100.00	99.99	100.00	100.00	100.01	100.00

N.B.: Thesis area intrusives are those with M before the sample number. Samples with TH are from Jensen (1978b). Jensen uses the Jensen Cation Plot to classify the volcanic rocks.

twenty-eight of thirty-five tholeiitic basalt samples with greater than 1.0 % TiO_2 and twenty-five of thirty-five samples with greater than 0.98 % TiO_2 in Thackeray, Elliot, Tannahill and Dokis Townships.

The peridotite-gabbro and gabbroic sills in the map area may have been intruded into an evolving volcanic succession so that their extrusive associates (if any) were likely lateral equivalents to the Kinojevis Group. These volcanics which conceivably had once overlain the Larder Lake Group in the thesis map area have since been eroded. This is compatible with the observation that where tholeiitic volcanics are absent, (south and southeast of Kirkland Lake) metamorphic grades are higher, reflecting greater depths of burial.

8-9 Genesis of the Peridotite-Gabbro and Gabbro Sills

Goodwin and Smith (1980) note that tholeiitic volcanic assemblages in the Kinojevis Group display chemical trends and patterns closely comparable to those of the modern oceanic basalt-plagiogranite series. By analogy, they attribute the origin of the Archean tholeiites to crystal fractionation from a mantle derived basaltic magma.

Through R.E.E. geochemistry, Capdevila et al. (1982) conclude that equal numbers of tholeiitic lavas are derived from highly depleted and slightly depleted mantle sources. R.E.E. patterns a and d in figure 8-6 are derived from

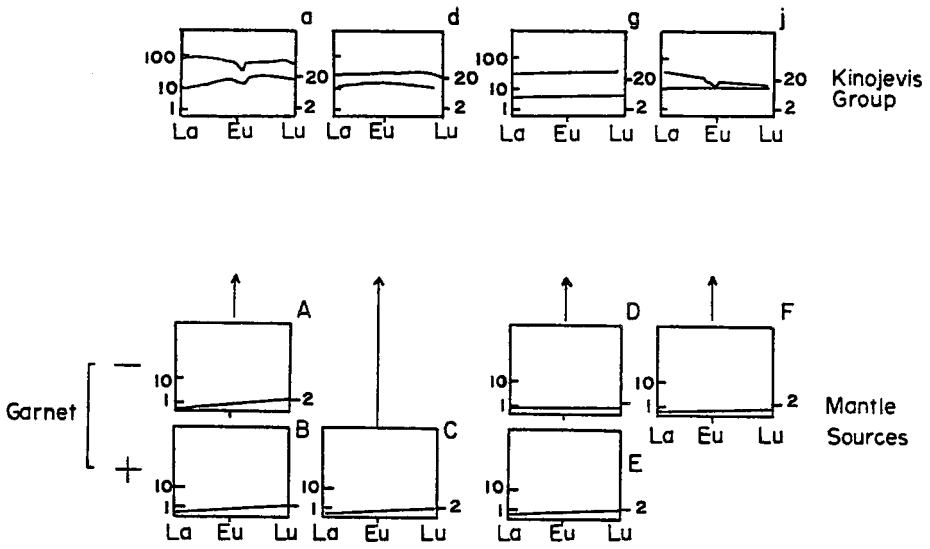

FIGURE 8-6 Chondrite-normalized R.E.E. patterns of Kinojevis Group basalts and inferred patterns of their source rocks after Capdevila et al. (1982). Garnet (+) or (-) indicates stability or instability of garnet in source area respectively and not necessarily presence or absence of garnet in residue of partial melting. Two lines envelope a number of Kinojevis Group samples with similar R.E.E. patterns. The R.E.E. patterns are not quantitive for mantle sources.

A,B,C, highly depleted mantle sources while g and j are derived from D,E,F slightly depleted mantle sources.

A mantle derived origin is reasonably attributed to the peridotite-gabbro and gabbro sills in the map area, bearing in mind the sills can be regarded as subvolcanic intrusions to the Kinojevis Group.

8-10 Cumulate Processes in the Sills

The observed layering in some of the sills in the map area points to an origin by fractional crystallization with crystal settling and accumulation. The basal peridotite zone can be attributed largely to the accumulation of olivine, the first solid phase on the liquidus, while the overlying pyroxenite zone largely reflects pyroxene accumulation. The gabbroic zone is a result of both clinopyroxene and plagioclase accumulation. Gabbros lower in the stratigraphically lowermost sill on the south limb of the Lebel Syncline contain more pyroxene than gabbros higher in the sill. The greater abundances of plagioclase in the upper cumulate portion may be due to settling of clinopyroxene and the upward flotation of plagioclase. Campbell *et al*. (1978) note that plagioclase has a tendency to float in basaltic liquids. The fine grained microgabbro phase is likely a quickly cooled marginal zone, an inference which is consistent with the absence of cumulate textures in thin sections of

microgabbro.

Most concordant gabbros plot in either the iron-rich tholeiitic basalt or magnesium-rich tholeiitic basalt fields on the Jensen Cation Plot. In the stratigraphically lowest sill on the south limb of the Lebel Syncline, this difference is a function of stratigraphic height with the magnesium-rich samples underlying the iron-rich samples. This feature may be applicable to the other gabbroic sills and may be caused by the late crystallization of magnetite in residual liquid in the uppermost portions of the sills.

Sills composed only of the gabbroic phase are more common higher in the stratigraphy on both limbs of the Lebel Syncline. If the stratigraphically highest sills were the last to be emplaced, then the absence of peridotitic phases there may reflect pre-intrusion fractional crystallization of olivine in the feeder system. Such a mechanism is proposed by Bedard et al. (1984) to explain similar lithologies in similar stratigraphic relations in the Cape Smith Fold Belt in Ungava, Quebec.

8-11 The Relationship Between the South Pit, Power Line and Contact Gabbros and the Blake River Group

The discordant gabbroic intrusions in the map area resemble gabbroic and quartz gabbroic stocks north of Kirkland Lake which were outlined by Jensen (1972, 1975 and 1978b). Jensen describes these stocks as massive, medium

grained, circular in shape, 900 to 1200 meters in diameter and locally containing country rock xenoliths. This description certainly fits that of the smaller South Pit Gabbro and is in part consistent with the other gabbroic intrusions in the thesis map area.

Jensen (1978b) describes the gabbros in the stocks as having an ophitic texture, with 40 to 50 % augite, 30 to 40 % plagioclase and 5 % magnetite and up to 2 % quartz and notes that where augite is totally replaced by uralite, chlorite and epidote, the original texture is lost. The mineral abundances in these gabbros and those in the map area are approximately the same. The original igneous texture of the thesis area gabbros may have been obliterated by metamorphism in a manner described by Jensen (1978b).

In table 8-4 , the average major element abundances of the discordant gabbros are compared to analyses for gabbro stocks from Jensen (1978b). It is seen that, except for TiO_2 abundances, the major element abundances are very similar.

The gabbro and quartz gabbro stocks north of Kirkland Lake are found in the Kinojevis and Blake River Groups and not in the Timiskaming Group. Jensen (1978b) notes that these stocks are cut by fine-grained dykes of andesite, dacite and rhyolite composition which are subvolcanic to the Blake River Group volcanics and that the stocks have similar chemistry to calc-alkalic volcanics

Table 8-4

Comparison of average composition of the discordant gabbros with three analyses taken from Jensen (1978b).

	Average of six discordant gabbros	TA20	E25	TA19
SiO_2	51.41	51.14	56.23	51.53
Al_2O_3	15.87	18.32	16.71	16.44
Fe_2O_3	9.22	7.76	7.02	9.23
MgO	8.45	8.68	7.67	10.64
CaO	10.58	10.80	7.41	9.19
Na_2O	2.53	2.01	2.56	1.42
K_2O	1.24	0.42	1.39	0.75
TiO_2	0.44	0.69	0.78	0.63
MnO	0.23	0.13	0.14	0.15
P_2O_5	0.06	0.04	0.95	0.03
Total	100.00	99.99	100.86	100.01

which host some of them. On this basis, Jensen (1978b) proposed that these gabbro and quartz gabbro stocks may represent feeders to the calc-alkalic volcanism (Blake River Group).

The similarities in lithology, form, mineralogy and major element abundances (except TiO_2) between the South Pit, Power Line and Contact Gabbros and the stocks described by Jensen (1978b) leads one to suspect that the two groups of intrusions are related to each other and to one event in the development of the Abitibi pile; namely, late calc-alkalic volcanism. The South Pit, Power Line and Contact Gabbros may have been part of a subvolcanic feeder system to calc-alkalic volcanism or perhaps were simply subvolcanic intrusions emplaced during calc-alkalic volcanism. The discordant nature of the South Pit Gabbro through the south limb succession is consistent with a feeder system affinity. Moreover if this intrusion was part of a feeder system, then it seems likely that lateral equivalents to the Blake River Group had once stratigraphically overlain tholeiitic volcanics (lateral equivalents to the Kinojevis Group and marked in the map area by the sills) which in turn had overlain the Larder Lake Group in the map area.

The discordant gabbros cannot be considered as comagmatic with komatiitic volcanics in the map area. The discordant gabbros appear to post-date the concordant gabbros which are considered comagmatic with the Kinojevis

Group and thus post-date komatiitic volcanism. Moreover, the discordant gabbros cross-cut and thus post-date all komatiitic volcanics now preserved on the south limb of the Lebel Syncline.

Based on R.E.E. geochemistry, Capdevila et al. (1982) recognize two types of calc-alkalic volcanics in the Blake River Group. Figure 8-7 outlines the characteristics of each and Capdevila et al.'s (1982) interpretations of them.

The low TiO_2 abundances in the discordant gabbros are consistent with the undepleted mantle source indicated by Capdevila et al. (1982). The low TiO_2 abundances can be explained by derivation of magma from a strongly depleted mantle source.

8-12 Alkali-rich Dykes and the Lebel Stock

Field relations indicate that the alkali-rich dykes post-date the sills and the discordant gabbro plugs. These dykes also post-date the greenschist metamorphic event as they do not contain greenschist metamorphic mineralogy and the alteration accompanying them replaces greenschist metamorphic assemblages in the rocks they intrude.

In Teck Township which borders the northwest corner

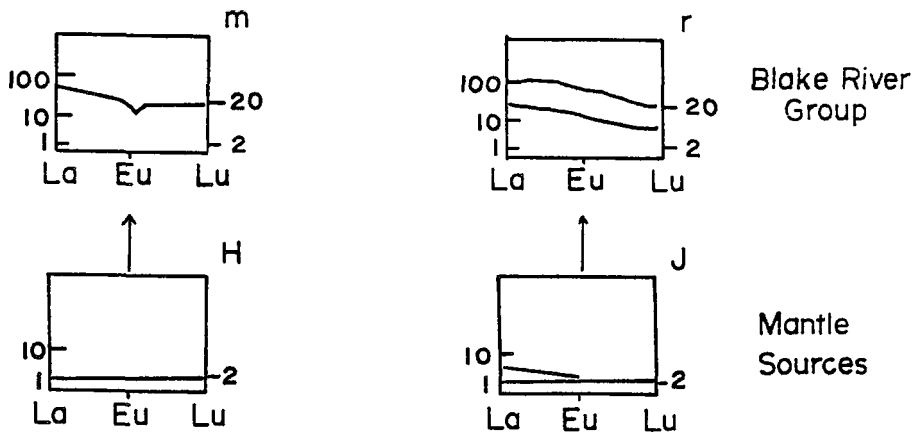

FIGURE 8-7 Chondrite-normalized R.E.E. patterns of Blake River Group basalts and inferred patterns of their source rocks after Capdevila et al. (1982). One calc-alkalic type is characterized by regularly fractionated, moderately enriched R.E.E. patterns (La_{IV}/Yb_{IV}=3 to 6), without Eu anomolies and with very moderate enrichment factors. This is represented by (r) and is derived by melting of undepleted or enriched mantle source with minor amounts of garnet in the residue (J). The other type represented by (m) is slightly enriched in light R.E.E. (La_{IV}/Sm_{IV}=1.2 to 25), flat or slightly depleted in heavy R.E.E., and often with a negative Eu anomaly and moderate enrichment factor. This is derived from melting of an undepleted mantle source with the presence of clinopyroxene but absence of garnet in the residue H.

of Boston Township, Thompson (1948) described three major types of alkali-rich intrusions hosted by the Timiskaming Group.

(1) Syenite which occurs as stocks, as irregular pipe-like bodies, and as dykes

(2) augite syenite or basic syenite which is found in close spatial association to syenite. It has sharp or gradational contacts with the syenite (Ploeger, 1980)

(3) Syenite-porphyry which are the latest dykes and cut the other two types.

Thompson (1948) also observed that lamprophyre dykes are later than the basic syenites.

Cooke and Moorhouse (1966) suggest that the mafic syenite (augite syenite) and the syenites were contemporaneous with Timiskaming volcanism, and that mineralogical and chemical similarities between syenite and leucitic lavas and mafic syenite and mafic trachytes points to common origins for each of the two pairs. They further emphasize that their chemical data suggest that the porphyry intrusions had a contrasting genesis with earlier non-porphyritic intrusions, and that structural evidence points to emplacement of the porphyry intrusions following the trachytic volcanism. Jensen (1977) observed that in the Larder Lake Group where syenite is in contact with komatiites and high MgO komatiitic basalts, mafic nepheline syenite develops. He sited the east margin of the Otto

Stock as an example.

Bearing these observations and interpretations in mind, the Lebel Stock can be regarded as a subvolcanic magma chamber, possibly feeding trachytic flows. Syenite dykes in the map area which mineralogically resemble the Lebel Stock may have emanated from it, although there is no field observations which substantiate this. The Lebel Stock is not bordered by mafic syenite possibly because the stock is in contact with the discordant gabbro which is more intermediate in composition than komatiite and high MgO komatiitic basalts. The biotite lamprophyre dykes which are later than the syenite dykes may have originated by mixing of mafic-ultramafic and felsic components following Jensen's (1977) suggestion for the origin of the mafic nepheline syenite. This mixing would not have occurred at the erosional level now exposed.

Feldspar porphyries or syenite porphyries (Thompson, 1948) are the latest alkali-rich intrusion in the map area and in the Timiskaming Group in Teck Township. In the immediate vicinity of Kirkland Lake, Ploeger (1980) observes numerous porphyry dykes and irregular bodies emanating from a central plug of syenite porphyry. Thompson (1948) infers that more than one of these plugs are present in Teck Township. Bearing this in mind, it is likely that the porphyry dykes in the thesis area emanated from one such plug, although not necessarily one now exposed in Teck

Township. The porphyry dykes did not likely emanate from the Lebel Stock.

8-13 Petrogenesis of Alkalic Rocks

Alkalic rocks are rare in the Superior Province with only four known examples:

(1) mafic trachytes, leucite flows and alkalic intrusives at Kirkland Lake (Cooke and Moorhouse, 1966)

(2) lamprophyres, syenodiorites and syenites in northeastern Minnesota (Arth and Hanson, 1975)

(3) alkalic intrusives and extrusives at Bijou Point, Ontario (Smith and Longstaffe, 1974)

(4) alkalic extrusive rocks of the Knee Lake-Oxford Lake greenstone belt, Manitoba (Hubregtse, 1976).

Brooks et al. (1982) defined the alkalic extrusive rocks of the Oxford Lake Group in the Knee Lake-Oxford Lake greenstone belt as a shoshonite to high-K andesite-dacite-rhyolite series. This series unconformably overlies tholeiitic volcanics of the Hayes River Group. Brooks et al. (1982) used trace element abundances and R.E.E. profiles to construct a three-fold model for the petrogenesis of the Oxford Lake Group as follows:

(1) Volatiles rich in L.I.L. elements modify a mantle or mafic crustal source region

(2) Partial melting of this source region leads to the formation of a parental liquid and shoshonite character.

(3) More evolved rock compositions are derived from this liquid principally by amphibole fractionation.

Brooks et al. (1982) suggest that a similar model can be applied to the Kirkland Lake alkalic volcanic rocks. As such, this model could account for the petrogenesis of the Lebel Stock, the syenite dykes and possibly the feldspar porphyry dykes.

8-14 The Relationship between the Diabase Dykes and Major Dyke Swarms in the Timmins-Kirkland Lake area

The two diabase dykes discussed in section 7-6 can be related to one of two major swarms of diabase dykes in the Timmins-Kirkland Lake area. The oldest swarm consists of north-trending "Matachewan type" diabase dykes which are centered near the town of Matachewan 30 km west of Kirkland Lake. These dykes intrude all Archean rocks and are overlain by the Proterozoic Gowganda Formation. They have been dated at 2,690±93 Ma by the Rb-Sr whole-rock isochron method (Gates and Hurley, 1973). Younger Nipissing dykes trend north to northeast and cut Proterozoic rocks south of the Abitibi Belt. Two dykes from this swarm have been dated (K-Ar) by Leech (1965) in the Timmins area at 1,930 Ma and 1,220 Ma.

Pyke (1978) suggests that only age dating might discriminate between north-trending diabase dykes. However, in the map area it is fortunate that both dykes have northeast trends which alone suggests that they are part of

the younger Nipissing swarm and are Proterozoic in age.

8-15 Summary

(1) Ultramafic liquids which are parent to the komatiites are derived from high degrees of partial melting of the mantle.

(2) High MgO komatiitic basalts are derived from an ultramafic liquid by fractional crystallization of olivine and chromite. Cr and Ni-rich low MgO komatiitic basalts and andesites may be a product of rapid cooling in a magma chamber which reduces or stops the precipitation of olivine and chromite. High Al_2O_3 volcanics may also be products of rapid cooling in a magma chamber. Rapid cooling lowers the temperature of feldspar crystallization.

(3) High Fe_2O_3, Al_2O_3 komatiitic basalt may have been derived from a liquid with the composition of a high Al_2O_3 komatiitic basalt.

(4) Evidence of rapid cooling in intrusive rocks is in textures found in the Bird River Sill.

(5) Sequence 1 basalts may have been parented by a magnesium-rich (MgO 12-18 %) mantle derived liquid.

(6) Peridotite sills were likely intruded during komatiitic volcanism and formation of the Larder Lake Group. The layered peridotite-gabbro and gabbroic sills were likely intruded during tholeiitic

volcanism and development of the Kinojevis Group.

(7) The peridotite-gabbro and gabbro sills are probably mantle derived, as is the Kinojevis Group.

(8) The observed layering in the sills points to an origin by fractional crystallization with crystal settling and accumulation.

(9) The map area discordant gabbros resemble gabbros which are likely comagmatic with the calc-alkalic volcanism preserved in the Blake River Group.

(10) Syenitic dykes may have emanated from the Lebel Stock. Lamprophyre dykes may have been produced by mixing of syenitic and ultramafic liquids. The feldspar porphyry dykes likely emanated from feldspar porphyry plugs.

Chapter 9

Paleogeography, Volcanism, Metamorphism, Alteration, Structural History and Geotectonic Models

9-1 Paleogeography

In the Abitibi Belt, komatiitic and tholeiitic volcanism is typically associated with a plain like topography (Dimroth et al., 1982). Komatiitic flows in sequence 5 which can be traced from the northwest trending power line to the northeast end of the Peria Pit a distance of approximately 5 km, are consistent with this.

An ultramafic sill found low in what is most likely sequence 2 is traceable laterally for 30 km southeast of the thesis map area (figure 9-1). Through this interval, it occupies a consistent level above the Skead/Larder Lake contact, suggesting a constant thickness for sequence 1 and the lowermost part of sequence 2. This is also consistent with a plain-like topography.

This plain hosted a submarine fan as discussed in chapter 6. It also flanked a topographic high(s) to the east or northeast as indicated respectively by the presence of sedimentary debris flow deposits and paleocurrents.

9-2 Volcanic Environment

The observed section of the Larder Lake Group in the

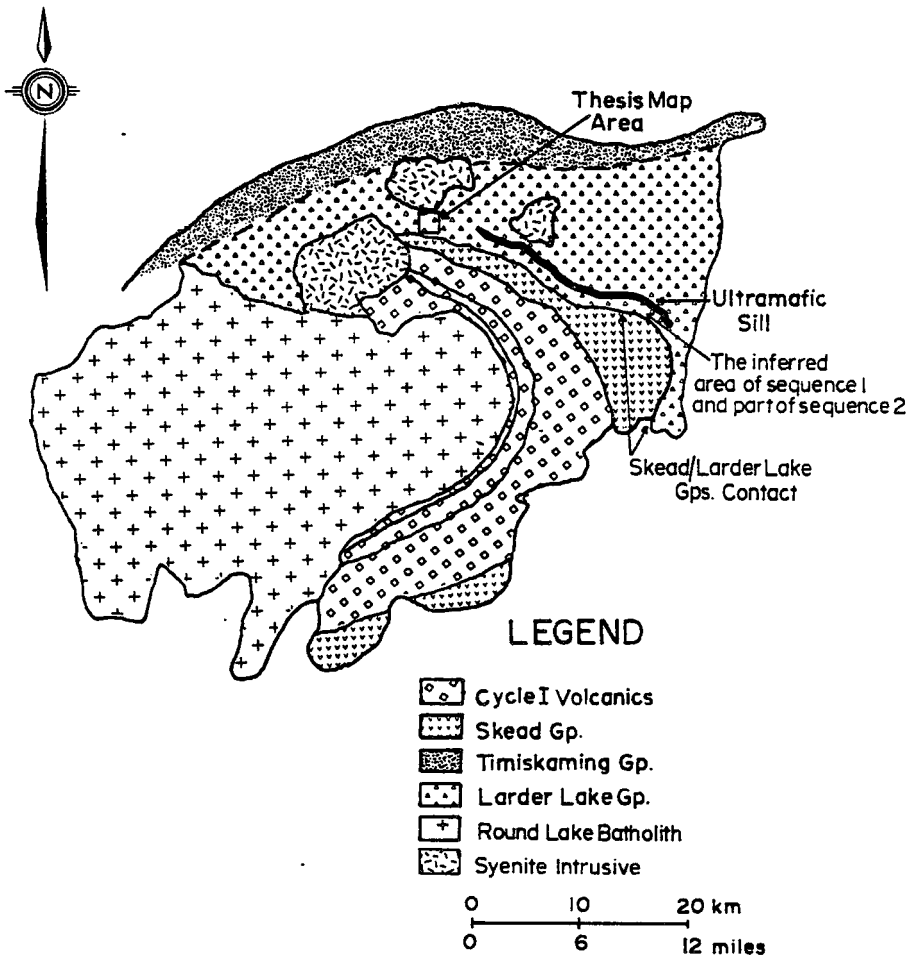

FIGURE 9-1 Generalized geology of the Abitibi greenstone belt south of Kirkland Lake from Jensen (1980) showing the thick peridotite sill in the Larder Lake Group and its apparent conformability with the Larder Lake/Skead Group contact. The thickness of the sill is exaggerated here.

thesis map area may reflect a volcanic environment distal to vents or fissure sites and to the magma chambers which lay beneath them. The absence of cross-cutting peridotite, amygdaloidal units and thick agglomerate zones and the scarcity of ultramafic tuffs is consistent with this interpretation. Williams (1979) associates these four features with a vent environment.

The probability that pillowed low MgO and high Al_2O_3 basalt and andesites flows are more abundant than massive low MgO and high Al_2O_3 komatiitic basalt and andesite flows further attests to a distal volcanic environment. Dimroth (1982) notes that massive basaltic submarine flows are usually proximal to the site of eruption while the opposite is true for pillowed flows.

9-3 Nature of the Magma Chambers

Separate new magma chambers may have existed for each of the seven komatiitic volcanic sequences on the south limb of the Lebel Syncline, each having formed with the periodic injection of primitive ultramafic liquids into the crust. This statement is based on Nesbitt and Chinner (1981) who interpret the interlayering of komatiites and basalts (komatiitic) at Ruth Well in western Australia as a function of the transient nature of the magma chambers.

They point out that new batches of high magnesium liquid entering a semi-permanent pre-existing magma chamber

would be trapped, as happens at fast-spreading mid-ocean ridges. New batches of liquid would enter from below. Being denser than the more evolved liquid (basaltic?) remaining in the chamber, a density stratification would develop with the denser high-magnesium liquid remaining below the less dense, more evolved basaltic liquid. The two liquids would convect but as separate magmas without mixing. Mixing would not occur until the lower liquid had cooled sufficiently and in so doing, becoming more like the evolved upper liquid. Prior to this mixing, only evolved liquid from the upper portion of the chamber would likely be tapped and erupted at the crust/seawater interface. Nesbitt and Chinner (1981) conclude that primitive liquids would not gain access to the surface and komatiites would be absent from all volcanic sequences overlying the first one.

High rates of cooling in a magma chamber has been suggested in chapter 8 as a mechanism to produce high Al_2O_3 komatiitic volcanics and low MgO komatiitic andesites. High cooling rates can be explained by injecting the primitive liquids into high levels of the crust, levels higher than those normally reached by primitive liquids in other Archean terranes. Primitive liquids could gain access to such higher crustal levels if the crust was rendered permeable by extensive pre and synvolcanic faulting and or fracturing.

There is no evidence for subvolcanic magma chambers in the 5.4 km of exposed crust (cycle I volcanics) below the

Larder Lake Group nor is there evidence for extensive faulting there. The contacts of the three cycle I groups are not disturbed by faulting, being conformable to the later Round Lake Batholith. This is consistent with interpretations made in section 9-2.

Synvolcanic faulting distal to the observed section may be recorded by abundant angular clasts of Larder Lake Group lithologies in sedimentary debris flows.

Sequences 6, 7 and 8 which are observed west of the mine site contain low MgO komatiitic andesites. On the mine site, high Al_2O_3 komatiitic basalts and andesites occupy the same stratigraphic position. This feature might be explained by variations in cooling rates between at least two separate high level magma chambers which existed simultaneously during formation of sequences 6, 7 and 8. High Al_2O_3 komatiitic volcanics were erupted from one, while low Al_2O_3, high Cr and Ni komatiitic volcanics were erupted from the other. In this model each chamber developed simultaneously with the injection of primitive ultramafic liquid.

9-4 Metamorphism of the Larder Lake Group

Jolly (1974) and Dimroth *et al*. (1982) established metamorphic facies patterns for the Abitibi greenstone belt. Their work is summarized in figure 9-2. It is clear from this figure that low grade metamorphic assemblages are

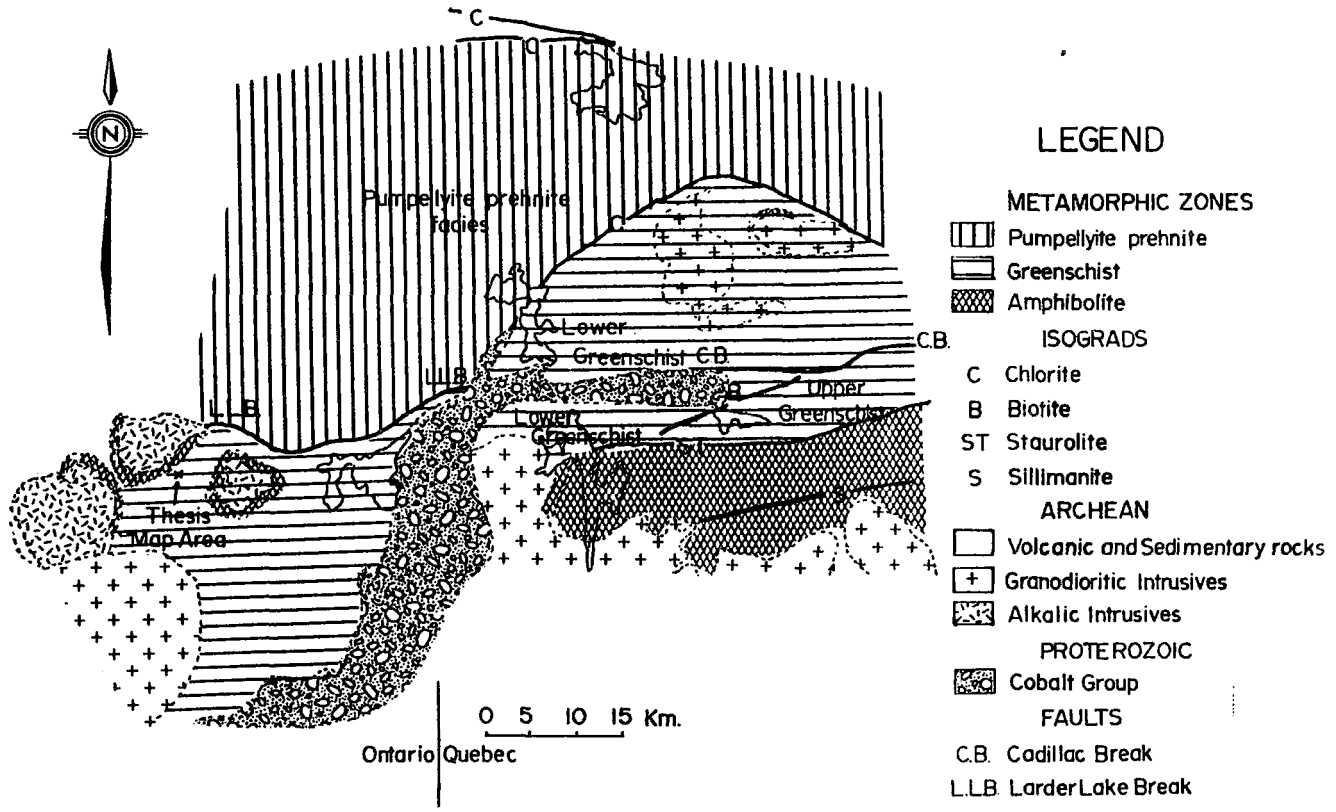

FIGURE 9-2 Metamorphic facies of the Abitibi Belt as modified from Jolly (1974) for Ontario and Dimroth (1983b) for Quebec.

pervasive north of the Larder Lake Break while higher grade assemblages are pervasive south of the Break.

Jolly (1974, 1978, 1980) attributed the widespread greenschist mineralogy south of the Break in Ontario to a contact effect about the Round Lake Batholith and the large alkalic stocks. Jolly believes that prehnite-pumpellyite assemblages developed during burial metamorphism and were converted to albite-epidote-actinolite assemblages and hornblende-almandine assemblages during contact metamorphism.

It is more likely however, that development of the greenschist facies is a regional event unrelated to the intrusions noted above. There are four lines of evidence which supports this line of reasoning.

1) The greenschist facies is regional in extent within the Larder Lake Group and in the underlying cycle I volcanics. Contact metamorphic effects are not regional, given the size of the alkalic stocks.
2) The greenschist facies extends eastward below the Proterozoic Cobalt Group into the Bellecombe gneiss belt in Quebec. Pelitic layers there display biotite, hornblende, garnet, staurolite and kyanite zones similar to a Barrovian type sequence (Jolly, 1980). The greenschist facies is thus part of a Barrovian type sequence which is characteristic of regional metamorphism, not local contact metamorphism.

3) The Round Lake Batholith may have been emplaced as a solid diapir (K. Card, personal communication). This interpretation is consistent with the absence of a high temperature contact metamorphic aureole around the batholith. Epidote-chlorite-actinolite mineral assemblages which border the batholith are similar in metamorphic grade to assemblages throughout the Larder Lake Group.
4) Tasillo-Hirt et al. (1982) report that clasts in the Timiskaming conglomerates have retained their pre-depositional magnetic remanence. Greenschist metamorphism would have destroyed this feature. The Timiskaming conglomerates pre-date intrusion of the alkalic stocks and are in general weakly metamorphosed. A regional greenschist metamorphic event did not accompany intrusion of the various alkalic stocks in the Timiskaming Group.

Hornblende-diopside-anthophyllite mineral assemblages which are observed adjacent to the Otto Stock (Jolly, 1974) can be attributed to a contact metamorphic event.

9-5 Metamorphism in the Thesis Map Area

Greenschist metamorphic mineral assemblages in the thesis map area can be attributed to a regional metamorphic event which has been shown to effect the entire Larder Lake Group prior to intrusion of the Lebel Stock. Hornblende

hornfels facies as recognized at Far Lake can be attributed to contact metamorphism immediately following intrusion of the Lebel Stock.

There is no evidence from this study to suggest unequivocally that garnet was formed during contact metamorphism. The fact that 1) garnet occurs within 1.5 km of the Lebel Stock and that (2) garnet is reported from the borders of three other alkalic stocks (Jolly, 1974) are consistent with its being a result of contact metamorphism. However, it is possible that deeper levels of regionally metamorphosed crust containing garnet were uplifted during emplacement of the Lebel Stock.

Garnets in low MgO and high Al_2O_3 komatiitic basalts and andesites are visible in hand specimen. They are fine grained, pale red and comprise 0.5 to 1 % of a specimen. Volcanic lithologies containing garnet were not studied petrographically or by electron microprobe. However, the garnets are likely almandine. Turner (1968) notes that garnet in amphibolite is almandine.

Garnets observed in siltstones and argillites were visible only petrographically. Garnet is in contact with quartz and albite here.

Within the 1.5 km wide garnet-bearing zone

1) garnet distribution is patchy
2) biotite rather than sericite is the most common mica in very fine grained quartz-rich sediments

3) actinolite occurs in low MgO komatiitic basalts (example M-298, map 1)
4) greenish-brown hornblende (example M-333, map 1) occurs in sandstones.

The presence of hornblende marks the hornblende hornfels facies. The distribution of hornblende in the thesis map area has not been studied in detail. This makes it difficult to place a southern boundary on the hornblende hornfels facies.

The lower temperature limit of the greenschist facies can be defined by the disappearance of pumpellyite and the appearance of actinolite. Figure 9-3 shows this position in P-T space for the reaction 4 pumpellyite + 2 chlorite + 47 quartz = 11 actinolite + 71 epidote + 109 H_2O from Winkler (1979). For low pressures, temperatures near 330°C can be expected. The Abitibi Belt is considered to have been metamorphosed at pressures less than 3 to 4 kbars according to Jolly (1983).

The lower temperature limit of the hornblende hornfels facies can be estimated from figure 9-4. At 1 Kb. pressure actinolite converts to hornblende near 390°C. At 3 Kb. pressure, this conversion occurs at 420°C.

Almandine can form under greenschist facies conditions (Turner, 1981). This is seen in the southern part of the garnet zone where hornblende is absent. This hornblende-free garnet zone may characterize the albite-

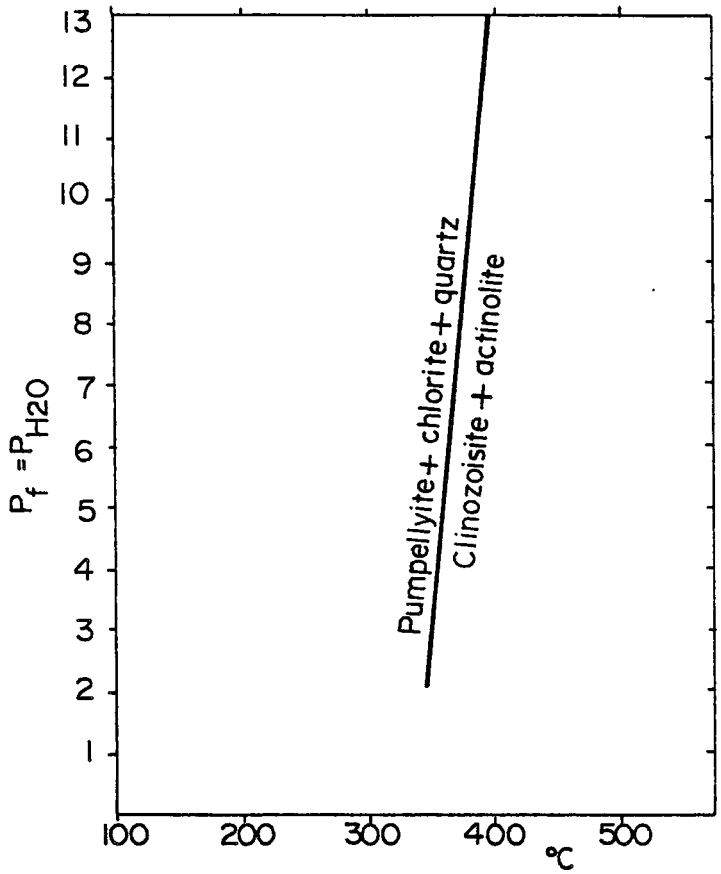

FIGURE 9-3 The reaction involving pumpellyite, chlorite, quartz, clinozoisite and actinolite in P-T space from Winkler (1979).

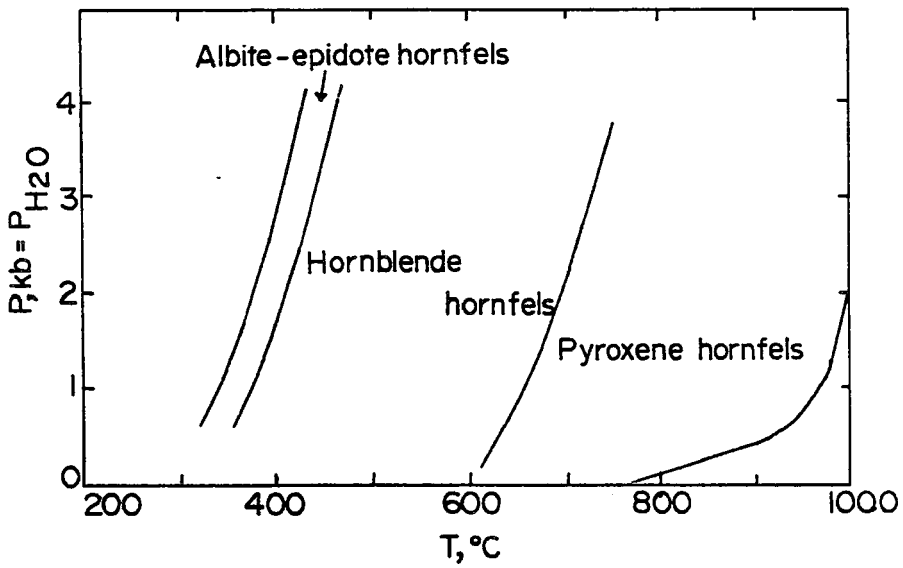

FIGURE 9-4 Temperature-pressure fields of facies of contact metamorphism from Turner (1981).

epidote facies if garnet is the result of contact metamorphism.

Jolly (1980) reports the following three assemblages in order of increasing metamorphic grade from basaltic rock surrounding the syenitic Otto Stock.

1) hornblende-plagioclase-epidote-chlorite.
2) hornblende-plagioclase-epidote-diopside.
3) hornblende-plagioclase-epidote-diopside-cummingtonite.

Hornblende-plagioclase assemblages in recrystallized discordant gabbro at Far Lake are comparable to assemblage 1. Assemblages 2 and 3 which mark the pyroxene hornfels facies were not observed in the thesis map area. However, it is likely that the hornblende hornfels facies gives way to the pyroxene hornfels facies (near the Lebel Stock) and that assemblages 2 and 3 are characteristic of it. Pyroxene hornfels assemblages mark temperatures in excess of 650°C (figure 9-4).

9-6 Potassic Alteration

It was noted in section 4-11 that:

1) biotite replaces greenschist metamorphic assemblages in komatiitic basalts and that
2) this explains their high K_2O abundances when compared to komatiitic basalts from other terranes.

In the thesis map area, this potassic alteration is understandably not restricted to the komatiitic volcanics.

Minor amounts of biotite and sericite are found in concordant and discordant gabbros and in sequence 1 basalts. This is reflected in tables comparing their major element compositions with samples from outside the map area. In six of seven comparisons made in table 8-3, the concordant gabbros have higher K_2O abundances than Kinojevis Group basalts of comparable major element composition. In table 8-4, the average K_2O abundance for discordant gabbros is greater than the two of the three Blake River Group gabbro stocks with comparable major element composition. In table 4-15, sequence 1 tholeiitic basalts have much higher K_2O abundances than the three Kinojevis Group tholeiitic basalts used for comparison.

Ridler (1969, 1970) notes that volcanic rocks enclosing B.I.F. units west, south and east of the Lebel Stock are relatively high in alkalies. These have likely been affected by potassic alteration. Ridler (1969, 1970) had grouped these volcanics with the Timiskaming Group trachytic volcanics on the basis of their high alkali content. Jensen (1978c) subsequently distinguished the Larder Lake Group from the Timiskaming Group on geological grounds.

Feldspars in rhyolitic volcaniclastic sediments at the Adams Mine are zoned (LaTour et al., 1984). An albite core is rimmed by K-feldspar which is in turn rimmed by albite. The development of K-feldspar may also be related

to the potassic alteration event. K-rich orthoclase can replace plagioclase in granitic type rocks as is seen within the potassic alteration zones associated with porphyry copper deposits.

The introduction of biotite and K-feldspar may be linked to the emplacement of K_2O-rich post-greenschist metamorphic syenite, feldspar porphyry and biotite lamprophyre dykes and the Lebel Stock. K-bearing magmatic fluids may have emanated from these late intrusions and interacted with the host rocks in the map area.

This fluid/rock interaction was apparently widespread (most volcanics and intrusives are altered) although generally not intensive (secondary biotite and sericite are minor in abundance). The scatter in the K_2O versus MgO variation diagram (figure 9-5) for komatiitic volcanics reflects variations in fluid/rock interaction during the potassic alteration event. This was likely governed by permeability (fractures in the rock) and possibly also by proximity to alkali-rich dykes.

Epidotization and carbonatization can also be related to intrusion of the dykes. Host lithologies adjacent to the dykes are often either epidotized or carbonatized. This alteration appears to be a function of rock lithology. Komatiites and high MgO komatiitic basalts are carbonatized while low MgO komatiitic andesites and high Al_2O_3 komatiitic volcanics are epidotized.

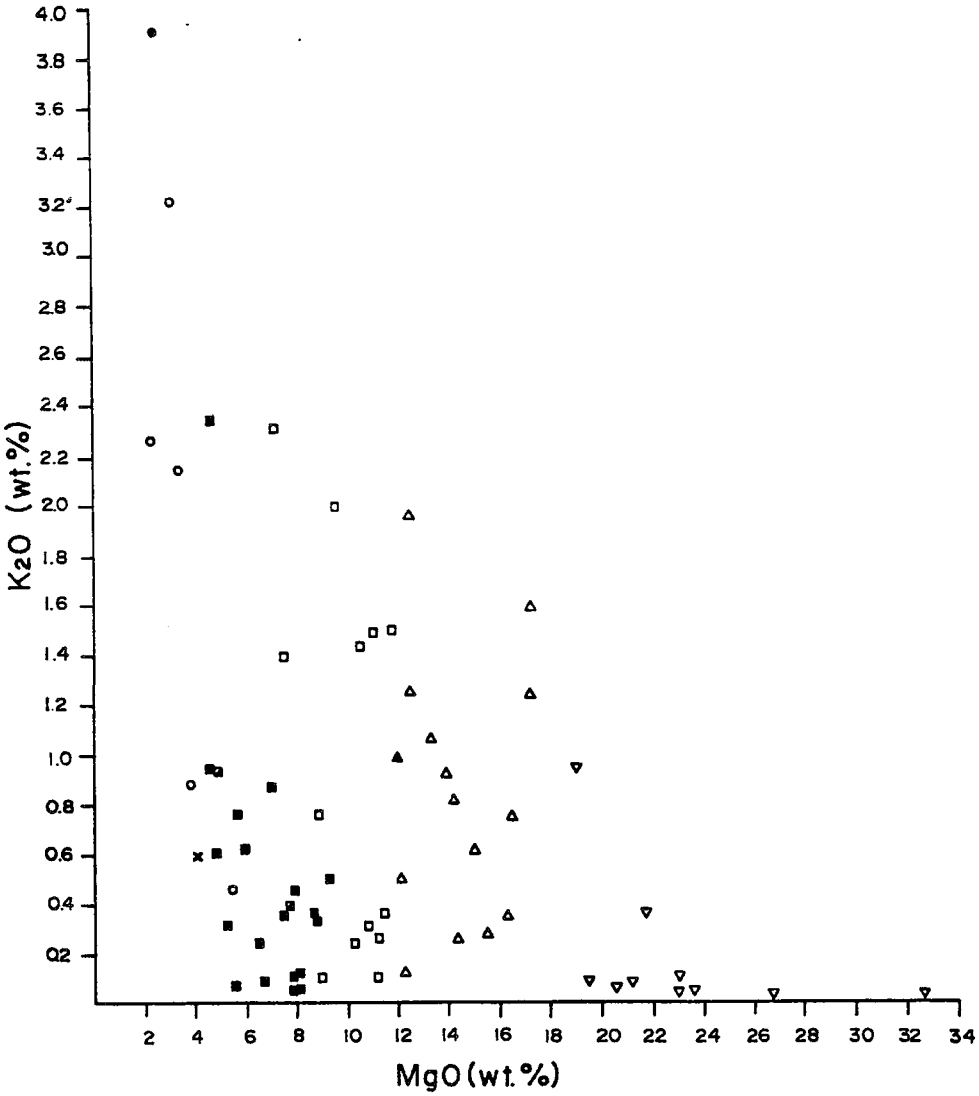

FIGURE 9-5 Variation diagram of K_2O versus MgO for komatiites and komatiitic volcanics

- ▽ Komatiite
- △ High MgO komatiitic basalt
- ▲ High MgO komatiitic andesite
- □ Low MgO komatiitic basalt
- ■ Low MgO komatiitic andesite
- ◪ Low Al_2O_3 komatiitic dacite
- ○ High Al_2O_3 komatiitic basalt and andesite
- ● High Al_2O_3 dacite
- × High Fe_2O_3, Al_2O_3 komatiitic basalt

9-7 Structural History of the Adams Mine Area

The structural history for the Adams Mine area is subdivided into five events which are outlined below.

1) Formation of the Lebel Syncline
2) Development of drag folding (west of the South Pit) and isoclinal folds with north-south trending axial surface traces (best recognized at the South Pit).
3) Mild warping of the Lebel synclinal axis and the strata about the Lebel Stock during its emplacement.
4) Late deformation following cessation of alkali rich dyke intrusions.
5) Movement along the Larder Lake Break. Uplift of the south block with respect to the north block.

Events 1 and 2 are believed to pre-date intrusion of the Lebel Stock. There is no direct evidence to substantiate this but several observations below are consistent with the concept.

1. Syenite dykes which may be contemporaneous with intrusion of the Lebel Stock cut
   a) strata folded by the Lebel Syncline
   b) B.I.F. in the South Pit which is deformed by folds with north-south trending axial surface traces.
2. Syenite dykes are accompanied by epidote-bearing alteration assemblages. Epidote veinlets cut stretched polygonal joints in flows south of Dry Lake near the interpreted fold axis of the Lebel Syncline.

3. The Timiskaming Group truncates older folded structures in the Keewatin (Larder Lake and Kinojevis Groups)(Hewitt, 1963). Since the Lebel Stock may have been a subvolcanic magma to trachytic flows which are part of the Timiskaming Group, then it is possible that there was folding prior to the stock's emplacement.
4. The folding observed in the thesis map area is not unlike that found east of Boston Township and north of Kirkland Lake which is clearly independent of large syenite stocks. In McElroy Township, isoclinal fold axes trend into the McElroy Stock (figure 9-6). The folding apparently shows no relationship to the stock. North of the Larder Lake Break in Jensen's (1978b) map area large syenite stocks are absent and tight isoclinal folds similar to the Lebel Syncline are abundant. These folds are closely spaced with easterly and southerly trending axes (figure 9-6). Easterly trending fold axes are warped, indicating two folding episodes unrelated to the syenite stocks as postulated in the thesis map area. Thinly bedded sedimentary rocks in the Bellecombe gneiss belt have been tightly folded in a manner similar to that in B.I.F. in the South Pit. There are no large, late syenite stocks in this belt.

Drag folding (event 2) post-dates development of the Lebel Syncline (event 1) for the simple reason that the axis of the Lebel Syncline is warped by drag folding west-

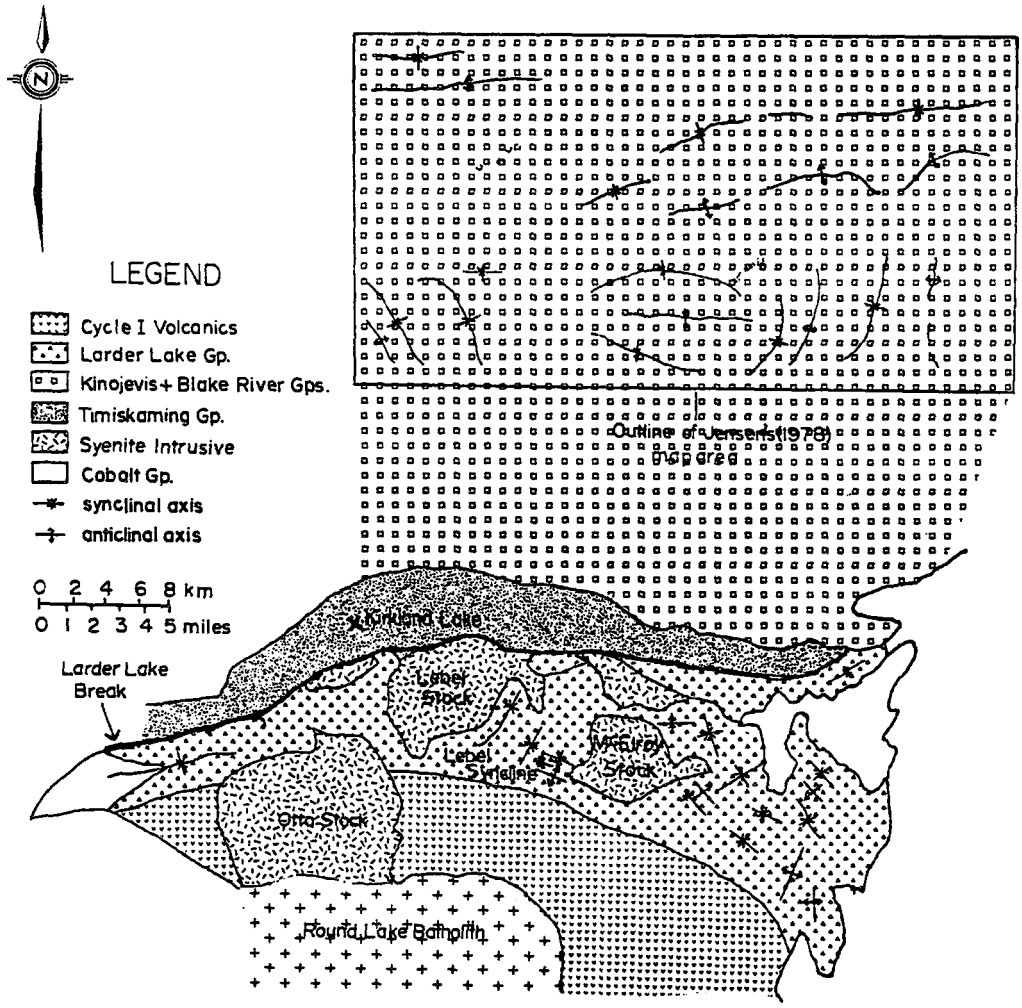

FIGURE 9-6 Location of fold axes in the Kirkland Lake Larder Lake area. Fold axes in the Larder Lake Group are from Thompson (1941). Fold axes in the Kinojevis and Blake River Groups are after Jensen (1978b). The Beaver Lake Syncline axis is from Hewitt (1963).

northwest of the South Pit. The drag folding may be contemporaneous with the tight isoclinal folding recorded in the South Pit. Difference in folding styles might be attributable to the fact that thinly bedded B.I.F. behaved more ductily than the strata containing numerous, relatively thick sills (40 to 50 meters average thickness) west of the South Pit Gabbro.

Deformation during events 1 and 2 may have been synchronous with regional metamorphism. Sericite in fine grained sedimentary samples (M-130 and M-89 near the Adams Mine road, map 1) and within the greenschist facies domain is preferentially orientated parallel to laminations. This sericite is believed to have formed during the greenschist metamorphic event and has clearly been influenced by stress during formation. The same stress may have been responsible for events 1 and 2.

In the Adams Mine area, the strata and the Lebel Syncline fold axis parallel the boundary of the Lebel Stock. This alone suggests that the stock has modified the trend of the fold axis (event 3).

Deformation in the thesis map area following the intrusion of a syenite dyke and thus the Lebel Stock is recognized by a boudinaged syenite dyke shown in plate 9-1 (event 4).

The Timiskaming Group north of the map area has been folded and then cut by the Larder Lake Break. Movement

PLATE 9-1 Boudinaged syenite dyke exposed on the face of a vertical exposure along the railroad tracks southwest of the Adams Mine mill.

along this break marks event 5. The temporal relationship between events 5 and 4 is not known. It is conceivable that they occurred at the same time. The temporal relationship between the folding of the Timiskaming Group and events 3 and 4 is also not known. This folding clearly pre-dates event 5.

Evidence for uplift of a southern block relative to a northern block at the Larder Lake Break is the widespread preservation of greenschist metamorphic assemblages on the south block and lower grade prehnite-pumpellyite assemblages on the north block. The absence of tholeiitic volcanics (Kinojevis Group equivalents) and calc-alkalic volcanics (Blake River Group equivalents) in the thesis map area is consistent with this. Erosion would have been greater on the elevated block relative to the lower block.

9-8 Geotectonic Models

Two basic models have been put forth to explain the origin and development of the Abitibi Belt. One model contends that the two volcano-sedimentary successions (cycles I and II) were initiated at zones of crustal extension and over mantle diapirs (Goodwin and Smith, 1980). The two successions sagged together following the accumulation of critical thicknesses. Goodwin and Smith (1980) use the term sag-duction for this process. A second model by Dimroth *et al.* (1983b) attributes the development

of the belt to processes analogous to those involved in modern (post-Mesozoic) global plate tectonics.

Figure 9-7 is a plate-tectonic model for the evolution of the Abitibi Belt as outlined by Dimroth et al. (1983b). It is briefly described below.

Phase 1: Where the oceanic lithosphere is fractured, subduction of a slab consisting of oceanic crust and mantle starts. This process first creates a mantle flow pattern that is analogous to back-arc convection. Convection induces mantle diapirism resulting in komatiitic and tholeiitic volcanism.

Phases 2 and 3: Magmas derived by partial melting of mantle (mantle plumes) are supplemented by and then replaced by magmas generated by fusion of the subducted slab. An arc develops as central volcanic complexes form above shallow level magma chambers.

Phases 3 and 4: Sediments derived from the arc are subducted with the slab resulting in the formation of greater amounts of calc-alkalic volcanics. With time, the K_2O/Na_2O ratios of these magmas increases.

Phase 5: At the Larder Lake Break, uplift occurs resulting in coarse grained sedimentation. These sediments are accompanied by alkalic volcanism (Timiskaming Group).

Phase 6: The island arc is shortened in a north-south direction with simultaneous addition of granitic magmas to the crust.

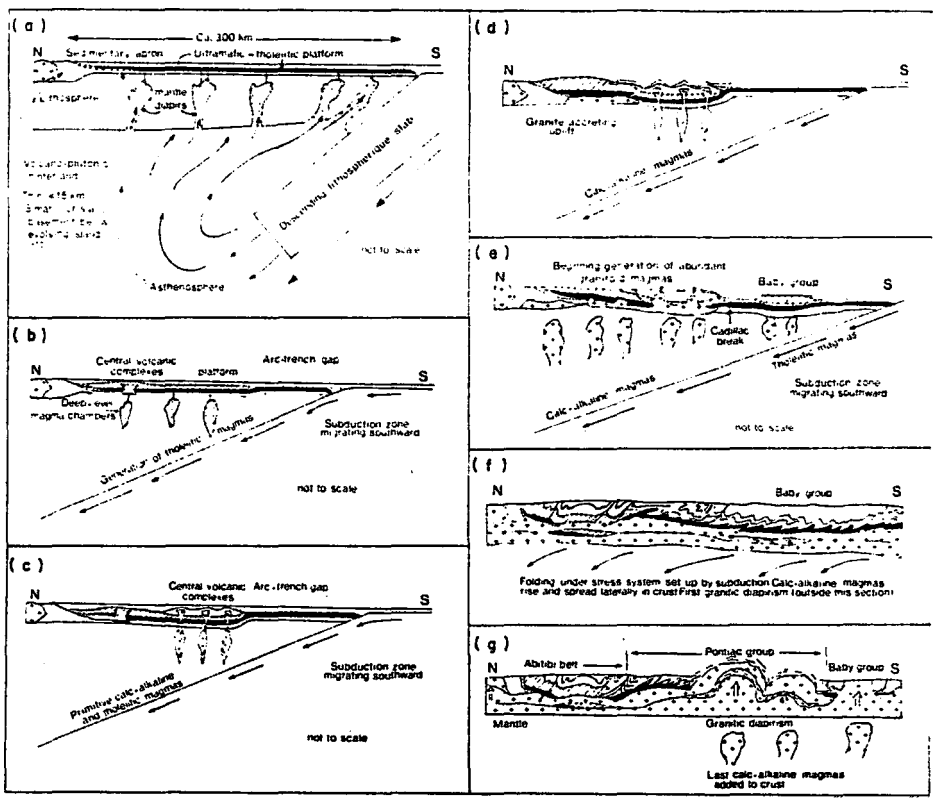

FIGURE 9-7 Model of the evolution of the region after Dimroth (1983b). Keyed to summary as follows: (a) phase 1; (b) phase 2; (c) phase 3; (d) phase 4; (e) phase 5; (f) commencement of orogeny; (g) final uplift and doming of Belle-combe Belt.

There are numerous lines of reasoning which give credibility to this model:

1) The R.E.E. patterns and L.I.L. element abundances of the Abitibi calc-alkalic volcanics and modern island arc andesitic rocks are comparable (Goodwin and Smith, 1980).
2) Potassium-rich volcanics (Timiskaming Group) resemble those found in the Roman Province in Italy (Brooks et al., 1982) which are part of an island arc assemblage.
3) Ophiolite/seawater interaction at mid-ocean ridges and the accompanying ^{18}O exchange between the two reactants is required in order to maintain the ^{18}O of Archean seawater near the observed value of 0±2 per mil (Beaty, 1980).

Beaty suggests that greenstone belts are not typical oceanic crust in the Archean whereas crust resembling Phanerozoic ophiolites was. The absence of this oceanic crust from the Archean geological record is explained by total subduction of such material with no survival through occasional obduction as is typical of Phanerozoic tectonics.

The plate-tectonic model is considered impractical by Goodwin and Smith (1980) who point out that under high thermal gradients which likely prevailed in the Archean (Green, 1975), a rigid lithosphere required for the subduction process would not have existed.

The author's views on this controversy are similar to those of Fyfe (1981) who felt that until good examples of

Archean ophiolite complexes are found, one cannot apply modern-type ocean-floor spreading to the Archean. Archean ophiolite complexes if they existed should have been found considering the abundance of greenstone belts. On this basis, the sag-duction model of Goodwin and Smith (1980) is favoured as an explanation for the origin and development of the Abitibi Belt.

Chapter 10

Conclusions and Recommendations

10-1 Conclusions

1. The Lebel Syncline is the major structural feature in the thesis map area. Its axis roughly follows the outline of the Lebel Stock. Faulting was observed locally and offsets strata only slightly.

2. The south limb of the Lebel Syncline hosts eight volcanic sequences, seven of which are komatiitic. The lowermost sequence is tholeiitic to calc-alkalic. Komatiitic volcanics are those which occur in sequences within which the flow composition changes from ultramafic to mafic or intermediate. Komatiitic volcanics stratigraphically overlie komatiites in one sequence. Komatiitic volcanics are subdivided into nine lithologies based on the abundances of two or more major oxides.

3. The thesis map area Cr and Ni-rich low MgO komatiitic basalts and the high Al_2O_3 and high Fe_2O_3, Al_2O_3 komatiitic volcanics are unique. They are not found in other Archean terranes where komatiites occur. Low

MgO komatiitic andesites which are abundant in the thesis map area are not common in other Archean terranes. Where found, they are volumetrically minor. Cr and Ni-rich komatiitic andesites are also found in Destor Township in Quebec. Komatiitic volcanics which resemble the low Al_2O_3 komatiitic dacites are not found elsewhere.

4. High Al_2O_3 komatiitic basalts and andesites are abundant in map areas NB-1 and NB-2 on the south limb of the Lebel Syncline. West of the mine site, low MgO komatiitic andesites with anomalously high Cr and Ni abundances are abundant.

5. Komatiitic volcanics are derived from ultramafic liquids by fractional crystallization of olivine and pyroxene. The unusual compositions of the komatiitic basalts and andesites is tentatively explained by rapid cooling in a magma chamber.

6. There are sixteen units of sedimentary rocks in the thesis map area. Clastic sedimentary rocks which make up a part of all of these units were deposited from turbidity currents and debris flows close to the slope of a submarine fan.

7. Sedimentary rocks 200 meters south of the South Pit are part of a regional body which is located west of the thesis map area. The McElroy Formation in Ontario and the Pontiac Group in Quebec make up this body.

8. Clastic sedimentary rocks in the map area are derived from a combined plutonic, volcanic and sedimentary source. The volcanic and sedimentary source is comprised of the Larder Lake, Skead and Catherine Groups. The plutonic source may be basement to the groups cited above.

9. Peridotite sills may have been intruded during development of the Larder Lake Group. Gabbroic sills and layered peridotite-gabbro sills may have been intruded during development of the Kinojevis Group. The discordant gabbroic intrusions (Power Line, South Pit, Contact Gabbros) may have been intruded during development of the Blake River Group.

10. The area has been metamorphosed to the greenschist and hornblende hornfels facies. The boundary between these two is not well defined but likely follows an east-west trend in the thesis map area immediately north of Beaver Lake and the South Pit parallel to the margin of the Lebel Stock. Greenschist mineralogy is charac-

teristic of the Larder Lake Group and cycle I.

11. Regional metamorphism was likely accompanyied by deformation which produced the a) Lebel Syncline and b) drag folding and tight isoclinal folding (best observed in the South Pit).

12. The Lebel Stock was intruded after regional metamorphism. Hornblende hornfels metamorphic assemblages developed at this time. Pyroxene hornfels assemblages were not observed but likely exist adjacent to the Lebel Stock.

13. The Lebel Stock may have readjusted the trend of the Lebel Syncline axis which, together with the strata, broadly warp about the stock.

14. The thesis map area hosts syenite, biotite lamprophyre and feldspar porphyry dykes and the Lebel Stock. The syenite dykes mineralogically resemble the Lebel Stock and may be emanations from that stock. Biotite lamprophyre may be the result of mixing of syenite magma and komatiite.

15. Most samples studied petrographically and chemically have been effected by potassic alteration. This

alteration is believed to be related to emplacement of the alkali-rich dykes and the Lebel Stock.

16. The Larder Lake Break represents a major fault zone. The block south of it was uplifted with respect to the block north of it. Evidence for this is the fact that greenschist facies mineralogy prevails on the south block while prehnite-pumpellyite facies occurs in the north block.

Uplift on the south block with respect to the north block explains why tholeiitic and calc-alkalic volcanics (extrusive equivalents to the peridote-gabbro and gabbro sills and discordant gabbros respectively) are absent from the thesis map area.

17. The two diabase dykes are not metamorphosed nor altered. They may be related to the Nipissing swarm which cuts Proterozoic rocks south of the Abitibi Belt.

10-2 Recommendations: Further Geological Studies

1. Due to lack of time, the whole-rock R.E.E. abundances of the various volcanic and intrusive lithologies were not measured. This is unfortunate because R.E.E. aid in petrogenetic interpretations.

2. To further aid in evaluating the role of feldspar fractionation during komatiitic volcanism, Sr abundances might be of value.

3. Microprobe studies could be made on the mineralogy of the komatiitic basalts, andesites and dacites. Although metamorphosed, unusual compositions might be detected in actinolite, for instance. and in pyrite. Pyrite is the main sulphide in Cr and Ni-rich volcanics and may host much of the Ni.

4. More detail could be paid to structure in the field to aid in creating a more concise structural geological interpretation. In particular, lineations could be measured and domains with contrasting degrees of ductile deformation could be delineated.

5. More detail could be paid to metamorphism, particularly the development of garnet. It is not clear from this study as to whether the garnet is the result of regional or contact metamorphism although it is likely a product of contact metamorphism.

References

Abbey, S., 1977. Studies in standard samples for use in the general analysis of silicate rocks and minerals; Geological Survey of Canada Paper, 77-34, Part 5, Edition of Usable Tables, 31p.

Abraham, E.M., 1950, Geology of McElroy and part of Boston Townships, Larder Lake area: Ontario Department of Mines, Annual Report, v. 59, pt. 6, 66p.

Arndt, N.T., 1977, Ultrabasic magmas and high degree melting of mantle: Contributions to Mineralogy and Petrology, v. 64, p. 205-221.

----------, Naldrett, A.J., and Pyke, D.R., 1977, Komatiitic and iron-rich tholeiitic lavas of Munro Township, northeast Ontario: Journal of Petrology, v. 18, p. 319-369.

----------, and Fleet, M.E., 1979, Stable and metastable pyroxene crystallization in layered komatiite lava flows: American Mineralogist, v. 64, p. 856-864.

----------, Francis, D., and Hynes, A.J., 1979, The field characteristics and petrology of Archean and Proterozoic komatiites: Canadian Mineralogist, v. 17, p. 147-163.

----------, and Nesbitt, R.W., 1982, Geochemistry of Munro Township basalts: In Komatiites, N.T. Arndt and E.G. Nisbet (editors), George Allen and Unwin, London, p. 309-329.

----------, and Nisbet, E.G., 1982, What is a komatiite?: In Komatiites, N.T. Arndt and E.G. Nisbet (editors), George Allen and Unwin, London, p. 19-27.

Arth, J.G. and Hanson, G.N., 1975, Geochemistry and origin of the early Precambrian crust of northeastern Minnesota, Geochimica and Cosmochimica Acta, v. 39, p. 325-362.

Auvray, B., Blais, S., Jahn, B.M., and Piquet, D., 1982, Komatiites and the komatiitic series of the Finnish greenstone belts: In Komatiites, N.T. Arndt and E.G. Nisbet (editors), George Allen and Unwin, London, p. 131-146.

Barley, M.E., Sylvester, G.C., Groves, D.I., Barley, G.D., and Rogers, N., 1984, Archaean calc-alkaline volcanism in the Pilbara Block, western Australia: Precambrian Research, v. 24, nos. 3-4, p. 285-320.

Beaty, D.W., 1980, The oxygen isotope geochemistry of the Abitibi greenstone belt: Unpublished Ph.D. Thesis, Part II, California Institute of Technology, Pasadena, 463p.

Bedard, J.H., Francis, D.M. and Hynes, A.J., and Nadeau, S., 1984, Fractionation in the feeder system of a Proterozoic rifted margin: Canadian Journal of Earth Sciences, v. 21, p. 489-499.

Best, M.G., 1982, Igneous and metamorphic petrology: W.H. Freeman and Company, San Francisco, 630 p.

Bickle, M.J., Ford, C.E., and Nisbet, E.G., 1977, The petrogenesis of peridotitic komatiites: evidence from high-pressure melting experiments: Earth and Planetary Science Letters, v. 37, p. 97-106.

----------, 1982, The magnesium contents of komatiitic liquids: In Komatiites, N.T. Arndt and E.G. Nisbet (editors), George Allen and Unwin, London, p. 479-494.

Binns, R.A., Hallberg, J.A., and Taplin, J.H., 1982, Komatiites in the Yilgarn Block, western Australia: In Komatiites, N.T. Arndt and E.G. Nisbet (editors), George Allen and Unwin, London, p. 117-130.

Blatt, H., Middleton, G.V., and Murray, R., 1980, Origin of sedimentary rocks, second edition: Prentice Hall Inc., Englewood Cliffs, New Jersey, 782p.

Blum, N., 1986, Geochemical studies of Archean iron formations and associated volcanic rocks: Ph.D. Thesis (in preparation), McMaster University, 410p.

Bouma, A.H., 1962, Sedimentology of some flysch deposits: Amsterdam, Elsevier, 168p.

Brooks, C., Ludden, J., Pigeon, Y., and Hubregtse, J.J.M.W., 1982, Volcanism of shoshonite to high-K andesite affinity in an Archean arc environment, Oxford Lake, Manitoba: Canadian Journal of Earth Sciences, v. 19, p. 55-67.

Byerly, G.R., Melson, W.G. and Vogt, P.R., 1976, Rhyodacites, andesites, ferro-basalts and ocean tholeiites from the Galopagos Spreading Center: Earth and Planetary Science Letters, v. 30, p. 215-221.

Cameron, W.E., and Nisbet, E.G., 1982, Phanerozoic analogues of komatiitic basalts: In Komatiites, N.T. Arndt and E.G. Nisbet (editors), George Allen and Unwin, London, p. 29-50.

Campbell, I.H., Roeder, P.L., and Dixon, J.M., 1978, Plagioclase buoyancy in basaltic liquids as determined with a centrifuge furnace: Contributions to Mineralogy and Petrology, v. 67, p. 369-377.

Capdevila, R., Goodwin, A.M., Ujike, O., and Gorton, M.P., 1982, Trace-element geochemistry of Archean volcanic rocks and crustal growth in southwestern Abitibi Belt, Canada: Geology, v. 10, p. 418-422.

Carter, N.L., 1970, Mineralogy and chemistry of the earth's upper mantle based on the partial fusion - partial crystallization model: Bulletin of the Geological Society of America, v. 81, p. 2021-2034.

Cooke, D.L., and Moorhouse, W.W., 1969, Timiskaming volcanism in the Kirkland Lake area, Ontario, Canada: Canadian Journal of Earth Sciences, v. 6, p. 117-132.

Cox, K.G., 1978, Komatiites and other high-magnesian lavas: some problems: Philosophical Transactions of the Royal Society of London, pt. A, v. 288, p. 599-609.

Crocket, J.H., McNutt, R.H., Schwarcz, H.P., Shaw, D.M., and Thode, H.G., 1981, Genesis of Precambrian iron formations - links with base and precious metal mineralization: unpublished manuscript, 20p.

Dimroth, E., Imreh, L., Rocheleau, M. and Goulet, N., 1982, Evolution of the south-central part of the Archean Abitibi Belt, Quebec. Part I: Stratigraphic and paleographic model: Canadian Journal of Earth Sciences, v. 19, p. 1729-1758.

Dimroth, E., Imreh, L., Goulet, N., and Rocheleau, M., 1983a, Evolution of the south-central segment of the Archean Abitibi Belt, Quebec. Part II: Tectonic evolution and geomechanical model: Canadian Journal of Earth Sciences, v. 20, p. 1355-1373.

Dimroth, E., Imreh, L., Goulet, N., and Rocheleau, M., 1983b, Evolution of the south-central segment of the Archean Abitibi Belt, Quebec. Part III: Plutonic and metamorphic evolution and geotectonic model: Canadian Journal of Earth Sciences, v. 20, p. 1374-1388.

Dubuc, F., 1966a, Geology of the Adams Mine: Transactions

of the Canadian Institute of Mining Metallurgy, v. 69, p. 67-72.

Dubuc, F., 1966b, Dyke map, South Pit: Unpublished map for Laughlin Steel Corporation, Kirkland Lake, Ontario, Scale 1" to 50'.

Ferguson, J. and Sheraton, J.W., 1979, Petrogenesis of kimberlitic rocks and associated xenoliths of southeastern Australia: In Kimberlites, Diatremes and Diamonds: Their Geology, Petrology, and Geochemistry, F.R. Boyd and H.O.A. Meyer (editors), American Geophysical Union, Washington, D.C.

Fleet, M.E. and MacRae, N.D., 1975, A spinifex rock from Munro Township, Ontario: Canadian Journal of Earth Sciences, V. 12, p. 928-939.

Fyfe, W.S., 1981, How do we recognize plate tectonics in very old rocks?: In Precambrian Plate Tectonics, A. Kroner (editor), Elsevier, Amsterdam, The Netherlands, p. 549-560.

Fyon, J.A., Crocket, J.H., and Schwarcz, H.P., 1983, The Carshaw and Malga iron-formation-hosted gold deposits of the Timmins area: In The Geology of Gold in Ontario, A.C. Colvine (editor), Ontario Geological Survey, Miscellaneous Paper 110, p. 98-110.

Gariepy, C., Allegre, C.J., and Lajoie, J., 1984, U-Pb systematics in single zircons from the Pontiac sediments, Abitibi greenstone belt: Canadian Journal of Earth Sciences, v. 21, p. 1296-1304.

Gates, T.M., and Hurley, P.M., 1973, Evaluation of Rb-Sr dating methods applied to Matchewan, Abitibi, MacKenzie and Sudbury dike swarms in Canada: Canadian Journal of Earth Sciences, v. 10, p. 900-919.

Gelinas, L., Brooks, C., Perrault, G., Carignan, J., Trudel, P., and Grasse, F., 1977, Chemo-stratigraphic divisions within the Abitibi volcanic belt, Rouyn-Noranda District, Quebec. In Volcanic Regimes in Canada, W.R.A. Barager, L.C. Coleman and J.M. Hall (editors), Geological Association of Canada, Special Paper, 16, p. 265-295

Gelinas, L., 1979a, Archean Abitibi Belt, peridotitic komatiites, Lamotte Township, Quebec: Unpublished manuscript, 13p.

----------, 1979b, Archean Abitibi Belt, pyroxenitic

komatiites, Destor Township, Quebec: Unpublished manuscript, 26p.

Gibb, F.G.F., 1974, Supercooling and the crystallization of plagioclase from a basaltic magma: Mineralogical Magazine, v. 39, p. 641-653.

Glikson, A.Y., and Hickman, A.H., 1981, Geochemical, stratigraphy and petrogenesis of Archean basic-ultramafic volcanic units, eastern Pilbara Block, western Australia: Special Publications, Geological Society of Australia Incorporated, No. 7, p. 287-300.

Goodwin, A.M., 1977, Archean volcanism in the Superior Province, Canadian Shield: In Volcanic Regimes in Canada, W.R.A. Barager, L.C. Coleman, and J.M. Hall (editors), Geological Association of Canada, Special Paper, 16, p. 205-241.

Goodwin, A.M. and Smith, I.E.M., 1980, Chemical discontinuities in Archean metavolcanic terrains and the development of Archean crust: Precambrian Research, v. 10, p. 301-311.

Goodwin, A.M., 1982, Archean volcanoes in southwestern Abitibi Belt, Ontario and Quebec: form, composition, and development: Canadian Journal of Earth Sciences, v. 19, p. 1140-1155.

Goulet, N., 1978, Stratigraphy and structural relationships across the Cadillac-Larder Lake Fault, Rouyn-Beauchastel area, Quebec: Unpublished Ph.D. Thesis, Queen's University, Kingston, Ontario.

Green, D.H., Nicholls, I.A., Viljoen, M. and Viljoen, R., 1975, Experimental demonstration of the existence of peridotitic liquids in earliest Archaean magmatism: Geology, v. 3, p. 11-14.

--------, 1975, Genesis of Archean peridotitic magmas and constraints on Archean geothermal gradients and tectonics: Geology, 3, p. 15-18.

Hanson, G.N., and Langmuir, C.H., 1978, Modelling of major elements in mantle-melt systems using trace element approaches: Geochimica et Cosmochimica Acta, v. 42, p. 725-741.

Hess, H.H., 1949, Chemical composition and optical properties of common clinopyroxenes, part I: American Mineralogist, v. 34, p. 621-666.

Hewitt, D.F., 1949, Geology of Skead Township, Larder Lake area: Ontario Department of Mines Annual Report, v. 58, pt. 6, 43p.

Hewitt, D.F., 1963, The Timiskaming series of the Kirkland Lake area: Canadian Mineralogist, v. 7, p. 497-523.

Houghton, H.F., 1980, Refined techniques for staining plagioclase and alkali feldspars in thin section: Journal of Sedimentary Petrology, v. 50, p. 629-631.

Hubregtse, J.J.M.W., 1976, Volcanism in the western Superior Province in Manitoba. In The Early History of the Earth, B.F. Windley (editor), J.Wiley and Sons, New York, N.Y., p. 279-287.

Hyde, R.S., 1978, Sedimentology, volcanology, stratigraphy, and tectonic setting of the Archean Timiskaming Group, Abitibi greenstone belt, northeastern Ontario, Canada: Unpublished Ph.D. Thesis, McMaster University, Hamilton, Ontario, 423p.

Ingram, R.L., 1954, Terminology for the thickness of stratification and parting units in sedmentary rocks: Geological Society of America Bulletin, v. 65, p. 937-938.

Irvine, T.N., 1967, Chromian spinel as a petrogenetic indicator part 2. petrologic applications: Canadian Journal of Earth Sciences, v. 4, p. 71-99.

Irvine, T.N., and Baragar, W.R.A., 1971, A guide to the chemical classification of the common volcanic rocks: Canadian Journal of Earth Sciences, v. 8, p. 523-548.

Irvine, T.N. 1975, Crystallization sequences in the Muskox intrusion and other layered intrusions - II. Origin of chromitite layers and similar deposits of other magmatic ores: Geochimica et Cosmochimica Acta, 1975, v. 39, p. 991-1020.

Jahn, B., Auvray, B., Blais, S., Capdevila, R., Cornichet, J., Vidal, F., and Hameurt, J., 1980, Trace element geochemistry and petrogenesis of Finnish greenstone belts: Journal of Petrology, v. 21, pt. 2, p. 201-244.

Jensen, L.S., 1972, Geology of Melba and Bisley Townships, District of Timiskaming: Ontario Division of Mines Geological Report 103, 27p.

----------, 1975, Geology of Clifford and Ben Nevis Townships, District of Cochrane: Ontario Division of

Mines, Geoscience Report 132, 55p.

----------, 1976a, A new cation plot for classifying subalkalic volcanic rocks: Ontario Division of Mines, Miscellaneous Paper 66, 22p.

----------, 1976b, Regional stratigraphy and structure of the Timmins-Kirkland Lake area, District of Cochrane and Timiskaming and Kirkland Lake area, District of Timiskaming: Ontario Division of Mines, Miscellaneous Paper 67, p. 87-95.

----------, 1977, Regional stratigraphy and structure of the Timmins-Kirkland Lake area, District of Cochrane and Timiskaming and Kirkland Lake-Larder Lake areas, District of Timiskaming: Ontario Geological Survey Miscellaneous Paper 75, p. 98-101.

Jensen, L.S., 1978a, Archean komatiitic, tholeiitic, calc-alkalic and alkalic volcanic sequences in the Kirkland Lake area: In Toronto '78 Field Trip Guidebook, A.L. Currie and W.O. Mackasey (editors), Geological Association of Canada, p. 237-259.

----------, 1978b, Geology of Thackeray, Elliot, Tannahill and Dokis Townships, District of Cochrane: Ontario Geological Survey, Report 165, 71p.

----------, 1978c, Regional stratigraphy and structure of the Timmins-Kirkland Lake area, Districts of Cochrane and Timiskaming and the Kirkland Lake-Larder Lake area, District of Timiskaming: Ontario Geological Survey, Miscellaneous Paper 82, p. 67-72.

----------, 1979, Larder Lake synoptic mapping project, Districts of Cochrane and Timiskaming: Ontario Geological Survey, Miscellaneous Paper 90, p. 64-69.

----------, 1980, Kirkland Lake-Larder Lake synoptic mapping project, Districts of Cochrane and Timiskaming: Ontario Geological Survey, Miscellaneous Paper 96, p. 55-60.

----------, and Langford, F.F., 1983, Geology and petrogenesis of the Archean Abitibi Belt in the Kirkland Lake area, Ontario: Ontario Geological Survey, Open File Report 5455, 520p.

----------, 1983, Kirkland Lake-Larder Lake synoptic mapping project, District of Timiskaming: Ontario Geological Survey, Miscellaneous Paper 116, p. 63-68.

Jolly, W.T., 1974, Regional metamorphic zonation as an aid in study of Archean terrains: Abitibi Region, Ontario: Canadian Mineralogist 12, p. 499-508.

----------, 1975, Subdivision of the Archean lavas of the Abitibi area, Canada, from Fe-Mg-Ni-Cr relations: Earth and Planetary Letters, v. 27, p. 200-210.

----------, 1978, Metamorphic history of the Archean Abitibi Belt: Geological Survey of Canada, Paper 78-10, p. 63-78.

----------, 1980, Development and degradation of Archean lavas, Abitibi area, Canada, in light of major element geochemistry: Journal of Petrology 21, p. 323-363.

----------, 1983, Progressive metamorphism of komatiites and related Archaean lavas of the Abitibi area, Canada: In Komatiites. N.T. Arndt and E.G. Nisbet (editors), George Allen and Unwin, London, p. 247-266.

Jones, J.G., 1969, Pillow lavas as depth indicators: American Journal of Science, v. 267. p. 181-195.

Kerrich, R., and Watson, G.P., 1984, The Macassa Mine Archean lode gold deposit, Kirkland Lake, Ontario: Geology, patterns of alteration, and hydrothermal regimes: Economic Geology, v. 79, no. 5, p. 1104-1130.

Kuno, H., 1960, High-alumina basalt: Journal of Petrology, v. 1, p. 121-145.

Kushiro, I., 1960, Si-Al relation in clinopyroxenes from igneous rocks: American Journal of Science, v. 258, p. 548-554.

Lajoie, J., and Ludden, J.N., 1984, Petrology of the Archean Pontiac and Kewagama sediments and implications for the stratigraphy of the southern Abitibi belt: Canadian Journal of Earth Sciences, 21, p. 1305-1314.

La Tour, T.E., Kerrich, R., and Barnett, R.L., 1984, Hydrothermal alteration and dynamic recrystallization of feldspar in an Archean iron-formation: Canadian Mineralogist, v. 22, p. 621-630.

Lawton, K.D., 1957, Geology of Boston Township and part of Pacaud Township: Ontario Department of Mines, Anual Report, v. 66, pt. 5, 55p.

Leech, A.V., 1965, A reconnaissance: basic intrusive rocks of the Precambrian Shield, Canada: Unpublished M.Sc.

Thesis, University of Alberta, Edmonton, Alberta.

Le Roex, A.P., Dick, H.J.B., Reid, A.M., and Erlank, A.J., 1982, Ferrobasalts from the Spiess Ridge segment of the Southwest Indian Ridge: Earth and Planetary Science Letters, v. 60, p. 437-451.

Ludden, J.N., and Gelinas, L., 1982, Trace element characteristics of komatiites and komatiitic basalts from the Abitibi metavolcanic belt of Quebec: In Komatiites, N.T., Arndt and E.G. Nisbet (editors), George Allen and Unwin, London, p. 331-346

MacMichael, T.P., 1981, VLF-EM survey conducted on the base metal claims in Boston Township for Marshall-Boston Iron Mines Limited by A.C.A. Howe International Limited: Unpublished report, 12p.

Mattison, G.D., 1973, CIPW computer program: Department of Geology, McMaster University, Hamilton, Ontario

McLeod, H.D., 1952, Geology of Leonard A. Marshall Option No.2, Boston Township: Unpublished Dominion Gulf Company Report, 4p.

Middleton, G.V., and Hampton, M.A., 1973, Sediment gravity flows: mechanisms of flow and deposition: In Turbidites and Deep-water Sedimentation, G.V. Middleton and A.H. Bouma (editors), S.E.P.M., Pacific Section Short Course Notes, p. 1-38.

Moore, J.G., 1965, Petrology of deep-sea basalt near Hawaii: American Journal of Science, v. 263, p. 40-52.

Naldrett, A.J. and Turner, A.R., 1977, The geology and petrogenesis of a greenstone belt and related nickel sulphide mineralization at Yakabindie, western Australia: Precambrian Research, v. 5, p. 43-105.

Naldrett, A.J., and Smith, I.S.E., 1981, Mafic and ultramafic volcanism during the Archean: In Basaltic Volcanism on the Terrestrial Planets, Pergamon Press, Inc., New York, p. 5-29.

Nesbitt, R.W., and Sun, S.S., 1976, Geochemistry of Archaean spinifex-textured peridotites and magnesian and low-magnesian tholeiites: Earth Planetary Science Letters, v. 31, p. 433-53.

Nesbitt, R.W., Sun, S.S., and Purvis, A.C., 1979, Komatiites: geochemistry and genesis: Canadian Mineralogist, v. 17, p. 165-186.

Nisbet, E.G., Bickle, M.J., and Martin, A., 1977, The mafic and ultramafic lavas of the Belingwe greenstone belt, Rhodesia: Journal of Petrology, 18, p. 521-566.

Nisbet, E.G., and Chinner, G.A., 1981, Controls of the eruptions of mafic and ultramafic lavas, Ruth Well Ni-Cu prospect, west Pilbara: Economic Geology, v. 76, p. 1729-1735.

Nisbet, E.G., Bickle, M.J., Martin, A., Orpen, J.L. and Wilson, J.F., 1982, Komatiites in Zimbabwe: In Komatiites. N.T. Arndt and E.G. Nisbet (editors), George Allen and Unwin, London, p. 97-104.

Nunes, P.D., and Jensen, L.S., 1980, Geochronology of the Abitibi metavolcanic belt, Kirkland Lake area - progress report: Ontario Geological Survey, Miscellaneous Paper 92, p. 40-45.

Osborne, E.F., 1959, Role of oxygen pressure in the crystallization and differentiation of basaltic magmas: American Journal of Science, v. 257, p. 609-647.

Page, C., 1983, The geology of the Cullaton B-Zone gold deposit, Northwest Territories: Unpublished M.Sc. Thesis, University of Waterloo, Waterloo.

Parks, T., 1952, Detailed mapping - Charles Marshall Option No. 2, Area No. 119, Boston Township: Unpublished report, 7p.

Pearce, T.H. and Birkett, T.C., 1974, Archean metavolcanic rocks from Thackeray Township, Ontario: Canadian Mineralogist, v. 12, p. 509-519.

Pettijohn, E.J., 1975, Sedimentary Rocks, Harper Row, New York, 628p.

Ploeger, F.R., 1980, Kirkland Lake gold study, District of Timiskaming: Ontario Geological Survey, Miscellaneous Paper 96, p. 188-190.

Pyke, D.R., 1978, Geology of the Redstone River area, District of Timiskaming: Ontario Division of Mines, Geoscience Report 161, 75p.

Ratcliffe, J.H., 1951, Ground magnetometer survey, Leonard A. Marshall Option Number 2, Boston Township, Ontario: Unpublished report, 2p.

Ridler, R.H., 1969, The relationship of mineralization to volcanic stratigraphy in the Kirkland Lake area,

northeastern Ontario, Canada: Unpublished Ph.D. Thesis, University of Wisconsin.

Ridler, R.H., 1970, Relationship of mineralization to volcanic stratigraphy in the Kirkland-Larder Lakes area, Ontario: The Geological Association of Canada, Proceedings, v. 21, p. 33-42.

Scoates, R.F.J., Duke, J.M., Eckstrand, O.R. and Williamson, B., 1986, Layer disruption, PGE mineralization and the role of supercooling in the crystallization of the Bird River Sill, Manitoba: Current Activities Forum 1986, Program with Abstracts, Geological Survey of Canada, Paper 86-8.

Smith H.S. and Erlank, A.J., 1982, Geochemistry and petrogenesis of komatiites from Barberton greenstone belt: In Komatiites, N.T. Arndt and E.G. Nisbet (editors), George Allen and Unwin, London, p. 347-397.

Smith, T.E., and Longstaffe, F.J., 1974, Archean rocks of shoshonitic affinities at Bijou Point, northwestern Ontario: Canadian Journal of Earth Sciences, v. 11, p. 1407-1413.

Streckeisen, A., To each plutonic rock its proper name: Earth-Science Reviews, v. 12, p. 1-33.

Sun, S.S., and Nesbitt, R.W., 1978, Petrogenesis of Archaean ultrabasic and basic volcanics: evidence from rare earth elements: Contributions to Mineralogy and Petrology, v. 65, p. 301-325.

Tasillo-Hirt, A.M., Geissman, J.W., and Strangway, D.W., 1982, Paleomagnetism of Late Archean metavolcanics and metasediments, Abitibi orogen, Canada: volcanics of the Blake River Group and sediments and volcanics of the Timiskaming Group: Canadian Journal of Earth Sciences, v. 19, p. 2100-2113.

Taylor, S.R., Kaye, M., White, A.J.R., Duncan, A.R., and Ewart, A., 1969, Genetic significance of Co, Cr, Ni, Sc and V content of andesites: Geochimica et Cosmochimica Acta, v. 33, p. 275-286.

Thompson, J.E., 1941, Geology of McGarry and McVittie Townships, Larder Lake area: Ontario Department of Mines, Annual Report, v. 50, pt. 7, 99p.

Thompson, J.E., 1947, Geology of Hearst and McFadden Townships: Ontario Department of Mines, Annual Report, v. 56, pt. 8, 34p.

Thompson, J. E., 1948, Geology of Teck Township and the Kenogami Lake area, Kirkland Lake Gold Belt: Ontario Department of Mines, Annual Report, v. 57, pt. 5, p. 1-53.

Turner, F.J., 1981, Metamorphic petrology: mineralogical, field and tectonic aspects, second edition: Hemisphere Publishing Corporation, New York, N.Y., 524p.

Viljoen, M.J., Viljoen, R.P., and Pearton, T.N., 1982, The nature and distribution of Archaean komatiite volcanics in South Africa: In Komatiites, N.T. Arndt and E.G. Nisbet (editors), George Allen and Unwin, London, p. 53-79.

Walker, R.G., and Pettijohn, F.J., 1971, Archaean sedimentation: analysis of the Minnitaki Basin, northwestern Ontario, Canada: Geological Society of America Bulletin, v. 82, p. 2099-2130.

----------, 1978a, A critical appraisal of Archean basin-craton complexes: Canadian Journal of Earth Sciences, v. 15, p. 1213-1218.

----------, 1978b, Deep water sandstone facies and ancient submarine fans: models for exploration for stratigraphic traps: American Association of Petroleum Geologists, Bulletin, v. 62, p. 932-966.

----------, 1979, Facies models 8. Turbidites and associated coarse clastic deposits. In Facies Models, R.G. Walker (editor), Geoscience Canada Reprint Series 1, p. 91-103.

Watson, G.P., and Kerrich, R., 1983, Macassa Mine, Kirkland Lake - production history, geology, gold ore types and hydrothermal regimes: In The Geology of Gold in Ontario, A.C. Colvine (editor), Ontario Geological Survey, Miscellaneous Paper 110, p. 56-74.

Wilkinson, J.F.G., 1968, The petrography of basaltic rocks. In Basalts, v. 1. H.H. Hess and A. Poldervaart (editors), Interscience, John Wiley and Sons, New York, p. 163-214.

Williams, D.A.C., 1979, The association of some nickel sulfide deposits within komatiitic volcanism in Rhodesia: Canadian Mineralogist, v. 17, p. 337-349.

Williams, H., Turner, F.J., Gilbert, C.M., 1954, Petrography, an introduction to the study of rocks in thin sections: W.H. Freeman and Company, San

Francisco, 406p.

Winkler, H.G.F., 1979, Petrogenesis of metamorphic rocks, fifth edition: Springer-Verlag, New York, Heidelberg, Berlin, 348p.

Appendix A

Geochemical Data

(The location of all samples in this appendix is given in map 1). Major element compositions are given as wt. % and are normalized to 100% on an anhydrous basis. Cr, Ni, Co and V abundances are in ppm. L.O.I. values are given as wt. %.

Table A-1 Geochemical data for volcanic rocks

Sequence 1

	tholeiitic basalt	tholeiitic basalt	calc-alkalic basalt	calc-alkalic basalt	calc-alkalic basalt
	M-516	M-162	M-204	M-208	M-225
SiO_2	49.77	49.84	53.84	52.48	52.84
Al_2O_3	15.57	12.74	14.89	14.80	15.53
Fe_2O_3	12.22	14.53	9.39	9.22	9.79
MgO	8.84	7.62	6.40	7.57	6.54
CaO	7.36	10.38	10.49	11.08	9.25
Na_2O	3.06	3.28	3.23	3.53	4.37
K_2O	2.04	0.36	0.61	0.32	0.50
TiO_2	0.83	0.92	0.85	0.78	0.92
MnO	0.24	0.25	0.14	0.14	0.17
P_2O_5	0.08	0.08	0.15	0.08	0.09
Total	100.00	100.00	100.00	100.00	100.00
L.O.I.	1.55	0.90	1.26	0.89	0.88
Cr	173	451	338	466	224
Ni	75	75	69	96	114
Co	56	34	87	79	114
V	191	207	205	203	228

N.B.

For sequences 2 to 8, and for komatiitic volcanics on the north limb of the Lebel Syncline, the subscripts at the top of each analysis indicate the rock name according to the legend below.

A: komatiite

B: high MgO komatiitic basalt

C: high MgO komatiitic andesite

D: low MgO komatiitic basalt

E: low MgO komatiitic andesite

F: low Al_2O_3 komatiitic dacite

G: high Al_2O_3 komatiitic basalt

H: high Al_2O_3 komatiitic andesite

I: high Al_2O_3 komatiitic dacite

J: high Al_2O_3, Fe_2O_3 komatiitic basalt

Sequence 2

	A M-564	D M-160	B M-134	D M-404	D M-436
SiO_2	43.81	53.00	50.39	50.62	50.05
Al_2O_3	10.65	10.10	11.54	13.48	11.09
Fe_2O_3	14.33	9.80	12.43	9.40	13.91
MgO	21.68	11.04	12.59	11.81	10.84
CaO	8.18	10.84	8.02	8.73	10.36
Na_2O	0.05	2.01	2.18	3.49	2.38
K_2O	0.36	1.49	1.97	1.49	0.32
TiO_2	0.53	0.82	0.57	0.75	0.59
MnO	0.26	0.20	0.21	0.17	0.40
P_2O_5	0.04	0.71	0.00	0.04	0.06
Total	100.00	100.00	100.00	100.00	100.00
L.O.I.	4.63	1.33	1.25	1.32	1.40
Cr	2854	527	1029	881	2958
Ni	1196	106	287	194	2124
Co	121	59	79	89	168
V	177	173	173	205	182

Note: All samples from sequence 2 were collected west of the mine site.

Sequence 3

	A	B	B	E	E	E	F	E	E	B	D
	M-138	M-29	M-116	M-139	M-1	M-126	M-31	M-220	M-218	M-163	M-117
SiO_2	45.61	50.92	49.45	54.49	57.37	56.48	65.61	55.79	59.66	49.20	51.05
Al_2O_3	9.79	9.92	11.01	14.31	12.43	14.79	10.69	13.14	10.86	9.85	15.09
Fe_2O_3	12.66	16.42	10.66	10.92	9.10	9.80	8.66	10.49	10.60	9.41	9.15
MgO	21.20	12.11	14.24	8.27	6.53	5.71	4.96	7.99	8.19	16.57	9.59
CaO	9.77	7.75	11.81	4.68	12.44	9.34	5.99	6.36	6.85	12.18	10.03
Na_2O	0.05	1.11	0.98	6.10	0.94	2.05	2.33	4.97	2.85	0.63	2.07
K_2O	0.08	0.50	0.82	0.06	0.24	0.76	0.93	0.05	0.12	0.75	2.00
TiO_2	0.59	0.54	0.60	0.81	0.65	0.79	0.55	0.75	0.52	0.60	0.82
MnO	0.17	0.65	0.29	0.28	0.24	0.22	0.20	0.35	0.33	0.21	0.16
P_2O_5	0.07	0.07	0.13	0.06	0.09	0.05	0.08	0.11	0.02	0.60	0.04
Total	100.00	100.00	100.00	100.00	100.00	100.00	100.00	100.00	100.00	100.00	100.00
L.O.I.	4.54	2.59	2.46	2.35	1.84	1.60	1.20	1.07	0.91	1.70	1.26
Cr	1725	4712	4642	2849	2433	2463	4286	5312	5719	1131	329
Ni	855	1368	1228	1017	611	805	799	1780	1909	511	152
Co	69	129	84	148	67	139	312	195	269	81	92
V	202	207	167	234	196	214	149	239	192	114	221

Notes: M-220 and M-218 were collected south of the South Pit on the mine site. The others were collected west of the mine site.

Sequence 4

	A M-141	B M-127	B M-213	D M-177	E M-3	E M-124	E M-11
SiO_2	43.92	49.42	50.64	51.27	61.97	55.95	55.45
Al_2O_3	7.19	12.42	8.04	11.65	11.97	12.17	14.88
Fe_2O_3	13.39	12.20	12.86	12.28	7.53	11.31	9.54
MgO	26.80	12.29	13.89	11.27	6.74	7.06	5.31
CaO	7.97	9.58	12.00	10.02	6.35	10.55	8.35
Na_2O	0.05	2.90	0.83	2.23	4.38	0.94	5.00
K_2O	0.03	0.12	0.93	0.10	0.08	0.87	0.31
TiO_2	0.42	0.71	0.42	0.61	0.67	0.67	0.81
MnO	0.22	0.22	0.31	0.46	0.22	0.32	0.26
P_2O_5	0.02	0.15	0.08	0.10	0.09	0.16	0.09
Total	100.00	100.00	100.00	100.00	100.00	100.00	100.00
L.O.I.	6.99	1.90	1.40	1.89	0.92	1.82	1.13
Cr	3212	1709	3173	5932	4596	2517	1068
Ni	1594	390	1958	1334	1043	603	203
Co	125	66	166	193	96	70	57
V	127	212	128	192	215	214	248

Notes: M-213 and M-177 were collected south of the South Pit on the mine site. The others were collected west of the mine site.

Sequence 5

	A	A	C	D
	M-227	M-44	M-105	M-174
SiO_2	42.88	42.87	52.80	54.31
Al_2O_3	9.31	7.50	18.42	18.16
Fe_2O_3	14.26	13.48	7.17	11.22
MgO	23.74	23.01	3.28	3.43
CaO	8.87	12.25	11.38	7.40
Na_2O	0.05	0.05	2.66	2.19
K_2O	0.04	0.04	3.27	2.16
TiO_2	0.57	0.40	0.58	0.63
MnO	0.28	0.30	0.23	0.48
P_2O_5	0.01	0.09	0.19	0.02
Total	100.00	100.00	100.00	100.00
L.O.I.	6.94	5.66	2.07	1.16
Cr	3496	3291	410	422
Ni	861	1838	25	123
Co	132	133	27	115
V	172	142	194	256

Notes: M-227, M-44 and M-105 were collected west of the mine site. M-174 was taken 10 meters south of the South Pit.

I

	M-260
SiO_2	63.40
Al_2O_3	16.43
Fe_2O_3	7.90
MgO	2.73
CaO	1.31
Na_2O	3.07
K_2O	3.91
TiO_2	0.72
MnO	0.13
P_2O_5	0.41
Total	100.00
L.O.I.	1.44
Cr	108
Ni	88
Co	26
V	94

M-260 was taken from a unit which directly overlies B.I.F. in the South Pit.

Sequence 6

	low MgO komatiitic basalt D M-47	D M-57	D M-97	low MgO komatiitic andesite E M-578
SiO_2	52.73	51.68	52.56	57.33
Al_2O_3	11.91	11.90	14.97	14.49
Fe_2O_3	13.04	12.14	11.31	8.16
MgO	8.69	10.30	7.18	6.00
CaO	11.04	10.02	6.18	8.74
Na_2O	1.16	2.67	4.41	3.68
K_2O	0.36	0.24	2.32	0.62
TiO_2	0.61	0.63	0.78	0.68
MnO	0.33	0.26	0.20	0.24
P_2O_5	0.13	0.16	0.08	0.06
Total	100.00	100.00	100.00	100.00
L.O.I.	1.49	1.90	0.93	0.75
Cr	2847	1636	1666	1202
Ni	885	331	381	303
Co	134	67	106	112
V	178	212	245	228

Notes: All analyzed samples in sequence 6 were collected west of the mine site.

Flows between B.I.F. in the South Pit and Sequence 8 at Fault Lake. M-197 is lower in the stratigraphy than is M-185

	J		G	
	M-197		M-185	
SiO_2	48.50		53.24	
Al_2O_3	16.76	M-197 is	17.17	M-185 is
Fe_2O_3	18.50	probably on	11.93	probably on
MgO	4.24	the same	3.93	the same
CaO	9.81	stratigraphic	9.29	stratigraphic
Na_2O	0.51	level as	2.02	level as
K_2O	0.59	Sequence 6	0.88	Sequence 6 or 7
TiO_2	0.55		0.56	
MnO	0.54		0.36	
P_2O_5	0.00		0.02	
Total	100.00		100.00	
L.O.I.	2.92		1.33	
Cr	443		214	
Ni	136		67	
Co	116		56	
V	220		248	

Sequence 7

	A M-231	B M-232	A M-233	A M-56	A M-103	A M-650	B M-59
SiO_2	43.92	48.34	47.94	48.93	46.84	47.50	47.47
Al_2O_3	6.18	11.77	7.41	6.81	8.04	8.69	10.84
Fe_2O_3	12.00	12.44	12.00	10.86	12.53	11.96	12.86
MgO	32.83	12.49	20.63	23.15	23.05	19.06	17.24
CaO	4.32	10.34	10.84	9.49	8.74	11.09	9.47
Na_2O	0.05	2.45	0.35	0.05	0.05	0.05	0.05
K_2O	0.03	1.25	0.06	0.11	0.05	0.95	1.24
TiO_2	0.34	0.61	0.47	0.36	0.48	0.44	0.57
MnO	0.27	0.22	0.20	0.21	0.15	0.25	0.26
P_2O_5	0.07	0.09	0.10	0.03	0.08	0.01	0.00
Total	100.00	100.00	100.00	100.00	100.00	100.00	100.00
L.O.I.	6.93	0.63	2.74	3.62	5.11	2.58	2.18
Cr	2478	1219	2916	2212	2760	2295	1550
Ni	2200	458	1369	876	1300	961	593
Co	135	92	110	96	81	115	103
V	115	187	137	105	129	130	168

Sequence 7 (continued)

	B M-98	B M-55	B M-26	B M-238	D M-199	D M-69
SiO_2	48.06	48.39	49.55	45.55	53.24	50.44
Al_2O_3	9.71	10.28	7.86	13.26	14.18	12.00
Fe_2O_3	11.73	12.57	12.88	15.63	11.75	11.18
MgO	16.38	15.05	15.56	13.30	7.52	9.00
CaO	11.62	10.70	12.33	8.92	9.91	15.86
Na_2O	1.34	1.45	0.68	0.98	0.96	0.37
K_2O	0.35	0.62	0.28	1.07	1.39	0.10
TiO_2	0.53	0.57	0.44	0.81	0.72	0.59
MnO	0.22	0.24	0.31	0.46	0.24	0.29
P_2O_5	0.05	0.12	0.12	0.03	0.10	0.16
Total	100.00	100.00	100.00	100.00	100.00	100.00
L.O.I.	1.32	4.05	3.45	2.98	1.95	2.45
Cr	2413	1859	2636	3174	3022	3105
Ni	688	366	950	1216	946	850
Co	95	70	84	140	139	80
V	154	179	121	243	216	182

Sequence 7 (continued)

	D	E	E	E	E	E
	M-71	M-70	M-269	M-107	M-106	M-76
SiO_2	53.88	57.08	56.76	58.13	59.62	58.12
Al_2O_3	11.27	9.45	12.53	11.19	13.28	11.85
Fe_2O_3	10.54	11.59	10.56	10.85	9.12	9.70
MgO	11.45	11.29	7.51	7.99	4.87	8.81
CaO	10.32	7.89	9.53	9.66	8.84	8.38
Na_2O	1.36	1.65	1.90	0.87	2.68	1.95
K_2O	0.36	0.26	0.35	0.45	0.60	0.33
TiO_2	0.58	0.46	0.63	0.57	0.66	0.62
MnO	0.20	0.26	0.21	0.23	0.21	0.16
P_2O_5	0.05	0.07	0.02	0.08	0.13	0.08
Total	100.00	100.00	100.00	100.00	100.00	100.00
L.O.I.	1.16	2.01	2.07	1.94	0.86	1.99
Cr	3125	4551	3146	3481	2976	3539
Ni	1015	1675	1134	1148	708	945
Co	150	110	192	96	165	82
V	189	168	193	202	206	208

Notes: All analyzed samples in sequence 7 were collected west of the mine site.

Sequence 8

	A	B	D	F
	M-202	M-272	M-413	M-115
SiO_2	46.81	49.89	51.02	63.72
Al_2O_3	8.59	7.97	12.99	10.13
Fe_2O_3	12.33	14.21	13.51	7.55
MgO	19.60	14.40	8.95	7.72
CaO	11.59	12.18	9.66	6.88
Na_2O	0.05	0.42	2.13	2.85
K_2O	0.08	0.26	0.76	0.39
TiO_2	0.48	0.31	0.61	0.49
MnO	0.36	0.37	0.34	0.22
P_2O_5	0.11	0.00	0.03	0.07
Total	100.00	100.00	100.00	100.00
L.O.I.	2.37	1.04	1.21	1.55
Cr	4017	2391	3476	3735
Ni	1125	1109	1386	927
Co	128	120	194	73
V	139	118	190	180

Notes: All analyzed samples in sequence 8 were collected west of the mine site.

Volcanics in the Dry Lake-Fault Lake Area

	E	E	G	H
	M-73	M-340	M-302	M-353
SiO_2	58.12	57.12	48.48	56.02
Al_2O_3	14.95	12.37	18.51	17.32
Fe_2O_3	9.71	10.58	10.29	9.68
MgO	4.70	7.88	5.43	2.26
CaO	6.57	9.04	12.53	10.03
Na_2O	2.29	2.06	3.30	1.56
K_2O	2.36	0.10	0.46	2.28
TiO_2	0.81	0.61	0.62	0.58
MnO	0.24	0.23	0.30	0.26
P_2O_5	0.26	0.00	0.06	0.01
Total	100.00	100.00	100.00	100.00
L.O.I.	2.20	1.56	2.21	1.58
Cr	407	3255	422	405
Ni	58	1032	84	45
Co	47	175	88	66
V	130	195	255	200

N.B.:

M-73 and M-353 may represent Sequence 9 which overlies the stratigraphically highest B.I.F. on the south limb of the Lebel Syncline.

M-340 may represent sequence 10.

Komatiitic Volcanics - North Limb of the Lebel Syncline

	B M-529	C M-522	D M-298	E M-330	E M-395	E M-612	D M-280
SiO_2	48.61	55.81	50.39	58.37	55.78	57.72	52.75
Al_2O_3	10.98	9.11	13.05	15.38	15.66	14.72	13.56
Fe_2O_3	11.44	9.17	12.76	8.88	8.65	8.33	13.63
MgO	17.37	12.06	10.43	4.73	5.79	7.07	6.51
CaO	9.07	10.21	8.76	6.90	9.67	7.42	8.73
Na_2O	0.05	1.92	2.30	3.65	2.98	3.27	2.53
K_2O	1.59	0.99	1.43	0.94	0.07	0.46	0.71
TiO_2	0.50	0.45	0.66	0.76	0.89	0.71	0.79
MnO	0.36	0.25	0.17	0.26	0.30	0.14	0.54
P_2O_5	0.03	0.02	0.06	0.13	0.20	0.16	0.26
Total	100.00	100.00	100.00	100.00	100.00	100.00	100.00
L.O.I.	1.81	0.87	1.23	1.61	0.77		0.95
Cr	1536	1670	603	333	520	268	355
Ni	357	165	152	142	195	143	181
Co	88	95	81	74	75	63	49
V	175	191	205	127	154	119	126

Table A-2 Geochemical data for intrusive rocks

Samples from Peridotite Sills

	M-563	M-104	M-416	M-312
SiO_2	48.49	46.27	47.04	42.02
Al_2O_3	6.26	4.19	4.50	3.13
Fe_2O_3	11.62	9.89	10.84	12.32
MgO	25.76	33.76	21.75	41.79
CaO	7.24	5.34	15.41	0.26
Na_2O	0.05	0.05	0.05	0.05
K_2O	0.11	0.04	0.09	0.09
TiO_2	0.24	0.25	0.08	0.15
MnO	0.23	0.13	0.21	0.17
P_2O_5	0.01	0.07	0.03	0.01
Total	100.00	100.00	100.00	100.00
L.O.I.	4.71	10.05	4.09	10.81
Cr	2205	2616	1915	6374
Ni	880	1759	1436	1879
Co	102	99	110	200
V	114	72	61	57

Samples from peridotite-gabbro and gabbroic sills - South Limb of the Lebel Syncline (sill number 1 north of Beaver Lake, map 5)

	pyroxenite M-417	gabbro M-114	gabbro M-112	gabbro M-418	gabbro M-111	gabbro M-19
SiO_2	49.89	51.96	52.92	47.05	48.94	52.24
Al_2O_3	7.56	17.83	14.62	16.80	16.41	13.25
Fe_2O_3	11.20	9.28	9.94	15.52	12.72	14.99
MgO	13.08	9.21	8.47	5.57	6.16	5.25
CaO	15.41	4.44	7.86	10.04	11.57	9.70
Na_2O	1.60	4.95	3.85	2.92	2.45	2.44
K_2O	0.61	1.35	1.30	1.01	0.68	0.43
TiO_2	0.30	0.70	0.68	0.76	0.67	1.25
MnO	0.23	0.16	0.19	0.13	0.22	0.28
P_2O_5	0.13	0.13	0.16	0.20	0.17	0.16
Total	100.00	100.00	100.00	100.00	100.00	100.00
L.O.I.	4.80	5.09	2.24	1.32	1.03	1.99
Cr	1604	299	118	909	298	4
Ni	613	93	222	209	104	63
Co	57	45	52	65	63	80
V	123	220	196	219	193	297

(M-642, 644 and 746 are from the sill number 1 near northwest trending power line, map 5)

	peridotite M-642	pyro-xenite M-644	gabbro M-746	gabbro M-423	gabbro M-729	pyro-xenite M-187	micro-gabbro M-275
SiO_2	45.07	47.57	54.33	51.32	49.69	50.71	53.48
Al_2O_3	4.68	12.73	14.33	17.07	14.78	14.77	16.11
Fe_2O_3	8.42	11.75	11.71	11.64	15.75	11.90	14.10
MgO	40.22	16.47	5.62	10.11	5.45	13.02	2.73
CaO	1.14	6.85	8.58	3.72	7.26	4.15	8.56
Na_2O	0.05	2.56	2.80	5.02	4.05	2.11	3.11
K_2O	0.13	1.43	1.19	0.09	1.32	2.47	0.62
TiO_2	0.13	0.48	1.09	0.72	1.28	0.64	0.96
MnO	0.13	0.13	0.26	0.21	0.30	0.18	0.28
P_2O_5	0.03	0.03	0.09	0.09	0.11	0.06	0.05
Total	100.00	100.00	100.00	100.00	100.00	100.00	100.00
L.O.I.	11.74	3.27	0.97	4.39	1.32	3.47	1.78
Cr	2586	583	87	280	6	291	70
Ni	811	240	63	88	16	81	54
Co	133	108	67	67	83	60	83
V	102	194	326	205	351	273	317

Samples from peridotite gabbro and gabbroic sills - North Limb of the Lebel Syncline

	micro gabbro M-325[1]	gabbro M-326[1]	gabbro M-424[1]	gabbro M-733[1]	gabbro M-732[1]	perido-tite M-530[2]	gabbro M-549[2]
SiO_2	50.91	52.37	51.23	57.78	56.67	45.55	52.34
Al_2O_3	13.14	13.48	14.39	12.31	14.97	4.28	14.34
Fe_2O_3	14.83	15.16	12.44	12.06	8.00	8.95	10.20
MgO	6.08	7.26	7.43	7.96	6.59	26.70	7.93
CaO	8.71	6.99	10.93	5.11	8.28	13.96	8.99
Na_2O	3.75	2.00	2.11	1.89	3.06	0.05	4.30
K_2O	0.85	1.20	0.21	1.25	1.49	0.29	0.77
TiO_2	1.35	1.14	0.90	1.33	0.71	0.06	0.75
MnO	0.26	0.20	0.26	0.17	0.15	0.15	0.33
P_2O_5	0.13	0.18	0.09	0.15	0.06	0.01	0.05
Total	100.00	100.00	100.00	100.00	100.00	100.00	100.00
L.O.I.	1.22	1.08	1.82	2.09	1.77	7.76	1.31
Cr	52	52	165	8	338	1598	385
Ni	68	63	86	49	66	2135	150
Co	101	86	68	101	87	104	92
V	335	302	220	276	183	83	227

Note:
[1] samples from Beaver-Spider Lake Area
[2] samples from North Lake Area

(Dry Lake Area)

	pyroxenite M-715	gabbro M-714	pyroxen-ite M-290	pyroxen-ite M-282
SiO_2	45.73	51.41	47.00	48.51
Al_2O_3	11.33	13.14	11.71	13.30
Fe_2O_3	13.98	17.53	14.26	13.87
MgO	19.96	5.79	16.84	12.74
CaO	7.59	6.75	7.31	6.34
Na_2O	0.05	2.34	1.87	1.27
K_2O	0.68	1.09	0.07	2.89
TiO_2	0.42	1.58	0.63	0.74
MnO	0.22	0.24	0.26	0.26
P_2O_5	0.04	0.12	0.05	0.09
Total	100.00	100.00	100.00	100.00
L.O.I.	4.59	1.97	3.95	2.71
Cr	1381	8	1282	209
Ni	437	15	408	95
Co	113	85	101	84
V	141	459	175	210

Discordant Gabbros

	M-150	M-305	M-300	M-648	M-558	M-74
SiO_2	51.85	52.00	51.60	47.35	52.26	53.40
Al_2O_3	15.47	15.37	15.96	16.03	16.90	15.47
Fe_2O_3	9.36	7.40	10.26	11.62	8.04	8.63
MgO	8.21	9.54	5.97	11.07	7.91	7.97
CaO	11.85	11.20	11.30	9.44	11.33	8.34
Na_2O	1.40	2.32	3.48	2.71	1.55	3.71
K_2O	1.12	1.66	0.73	1.07	1.28	1.55
TiO_2	0.46	0.36	0.39	0.33	0.55	0.55
MnO	0.18	0.15	0.29	0.34	0.16	0.23
P_2O_5	0.11	0.00	0.00	0.06	0.03	0.16
Total	100.00	100.00	100.00	100.00	100.00	100.00
L.O.I.	1.75	1.80	1.62	1.45	2.12	1.88
Cr	589	833	371	551	665	293
Ni	115	117	59	72	122	90
Co	52	70	91	75	72	39
V	191	127	197	194	144	127

Diabase Dyke

	M-80
SiO_2	50.20
Al_2O_3	13.36
Fe_2O_3	14.45
MgO	7.03
CaO	9.67
Na_2O	2.34
K_2O	1.16
TiO_2	1.37
MnO	0.22
P_2O_5	0.21
Total	100.00
L.O.I.	1.43
Cr	139
Ni	88
Co	65
V	261

Appendix B

Analytical Procedures and Errors

Analytical Procedures and Errors

B-1 X-Ray Fluorescence Spectrometry

Major elements and the trace elements Cr, Ni, Co and V were determined on a Phillips PW 1450 automatic sequential spectrometer.

A fused glass bead procedure was followed in the analyses of the major elements. 500 mg of -200 mesh sample powder was mixed with 3.00 g of lithium metaborate-tetraborate (1:1) flux. The mixture was then fused in a platinum crucible over a hot burner and cast in a platinum mold.

Trace elements determinations were made using a compressed powder pellet. Five g of powder was mixed in a plastic vial with three drops of Mowiol binding solution. This was placed in aluminum pellet cups and compressed to twenty tons using a Spex 30 ton press. Na_2O was also determined on compressed powder pellets.

Na_2O abundances obtained by analyses of compressed powder pellets were considered better than those obtained from the fused pellets. This is because the counts per second (C.P.S.) for Na on glass beds in the spectrometer are very low. The C.P.S. for Na on powder pellets are approximately ten times higher (Otto Mudrock, personal communication). Otto Mudrock also points out that precision

for Na using glass beads is poor.

The Na_2O abundances listed in appendix A and in the text are those obtained from analyses of compressed powder pellets. Na_2O abundances (pressed pellets) were substituted for Na_2O abundances (fused pellets). The major oxides were then normalized to 100%.

The standards GSP-1, SY-2, BCR-1, AGV-1, NIM-G, NIM-D, JB-1 and ARSEN used from mid-1983 to mid-1984 to form calibration curves for trace element determinations in the x-ray fluorescence spectrometer. The standards NIM-P, NIM-G, MRG-1, STM-1, G-2, NIM-N, JB-1, W-1 and GSP-1 were used in late 1984 for trace element and Na determinations. Otto Mudrock changed the standards with introduction of a new program.

For the major element determinations on glass beads B-3, NIM-G, GSP-1, AGV-1, W-1 and MRG-1 were used for calibration throughout the study.

B-2 Accuracy

The standard JB-1 was used to measure the accuracy of major element determinations in late 1984. The standard NIM-N was used from mid-1983 to mid-1984. This includes Na as measured on fused pellets. Table B-1 shows that the major element compositions of these two standards determined during this study are in good agreement with literature values (Abbey, 1977) except for K_2O and P_2O_5 with NIM-N.

Table B-1 Accuracy (major elements)

	JB-1				NIM-N			
	X	literature	Diff.	% Diff.	X	literature	Diff.	% Diff.
SiO_2	53.02	52.62	0.40	0.76	53.13	52.56	0.43	0.82
Al_2O_3	14.59	14.62	0.03	0.21	16.19	16.54	0.35	2.12
Fe_2O_3	9.01	9.01	0	0	9.14	8.91	0.25	2.81
MgO	7.86	7.76	0.10	1.29	7.24	7.48	0.24	3.21
CaO	9.34	9.35	0.01	0.11	11.46	11.46	0.00	0.00
Na_2O	2.96	2.79	0.17	6.09	2.30	2.46	0.14	5.69
K_2O	1.53	1.42	0.11	7.75	0.11	0.25	0.14	56.00
TiO_2	1.28	1.34	0.06	4.48	0.19	0.20	0.01	5.00
MnO	0.16	0.15	0.01	6.67	0.19	0.18	0.01	5.56
P_2O_5	0.28	0.26	0.02	7.69	0.05	0.03	0.02	66.67

X for JB-1 is the mean (in weight %) of six determinations.
X for NIM-N is the mean (in weight %) of three determinations.

Table B-2 shows the accuracy of Na abundances, as measured on pressed powder pellets is good.

The average abundances of Cr, Ni, Co and V for BR are in good agreement with those reported by Abbey (1977) (table B-3).

B-3 Precision

A glass bead for M-116 was made and included in every set of a major element determinations for the measure of precision. Table B-4 shows the mean, standard deviation and variance for this sample. It is seen that the precision is good (less than 5 %) for SiO_2, Al_2O_3, Fe_2O_3, MgO, CaO and TiO_2 and poor (greater than 5 %) for Na_2O (glass bead), K_2O, MnO and P_2O_5.

The mean, standard deviation and variance for the standards JB-1 and NIM-N are shown in table B-5. For JB-1, precision is good for SiO_2, Al_2O_3, Fe_2O_3, MgO, CaO and TiO_2 and poor for Na_2O (glass bead), K_2O, MnO and P_2O_5 as in M-116. For NIM-N, precision is poor for Na_2O (glass bead), P_2O_5, and MgO.

Precision is good for Na_2O on pressed pellets of JB-1 (table B-5).

A separate pressed powder pellet was made of M-57 and included in each set of trace element determinations. Precision is good (less than 5%) for Cr, Ni and V and poor for Co (table B-6). For BR, the standard used for accuracy,

Table B-2 Accuracy (Na -pressed pellets)

JB-1

	X	literature	Diff.	% Diff.
Na_2O	2.90	2.79	0.11	3.94

X for JB-1 is the mean (in weight %) of two determinations.

Table B-3 Accuracy (trace elements)

BR

	X	literature	Diff.	% Diff.
Cr	316	380	64	16.84
Ni	260	260	0	0.00
Co	59	50	9	18.00
V	246	240	6	2.50

X for BR is the mean in ppm of five determinations.

Table B-4 Precision (major elements)

	M-116			JB-1			NIM-N	
	X	S.D.	C.V.%	X	S.D.	C.V.%	X	S.D.	C.V.%
SiO_2	49.63	0.43	0.87	53.02	0.28	0.52	53.13	0.61	1.14
Al_2O_3	11.14	0.22	1.92	14.59	0.19	1.28	16.19	0.16	0.98
Fe_2O_3	10.68	0.16	1.51	9.01	0.24	2.70	9.14	0.04	0.44
MgO	13.89	0.43	3.10	7.86	0.28	3.64	7.24	0.50	6.90
CaO	11.91	0.24	1.99	9.34	0.21	2.23	11.46	0.08	0.71
Na_2O	0.84	0.10	12.19	2.96	0.44	14.99	2.30	0.26	11.40
K_2O	0.87	0.10	10.98	1.53	0.12	7.73	0.11	0.00	0.00
TiO_2	0.60	0.03	4.17	1.28	0.05	4.06	0.19	0.01	3.04
MnO	0.32	0.03	8.41	0.16	0.01	6.25	0.19	0.01	3.04
P_2O_5	0.06	0.05	81.02	0.28	0.04	12.78	0.05	0.04	83.20

X for M-116 is the mean in weight % of nine determinations.
X for JB-1 is the mean in weight % of six determinations.
X for NIM-N is the mean in weight % of three determinations.

Table B-5 Precision (Na - pressed pellet)

	JB-1		
	X	S.D.	C.V.%
Na_2O	2.90	0.14	4.88

X for JB-1 is the mean in weight % of two determinations.

Table B-6 Precision (trace elements)

	M-57			BR		
	X	S.D.	C.V.%	X	S.D.	C.V.%
Cr	1,556	45.93	2.95	316	33.10	10.47
Ni	355	13.98	3.94	260	9.74	3.75
Co	86	10.85	12.65	59	2.65	4.49
V	197	4.99	2.53	245	21.89	8.90

X for M-57 and BR are the means in ppm of five determinations.

precision is good for Ni and Co and poor for V and Cr (table B-6).

B-4 Determination of L.O.I.

Loss on ignition (L.O.I.) was determined by heating 1.3 g of powdered sample in an electric furnace for one hour at a temperature of 1100°C.

Appendix C

C.I.P.W. Norms

C-1 Calculation of C.I.P.W. Norms

Norms were calculated using the C.I.P.W. program of Mattison, (1973). This program was run on the Cyber 170/815 computer at McMaster University.

C.I.P.W. Norms of Volcanic Rocks

Table C-1

Komatiites

	Qtz	Or	Ab	An	Cor	Ne	Mt	Il	Ap	Ol	Di	Hy
M-564	0.00	2.16	0.43	28.15	0.00	0.00	2.98	1.02	0.00	34.18	10.20	20.79
M-138	0.00	0.48	0.43	26.54	0.00	0.00	3.06	1.13	0.16	24.26	17.57	26.37
M-231	0.00	0.18	0.43	16.72	0.00	0.00	2.70	0.65	0.16	51.06	3.54	24.57
M-141	0.00	0.18	0.43	19.53	0.00	0.00	2.82	0.81	0.47	42.93	16.21	17.06
M-227	0.00	0.24	0.43	23.37	0.00	0.00	3.04	1.10	0.02	41.26	15.28	13.27
M-56	0.00	0.66	0.43	18.20	0.00	0.00	2.72	0.69	0.07	15.83	23.15	38.26
M-44	0.00	0.00	0.00	20.36	0.00	0.23	2.79	0.77	0.21	43.50	31.96	0.00
M-103	0.00	0.30	0.43	21.80	0.00	0.00	2.90	0.92	0.19	22.56	17.14	33.76
M-650	0.00	5.70	0.43	20.89	0.00	0.00	2.84	0.02	20.18	27.70	21.43	
M-202	0.00	0.48	0.43	23.22	0.00	0.00	2.90	0.92	0.26	18.54	27.34	25.92

High MgO Komatiitic Basalts

	Qtz	Or	Ab	An	Cor	Ne	Mt	Il	Ap	Ol	Di	Hy
M-529	0.00	9.5	0.43	25.28	0.00	0.00	2.93	0.96	0.07	12.90	15.97	31.98
M-59	0.00	7.41	0.43	25.97	0.00	0.00	3.03	1.09	0.00	15.82	17.28	28.96
M-163	0.00	4.47	5.37	22.00	0.00	0.00	3.07	1.15	1.40	8.54	27.80	26.22
M-98	0.00	2.09	11.45	19.64	0.00	0.00	2.97	1.02	0.12	21.67	30.67	10.38
M-26	0.00	1.67	5.82	17.76	0.00	0.00	2.84	0.85	0.28	7.71	34.89	28.18
M-55	0.00	3.70	12.40	19.92	0.00	0.00	3.03	1.09	0.28	19.09	26.52	13.95
M-272	0.00	1.56	3.60	19.33	0.00	0.00	2.66	0.60	0.00	2.45	33.95	35.87
M-116	0.00	4.89	8.37	23.43	0.00	0.00	3.07	1.15	0.30	9.14	27.91	21.75
M-213	0.00	5.56	7.10	15.64	0.00	0.00	2.82	0.81	0.19	5.27	35.60	27.03
M-238	0.00	6.41	8.40	29.01	0.00	0.00	3.39	1.56	0.07	23.52	12.73	14.91
M-134	0.00	11.78	18.66	16.07	0.00	0.00	3.04	1.10	0.00	19.57	19.55	10.25
M-127	0.00	0.72	24.79	20.72	0.00	0.00	3.24	1.36	0.35	18.59	21.23	9.00

Low MgO Komatiitic Basalts

	Qtz	Or	Ab	An	Cor	Ne	Mt	Il	Ap	Ol	Di	Hy
M-404	0.00	8.87	25.37	16.84	0.00	2.37	3.29	1.44	0.09	20.51	21.22	0.00
M-177	0.00	0.60	19.07	21.71	0.00	0.00	3.09	1.17	0.23	2.42	22.60	29.12
M-160	1.19	8.87	17.14	14.24	0.00	0.00	3.39	1.57	1.66	0.00	28.28	23.67
M-436	0.00	1.91	20.38	18.86	0.00	0.00	3.07	1.34	0.14	11.48	26.73	16.30
M-298	0.00	8.54	19.67	21.29	0.00	0.00	3.17	1.27	0.14	12.56	18.08	15.30
M-117	0.00	11.90	17.64	26.16	0.00	0.00	3.39	1.57	0.09	7.8	19.00	12.46
M-413	0.00	4.54	18.23	23.91	0.00	0.00	3.10	1.17	0.70	1.78	19.97	27.23
M-47	7.17	2.15	9.92	26.52	0.00	0.00	3.09	1.17	0.31	0.00	22.94	26.74
M-199	8.19	8.29	8.20	30.57	0.00	0.00	3.25	1.38	0.23	0.00	15.06	24.83
M-97	0.00	13.84	34.62	14.33	0.00	1.65	3.34	1.50	0.19	17.41	13.14	0.00
M-29	1.67	3.00	9.53	20.91	0.00	0.00	3.00	1.04	0.17	0.00	14.45	46.24
M-280	4.05	4.24	21.65	23.82	0.00	0.00	3.36	1.52	0.61	0.00	15.13	25.63

High MgO Komatiitic Andesites

	Qtz	Or	Ab	An	Cor	Ne	Mt	Il	Ap	Ol	Di	Hy
M-522	4.55	5.89	16.37	13.42	0.00	0.00	2.85	0.86	0.05	0.00	30.04	25.98

Low MgO Komatiitic Andesites

	Qtz	Or	Ab	An	Cor	Ne	Mt	Il	Ap	Ol	Di	Hy
M-70	11.23	1.55	14.10	17.78	0.00	0.00	2.87	0.88	0.16	0.00	17.23	34.20
M-76	14.16	1.97	16.63	22.78	0.00	0.00	3.10	1.19	0.19	0.00	15.01	24.99
M-107	18.30	2.68	7.43	25.52	0.00	0.00	3.03	1.09	0.19	0.00	18.16	23.61
M-220	0.14	0.30	42.41	13.51	0.00	0.00	3.29	1.44	0.26	0.00	14.28	24.38
M-269	12.53	2.09	16.21	24.84	0.00	0.00	3.12	1.21	0.05	0.00	18.50	21.46
M-124	14.15	5.19	8.03	26.66	0.00	0.00	3.18	1.28	0.37	0.00	20.56	20.59
M-3	13.88	0.46	37.26	12.84	0.00	0.00	3.16	1.28	0.21	0.00	14.67	16.23

Low MgO Komatiitic Andesites (cont.)

	Qtz	Or	Ab	An	Cor	Ne	Mt	Il	Ap	Ol	Di	Hy
M-1	18.01	1.43	7.59	29.13	0.00	0.00	3.14	1.24	0.21	0.00	26.11	12.86
M-578	7.43	3.69	31.33	21.32	0.00	0.00	3.18	1.30	0.14	0.00	17.74	13.89
M-139	0.00	0.36	52.08	11.59	0.00	0.00	3.38	1.55	0.14	16.60	9.29	5.02
M-218	14.08	0.72	24.33	16.63	0.00	0.00	2.95	1.00	0.05	0.00	14.26	26.00
M-395	9.86	0.42	25.38	29.34	0.00	0.00	3.49	1.7	0.47	0.00	14.29	15.06
M-126	12.67	4.53	17.48	29.13	0.00	0.00	3.35	1.51	0.18	0.00	14.08	17.14
M-11	0.54	1.85	42.62	17.37	0.00	0.00	3.37	1.55	0.21	0.00	19.43	13.06
M-330	10.65	5.59	31.09	22.96	0.00	0.00	3.30	1.45	0.30	0.00	8.71	15.95
M-73	12.81	14.05	19.52	23.72	0.00	0.00	3.37	1.55	0.61	0.00	6.09	18.30

Low Al_2O_3 Komatiitic Dacites

	Qtz	Or	Ab	An	Cor	Ne	Mt	Il	Ap	Ol	Di	Hy
M-115	20.77	2.32	24.25	13.77	0.00	0.00	2.90	0.94	0.16	0.00	16.14	18.76
M-31	27.58	5.53	19.85	16.07	0.00	0.00	3.00	1.05	0.19	0.00	10.89	15.85

High Al_2O_3 Komatiitic Basalts

	Qtz	Or	Ab	An	Cor	Ne	Mt	Il	Ap	Ol	Di	Hy
M-302	0.00	2.74	21.97	34.63	0.00	3.35	3.10	1.19	0.14	10.13	22.75	11.55
M-105	0.00	19.43	22.58	28.82	0.00	0.02	3.03	1.12	0.44	2.68	21.88	0.00
M-185	8.34	5.29	17.37	35.75	0.00	0.00	3.04	1.08	0.47	0.00	9.18	19.92

High Al_2O_3 Komatiitic Andesites

	Qtz	Or	Ab	An	Cor	Ne	Mt	Il	Ap	Ol	Di	Hy
M-174	7.18	12.88	18.70	33.65	0.00	0.00	3.12	1.21	0.05	0.00	2.74	20.47
M-353	12.25	13.58	13.30	33.78	0.00	0.00	3.04	1.11	0.02	0.00	13.76	9.16

High Al_2O_3 Komatiitic Dacite

	Qtz	Or	Ab	An	Cor	Ne	Mt	Il	Ap	Ol	Di	Hy
M-260	21.97	23.24	26.12	3.85	8.78	0.00	3.24	1.38	0.96	0.00	0.00	13.48

High Fe_2O_3, Al_2O_3 Komatiitic Basalt

	Qtz	Or	Ab	An	Cor	Ne	Mt	Il	Ap	Ol	Di	Hy
M-197	5.88	3.55	4.39	42.40	0.00	0.00	3.02	1.06	0.00	0.00	6.04	33.67

Sequence 1 Basalts
(Tholeiitic)

	Qtz	Or	Ab	An	Cor	Ne	Mt	Il	Ap	Ol	Di	Hy
M-162	0.00	2.15	28.10	19.21	0.00	0.00	3.55	1.77	0.19	13.46	26.70	4.88
M-516	0.00	12.18	26.15	22.95	0.00	0.00	3.41	1.59	0.19	21.18	10.91	1.44

(Calc-alkalic)

	Qtz	Or	Ab	An	Cor	Ne	Mt	Il	Ap	Ol	Di	Hy
M-225	0.00	2.98	37.25	21.44	0.04	0.00	3.54	1.76	0.21	7.24	19.65	5.94
M-204	3.02	3.63	27.53	24.51	0.00	0.00	3.43	1.63	0.35	0.00	21.85	14.06
M-208	0.00	1.90	30.08	23.76	0.00	0.00	3.33	1.50	0.19	3.45	25.09	10.71

Appendix D

Cation Molar Proportions
(as plotted on the Jensen Cation Plot)

D-1 Calculation of Cation Molar Proportions

Cation molar proportions were calculated for the Jensen Cation Plot using a program written by Abdul Kabir. This program was run on the Cyber 170/815 computer at McMaster University.

Cation percentages are calculated from analyzed weight % data which has been normalized to 100 % on an anhydrous basis. Each oxide is divided by its corresponding equivalent molecular weight and multiplied by 1000. As cation percentages are based on each oxide having one cation, one half of the molecular weights of Al_2O_3, Na_2O, K_2O, Fe_2O_3 and P_2O_5 are used. Values obtained from this calculation are added together and percentages of each cation are calculated. For the Jensen Cation Plot, Al_2O_3, Fe_2O_3, FeO, MgO and TiO_2 are totalled and normalized to 100 %. The addition of Fe_2O_3, FeO and TiO_2 forms one value on the Jensen Cation Plot. Al_2O_3 and MgO form the other values.

Table D-1 Cation Molar Proportions

	Al_2O_3	MgO	Fe_2O_3+FeO+TiO_2
M-44	16.50	64.09	19.41
M-163	26.62	56.72	16.66
M-522	29.86	30.00	20.13
M-404	39.01	43.27	17.72
M-436	32.63	40.39	26.98
M-47	37.84	34.95	27.21
M-3	47.00	33.50	19.50
M-395	54.53	25.48	19.99
M-126	52.00	25.42	22.57
M-302	57.57	21.33	21.10
M-353	65.24	10.76	24.00
M-260	64.72	13.60	21.68
M-115	40.48	39.02	20.51
M-197	48.88	15.64	35.48
M-714	40.23	22.42	37.35
M-19	44.64	22.41	32.95
M-325	43.09	25.24	31.67
M-326	41.49	28.27	30.24
M-280	43.88	26.70	29.42
M-746	48.40	27.60	24.01
M-418	49.61	20.84	29.55
M-729	45.41	21.18	33.41
M-275	56.00	11.99	32.00
M-111	50.49	24.01	25.50
M-732	51.86	28.88	19.26
M-114	50.17	32.81	17.01
M-733	39.80	32.56	27.64
M-424	45.07	29.45	25.48
M-549	45.73	31.98	22.29
M-112	45.94	33.68	20.38
M-423	45.58	34.16	20.26
M-190	55.02	18.97	26.02
M-300	52.65	24.91	22.43
M-558	52.18	30.89	16.93
M-150	48.41	32.49	19.10
M-74	49.53	32.30	18.10
M-648	42.56	37.18	20.26
M-305	47.58	37.43	14.99

MAP I : SAMPLE LOCATIONS : THESIS MAP AREA

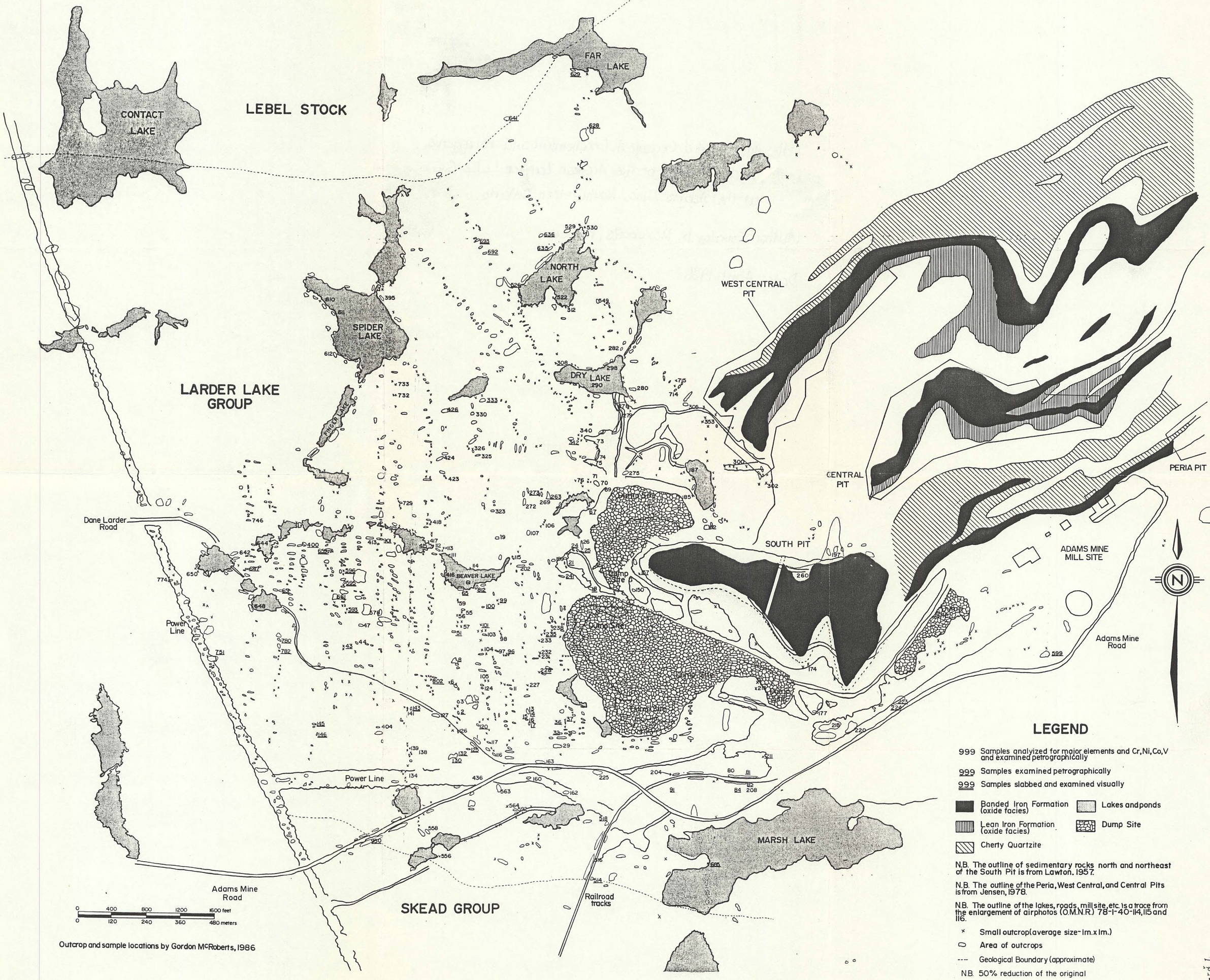

Outcrop and sample locations by Gordon McRoberts, 1986

LEGEND

999 Samples analyzed for major elements and Cr, Ni, Co, V and examined petrographically

999 Samples examined petrographically

999 Samples slabbed and examined visually

Banded Iron Formation (oxide facies)

Lean Iron Formation (oxide facies)

Cherty Quartzite

Lakes and ponds

Dump Site

N.B. The outline of sedimentary rocks north and northeast of the South Pit is from Lawton, 1957.

N.B. The outline of the Peria, West Central, and Central Pits is from Jensen, 1978.

N.B. The outline of the lakes, roads, mill site, etc. is a trace from the enlargement of airphotos (O.M.N.R.) 78-1-40-114, 115 and 116.

× Small outcrop (average size - 1m. x 1m.)

Area of outcrops

--- Geological Boundary (approximate)

N.B. 50% reduction of the original

MAP 2: GEOLOGY OF THE THESIS MAP AREA

LEBEL STOCK

CONTACT LAKE

FAR LAKE

NORTH LAKE

SPIDER LAKE

DRY LAKE

FINGER LAKE

BEAVER LAKE

LARDER LAKE GROUP

Lebel Syncline fold axis

Dane Larder Road

Power Line

Power Line

Adams Mine Road

SKEAD GROUP

Railroad Tracks

MARSH LAKE

WEST CENTRAL PIT

CENTRAL PIT

SOUTH PIT

PERIA PIT

ADAMS MINE MILL SITE

Adams Mine Road

0 400 800 1200 1600 feet
0 120 240 360 480 meters

Geology of the Thesis Map Area by Gordon McRoberts, 1986

LEGEND

1 SKEAD GROUP
- 1a Massive Felsic Flow
- 1b Feldspar Phyric Flow
- 1c Thinnly Laminated Tuff

2 SEQUENCE I VOLCANICS
- 2a Massive Flow
- 2b Pillowed Flow

3 KOMATIITIC VOLCANICS
- 3a Komatiite
- 3b High MgO Komatiitic Basalt
- 3c Low MgO Komatiitic Basalt
- 3d High MgO Komatiitic Andesite
- 3e Low MgO Komatiitic Andesite
- 3f High Al_2O_3 Komatiitic Basalt and or Andesite
- 3g High Fe_2O_3, Al_2O_3 Komatiitic Basalt or Andesite
- 3h High Al_2O_3 Komatiitic Dacite
- 3i Low Al_2O_3 Komatiitic Dacite
- 3j Mafic Tuff

4 SEDIMENTARY ROCKS
- 4a Sandstone, Massive Appearing
- 4b Sandstone and or siltstone Thinnly Laminated
- 4c Granule Conglomerate
- 4d Pebble Conglomerate
- 4e Cobble Conglomerate
- 4f Banded Iron Formation (oxide facies)
- 4g Chert
- 4h Carbonaceous Sediment/Chert
- 4i Argillite

- * Banded Iron Formation (oxide facies)
- * Lean Iron Formation
- * Chert
- * From Lawton, 1957

5 INTRUSIVES (CONCORDANT)
- 5a Peridotitic sill
- 5b Peridotitic phase of a layered Peridotite Gabbro Sill
- 5c Pyroxenitic phase of a layered Peridotite Gabbro Sill
- 5d Gabbroic phase of a layered Peridotite Gabbro Sill or a Gabbroic Sill
- 5e Microgabbroic phase of a layered Peridotite Gabbro Sill or a Gabbroic Sill

6 INTRUSIVES (DISCORDANT)
- 6a Gabbro
- 6b Syenite(Stock)
- 6c Diabase
- 6d Syenite(Dyke)
- 6e Lamprophyre
- 6f Fspar Porphyry

N.B. The outline of sedimentary rocks north and northeast of the South Pit is from Lawton, 1957. The outlines of the Peria, West Central and Central Pits are from Jensen 1978. The outlines of the lakes, roads, mine dump sites, etc. are traces from enlargements of O.M.N.R. airphotos 78-1-40-114, #5, and 116.

SYMBOLS
- x small outcrop (av. size) 1m x 1m
- area of outcrop
- bedding, inclined
- vertical
- flow top (arrow) from shape and packing of pillows
- schistosity, inclined
- vertical
- fault
- shear zone
- Lebel Syncline fold axis
- trace of the axial surfaces of folds which lies on the limbs of the Lebel Syncline
- geological boundary (approximate)
- mine dump site
- stratigraphic top as indicated by variations in a spinifex textured flow
- stratigraphic top as indicated by variations in a layered sill

NB. 50% reduction of the original

MAP 3: GEOLOGICAL COMPILATION OF THE ADAMS MINE AREA

LEBEL STOCK

FAR LAKE

CONTACT LAKE

NORTH LAKE

SPIDER LAKE

WEST CENTRAL PIT

Lebel Syncline fold axis

DRY LAKE

LENS LAKE

PERIA PIT

LARDER LAKE GROUP

Lebel Syncline fold axis

Dane Larder Road

Dump Site

SOUTH PIT

ADAMS MINE MILL SITE

BEAVER LAKE

Dump Site

Dump Site

Dump Site

Power Line

Area between double dashed lines is covered by overburden

N

Adams Mine Road

Power Line

Power Line

MARSH LAKE

0 400 800 1200 1600 feet
0 120 240 360 480 meters

SKEAD GROUP

Railroad Tracks

Geology of the Thesis Map Area by Gordon McRoberts, 1986

LEGEND

VOLCANIC ROCKS
- Komatiite and or High MgO Komatiitic Basalt
- Low MgO Komatiitic Basalt and or Andesite and or Low Al_2O_3 Komatiitic Dacite
- High Al_2O_3 Komatiitic Basalt and or Andesite
- High Al_2O_3 Komatiitic Dacite
- High Fe_2O_3, Al_2O_3 Komatiitic Basalt
- Tholeiitic and Calc alkaline Basalt

N.B. The outline of volcanic lithologies in the Central Pit and Peria Pit areas is based on the interpretation of field and geochemical data in Blum, 1986

SEDIMENTARY ROCKS
- Pebble and or Cobble Conglomerate
- Predominantly very fine to medium grained Clastic Sediments with or without minor amounts of Chemical Sediments
- Chert with or without minor amounts of Clastic Sediments
- Carbonaceous Sediments and Carbonaceous Chert
- Banded Iron Formation (oxide facies)
- Lean Iron Formation (oxide facies)
- Cherty Quartzite

N.B. Lean Iron Formation and Cherty Quartzite are terms from Lawton, (1957) and do not apply to the thesis map area
N.B. BIF, LIF and Cherty Quartzite north and northeast of the South Pit are outlined after Lawton, (1957)

INTRUSIVE ROCKS
- Peridotitic Sill
- Peridotitic phase of a layered Peridotite Gabbro Sill
- Pyroxenitic phase of a layered Peridotite Gabbro Sill
- Gabbroic phase of a layered Peridotite Gabbro Sill or a Gabbroic Sill
- Microgabbroic phase of a layered Peridotite Gabbro Sill or a Gabbroic Sill
- Discordant Gabbroic Intrusive
- Lebel Syenite Stock

N.B. Intrusive rocks shown between the West Central Pit and the Mill Site are outlined after Blum, (1986)

SYMBOLS
- synclinal fold axis
- geological boundary (approximate)

N.B. 50% reduction of the original

MAP 4: VOLCANIC LITHOLOGIES : ADAMS MINE AREA

LEBEL STOCK

CONTACT LAKE

FAR LAKE

NORTH LAKE

SPIDER LAKE

DRY LAKE

FINGER LAKE

LARDER LAKE GROUP

Lebel Syncline fold axis

WEST CENTRAL PIT

CENTRAL PIT

SOUTH PIT

PERIA PIT

ADAMS MINE MILL SITE

Dane Larder Road

Power Line

Adams Mine Road

BEAVER LAKE

SEQUENCE 1

SEQUENCE 2

SEQUENCE 3

SEQUENCE 4

SEQUENCE 5

SEQUENCE 6

SEQUENCE 7

SEQUENCE 8

MARSH LKE

SKEAD GROUP

Railroad Tracks

0 400 800 1200 1600 feet
0 120 240 360 480 meters

Geology of the Thesis Map Area by Gordon McRoberts, 1986

LEGEND

VOLCANIC ROCKS

- Komatiite and or High MgO Komatiitic Basalt
- Low MgO Komatiitic Basalt and or Andesite and or Low Al_2O_3 Komatiitic Dacite
- High Al_2O_3 Komatiitic Basalt and or Andesite
- High Al_2O_3 Komatiitic Dacite
- High Fe_2O_3, Al_2O_3 Komatiitic Basalt
- Tholeiitic and Calc alkalic Basalt

N.B. The outline of volcanic lithologies in the Central Pit and Peria Pit areas is based on interpretation of field and geochemical data in Blum, 1986.

N.B. 50% reduction of the original

SEDIMENTARY ROCKS

- Banded Iron Formation (oxide facies)
- Lean Iron Formation (oxide facies)
- Chert

N.B. The outline of B.I.F, L.I.F and Cherty Quartzite north and northeast of the South Pit is from Lawton, 1957. The outline of the Peria, West Central and Central Pits is from Jensen, 1978. The outlines of the lakes, roads, dump sites, etc. are traces from enlargements of O.M.N.R. airphotos 78-1-40-114, 115 and 116.

- Mine Dump Site

SYMBOLS

- Geological Boundary (Approx)
- Synclinal Fold Axis

MAP 5 : INTRUSIVE LITHOLOGIES : ADAMS MINE AREA

LEBEL STOCK

CONTACT LAKE

FAR LAKE

Contact Gabbro

NORTH LAKE

SPIDER LAKE

Contact Gabbro

LARDER LAKE GROUP

DRY LAKE

WEST CENTRAL PIT

South Pit Gabbro

CENTRAL PIT

PERIA PIT

Lebel Syncline fold axis

EINDER LAKE

Location for Figure 7-3

Dane Larder Road

BEAVER LAKE

South Pit Gabbro

SOUTH PIT

ADAMS MINE MILL SITE

Power Line Gabbro

South Pit Gabbro

Adams Mine Road

Power Line

Power Lire

Power Line

MARSH LAKE

Adams Mine Road

South Pit Gabbro

SKEAD GROUP

Railroad Tracks

0 400 800 1200 1600 feet
0 120 240 360 480 meters

Geology of the Thesis Map Area by Gordon McRoberts, 1985

LEGEND

CONCORDANT INTRUSIVES
- Peridotitic Sill
- Peridotitic phase of a layered Peridotite-Gabbro Sill
- Pyroxenitic phase of a layered Peridotite-Gabbro Sill
- Gabbroic phase of a layered Peridotite-Gabbro Sill or a Gabbroic Sill
- Microgabbroic phase of a layered Peridotite-Gabbro Sill or a Gabbroic Sill

DISCORDANT INTRUSIVES
- Gabbro
- Syenite Stock
- Diabase
- S Syenite Dyke
- S.M. Mafic Syenite
- L Lamprophyre Dyke
- F.P. Feldspar Porphyry Dyke

SEDIMENTARY ROCKS
- Banded Iron Formation (oxide facies)
- Lean Iron Formation (oxide facies)
- Cherty Quartzite

N.B. The outline of sedimentary rocks north and northeast of the South Pit is from Lawton, 1957. The outline of the Peria, West Central and Central Pits is from Jensen, 1978. The outline of the lakes, roads, mill site, etc. is a trace from the enlargement of airphotos (O.M.N.R.) 78-1-40-114, 115 and 116.

- Mine Dump Site
- Trend of dyke
- × Outcrop which is probably part of an alkali rich dyke
- Synclinal fold axis
- Geological boundary (approx.)
- 1,2,3,4 Indicates the stratigraphic position of the Peridotite-Gabbro and Gabbroic Sills on the south limb of the Lebel Syncline

NB. 50% reduction of the original

MAP 6 : SEDIMENTARY LITHOLOGIES : ADAMS MINE AREA

LEBEL STOCK

CONTACT LAKE

FAR LAKE

Group 1

Group 2

Group 3

Group 4

Group 5

Group 6

NORTH LAKE

SPIDER LAKE

DRY LAKE

FINGER LAKE

LARDER LAKE GROUP

Lebel Syncline fold axis

WEST CENTRAL PIT

CENTRAL PIT

SOUTH PIT

PERIA PIT

ADAMS MINE MILL SITE

Adams Mine Road

Dump Site

Dump Site

Dump Site

Dump Site

Dump Site

Dump Site

Sedimentary rocks considered as lateral equivalents to B.I.F. in the West Central Pit

Dane Larder Road

Sedimentary rocks considered as lateral equivalents to B.I.F. in the Central Pit

BEAVER LAKE

Power Line

Sedimentary rocks considered as lateral equivalents to B.I.F. in the South and Peria Pits

Sedimentary rocks considered as lateral equivalents to the McElroy Formation

Power Line

MARSH LAKE

Adams Mine Road

Railroad Tracks

SKEAD GROUP

0 400 800 1200 1600 feet

0 120 240 360 480 meters

Geology of the Thesis Map Area by Gordon McRoberts, 1986

LEGEND

SEDIMENTARY ROCKS

- Pebble and or Cobble Conglomerate
- Predominantly very fined to medium grained clastic sediments with or without minor amounts of chemical sediments
- Chert with or without minor amounts of clastic sediments
- Carbonaceous Sediments and Carbonaceous Chert
- Banded Iron Formation (oxide facies)
- Lean Iron Formation (oxide facies)
- Cherty Quartzite

N.B. Lean Iron Formation and Cherty Quartzite are terms from Lawton,(1957) and do not apply to the thesis map area

N.B. B.I.F, L.I.F and Cherty Quartzite north and northeast of the South Pit are outlined after Lawton,1957)

N.B. Clastic sedimentary rocks between the West Central and Peria Pits are outlined from Blum, 1986

SYMBOLS

- ----- Geological Boundary (Approx.)
- Synclinal Fold Axis

N.B. 50% reduction of the original